THE HONG KONG POLYTECHNIC UNIVERSITY

DEPARTMENT OF CIVIL AND STRUCTURAL ENGINEERING

FIELD INVESTIGATION OF WATER SOLUBLE IONIC SPECIES IN AEROSOLS AND THE FORMATION OF FINE SULFATE AND NITRATE IN THE ATMOSPHERE

BY

WAI SHING WU

A thesis submitted in partial fulfillment of

the requirements for the degree of Doctor of Philosophy

March 2009

CERTIFICATE OF ORIGINALITY

I hereby declare that this thesis is my own work and that, to the best of my knowledge and belief, it reproduces no material previously published or written, nor material that has been accepted for the award of any other degree or diploma, except where due acknowledgement has been made in the text.

Wai Shing Wu

FIELD INVESTIGATION OF WATER SOLUBLE IONIC SPECIES IN AEROSOLS AND THE FORMATION OF FINE SULFATE AND NITRATE IN THE ATMOSPHERE

Wai Shing Wu

Environmental Engineering
The Hong Kong Polytechnic University

ABSTRACT

Water soluble ionic species in $PM_{2.5}$ play an important role in the climate forcing, heterogeneous chemistry, cloud formation as well as human health. In this study, the data of both one hour and twenty-four hour water soluble ions were obtained. These two types of data are important for interpreting the behaviors of ion species in the atmosphere. Secondly, this study was conducted in the megacities of China which has long been known for its severe air pollution caused by high concentrations of particulate matter. In addition, there is limited knowledge on the distribution of aerosols in suburban and/or rural areas and on the formation of secondary aerosols in China. Such knowledge is essential for evaluating the impact of a megacity's emission on regional air quality and climate. Thus, this study is valuable and important for the more in-depth understanding of the water soluble ion species as well as the current air pollution situation in China.

The objectives of this study include the determination of the data accuracy and quality of the recently developed Ambient Ion Monitor (AIM). The field studies document the present levels of the water soluble ion species at different parts of China. This study also provides more in-depth analysis of the behaviors of ion species as well as the formation of fine sulfate and nitrate in the atmosphere. The comparison of the water soluble ion species in different parts of China was also made. Finally, the visibility problem in China was demonstrated.

Data accuracy and quality of the AIM

Two kinds of comparison have been preformed to verify the AIM instrument. The comparison of the AIM with another semi-continuous sulfate and nitrate instruments showed an overall similar pattern. However, the AIM showed generally smaller sulfate (AIM: 13.4 ± 8.2μg/m^3 and APSM: 18.5 ± 9.1μg/m^3) and higher nitrate concentrations (AIM: 3.4 ± 2.0μg/m^3 and APNM: 3.0 ± 1.7μg/m^3). In addition, at the days with high sulfate pollution plumes, the sulfate results were reversed. Secondly, the comparison between the AIM and the filter analysis has shown that the two methods had a good overall correlation for sulfate and nitrate, but showed discrepancies in absolute concentrations. At low levels of sulfate and SO_2, the AIM data agreed with the filter result in Beijing (AIM = 0.97 x filter + 0.60, $R^2 = 0.94$). However, the AIM gave much higher sulfate values at high SO_2 concentrations (in Shanghai). At high sulfate and nitrate loading, on the other hand, the AIM gave a much smaller reading.

Analysis of the water soluble ion species collected from the AIM

The temporal and diurnal variations of the $PM_{2.5}$ mass and water soluble ion species collected in Beijing, Shanghai and Hong Kong were presented. Analysis of the collected dataset suggested that meteorological and chemical factors contributed to the high $PM_{2.5}$ aerosol concentrations (Beijing: 79.3 ± 65.4μg/m^3, Shanghai: 59.7 ± 47.4μg/m^3). The diurnal profiles of sulfate and nitrate were different at different places.

Analysis of the water soluble ion species collected from the filters

The water soluble ion species collected from the filters at four different places (Shanghai, Beijing, Lanzhou and Guangzhou) were analyzed. In these four places, the abundant of the $PM_{2.5}$ mass were found to be similar (60 – 70μg/m^3). The concentrations of the water soluble ion species were found to be much higher than other countries such as US. Sulfate, nitrate and ammonium were generally the major components of the water soluble ions in these places. From the nitrate to sulfate ratio (<0.44 for all the sampling sites), the results suggested that all the sampling locations were more affected by the stationary sources such as factories over the mobile sources. The analysis of the sulfur and nitrogen oxidation ratio suggested that Shanghai and Lanzhou experienced similar degree of oxidation (SOR: ~0.2, NOR: ~0.1) while Beijing showed a bit higher (SOR: ~0.5, NOR: ~0.2).

Formation routes of sulfate and nitrate and visibility reduction in Beijing

25 – 67% of SO_2 were found to have been converted to sulfate in seven urban pollution plumes examined in Beijing. An examination of SO_2 versus total sulfur under different humidity conditions indicated that the conversion of SO_2 was most efficient under humid conditions in Beijing, but not in Shanghai. The nitrate formation pathways at four study sites were different. Lanzhou and Guangzhou were mainly through gas-phase homogeneous reaction between ammonia and nitric acid, while Beijing and Shanghai were through heterogeneous hydrolysis of N_2O_5.

In addition, the visibility problem in Beijing was very serious. Results suggested that fine particulates (sulfate, nitrate and ammonium) were the major visibility reducing aerosol components in the polluted atmosphere in Beijing. Furthermore, ammonium sulfate and ammonium nitrate contributed to the high fraction of the light extinction, especially during the episode days. This suggested that water soluble ions played a significant role in the visibility impairment in the Beijing area.

Signature: ___________________________

ACKNOWLEDGEMENTS

I would like to thank my supervisor Prof. Tao Wang for providing me the opportunity to be involved in the field of Atmospheric research. His unwavering support, constant encouragement, and expert guidance were what inspired me to strive for more achievements.

I am indebted to Dr. Aijun Ding for his valuable suggestions and generous help, especially in data analysis part. Without his help, my thesis work would not have been completed.

I would like to thank a number of colleagues who have assisted me in numerous ways. Mr. Steven Poon provided all the logistic work and technical support. Dr. Yu Ren provided part of the filter analysis. Mr. Joey Kwok provided the data reduction work.

Special thanks to my friends Mr. Anson Wong and Mr. Joe Cheung for their valuable encouragement and support throughout my study.

Financial support was provided to me as Postgraduate Studentship from the Hong Kong Polytechnic University.

Finally, I would like to thank my parents and my wife Dr. Cindy Yang for their love, support and care.

TABLE OF CONTENTS

CHAPTER 1 AEROSOLS AND WATER SOLUBLE ION SPECIES IN THE ATMOSPHERE

CHAPTER 2 IMPORTANCE OF ATMOSPHERIC AEROSOLS AND WATER SOLUBLE ION SPECIES

CHAPTER 3 REVIEW ON THE WATER SOLUBLE ION SPECIES IN THE ATMOSPHERE

CHAPTER 4 BACKGROUND INFORMATION OF THE SAMPLING LOCATION

CHAPTER 5 INSTRUMENT DESCRIPTIONS AND FILTER ANALYSIS

CHAPTER 6 INTERCOMPARISON OF THE AIM WITH DIFFERENT SAMPLING METHODS

CHAPTER 7 MEASUREMENT RESULTS IN BEIJING, SHANGHAI, AND HONG KONG

CHAPTER 8 RESULTS AND ANALYSIS OF PM2.5 MASS AND WATER SOLUBLE ION SPECIES FROM FILTER MEASUREMENTS

CHAPTER 9 FORMATION MECHANISMS OF SULFATE, NITRATE AND THE CONTRIBUTION OF AEROSOLS TO THE VISIBILITY IMPAIRMENT IN BEIJING

LISTS OF FIGURES

LIST OF TABLES

ABBREVIATIONS

AGL	Above Ground Level
AIM	Ambient Ion Monitor
AOD	Aerosol Optical Depth
APNM	Ambient Particulate Nitrate Monitor
APSM	Ambient Particulate Sulfate Monitor
a.s.l.	Above Sea Level
Br^-	Bromide
$C_2H_2O_4$	Oxalic acid
$C_2O_4^{2-}$	Oxalate
Ca^{2+}	Calcium
$CaCO_3$	Calcium carbonate
$Ca(NO_2)_2$	Calcium nitrite
$Ca(NO_3)_2$	Calcium nitrate
CCN	Cloud Condensation Nuclei
CH_3COO^-	Acetate
CH_3COONH_4	Ammonium acetate
Cl^-	Chloride
Cl_2O_2	Chlorine peroxide
ClO	Hypochlorite
$ClONO_2$	Chlorine nitrate
CO	Carbon monxide

CO_2	Carbon dioxide
EC	Elemental Carbon
F^-	Fluoride
Fe_2O_3	Iron (III) oxide
Fe^{3+}	Iron
F_n	Nitrogen conversion ratio
F_s	Sulfur conversion ratio
H^+	Hydrogen
H_2O	Water
H_2O_2	Hydrogen peroxide
$H_2PO_4^-$	Dihydrogen phosphate
H_2SO_3	Sulfurous acid
H_2SO_4	Sulfuric acid
HCl	Hydrochloric acid
$HCOONH_4$	Ammonium Formate
HKEPD	Hong Kong Environmental Protection Department
HNO_2	Nitrous acid
HNO_3	Nitric acid
$HO_2\cdot$	Hydroperoxyl radical
HSO_3^-	Bisulfate
HYSPLIT	HYbrid Single-Particle Lagrangian Integrated Trajectory
IC	Ion chromatography
IN	Ice Nuclei

K^+	Potassium
K_2SO_4	Potassium sulfate
KCl	Potassium chloride
Li^+	Lithium
Mg^{2+}	Magnesium
$MgCO_3$	Magnesium carbonate
MgO	Magnesium oxide
Milli-Q	Millipore
MODIS	MODerate-resolution Imaging Spectroradiometer
MoO	Molybdenum oxide
Mn^{2+}	Manganese
MnO_2	Manganese dioxide
N_2O_5	Dinitrogen pentoxide
NCEP	National Centre for Environmental Prediction
NPN	N-propylnitrate
Na^+	Sodium
Na_2SO_4	Sodium sulfate
NaCl	Sodium chloride
$NaNO_3$	Sodium nitrate
NCPs	North China Plains
NH_3	Ammonia
NH_4^+	Ammonium
$(NH_4)_2C_2O_4$	Ammonium oxalate

$(NH_4)_2CO_3$	Ammonium carbonate
NH_4Cl	Ammonium chloride
NH_4NO_3	Ammonium nitrate
$(NH_4)_2SO_4$	Ammonium sulfate
nm	nanometer
NO	Nitric oxide
NO_2	Nitrogen dioxide
NO_2^-	Nitrite
NO_3^-	Nitrate
NOR	Nitrogen Oxidation Ratio
NO_x	Nitrogen oxide
NO_y	Nitrogen oxide
N-ratio	Nitrogen conversion ratio
O_2	Oxygen
O_3	Ozone
OC	Organic Carbon
OH·	Hydoxide radical
PAHs	Polycyclic Aromatic Hydrocarbons
PAN	Peroxy Acetyl Nitrate
PFA	Perfluoroalkoxy
PM_{10}	Particulate matter with aerodynamic diameter less than 10μm
$PM_{2.5}$	Particulate matter with aerodynamic diameter less than 2.5μm
PO_4^{3-}	Phosphate

QA	Quality assurance
QC	Quality control
RH	Relative Humidity
RMA	Reduced Major Axis regression
$RO_2\cdot$	Alkperoxy radical
RSP	Respirable Suspended Particulate
SH	Specific Humidity
SO_2	Sulfur dioxide
SO_3	Sulfur trioxide
SO_4^{2-}	Sulfate
SOR	Sulfur Oxidation Ratio
SO_x	Sulfur oxide
S-ratio	Sulfur conversion ratio
TEI	Thermo Environmental Instrument
TEMP	Temperature
TEOM	Tapered Element Oscillating Microbalance
TSP	Total Suspended Particulate
US	United States
UV	Ultra-violet
V_2O_5	Vanadium (V) oxide
$\mu g/m^3$	Microgram per cubic meter
µm	Micrometer

Section I: Introduction

Chapter 1: Aerosols and water soluble ion species in the atmosphere

1.1 Atmospheric aerosols

Aerosol is technically defined as a suspension of fine solid or liquid particles in a gas. Atmospheric aerosols are generally considered to be the particles that range in size from a few nanometers (nm) to tens of micrometers (µm) in diameter [Seinfeld and Pandis, 1998].

Atmospheric aerosols can be classified according to the sources or sizes. Based on the sources, they can be classified as natural as well as anthropogenic aerosols. Natural aerosols consist of: (1) products of sea spray evaporation; (2) mineral dust wind-driven to the atmosphere; (3) volcanic aerosols; (4) particles of biogenic origin; (5) smokes from biota burning on land; and (6) products of natural gas-to-particle conversion whereas anthropogenic aerosols consist of (1) direct industrial emissions of particles; and (2) products of gas-to-particle conversion [Kondratyev et al., 2006]. Apart from the above classification, atmospheric aerosols can also be divided into primary as well as secondary. Primary aerosols such as elemental carbon are emitted directly as particles whereas secondary aerosols such as sulfate (SO_4^{2-}) and nitrate (NO_3^-) are formed in the atmosphere by gas-to-particle conversion processes [Seinfeld and Pandis, 1998].

According to their sizes, the aerosol particulates can be divided into total suspended particulate (TSP), coarse particles (PM_{10}) and fine particles ($PM_{2.5}$). TSP, PM_{10} and $PM_{2.5}$ can be defined as particles with aerodynamic diameter smaller than 100µm, 10µm and 2.5µm, respectively [Wang et al., 2006; Zheng et al., 2005].

Besides, atmospheric aerosol particles consist of numerous kinds of species. It contains both organic and inorganic fractions. Organic aerosols such as aldehydes, polycyclic aromatic hydrocarbons (PAHs) contribute only small fraction of the aerosol particles while the majority of them are made up of inorganic fractions such as sulfate, nitrate.

1.2 Atmospheric water soluble ion species

Water soluble ion species are a group of inorganic species which contribute to large fraction of atmospheric aerosols. They include many species such as sulfate, nitrate, ammonium (NH_4^+), sodium (Na^+), chloride (Cl^-). They consist of both primary (e.g. Na^+ and Cl^- from sea salt) as well as secondary (e.g. NH_4^+ and NO_3^- from gas to particle conversion) origin.

Chapter 2: Importance of atmospheric aerosols and water soluble ion species

2.1 Importance of atmospheric aerosols

Aerosol particles play an important role in both physical and chemical processes in the atmosphere such as climate forcing, heterogeneous chemistry and cloud formation. They have also been proposed as a major factor in producing adverse human health effects. In the following section, the effects of aerosol particles to the atmosphere and the human beings are presented.

Effects on clouds, climate , and ozone

Cloud formations as well as cloud properties are substantially influenced by the physical and chemical characteristics of the aerosols present in the air. In reverse, clouds could also modify the preexisting aerosols by removal and/or by aqueous reactions.

Since cloud condensation nuclei (CCN) and ice nuclei (IN) impart initial cloud characteristics, and consequently influence the evolution of clouds, the CCN will be able to influence climatic changes, especially through the cloud albedo. Moreover, the continental anthropogenic aerosol may also influence maritime clouds. Nitrate and sulfate concentrations in oceans are increasing, probably via transport of continental particulate air pollutants. The anthropogenic CCN significantly affect clouds and modify the greenhouse effect, forcing increased concentrations of CO_2. Furthermore, the particle size, chemical composition, and reactivity of emitted anthropogenic aerosols substantially influence the optical properties of the global atmosphere. Increasing concentrations of a number of atmospheric chemicals, including aerosols, lead to concern about the possibility of the resulting climatic changes. They also affect the environment by degrading visibility and affecting regional and global climate [Drewnick, 2003; Jeong et al., 2004; Park et al., 2005].

Another role played by aerosol chemistry involves atmospheric chemical reactions. For example, organosulfur species are oxidized in the marine atmosphere and form CCN.

In addition, the study of the role of aerosols in stratospheric ozone photochemistry has shown that heterogeneous reactions on aerosols can play a significant role in ozone depletion mechanisms. In the stratosphere, low temperature reactions on nitric acid trihydrate, on water ice particles, or on particles consisting of ternary supercooled solutions of sulfuric acid, nitric acid, and water, lead to rapid conversion of HCl and $ClONO_2$ species into active chlorine species (Cl, ClO, Cl_2O_2), which act catalytically to rapidly destroy ozone [Crutzen, 1996; Dentener et al., 1996; Spurny, 2000].

Health effects of fine atmospheric aerosols

Many previous studies suggested that both physical (particle size, shape, surface, and biopersistence) and chemical (solved and leached toxic chemicals, and surface catalytic reactions) properties of fine particulate fractions are involved in several health effects.

1. Air particulate epidemiology

Many epidemiological studies have shown a strong correlation between increased PM concentrations and increased morbidity, mortality as well as respiratory symptoms. For instance, Dockery et al. (1993) examined particulate air pollutant concentrations in relation to health statistics and concluded that elevated fine-particle matter concentrations are associated with increased mortality and morbidity in the general population, and especially in vulnerable children and elderly people. Figure 2.1 summarized the results of such investigation. The ambient air concentrations of fine particulates correlated well with excess mortalities of six US cities. However, the mechanisms responsible for the observed increases in mortality and morbidity were virtually unknown [Dockery et al., 1993; Spurny, 2000].

Figure 2.1. Estimated adjusted mortality rate ratios and pollution levels ($PM_{2.5}$) in six US cities: Portage, WI (P); Topeka, KS (T); Watertown, MA (W); St. Louis, OH (L); Harrison, TN (H); and Steutenville, OH (S) [Dockery et al., 1993].

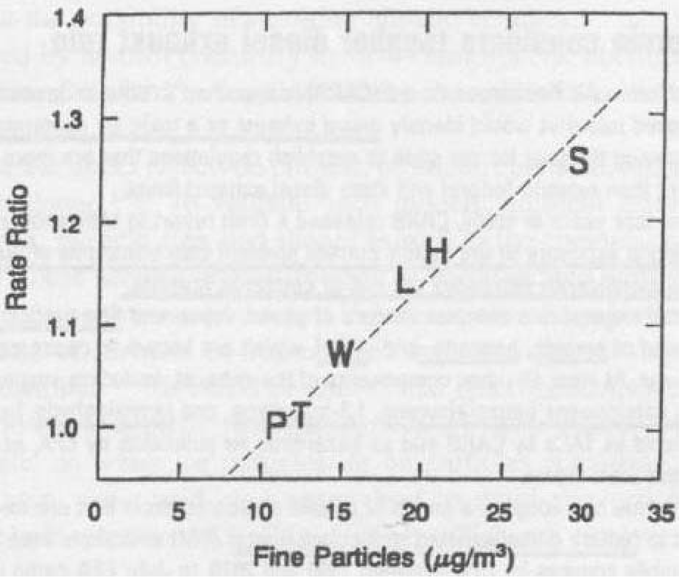

2. Toxicology of fine particulates

Some previous epidemiological studies have shown that physical and chemical properties of single particles are involved in the toxic, genotoxic, and carcinogenic health effects of inhaled atmospheric particulates. Particle size, shape, electric charge, particulate surface, and solubility are the most important physical parameters that have been correlated with the observed toxic effects. These parameters also influence substantially the particle lung deposition and lung clearance rates. Some reports have shown that the impacts of fine particles ($PM_{2.5}$ or less) on human health are greater than the impacts of large particles because small particles can be inhaled deep into the unciliated and alveolar sections of the lungs [Pathak et al., 2003]. Fine and very fine particles penetrate into the deep lung compartments, and their deposited fraction depends strongly on particle diameter and breathing rates. Furthermore, the electric charge of fine particles enhances airway deposition. Similarly, particle clearance in the lung depends on the particle size. The hypothesis that fine and very fine particles, when inhaled, can be very toxic to the lung is therefore supported by their high deposition efficiency in the lower respiratory tract, by slow clearance rates, by their large numbers per unit mass, and by the increased surface areas available for interactions with cells [Cheng and Swift, 1995; Cohen et al., 1996; Ferin et al., 1990; Oberdörster et al., 1995; Seaton et al., 1995; Spurny, 2000].

2.2 Importance of water soluble ion species in the atmosphere

As fine aerosols have greater impact to the human beings, more focus has been put on the fine particulate matters ($PM_{2.5}$) recently. Since $PM_{2.5}$ is complex mixture of chemical species, we firstly need to know the chemical compositions of $PM_{2.5}$. The speciation studies for $PM_{2.5}$ have shown that sulfate, nitrate, ammonium, organic carbon (OC) and elemental carbon (EC) are the major components of $PM_{2.5}$ in the atmosphere [Lin, 2002]. Figure 2.2 showed one of the speciation results of aerosols in southern California. Sulfate, nitrate, ammonium and black carbon have already accounted for about 50% of the total $PM_{2.5}$ and about one-third was come from the organic components [McMurry et al., 2004].

Figure 2.2. Speciation results of aerosols in southern California.

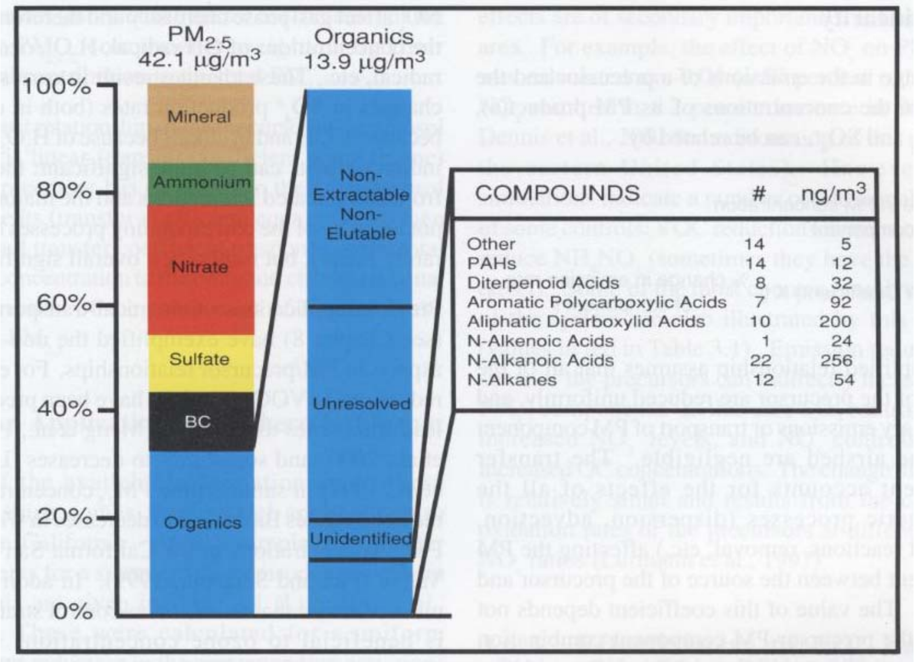

Among these components, volatile inorganic species, such as nitrate, chloride and ammonium, are of great concern in urban and regional air pollution problems because aerosol acidity and its impact on environmental acidification are predominantly controlled by these species, together with sulfate [Ueda et al., 2000]. Due to their abundance, water soluble ion species in $PM_{2.5}$ play a central role in affecting the earth’s radiation balance directly by scattering and absorbing incoming solar radiation, and indirectly via their effects on cloud properties [Hillamo et al., 1998]. Therefore, understanding the composition, variation, sources, and the formation of secondary ionic species, with an emphasis on sulfate and nitrate, have been the key issue and hence the urgency in the study on air quality and its control policy [Wang et al., 2005].

Chapter 3: Review on the water soluble ion species in the atmosphere

In order to know the importance of this study in comparison with the previous ones, we need to have a complete picture on the current knowledge of these species. In this chapter, I will review the water soluble ion species in the atmosphere in different aspects such as the sources, ambient levels, the formation mechanisms based on the previous studies.

Water soluble ions contain numerous kinds of species. Some of them are in greater abundance such as sulfate, nitrate, ammonium, whereas some of them are in trace amount such as oxalate ($C_2O_4^{2-}$), acetate (CH_3COO^-), dihydrogen phosphate ($H_2PO_4^-$). In this study, thirteen ions were determined totally as these ions have greater effect to the climate change as well as human beings due to the greater abundance in comparison with the others. Six cations, namely sodium (Na^+), potassium (K^+), calcium (Ca^{2+}), magnesium (Mg^+), ammonium (NH_4^+), and lithium (Li^+) as well as seven anions, namely fluoride (F^-), chloride (Cl^-), sulfate (SO_4^{2-}), nitrate (NO_3^-), bromide (Br^-), nitrite (NO_2^-), and phosphate (PO_4^{3-}) were determined in this study. Therefore, I will focus on the above selected ion species in this review section.

3.1 Sources of water soluble ionic species and their precursor gases

In order to improve visibility, reduce ecological damage as well as protect human health, we need to control the particulate matter concentrations. Knowing the sources of the pollutants are the first important step because it can provide us more information on their origin and in turn understand the formation mechanisms of secondary pollutants such as sulfate, nitrate. Finally, it can help in establishing any control policy to reduce the pollution problems.

Different water soluble ions have different sources. Moreover, each ion can have various sources and have both natural and anthropogenic origin. For example, part of the Na^+ and Cl^- come from ocean and can regard as natural source, while industrial activities emit Ca^{2+} and can regard as anthropogenic source. The summary of the sources of cations and anions are illustrated in Tables 3.1 and 3.2, respectively.

Table 3.1. Sources of water soluble cation species.

Ion species	**Sources**
Magnesium	1. Soil
Calcium	1. Soil 2. Vehicle exhaust 3. Industrial activity 4. Building material
Potassium	1. Soil 2. Ocean 3. Vegetation 4. Biomass burning 5. Incinerator emission
Sodium	1. Soil 2. Ocean 3. Vehicle exhaust
Ammonium	1. Fertilizer from the agricultural area 2. By the reaction of NH_3 vapors with acidic gases such as H_2SO_4, HNO_3, HCl 3. Reaction or condensation of NH_3 vapor on an acidic particle surface of anthropogenic origin 4. By the reaction of NH_3 gas on sulfate or nitrate enriched sea salt and/or soil particle when excess NH_3 gas was available 5. From salts of carbonic acid such as $(NH_4)_2CO_3$, NH_4NO_3 and salts of organic acids via CH_3COONH_4 or $HCOONH_4$. These may be formed by the reaction of NH_3 gas with aqueous aerosols

Table 3.2. Sources of water soluble anion species.

Ion species	**Sources**
Chloride	1. Ocean 2. Biomass burning 3. Combustion process
Fluoride	1. Industrial activity such as brick kiln, lime pulverization unit
Bromide	1. Ocean 2. Biogenic
Sulfate	1. Ocean 2. Biomass burning 3. Combustion process 4. By droplet-phase oxidation of SO_2 in cloud 5. SO_2 or H_2SO_4 react with aqueous carbonates such as dissolved $CaCO_3$, $MgCO_3$ on soil particles 6. H_2SO_4 gas can condense on sea-salt particles and react with NaCl
Nitrate	1. Combustion process 2. By the reaction of HNO_3 with sea-salt particles 3. HNO_3 reacts with aqueous carbonates such as dissolved $CaCO_3$, $MgCO_3$ on soil particles $2HNO_3(g) + CaCO_3(s) \rightarrow Ca(NO_3)_2(s) + H_2O + CO_2(g)$

[Cheng et al., 2000; Erduran and Tuncel, 2001; McMurry et al., 2004; Mouli, et al., 2003; Zhuang et al., 1999]

As water soluble ion species such as sulfate, nitrate, ammonium are mainly secondary in origin, most of these are formed in the atmosphere by gas to particle conversion from the primary emissions of gaseous sulfur dioxide (SO_2), nitrogen oxide (NO_x), and ammonia (NH_3). Therefore, knowing the sources of the precursor gases are also helpful and important for studying water soluble ion species in the atmosphere. Table 3.3 summarized the sources of SO_2, NO_x, and NH_3 gases.

Table 3.3. Sources of SO_2, NO_x, and NH_3 gases.

Gases	**Sources**
Ammonia	1. Fertilizer from the agricultural area 2. Livestock 3. Ammonia-based chemical fertilizer 4. Human beings 5. Sewage treatment plant 6. Catalytic converter equipped vehicle
Sulfur dioxide	1. Combustion of sulfur-containing fossil fuel 2. Power station 3. Fuel combustion 4. Marine vessel 5. Vehicle
Nitrogen oxides	1. Combustion process 2. Power station 3. Motor vehicle e.g. diesel vehicle

[Air Services Group, 2003; Bari et al., 2003; Erduran and Tuncel, 2001]

3.2 Ambient levels of water soluble ion species

After reviewing the sources of the ion species in the atmosphere, I will give a comprehensive review on the ambient concentrations of the ionic species conducted from different areas. This kind of summary can give us information on the concentrations in different types of environment (e.g. urban, rural) as well as in different countries (e.g. China, United States) so that comparisons can be made between our measurement results and others from different geographical locations in future. In addition, it can also give us an idea on the seriousness of the pollution problems in this study. The location and the time for conducting the measurement and the concentrations of cations and anions are summarized in Tables 3.4 and 3.5, respectively.

Table 3.4. Summary of the ambient concentrations of cations.

Location	**Period**	**NH_4^+**	**Ca^{2+}**	**Na^+**	**K^+**	**Mg^{2+}**	**Reference**
Leipzig (Germany)	Jan 93 – Dec 95	-- 2.9 ± 2.1	-- 1.1 ± 0.7				Müller (1999)
Melpitz (Germany)	Jan 93 – Dec 95	-- 2.7 ± 1.9	-- 0.6 ± 0.4				Müller (1999)
Cape D'Aguilar (China)	Apr 95 – Apr 96	0.073 – 4.96 1.08 ± 1.10	0.09 – 7.42 0.91 ± 0.91	0.98 – 32.67 11.13 ± 7.98	0.075 – 2.78 0.78 ± 0.60	0.13 – 4.45 1.38 ± 1.02	Cheng et al. (2000)
Küçük Çalticak (Turkey)	Aug 95 – Apr 96	0.02 – 6.08 2.19 ± 1.17					Erduran and Tuncel (2001)
Veszprém (Hungary)	Sept 95 – Aug 96	-- 4.162	-- 0.355	-- 0.218	-- 1.572	-- 0.036	Krivácsy and Molnár (1998)
The Hong Kong University of Science and Technology (China)	Jul 97 – Dec 97		0.005 – 0.880 --	0.207 – 2.328 --			Zhuang et al. (1999)
Thessaloniki (Greece)	Jul 97 – Jul 98	0.49 – 7.58 2.67 ± 1.61	0.07 – 3.27 1.10 ± 0.72	0.10 – 3.097 0.639 ± 0.567	0.19 – 2.619 0.719 ± 0.593	0.03 – 0.23 0.11 ± 0.04	Tsitouridou et al. (2003)
Shanghai (China)	Mar 99 – Mar 00	1.60 – 11.99 5.67	0.12 – 2.06 0.54	0.19 – 0.88 0.45	0.24 – 6.09 1.66	0.00 – 0.59 0.19	Ye et al. (2003)
Shanghai (China)	May 99 – Mar 00	1.51 – 12.44 6.07	0.15 – 1.35 0.55	0.00 – 1.13 0.49	0.27 – 9.82 1.98	-- 0.19	Ye et al. (2003)
Beijing (China)	Jul 99 – Sept 00	1.1 – 21.9 6.2	0.2 – 1.5 0.7	BDL – 3.2 0.7	0.6 – 8.1 2.2	BDL – 0.8 0.3	Yao et al. (2002)
Beijing (China)	Jul 99 – Sept 00	1.2 – 23.6 6.5	0.3 – 0.9 0.8	BDL – 1.9 0.7	2.1 – 3.6 2.2	BDL – 1.1 0.4	Yao et al. (2002)
Fukue Island (Japan)	Mar 00 – Apr 02	-- 2.5	-- 1.07				Hayami (2005)

Table 3.4. Summary of the ambient concentrations of cations. (Continued)

Location	**Period**	**NH_4^+**	**Ca^{2+}**	**Na^+**	**K^+**	**Mg^{2+}**	**Reference**
Tsuen Wan (China)	Nov 00 – Oct 01	--		--	--		Louie et al. (2005)
		2.91 ± 2.15		0.40 ± 0.29	0.49 ± 0.48		
Tirupati (South India)	Apr 01 – Sept 01	0.410 – 1.195	0.230 – 0.572	0.401 – 1.147	0.125 – 0.323	0.011 – 0.072	Mouli et al. (2003)
		0.770 ± 0.240	0.382 ± 0.099	0.751 ± 0.239	0.215 ± 0.061	0.045 ± 0.020	
Beijing (China)	01 – 03	--	--	--	--	--	Wang et al. (2005)
		8.72 ± 7.66	1.63 ± 1.90	0.55 ± 0.54	1.55 ± 1.63	0.17 ± 0.16	
Note:	The first row represents the concentration range of respective ion. The second row represents the mean and the standard derivation of respective ion. Unit: µg/m^3 Li^+ is omitted in the table due to the absent in the ambient samples.						

Table 3.5. Summary of the ambient concentrations of anions.

Location	**Period**	**NO_3^-**	**SO_4^{2-}**	**Cl^-**	**F^-**	**NO_2^-**	**PO_4^{3-}**	**Reference**
Leipzig (Germany)	Jan 93 – Dec 95	-- 2.9 ± 2.9	-- 9.1 ± 7.4					Müller (1999)
Melpitz (Germany)	Jan 93 – Dec 95	-- 2.3 ± 2.6	-- 7.7 ± 5.9					Müller (1999)
Cape D'Aguilar (China)	Apr 95 – Apr 96	0.20 – 15.70 4.21 ± 3.22	1.40 – 34.67 10.77 ± 6.94	0.19 – 52.39 16.80 ± 13.19				Cheng et al. (2000)
Küçük Çalticak (Turkey)	Aug 95 – Apr 96	0.09 – 8.94 2.28 ± 1.77	0.25 – 12.5 2.35 ± 2.01	0.09 – 58.3 4.30 ± 6.94				Erduran and Tuncel (2001)
Veszprém (Hungary)	Sept 95 – Aug 96	-- 4.365	-- 7.267	-- 1.577				Krivácsy and Molnár (1998)
The Hong Kong University of Science and Technology (China)	Jul 97 – Dec 97	0.659 – 3.263 --	0.248 – 2.973 --	0.132 – 2.225 --				Zhuang et al. (1999)
Thessaloniki (Greece)	Jul 97 – Jul 98	0.87 – 6.66 2.81 ± 1.38	1.10 – 10.76 4.80 ± 2.06	0.20 – 2.45 0.87 ± 0.53				Tsitouridou et al. (2003)
Bronx, New York (US)	Jan 99 – Nov 00		0.04 – 4.96 0.9 ± 4.96					Bari et al. (2003)
Manhattan, New York (US)	Jan 99 – Nov 00		0.07 – 6.08 1.08 ± 0.96					Bari et al. (2003)
Shanghai (China)	Mar 99 – Mar 00	0.40 – 18.20 5.77	5.68 – 28.74 13.48	0.01 – 5.99 1.45				Ye et al. (2003)
Shanghai (China)	May 99 – Mar 00	0.50 – 16.6 6.30	3.30 – 29.95 14.56	0.00 – 6.90 1.81				Ye et al. (2003)

Table 3.5. Summary of the ambient concentrations of anions. (Continued)

Location	**Period**	**NO_3^-**	**SO_4^{2-}**	**Cl^-**	**F^-**	**NO_2^-**	**PO_4^{3-}**	**Reference**
Beijing (China)	Jul 99 – Sept 00	1.6 – 54.0 10.3	3.9 – 62.4 18.4	0.1 – 9.3 1.6				Yao et al. (2002)
Beijing (China)	Jul 99 – Sept 00	2.2 – 49.6 9.9	4.0 – 55.7 16.9	0.1 – 9.2 1.8				Yao et al. (2002)
Fukue Island (Japan)	Mar 00 – Apr 02	-- 4.16	-- 6.93					Hayami (2005)
Tsuen Wan (China)	Nov 00 – Oct 01	-- 1.29 ± 1.61	-- 9.09 ± 5.13	-- 0.14 ± 0.36				Louie et al. (2005)
Tirupati (South India)	Apr 01 – Sept 01	0.197 – 1.512 0.843 ± 0.432	1.322 – 3.571 2.485 ± 0.761	0.145 – 0.333 0.232 ± 0.053	0.013 – 0.030 0.020 ± 0.005			Mouli et al. (2003)
Beijing (China)	01 – 03	-- 11.52 ± 11.37	-- 17.07 ± 16.52	-- 3.07 ± 3.13	-- 0.29 ± 0.31	-- 0.41 ± 0.51	-- 0.26 ± 0.29	Wang et al. (2005)
Baltimore (US)	Feb 02 – Nov 02	0.10 – 13.9 1.7 ± 1.6						Park et al. (2005)
Rochester, New York (US)	Jun 02		-- 3.4 ± 3.2					Jeong et al. (2004)
Philadelphia, Pennsylvania (US)	Jul 02 – Aug 02		-- 8.5 ± 8.9					Jeong et al. (2004)
Note:	The first row represents the concentration range of respective ion. The second row represents the mean and the standard derivation of respective ion. Unit: µg/m^3 Br^- is omitted in the table due to the absent in the ambient samples.							

Generally speaking, sulfate, nitrate and ammonium are the major components of water soluble ion species according to Tables 3.4 and 3.5. Ions such as potassium, calcium, chloride contain only trace amounts (about several $\mu g/m^3$), however, ions such as lithium, bromide usually do not exist or exist in very tiny amount in the atmosphere.

In addition, the concentrations of water soluble ion species in China are much higher than in other countries such as US, Japan. China usually has several folds of ion concentrations in comparison with other clean countries (e.g. US). The previous studies indicated the seriousness of the air pollution problems and the urgency for improving the air quality in China.

3.3 Diurnal profiles of sulfate and nitrate

The determination of the diurnal profiles of water soluble ion species is impossible in the past because of the much longer sampling time of filters. With the development of semi-continuous ion instruments in the recent year, the diurnal profiles of water soluble ions have been reported. In this section, I will review the diurnal profiles of sulfate and nitrate that have done previously.

3.3.1 Diurnal profile of sulfate

Wittig et al. (2004) conducted the measurement of the diurnal profiles of sulfate in Pittsburgh, US for July, October 2001 and January, March 2002. The result is shown in Figure 3.1. During the summer months, the profiles exhibited a characteristics diurnal pattern, with maximum sulfate observed a couple hours before sunset. In fall, winter, and spring, the profiles on average did not exhibit a diurnal pattern. This is because sulfate is formed via gas phase OH radical oxidation of SO_2 and OH radical is principally formed during daytime, tracking the changes in solar actinic flux. Thus, a diurnal pattern was more likely to be observed during summer months due to the increased in photochemical activity [Rattigan et al., 2006].

Figure 3.1. Average diurnal $PM_{2.5}$ sulfate profiles for July 2001, October 2001, January 2002, and March 2002.

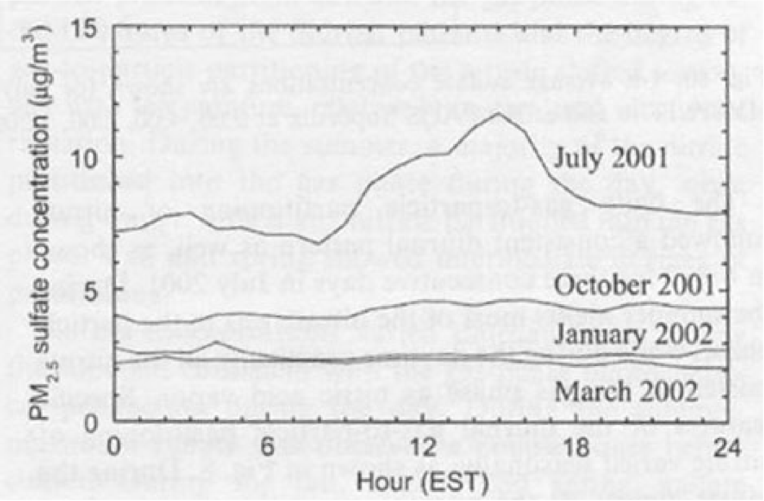

Rattigan et al. (2006) also reported the diurnal profile of sulfate at South Bronx in US. The result for the South Bronx is shown in Figure 3.2. As shown in the figure, the median sulfate concentration did not show a pronounced diurnal pattern, whereas the mean, 25th and 75th percentiles exhibited a rise in concentrations centering around 12 – 2pm. Rattigan et al. (2006) explained that there was a large and variable background regional sulfate signal in the northeastern US. This together with the changing meteorology made it difficult to observe a strong sulfate diurnal within the overall pattern.

Figure 3.2. Average diurnal sulfate for August 2004, at the South Bronx site (box) along with the median (horizontal bar), and 25th and 75th percentiles (whiskers). The right axis indicates the mean SO_2 concentration (circle) and temperature (cross).

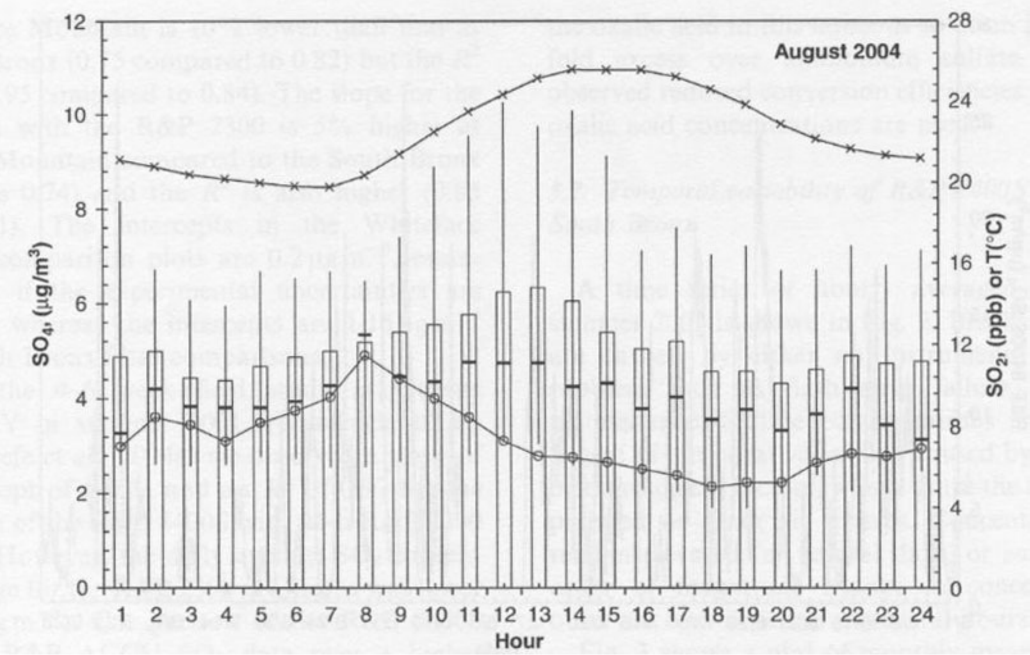

3.3.2 Diurnal profile of nitrate

The diurnal profiles of nitrate for July, October 2001 and January, March 2002 reported by Wittig et al. (2004) in Pittsburgh, US is shown in Figure 3.3. The profiles exhibited a strong diurnal pattern, with the maximum nitrate observed in the early morning a little before sunrise and minimum nitrate observed a couple hours before sunset. The time of the maximum and minimum nitrate shifted on a seasonal basis, consistent with the changes in the ultraviolet radiation and temperature. The magnitudes of the maximum and minimum nitrate also changed on a seasonal basis and were greatest during the winter months. The minimum $PM_{2.5}$ nitrate concentration during the winter months was non-zero and correlated with low ambient temperature measured at Pittsburgh Air Quality Study.

Figure 3.3. Average diurnal $PM_{2.5}$ nitrate monthly profiles for July 2001, October 2001, January 2002, and March 2002.

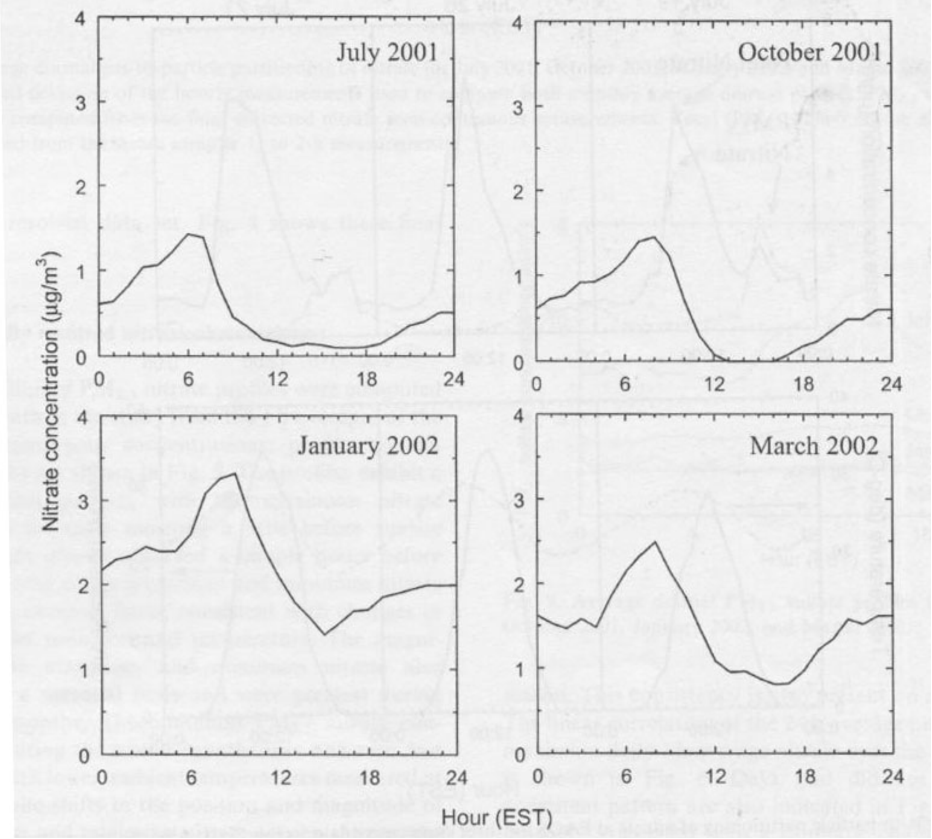

Figure 3.4 showed the average diurnal nitrate concentrations along with the median, 25th and 75th percentiles at the South Bronx in August 2003. Peak nitrate concentrations were observed in the morning hours, 7 – 10am, followed by a decline in the afternoon, and a subsequent rise later in the day. Rattigan et al. (2006) suggested that the morning NO_x pulse contributed to the nitrate peak. During elevated temperatures NH_4NO_3, however, undergone thermal decomposition, shifting nitrate into nitric acid. Variations in the boundary layer height in response to temperature changes, also likely contributed to some of the observed concentration variations. Therefore, nitrate concentrations declined in the late morning and remained low until after 6pm reaching a plateau around 11pm.

Figure 3.4. Average diurnal nitrate at the South Bronx for August 2003 (box) along with the median (horizontal bar), 25th and 75th percentiles (whiskers). The right axis indicates the mean NO_x concentration (circle) and temperature (cross).

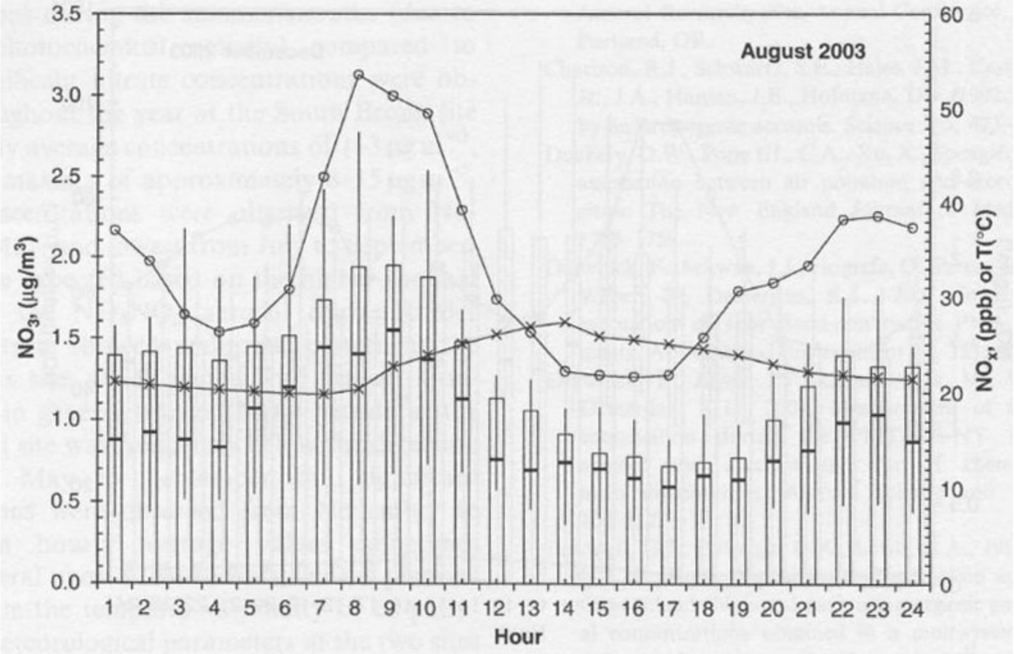

3.4 Fundamental mechanism of gas to particle conversion and its importance

Some water soluble ion species such as sulfate, nitrate are mainly secondary in origin, only trace amount of them are emitted directly from sources. In fact, most of these species are formed by the gas to particle conversion. Thus, knowing gas to particle conversion is important for studying water soluble ion species, especially for sulfate and nitrate. In this section, I will briefly introduce the fundamental mechanism of the gas to particle conversion as well as its importance in the atmosphere.

Trace gases such as SO_2 and NO_x are continuously injected into the atmosphere. Part of these gases are removed by dry deposition, however, some of them will change from the gas phase into the particulate phase. Gases that are condensable and supersaturated can change via chemical reactions in air to form products of low vapor pressure. A mass transfer is then taking place from the gas phase into the particulate phase. We often refer this process as gas to particle conversion [Foltescu et al., 1996; Juozaitis et al., 1996].

Gas to particle conversion can be linked to photochemical processes because large fraction of the suspended materials in secondary aerosols are derived from atmospheric photochemical reactions of reactive gases, including SO_2, NO_x, and organic vapors [Foltescu et al., 1996]. Moreover, the formation of aerosols is affected by the presence of condensable vapors as well as the characteristics of the pre-existing particles. The formation of aerosol particles by gas to particle conversion can take place through several different mechanisms, including (1) Reaction of gases to form low vapor pressure products, (2) One- or multi-component (in the atmosphere generally with water vapor) nucleation of those low pressure vapors, (3) Vapor condensation onto surfaces of preexisting particles, (4) Reaction of gases at the surfaces of existing particles, and (5) Chemical reactions within the particles. Step 1, 4 and 5 affect the compositions of both vapor and liquid phases. Step 2 initiates the actual phase transition and increases aerosol particle number concentration, while step 3 increases aerosol mass [Hämeri et. al, 1996; Spurny, 2000].

Broadly speaking, gas to particle conversion may result from homogeneous gas-phase processes or it may be controlled by processes in the particulate phase. Gas-phase processes, either physical or chemical, can produce a supersaturated state which then collapses by aerosol formation. Physical processes producing supersaturation include adiabatic expansion or conductive cooling. Gas-phase chemical reactions such as the oxidation of SO_2 to sulfuric acid in the atmosphere also generate condensable products.

Once a condensable species has been formed in the gas phase, the system is in a non-equilibrium state. It may pass towards equilibrium by the generation of new particles (homogeneous nucleation) or by condensation on existing particles (heterogeneous nucleation). If all collisions among condensable molecules are effective, the process resembles aerosol coagulation. However, in certain important cases, small molecular clusters are unstable, an energy barrier must be surmounted before stable nuclei can form. Heterogeneous condensation may be limited by gas-phase transport processes or by chemical reactions in the aerosol particles. Measurements of the change in the size distribution function with time can be used to determine the form of particle growth laws. Inferences can then be drawn concerning the mechanism of growth. Homogeneous and heterogeneous condensation can occur in the same parcel of gas either sequentially or simultaneously. In the flow systems, this can lead to sustained oscillations in particle number density.

Homogeneous nucleation

The below experiments carried out by Wilson at the end of the nineteenth century has illustrated the homogeneous nucleation. He conducted the cloud chamber experiments to demonstrate the nature of the condensation process at various saturation ratios with and without foreign particles. The air in a chamber is first saturated with water vapor. By rapid expansion of the chamber contents, both pressure and temperature fell, carrying the system into a supersaturated state. At first, condensation took place on small particles initially present in the air. By repeatedly expanding the chamber contents and allowing the drops to settle, the vapor-air mixture could be cleared of these particles.

With the clean system, no aerosol formed unless the expansion exceeded a limit corresponding to a saturation ratio of about four. At this critical value, a shower of drops formed and fell. The number of drops in the shower remained about the same no matter how often the expansion process is repeated, indicating that these condensation nuclei are regenerated.

Further experiments showed a second critical expansion ratio corresponding to a saturation ratio of about eight. At higher saturation ratios, dense clouds of fine drops formed, the number increasing with the supersaturation. The number of drops produced between the two critical values of the saturation ratio was small in comparison with the number above the second limit.

Wilson suggested that the nuclei that act between the critical saturation limits were air ions normally present in a concentration of about 1000/cm^3. We know now that this result largely from cosmic rays and the decay of radioactive gases emitted by the soil. Wilson supported this interpretation by inducing condensation at saturation ratios between the saturation limits by exposing the chamber to x rays that produced large numbers of air ions. Wilson proposed that the vapor molecules themselves served as condensation nuclei when the second limit is exceeded, leading to the formation of very high concentrations of very small particles. The original experiments were carried out with water vapor. Similar results were found with other condensable vapors, but the value of the critical saturation ratio changed with the nature of the vapor.

Heterogeneous condensation

When high concentrations of particles are present and the supersaturation is low, condensation takes place on the existing particles without formation of new nuclei. We call this process heterogeneous condensation. Cloud droplet formation in the atmosphere takes place in this way because supersaturations are usually less than a few percent and the concentrations of the particles are high [Friedlander, 2000].

Importance of gas to particle formation

Gas to particle conversion is a ubiquitous process in the atmosphere. The formation and growth of aerosol particles in the presence of condensable vapors change the dynamics of an aerosol population. This kind of conversion also determines the size and composition of particles from the polluted urban atmosphere to the remote marine boundary layer. Understanding the detailed chemistry and physics of atmospheric gas to particle conversion allows us to predict the effects of primary gaseous and particulate emissions that changes on airborne particulate matter in the urban and regional setting as well as the effects of sulfur and other species on the generation of cloud condensation nuclei in the remote atmosphere. Furthermore, the physical and chemical aspects of aerosol dynamics are very closely coupled. For example, the size distributions of the aerosols are governed partially by particle compositions. In short, chemical reactions determine particle compositions and modify their dynamics significantly, while the number, size and composition of aerosol particles determine conditions for heterogeneous and liquid-phase chemical reactions.

Thus, the study of the gas to particle formation is important [Hämeri et. al, 1996; Spurny, 2000].

3.5 Possible routes for the formation of sulfate and nitrate

To investigate the formation mechanisms of secondary aerosols, we firstly need to know the possible routes for the formation of secondary aerosols. In this section, I will review the formation of secondary pollutants – sulfate and nitrate in the atmosphere.

3.5.1 Formation of sulfate

The formation of sulfate includes gas and aqueous phase reactions as well as heterogeneous reactions occurring on the surface of soot aerosols. Figure 3.5 showed the schematic diagram for the formation of sulfate in the atmosphere.

Figure 3.5. Schematic of the three pathways (Reaction in the gas, cloud and condensed phases) for the formation of sulfate in the atmosphere [McMurry et al., 2004].

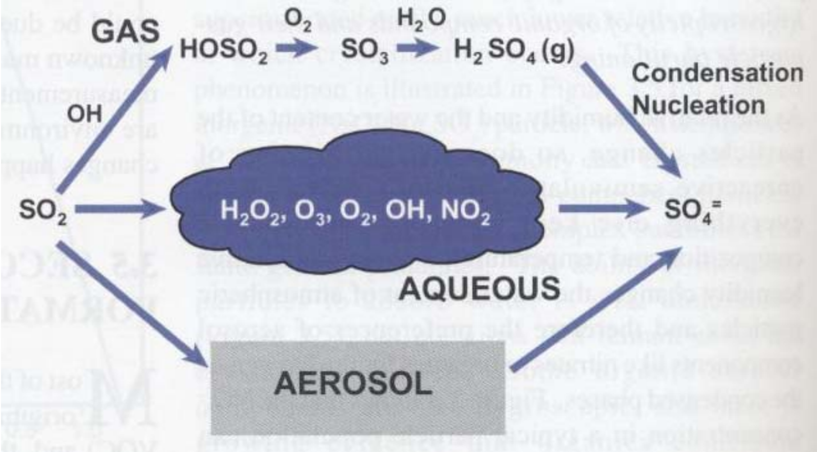

Gas phase reaction

Although there are many possible reactions for the oxidation of ground state SO_2 in the gas phase, the only process which is efficient enough is the reaction of SO_2 with the OH radical [Hämeri et al., 1996]. This gas phase oxidation tends to be slow. In the absence of catalysis or highly reactive species ($OH\cdot$, $HO_2\cdot$, $RO_2\cdot$, O_3), the reaction does not occur at a significant rate. The gas-phase oxidation of SO_2 leads to the formation of sulfuric acid as shown from the following equation which, due to its low vapor pressure, is subsequently transported to the aerosol phase.

$$OH\cdot + SO_2 + (H_2O + O_2) \rightarrow H_2SO_4 + HO_2\cdot$$

Kulmala et al. [1995] stated that the rate determining reaction for the oxidation of ground state SO_2 in the gas phase is the reaction of SO_2 with the OH radical. According to Luria and Sievering [1991], the gas-phase oxidation pathway dominates sulfate formation for summer daytime conditions.

Aqueous phase reaction

A large fraction of SO_2 is converted by aqueous phase reaction as shown below [Khoder, 2002].

$$SO_2 + H_2O \rightarrow H_2SO_3$$

Aqueous reactions leading to the formation of H_2SO_4 can proceed in droplets of clouds, fog and rain as well as in deliquescent aerosol droplets at high relative humidities and in surface films on “wet” aerosol particles [Foltescu et al., 1996]. The reaction within water drops is relatively fast and is catalyzed by the presence of certain trace compounds, provided that the pH is above 5. At higher pH, the oxidation occurs at a significant rate even without the presence of catalysts. Major aqueous sulfate formation mechanisms include the reactions of dissolved SO_2 with H_2O_2, O_3 and O_2 (catalyzed by Mn^{2+} and Fe^{3+}) as shown in the following equations.

$$S\,(IV) + \tfrac{1}{2}\,O_2 + Mn^{2+} \text{ or } Fe^{3+} \rightarrow S\,(VI)$$

$$S(IV) + H_2O_2 \rightarrow S(VI) + H_2O$$

$$S(IV) + O_3 \rightarrow S(VI) + O_2$$

Atmospheric sulfate production is dominated by aqueous-phase pathways at night. Moreover, the contribution of the aqueous-phase reaction of SO_2 with O_2 depends strongly on Fe^{3+} and Mn^{2+} concentrations and on the liquid water content of aerosols which, in turn, is dependent on the relative humidity and the background concentrations of sulfate, nitrate and ammonia. The aqueous reaction of SO_2 with H_2O_2 becomes important only at low temperatures when the solubility of these gases is relatively high. The aqueous-phase oxidation of SO_2 by O_3 and other oxidants such as PAN, HNO_2 are not important for aerosols because atmospheric aerosols are generally too acidic for these reactions which become significant only at relatively high pH. However, Sievering et al. [1994] suggested that O_3-oxidation of SO_2 to SO_4^{2-} in aerosol water is an important contributor to the high sulfate concentrations observed in the coarse mode due to the relatively high concentrations of SO_2 and O_3.

Heterogeneous reaction

Oxidation of SO_2 may occur in a thin film of water on surface of the solids in the air, making both solid surfaces and atmospheric water content important for oxidation. There can also be photochemically induced oxidation processes that may be taking place on surfaces of particulate [Saxena and Seigneur, 1987; Sharma et al., 2003].

Relative importance of different sulfate formation mechanisms

Middleton et al. [1980] theoretically investigated the relative contributions of different pathways to overall sulfate formation. Their calculations showed that under daytime conditions, the gas-phase formation of H_2SO_4 and its subsequent condensation on aerosols and aqueous-phase oxidation of SO_2 by H_2O_2 were the principal mechanisms for the atmospheric sulfate formation. They also found that sulfate formation at night was dominated by aqueous-phase mechanism and was generally lower than the daytime sulfate formation.

3.5.2 Formation of nitrate

Nitrates are formed from the oxidation of NO and NO_2 (NO_x) either during the daytime (reaction with OH radical) or during the night (reactions with ozone and water) [Wayne et al., 1991]. Nitric acid is continuously transferred between the gas and the condensed phases (condensation and evaporation) in the atmosphere. It naturally prefers the gas phase (when left alone), but reactions with gas-phase NH_3, sea salt, and dust result in its transfer to the condensed phase [McMurry et al., 2004; Seinfeld and Pandis, 1998]. Figure 3.6 showed the schematic diagram for the formation of nitrate in the atmosphere.

Figure 3.6. Schematic diagram for the formation of HNO_3 and particulate NO_3^- in the atmosphere [McMurry et al., 2004].

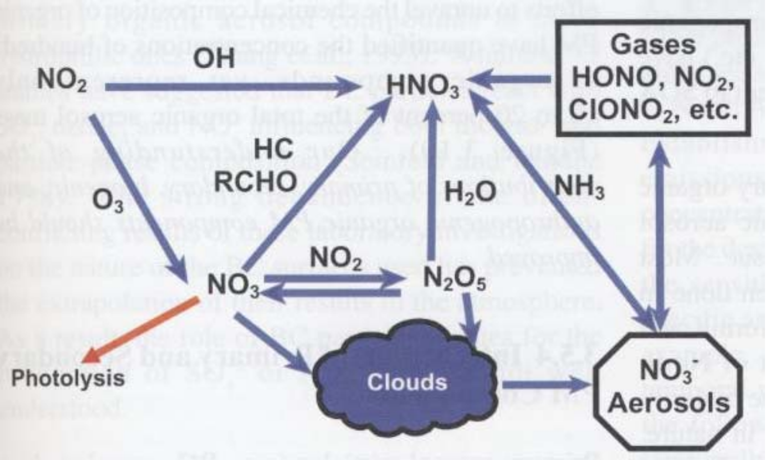

The formation of particulate nitrate may occur through nighttime heterogeneous reactions of gaseous NO_3 and N_2O_5 on the wet surface of sulfate particles. The process that results in the generation of fine nitrate particles is the reaction of gaseous nitric acid with gaseous ammonia. This reaction is important only when NH_4^+ is in excessive in comparison with SO_4^{2-} in the particles.

$$NH_3(g) + HNO_3(g) \rightarrow NH_4NO_3(s)$$

The reactions in which HNO_3 is replaced by water-soluble particulate formate, acetate and oxalate are also important for the formation of fine nitrate particles.

$$(NH_4)_2C_2O_4(s) + 2HNO_3(g) \rightarrow 2NH_4NO_3(s) + C_2H_2O_4(g)$$

The formation of aerosol NH_4NO_3 is favored by the availability of NH_3, low temperature, and high relative humidity. The resulting NH_4NO_3 is usually in the sub-micrometer particle range [McMurry et al., 2004].

Coarse nitrate particles can be produced by the reactions of gaseous nitric acid with mineral aerosols and/or with sea (or lake) salt aerosols [Ma et al., 2003].

$$CaCO_3(s) + 2HNO_3(g) \rightarrow Ca(NO_3)_2(s) + H_2O + CO_2(g)$$

$$NaCl(s) + HNO_3(g) \rightarrow NaNO_3(s) + HCl(g)$$

The availability of significant HNO_3 vapor in an area (even if the particulate NO_3^- concentrations are low or zero) is an indication of the potential for the future formation of NO_3^--containing particles. Heterogeneous reactions and perhaps photolysis lead to the reduction of particulate NO_3^- and return nitrogen oxides to the gas phase. However, these reactions are still poorly understood at this moment [Honrath et al., 2000; McMurry et al., 2004].

3.6 Conversion ratios of sulfur (F_s) and nitrogen (F_n)

Conversion ratios of sulfur and nitrogen could offer us the first in-sight on the degree of oxidation of gas species to particle species. Lin [2002] stated that it could be utilized as an index of occurrence as well as the level of the secondary aerosol formation. The two equations below are the most commonly used equations for calculating the conversion ratios of sulfur and nitrogen [Kadowaki, 1986].

$$F_s = [\text{f } SO_4^{2-}] / ([SO_2] + [\text{f } SO_4^{2-}])$$

where $[\text{f } SO_4^{2-}]$ = Fine sulfate concentration, $[SO_2]$ = Gas-phase SO_2 concentration

$$F_n = [\text{p } NO_3^-] / ([NO_2] + [\text{p } NO_3^-])$$

where $[\text{p } NO_3^-]$ = Total particulate nitrate concentration, $[NO_2]$ = Gas-phase NO_2 concentration

The above two equations are to clarify the difference between the oxidation process of NO_2 to nitrate and SO_2 to sulfate [Khoder, 2002]. The sulfur conversion ratio expresses the degree of oxidation of sulfur in terms of the ratio of sulfate sulfur to total sulfur (in sulfate plus sulfur dioxide). Similarly, the nitrogen conversion ratio expresses the degree of oxidation of nitrogen in terms of the ratio of nitrate nitrogen to total nitrogen (in nitrate plus nitrogen dioxide). Higher values of F_s and F_n suggested that the photochemical oxidation would have occurred and more secondary aerosols could exist in the atmosphere [Lin, 2002]. Below is the summary of the previous publications that utilize the above equations.

Kadowaki [1986] made the measurements in a mixed residential / light industrial area in Nagoya. He calculated the average F_s and F_n and the results were tabulated in Table 3.6. He found that at a Nagoya urban site, F_s and F_n in summer were about 2 and 4 times higher than those in winter, respectively.

Table 3.6. Comparison of sulfur conversion ratio (F_s) and nitrogen conversion ratio (F_n) at a Nagoya urban site.

Sampling periods	Average F_s (%)			Average F_n (%)		
	Day	Night	Mean	Day	Night	Mean
June	6.7	7.8	7.3	12.1	7.7	9.9
Aug	10.4	9.1	9.8	12.0	8.2	10.1
Dec and Jan	4.0	3.9	4.0	2.9	1.9	2.4

Moreover, F_n was always higher in the daytime than in the nighttime and did not change under the two different summertime conditions. On the other hand, there was hardly any difference in F_s for daytime and nighttime. Under the two different summertime conditions, F_s was higher in August than in June. The results of F_s and F_n implied that photochemical oxidation played an important role in the oxidation of SO_2 and NO_2. Furthermore, the SO_2 oxidation might be enhanced at high relative humidities.

Khoder [2002] conducted the measurements in an urban area in Dokki, Giza, Egypt. He also used the above equations to calculate the sulfur and nitrogen conversion ratios. The results were shown in Table 3.7. The daily nitrogen conversion ratio ranged from 1.08% – 5.30% (with a mean value of 2.86%) in winter and from 4.62% – 16.10% (with a mean value of 8.48%) in summer. Nitrogen conversion ratio in summer was about 2.97 times higher than that in winter. However, the daily sulfur conversion ratios covered the range from 3.22 – 14.88% (with a mean value of 7.55%) during the winter and 8.77 – 27.99% (with a mean value of 16.77%) in the summer season. Sulfur conversion ratio in summer was about 2.22 times higher than that in winter. The daytime and nighttime nitrogen and sulfur conversion ratios were also calculated and presented graphically in Figure 3.7. The highest values of F_s and F_n were found in the daytime during the winter and summer seasons.

Table 3.7. Sulfur conversion ratio (F_s) and nitrogen conversion ratio (F_n) during the summer and winter seasons.

Sampling periods	F_s (%)		F_n (%)	
	Mean	S.D.	Mean	S.D.
Summer	16.77	5.32	8.48	2.96
Winter	7.55	3.34	2.86	1.12

Figure 3.7. Daytime and nighttime nitrogen conversion ratio (F_n) and sulfur conversion ratio (F_s) on some days during the winter and summer seasons.

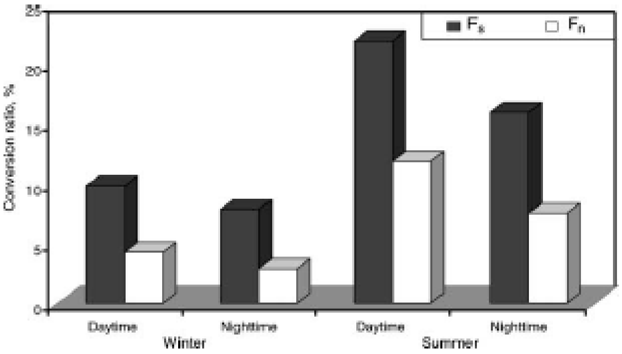

The highest nitrogen and sulfur conversion ratios were found in daytime during both seasons. Moreover, the sulfur conversion ratio and nitrogen conversion ratio in summer were about 2.22 and 2.97 times higher than those in winter, respectively. These results indicated that the oxidation of SO_2 to sulfate and NO_2 to nitrate as well as their conversions depended on the photochemical oxidation.

Higher S-ratios and lower N-ratios were typical for conditions of high relative humidity. It was conceivable that condensed phase chemistry was of major importance in the SO_2 oxidation and that HNO_3 was absorbed onto the wet aerosol particles. More generally, a low N-ratio indicated efficient depletion of gaseous HNO_3 which could deposit either on suspended atmospheric particles or on the ground surface.

More N in the particulate form (as NO_3^-) than gaseous (as HNO_3) yielded a subunity N-ratio ranging from 0.24 to 0.93 at Lista. At South Uist, there were two occasions with a factor of 2 – 3 higher in the gas phase. These two cases corresponded to episodes of pollution accumulation over Germany, Netherlands, and southern North Sea.

Stagnation of air masses over source regions of high emission densities and rates resulted in accumulation of pollution. The S-ratios in such conditions were high due to the longer time of transport [Foltescu et al., 1996].

Furthermore, Lin [2002] made the measurements in Taiwan and the average values of F_s and F_n were shown in Figure 3.8. He found that F_s was higher in the northern part of the urban area than those in the southern area. Since the major emissions of SO_2 were mostly distributed in the southern part of the city, areas with high emissions of SO_2 should have lower values of F_s. The average F_s at Kaohsiung City were 0.25 ± 0.12 and 0.29 ± 0.13 for $PM_{2.5}$ and PM_{10}, respectively. The high F_s values suggested that secondary formation of SO_4^{2-} from SO_2 occurred in the atmosphere during the sampling periods in Kaohsiung City.

Figure 3.8. Calculated F_s and F_n at the six sampling sites in Kaohsiung City.

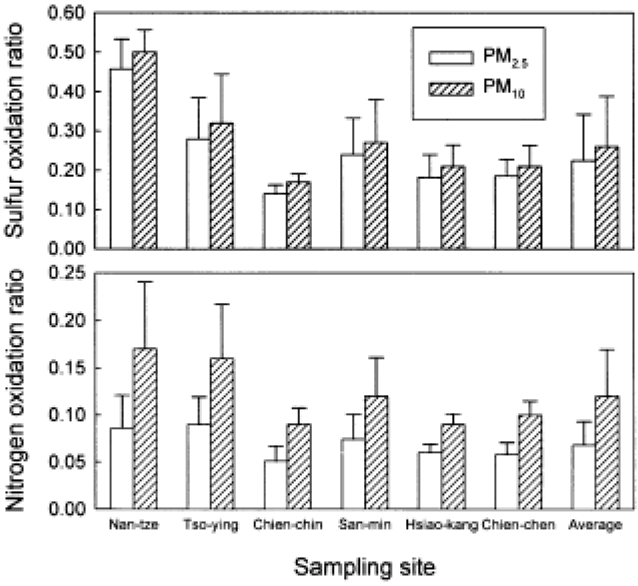

The average F_n values in Kaohsiung City were 0.07 ± 0.03 and 0.12 ± 0.05 for $PM_{2.5}$ and PM_{10}, respectively. The high F_n values suggested that secondary formation of NO_3^- from NO_x occurred in the atmosphere during the sampling periods in Kaohsiung City [Lin, 2002].

3.7 Factors affecting gas to particle conversion

In addition to the formation routes, we also need to know the controlling factors that affect the formation of sulfate and nitrate in order to determine the formation pathways of them. For example, environmental parameters (both physical and chemical) that affect the SO_4^{2-} formation include the concentrations of SO_2, PM_{10}, NH_3, $OH\cdot$, pH, atmospheric water content and other metal catalysts [Sharma et al., 2003].

According to Sharma et al. [2003], conversion of SO_2 to SO_4^{2-} was significant in cities in India. They calculated the SO_4^{2-} to SO_2 ratio and compared with the studies from others as shown in Figure 3.9. The ratio of SO_4^{2-}/SO_2 varied between 0.94 and 1.35 with a mean value of 1.11. However, the ratio was

0.63 at IIT Kanpur. The possible reasons for the lower ratio at that site included lower levels of PM_{10} and SO_2, which possibly represented equilibrium background concentration at which further conversion of SO_2 did not take place. They showed that SO_4^{2-} levels were positively correlated with SO_2, PM_{10} and Ca. They suggested that the absorption of SO_2 on the surfaces of atmospheric particulate matter, followed by its oxidation and formation of sulfuric acid and eventually neutralized by these particulate matters (alkaline nature) appeared to be occurring in the study area.

Figure 3.9. SO_4^{2-} to SO_2 ratio at various locations (IIT – IIT Kanpur, GT – GT Road, AU – Agriculural University, Nave – Naveen Market, and Laj – Lajpat Nagar), Altshuller (1976) (EC – East Coast and IP – Indianapolis), and Sandberg et al. (1976) (St. Louis).

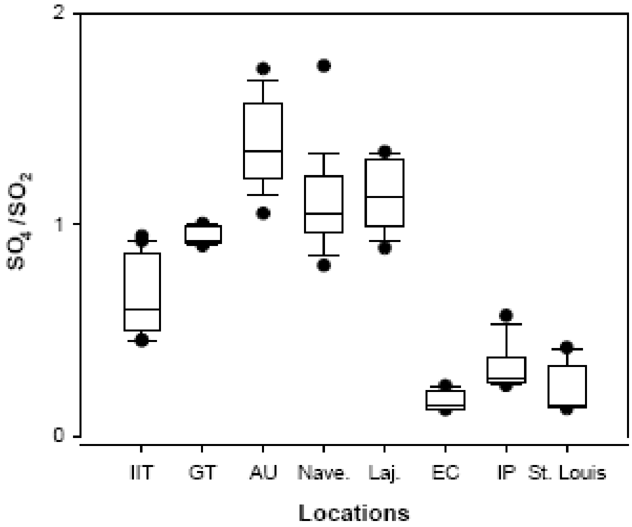

Furthermore, the reason for the positive correlation between SO_4^{2-} and Ca is that Ca raises the pH and advances the oxidation of SO_2 to SO_3.

Catalysts can also enhance the oxidation of SO_2. Moreover, the oxidation of SO_2 to SO_3 can also increase with the increase in pH [Beilke et al., 1975]. Carbon surfaces and other types of surfaces, including alumina, fly ash, soil, MgO, V_2O_5, Fe_2O_3, and MnO_2, have been shown to oxidize SO_2 and/or remove it from the gas phase. The rate of removal depends on the nature of the particulate surface, the increase rate of removal with increasing water vapor suggested that oxidation of SO_2 may occur in a thin film of water on surface of the solid.

Figures 3.10 and 3.11 showed the relationships between sulfur oxidation ratio (F_s), nitrogen oxidation ratio (F_n), and oxidant concentrations, respectively. In these figures, data sets observed at relative humidity above 75% were distinguished from the others as a black circle, because liquid-phase reactions might be predominant at high relative humidities. However, F_s had an indistinct correlation to oxidant concentration at relative humidity less than 75%.

Figure 3.10. Scatter diagram of oxidant concentration and sulfur conversion ratio (F_s) observed at a Nagoya urban site.

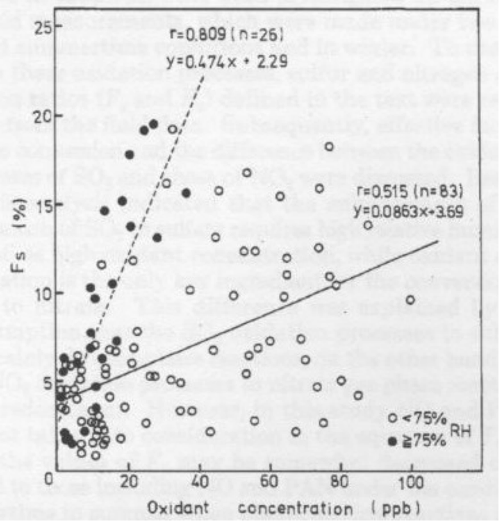

Figure 3.11. Scatter diagram of oxidant concentration and nitrogen conversion ratio (F_n) observed at a Nagoya urban site.

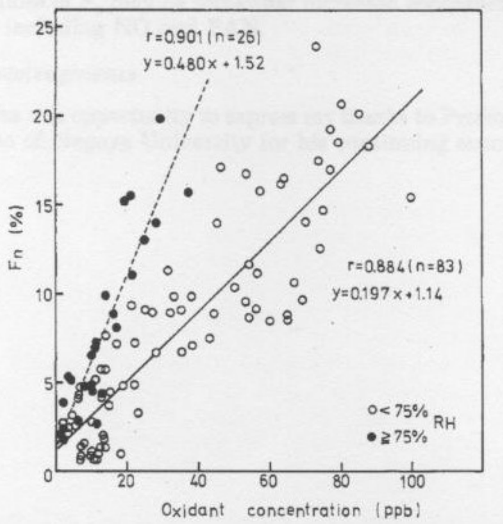

Figures 3.12 and 3.13 showed the relationship between F_s, F_n and relative humidity, respectively, when oxidant concentration exceeded 20ppb and photochemical oxidation took place in some degree. Good correlation was obtained between F_s and relative humidity, but no correlation could be found between F_n and relative humidity.

Figure 3.12. Scatter diagram of relative humidity and sulfur conversion ratio (F_s) observed at a Nagoya urban site.

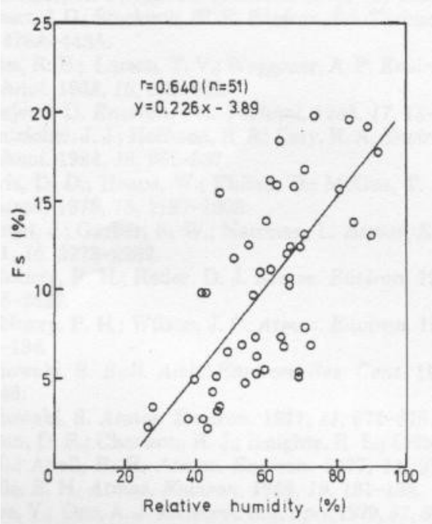

Figure 3.13. Scatter diagram of relative humidity and nitrogen conversion ratio (F_n) observed at a Nagoya urban site.

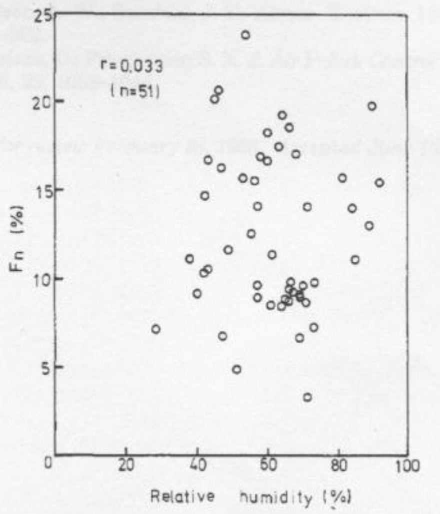

The results observed in Figures 3.10 – 3.13 suggested that for the conversion of SO_2 to sulfate, relative humidity as well as oxidant concentration (e.g. sunlight) were important factors, while oxidant concentration was the only key ingredient for the conversion of NO_2 to nitrate. Hence, SO_2 oxidation processes were mainly droplet-phase reactions, while gas-phase reactions were predominant for NO_2 oxidation processes [Kadowaki, 1986].

Khoder [2002] suggested that atmospheric oxidation of SO_2 occurred by both heterogeneous and homogeneous pathways and the oxidation rate was increased with increasing relative humidity through both pathways involving OH radical production. He also showed that significant positive correlation coefficients were found between the sulfur conversion ratio (F_s) and the relative humidity as well as ozone concentration. Significant positive correlation coefficients were found between the nitrogen conversion ratio (F_n) and ozone concentration during summer and winter. On the other hand, insignificant positive correlation coefficients were found between F_n and relative humidity during both seasons. The results were summarized in Table 3.6. They concluded that ozone and relative humidity were important factors for the conversion of SO_2 to sulfate. The enhancement of the conversion required high relative humidity and ozone concentration.

Table 3.8. Correlation coefficients between ozone concentration, relative humidity, and sulfur conversion ratio (F_s), nitrogen conversion ratio (F_n) during the winter and summer seasons (1999 – 2000).

Conversion ratio (%)	Winter		Summer	
	Ozone	Relative humidity	Ozone	Relative humidity
Nitrogen conversion ratio	0.77	0.20	0.91	0.15
Sulfur conversion ratio	0.55	0.81	0.89	0.78

Furthermore, Baldwin [1982] suggested that NO_2 and SO_2 were essentially adsorbed independently on different sites on the surface of the carbon. Thus, there was no effect of the NO_2 on SO_2 adsorption.

After the comprehensive review on the water soluble ion species, it seemed that there were quite a lot of researches on the water soluble ions in the past. However, most of the studies mentioned before were based on the traditional filter analysis method. This method is more labor demanding, suffers from known sampling artifact such as evaporation of volatile nitrate during sampling, and more importantly, requires longer sampling time (usually 12 to 24 hours) to get enough samples for analysis. In the past few years, higher resolution (1 hour) of the water soluble ion data can be obtained by using the recently developed semi-continuous instrument for measuring ion species. This is very important for interpreting the behaviors of ion species in the atmosphere, especially for the short term variability as the meteorological parameters, emission sources, etc. change rapidly within a day.

In addition, hourly data is also more useful in investigating the formation of ions. As discussed previously, there are different pathways for the conversion of secondary pollutants. We still don't clearly understand what the conversion pathway is. Is the conversion process different at different locations? At this moment, there is very limited research concerning the formation of ion species. By using higher resolution data, more accurate interpretation of the formation of ions can be obtained. This is an important issue because knowing the formation of ions may lead us to have more ideas on solving the pollution problems.

Finally, this study is conducted in the megacities of China (e.g. Hong Kong, Guangzhou, Shanghai, Beijing, and Lanzhou) which has long been known for its severe air pollution caused by extremely high concentrations of airborne particulate matters (e.g. Duan et al., 2006; He et al., 2001; Molina and Molina, 2004; Streets et al., 2007; Wang et al., 2006; Wei et al., 1999; Winchester and Bi, 1984; Zheng et al., 2005). Moreover, most of the previous studies of particulates in China were conducted in the urban area; there is limited knowledge on the distribution of aerosols in rural areas and on the formation of secondary aerosols. Such knowledge is essential for evaluating the impact of a megacity's emission on regional air quality and climate. In view of the above, this study is valuable and important. It can provide us more in-depth knowledge of the water soluble ion species in the atmosphere and know clearly the regional air quality in China.

In view of the above, I have the following objectives to achieve in this study.

1. Data accuracy and quality

Part of my research focuses on the data accuracy and quality for the field measurements of water soluble ion species because the semi-continuous instrument (Model: URG9000B) used in this study for measuring ions is developed recently. To my knowledge, there is still no publication thus far using the same model of instrument for conducting the ion measurements. Therefore, data accuracy and quality is one of the most important issues in this study.

2. A more in-depth understanding of the behaviors of ion species in the atmosphere such as the concentrations, the diurnal patterns.
3. To have the comparison between different parts of China.
4. To investigate the formation of fine sulfate and nitrate.
5. To investigate the visibility problems in Beijing.

Section II: Experimental section

Chapter 4: Background information of the sampling locations

The field measurements in this study were conducted at five different locations of China. These five monitoring sites were located in Guangzhou, Hong Kong, Shanghai, Beijing, and Lanzhou which represented the southern (Guangzhou and Hong Kong), eastern, northern and interior part of China, respectively. These five sampling sites covered different land use areas – urban, sub-urban as well as rural areas. The sampling locations in this study were shown in Figure 4.1. The detailed description of each sampling site was described in the following section.

Figure 4.1. The map showing the sampling locations in this study.

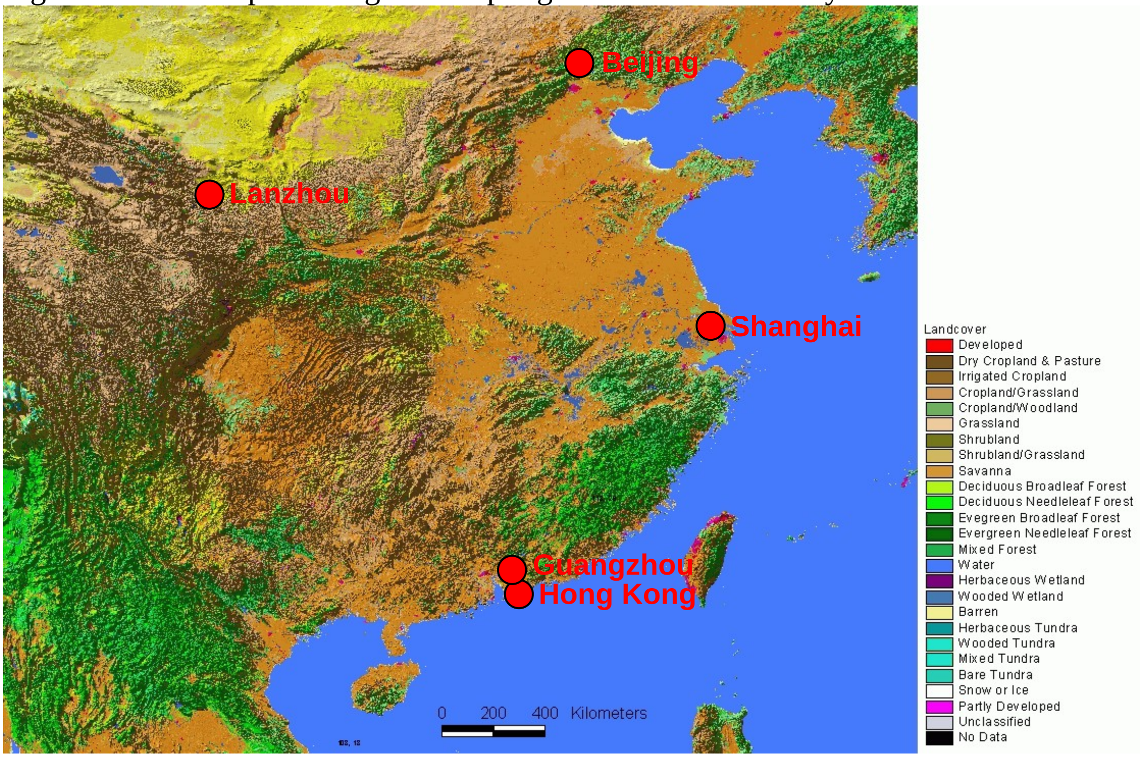

General description of each sampling site

4.1 Guangzhou – Wan Qing Sha

The first field measurement was conducted at Wan Qing Sha, Guangzhou. Guangzhou is located in the middle south of Guangdong Province, north of the Pearl River Delta. It lies close to the South China Sea, Hong Kong, and Macau. Covering an area of 7434.4 square kilometers, Guangzhou is home to more than 11 million people, including a 3.7 million transitory population. The climate of Guangzhou is sub-tropical. The average year-round temperature is 22°C. August is the hottest month with an average temperature of 28°C. January is the coldest month with an average of 13°C. The rainy season falls between April and August with an average annual rainfall of 1720mm. The major emission sources in Guangzhou include vehicles, industries, and construction sites.

Wan Qing Sha is located at the southeastern part of Guangzhou. The map showing the location of Wan Qing Sha was shown in Figure 4.2. Wan Qing Sha is a sub-urban, residential area. The population density is not very high. The instrument was set up on the rooftop of a secondary school with about 17m high. Figures 4.3a and b showed the surrounding views of the sampling site. Two weeks of measurements have been done starting from 15 May 2004 until 27 May 2004. During that period of time, the weather was usually cloudy and humid.

Figure 4.2. The map showing the location of Wan Qing Sha.

Figure 4.3. The surrounding views of the sampling site.

(a)

(b)

<u>Selection of Wan Qing Sha sampling site</u>

As we know, Guangzhou is one of the most polluted cities in China due to its fast-paced growth in population and energy use [Hagler et al., 2006; Qian et al., 2001]. This poor air quality has large impact to the environment as well as human beings. Our study site – Wan Qing Sha is a sub-urban area, conducting the field measurement there can let us knowing the regional air pollution problems in the Guangzhou region.

4.2 Hong Kong – Tsuen Wan

The second field measurement was conducted in Tsuen Wan, Hong Kong. Hong Kong is one of the most developed regions in Asia. With more than 6.8 million residents living in an 1100km^2 area, this metropolitan region has one of the highest population densities in the world [Louie et al., 2005]. Its climate is sub-tropical, tending towards temperate for nearly half the year. The major emission sources in Hong Kong include power plants, vehicles, and industries.

Tsuen Wan is located at the centre of Hong Kong. The topography of Hong Kong showing the location of Tsuen Wan was shown in Figure 4.4. Tsuen Wan is an urban, highly populated, residential site with mixed commercial and industrial developments in the New Territories. The instrument was set up on the rooftop of a community centre with 17 meters high. The photo showing the outlook of the monitoring station in Tsuen Wan was shown in Figure 4.5. Figures 4.6a and b showed the surrounding views of the sampling site. The measurement lasted for about six weeks and conducted from 16 January 2005 to 7 March 2005. During that period of time, the weather was usually cloudy and humid.

Figure 4.4. The topography of Hong Kong showing the location of Tsuen Wan.

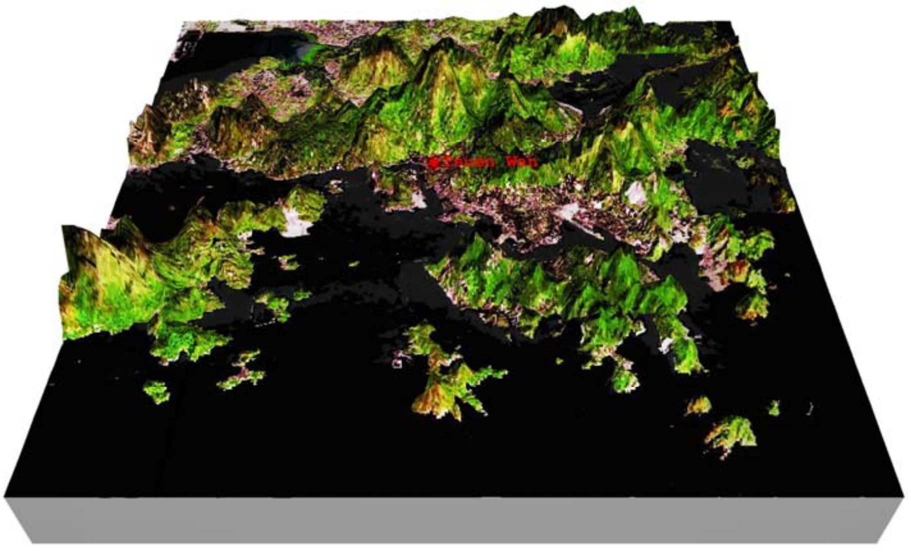

Figure 4.5. Photo showing the outlook of the monitoring station in Tsuen Wan.

Figure 4.6. The surrounding views of the sampling site in Tsuen Wan.

(a)

(b)

Selection of Tsuen Wan sampling site

Due to the large population (6.8 million) and limited area, Hong Kong is one of the most densely populated cities in the world. The limitation of available land and various industrial developments, causing the high levels of air pollutants in Hong Kong which may in turn affect the health of the citizens. Air quality has become an issue of major concern in Hong Kong [Ho et al., 2002]. Tsuen Wan is set from heavily traveled roads in a highly populated residential area with many stores, offices, and light industry as described before. Thus, we can know more clearly the concentrations and the behaviors of water soluble ion species in Hong Kong and then compare with other regions of China.

Secondly, we want to have a comparison between our instrument (URG9000B) and other semi-continuous instruments for measuring ions. Tsuen Wan is a suitable place to achieve this purpose as there is other semi-continuous instruments (R&P 8400N and R&P 8400S) available which are operated by the Hong Kong Environmental Protection Department (HKEPD). Therefore, we have chosen Tsuen Wan site to conduct our second measurement.

4.3 Megacities

Apart from Guangzhou and Hong Kong, two other sampling sites were located in Shanghai and Beijing, China. Shanghai and Beijing are two of the largest cities in China. Both cities have populations of over 10 million. These two urban areas have experienced rapid increase in the use of vehicles, concurrent with large increases in energy consumption [Yao et al., 2002].

4.3.1 Shanghai – Tai Cang

Shanghai is situated at the mouth of the Yangtze river in Jiangsu province with a total area of 6,340 square kilometers and a population of over 15 million. It is the largest city and port in China. Besides, it has a strong commercial and industrial base with China's largest petrochemical complex, its largest steel output, and other major industries [Ye et al., 2003]. With a pleasant northern subtropical maritime monsoon climate, Shanghai has four distinct seasons, generous sunshine and abundant rainfall every year. Its spring and autumn are relatively short comparing with the summer and winter. The average annual temperature is 16 degree Celsius. The city has a frost-free period lasting as long as 230 days a year, and receives an average annual rainfall of 1,200 millimetres. However, nearly 60% of the precipitation comes during May to September flood season. Major emission sources in Shanghai include industries and vehicles.

The sampling site was located at Tai Cang, northwest of Shanghai (Figure 4.7). It is a sub-urban area with several power plants and industries nearby. The instruments were set up on the rooftop of the Tai Cang Meteorological Agency (31º27´N, 121º06´E) with about 15 meters tall. The outlook of the monitoring station was shown in Figure 4.8. Figures 4.9a and b showed the surrounding views of the sampling site. The measurement lasted for six weeks and conducted from 5 May 2005 to 15 June 2005. During the measurement, the weather was usually cloudy with moderate wind.

Figure 4.7. Location of the sampling site – Tai Cang, northwest of Shanghai.

Figure 4.8. Photo showing the outlook of the sampling site in Tai Cang, Shanghai.

Figure 4.9. Photos showing the surrounding views of the sampling site in Tai Cang, Shanghai.

(a)

(b)

4.3.2 Beijing – Hei Shan Zhai

Beijing is the capital of China with around 14.6 million inhabitants distributed over 16,800km^2. It lies in the continental monsoon region in the warm temperature zone and its climate represents as hot and rainy in summer and cold and dry in winter. The four seasons in Beijing are distinct. It is dry, windy and sandy in spring while it is hot and rainy in summer. The air is crisp, mild and humid in autumn. However, winter is cold and dry with little snow. The average temperature throughout a year is 11.7 degree Celsius.

The measurement was conducted at Hei Shan Zhai, a rural mountainous site ($40^o21'$N, $116^o18'$E, 280m above sea level) approximately 50 km north of the center of Beijing (Tiananmen Square). The map showing the location of the sampling site was shown in Figure 4.10. Another large city, the Tianjin Municipality (population: ~10 million) is 150km southeast. Chang Ping, a satellite town of Beijing with a population of 110,000, is 15km southwest. Within 10km around the site, there are only small villages and agricultural-related activities such as fruit planting, with low population density and thus very sparse anthropogenic emission sources. The study site is a fruit farm growing peaches and apricots, and the surrounding mountainous areas are densely covered by trees and other vegetations in the summer season. The instruments were set up at 5 meters high. The outlook of the sampling site was shown in Figure 4.11. Figures 4.12a and b showed the surrounding views of the monitoring station in Beijing. The measurement was made from 20 June 2005 to 6 August 2005 and was usually cloudy with small wind during the measurement period.

Figure 4.10. Location of the Beijing sampling site.

Figure 4.11. The outlook of the Beijing sampling site.

Figure 4.12. The surrounding views of the Beijing sampling site.

(a)

(b)

Selection of Shanghai and Beijing sampling sites

Shanghai and Beijing are the two largest urban centers in eastern and northern regions of China. These highly populated centers suffered from serious urban air pollution problems due to the increased burning of fossil fuels with the annual coal consumption of 4.7×10^7t [Wang et al., 2005] as a result of rapid industrialization and transportation development.

There are many power plants located around Beijing and the top five coal burning power plants are Jingneng, Datang, Huaneng, Guohua, and Jingfeng. They provided around 48% of the total electricity consumption in Beijing in

2008. The emissions of SO_2, NO_x and PM_{10} in 2008 of these power plants are tabulated below [Hao et al., 2007].

Table 4.1. Emissions of power plants in Beijing in 2008.

Plant	SO_2 emission (t/yr)	NO_x emission (t/yr)	PM_{10} emission (t/yr)
Jingneng	2190	14775	784
Datang	1364	3366	116
Huaneng	1030	5086	225
Guohua	414	11028	153
Jingfeng	825	4018	167

Most of the previous studies in Shanghai and Beijing were mainly concerned with the pollution within the urban centers and the effects on human health. While the importance of urban pollution to the regional environment is widely acknowledged, there have been limited investigations concerning the impact of urban pollution on regional scales. This study can form a more complete picture of the regional impact of urban pollution in different parts of China. Moreover, as water soluble ions such as sulfate and nitrate are secondary pollutants, the two sampling sites that are downwind of the two major urban centres of Beijing and Shanghai (40 – 50km) can help to examine the chemical transformation in urban plumes that have aged for 0.5 to 2 days. Because such a distance should allow us to sample plumes that have undergone chemical processing and mixing of different urban sources during the transport to the sampling site.

4.4 Lanzhou – Renshoushan Park

Lanzhou is the capital city of northwest Gansu Province. It is located in the geometrical center of China with an area of 1631.6 square kilometers. It has a population of 3.14 million with mountains in the south and north of the city and the Yellow River flowing from the east to the west. The Gansu province has an average elevation of 1000 – 3000 meters above sea level. Deserts in the northwestern part cover about 15% of the total area.

Lanzhou is located in an inland area with a typical temperate, semi-arid continental monsoon climate. It is dry with plenty sunshine. Spring is ephemeral with changeable weather. Summer is short, but it is not too hot with an average temperature of 22.4°C. Autumn sees a rapid decrease in temperature while winter is long and chilly with an average temperature of -7.3°C. The annual precipitation is 328mm, which is concentrated during the summer.

The sampling site was located at Renshoushan Park, northwest of the urban centre of Lanzhou (Figure 4.13). It is a sub-urban mountainous area with the industrial region located at the southwestern side. The instruments were set up inside a small house. The outlook of the monitoring station was shown in Figure 4.14. Figures 4.15a and b showed the surrounding views of the sampling site. The measurement lasted for one month and conducted from 18 June 2006 to 17 July 2006. During the measurement, the weather was usually sunny with little wind.

Figure 4.13. The map showing the location of the monitoring site in Lanzhou.

Figure 4.14. The outlook of the monitoring station in Lanzhou.

Figure 4.15. The surrounding views of the monitoring station in Lanzhou.

(a)

(b)

Selection of Lanzhou sampling site

Lanzhou is a major city and industrial center in the northwestern part of China. This highly populated center has suffered from serious urban air pollution largely due to the increased burning of fossil fuels as a result of rapid industrialization and transportation development. The sampling site is situated at suburban area. This could provide us an opportunity to investigate the impacts of urban pollution on the chemistry and the environmental implications on regional scale. In addition, the results from Lanzhou could be compared with other parts of China (Guangzhou, Hong Kong, Shanghai, and Beijing) so that more complete picture about the pollution problems from different regions of China could be obtained.

Chapter 5: Instrument descriptions and Filter analysis

In order to study the water soluble ion species in the atmosphere, we firstly need to collect the field data. In this chapter, the instruments that I have used in this study will be described. Apart from the instrument descriptions, the quality assurance (QA) and quality control (QC) that have been performed for each instrument will also be mentioned.

5.1 Instrument descriptions

5.1.1 Ambient Ion Monitor

Thirteen ions in $PM_{2.5}$ are measured hourly using a commercially available instrument, Ambient Ion Monitor (AIM, URG Corporation, URG9000B). The photo of the AIM instrument is shown in Figure 6.1. It is capable of collecting both cationic species, namely calcium (Ca^{2+}), sodium (Na^{+}), ammonium (NH_4^{+}), potassium (K^{+}), magnesium (Mg^{2+}), and Lithium (Li^{+}) and anionic species, namely sulfate (SO_4^{2-}), nitrate (NO_3^{-}), fluoride (F^{-}), nitrite (NO_2^{-}), chloride (Cl^{-}), bromide (Br^{-}), and phosphate (PO_4^{3-}). The system consists of a particle collection unit and two ion chromatographies (IC) for chemical analyses. The AIM uses a modified version of the steam-jet aerosol collector described by Khlystov et al. (1995).

Figure 5.1. The photo showing the AIM instrument.

The schematic diagram of the Ambient Ion Monitor is shown in Figure 5.2. The air first passes through a 3-m long sample inlet at a flow rate of 3Lpm. The sample inlet is equipped with a $PM_{2.5}$ sharp cut cyclone that separates out the particles with aerodynamic diameters larger than 2.5µm from the air stream. The air then penetrates through a liquid diffusion denuder in which ultra-pure water is running continuously around the denuder in order to remove interfering gases such as SO_2 and HNO_3. The denuder is an annular type which has an outer diameter of 17mm, an inner diameter of 13mm and a length of 300mm. The residence time of air sample in the denuder is 0.23 seconds, and the collection efficiency for SO_2, based on the diffusion theory, should be 99% (Simon and Dasgupta, 1993). After passing through the denuder, the particles enter the aerosol supersaturation chamber (diameter: 15mm, length: 75mm) consisting of a steam generator and a mixing chamber. When the particles enter the chamber, the water vapour generated from the steam generator at a flow rate of 0.2mL/min mixes with the particles. The resulting high supersaturation causes aerosol particles to grow rapidly into droplets. The residence time in this chamber is approximately 0.2 seconds. The enlarged particles pass through an inertial particle separator and are stored in an aerosol sample collector. The collector automatically injects the samples into the two ICs for both cation and anion analysis once an hour. The expected collection efficiency of the AIM is greater than 99%, according to the manufacturer. The detection limit of the AIM is about 0.1μg/m^3 for the various ionic components. All the information, including the flow rate of the AIM and the analysis results, are stored in a computer. Hourly data are obtained for the concentrations of the above ions.

Figure 5.2. Schematic diagram of the AIM.

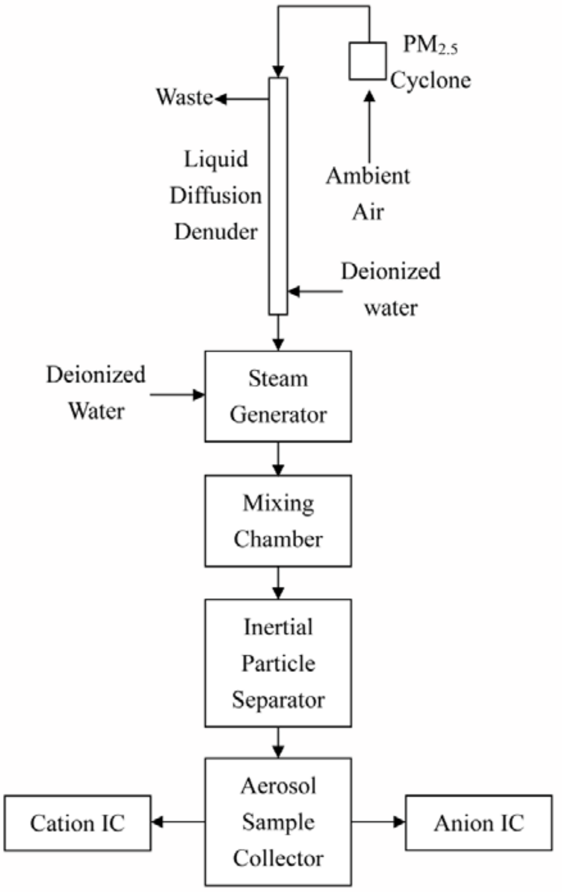

Each IC (Dionex Corporation, ICS-1000) consists of a guard column (CG12A for cation and AG14A for anion) and an analytical column (CS12A for cation and AS14A for anion). An electrolytic suppressor (Cation Atlas electrolytic suppressor for cation and Atlas anion electrolytic suppressor for anion) is used to stabilise the baseline. The analysis is performed by using 20mM methanesulfonic acid for the cation analysis and 0.08mM sodium carbonate / 0.01mM sodium bicarbonate for the anion system. Both ICs are operated in isocratic elution at a flow rate of 0.5mL/min.

Quality control and assurance of the AIM

The flow rate of the AIM was checked weekly at the sample inlet with a certified flow meter (Sensidyne, Gilian Gilibrator 2) after setting up the instrument. By using the equation below, I can determine whether the sampler flow rate is within 5% of the standard device.

(Sampler flow – Standard flow) / Standard flow × 100% = (should be within 5%)

The flow rate of the AIM in these studies was kept at 3L/min. with standard derivation of less than 1%.

Multi-point calibrations were performed after setting up the instrument at each sampling site as well as bi-weekly for both ICs by using calibration standard solutions (Dionex Corporation, Six Cation-II standard for cation and seven anion standard for anion). Calibration curves of each ion were established by using available ion standard. The standard concentrations of individual ionic species ranged from 0.004 to 1µg for fluoride, 0.006 to 1.5µg for chloride, 0.02 to 5µg for nitrite, bromide and nitrate, 0.03 to 7.5µg for phosphate and sulfate, 0.0025 to 0.5µg for lithium, 0.01 to 2µg for sodium, 0.0125 to 2.5µg for ammonium and magnesium, 0.025 to 5µg for potassium and calcium. One of the calibration results in the Beijing study was shown in Table 5.1. Good calibration curves (R^2 >0.99) were obtained except fluoride. The poor linearity of fluoride may possibly due to the poor separation of the fluoride peak with the water peak. However, this does not have great impact to this study as fluoride has negligible amount in the atmosphere.

Table 5.1. Calibration results of the ionic species in Beijing.

Species	Slope	Offset	R^2
Fluoride	2.1726	0.8651	0.622
Chloride	8.8814	0.1439	0.998
Nitrite	7.7296	0.9266	0.999
Bromide	6.3697	-0.3540	0.999
Nitrate	12.2842	-0.9439	0.999
Phosphate	5.1362	-0.7124	0.996
Sulfate	15.6331	-1.7613	0.998
Lithium	65.253	0.1011	1.000
Sodium	21.559	0.6389	1.000
Ammonium	4.6577	1.0195	0.990
Potassium	14.0856	0.0663	1.000
Magnesium	30.8102	1.6967	0.996
Calcium	25.4703	1.2057	0.999

Calculation of the concentrations of ionic species

The concentration of the ionic species is calculated based on the calibration curve. The area of the target species is firstly obtained from the chromatogram and then calculates according to the following equation.

$$\text{Amount } (\mu g) = \{[\text{Area of the target species} - \text{Offset (From calibration curve)}] / \text{Slope (From calibration curve)}\} \times \text{Response factor}$$

$$\text{Concentration } (\mu g/m^3) = \text{Amount } (\mu g) / \text{Volume } (m^3)$$

5.1.2 Thermo Andersen Chemical Speciation Monitor

The twenty-four hour $PM_{2.5}$ samples were collected by using Thermo Andersen Chemical Speciation Monitor (Thermo Electron Corporation, RAAS2.5-400). The photo showing the interior structure of the sampler is shown in Figure 5.3. The sampler is equipped with a cyclone which separates out the particles with aerodynamic diameters larger than 2.5µm when a vacuum pump draws air at a rate of 24L/min. The flow is then divided into two ways by a flow splitter. Each of the two airstreams then enters a manifold which redirects the air into two separate flow paths whose flow rate is individually controlled at 7.3L/min and 16.7L/min by a critical orifice. One of the airstreams is connected to two Teflon filters (Zeflour^{TM}, 2µm pore size and 47mm diameter, Pall Gelman Inc.), and the other is connected to one Teflon filter (flow rate: 7.3L/min) and one quartz filter (Pallflex #2500 QAT-UP, Pall Gelman Inc., flow rate: 16.7L/min) [Cheung et al., 2005].

Figure 5.3. The photo showing the interior structure of the Thermo Andersen Chemical Speciation Monitor.

Quality control and assurance of the Thermo Andersen Chemical Speciation Monitor

Before sampling, the quartz filters were baked at 600ºC for at least 3 hours and then wrapped by the aluminum foils. Moreover, one of the Teflon filters was weighed before and after sampling so as to obtain the mass concentrations of the particulates. Before weighing, the filters were conditioned in the desiccator in which the temperature and relative humidity were kept at 20°C and 40%, respectively for 24 hours. Each filter was weighed for three times in a 6 digit balance in order to get the mean values. The flow rate of the $PM_{2.5}$ sampler was calibrated by a certified dry gas meter before the measurement. Field blanks were collected at the start and the end of the sampling period. The field blank was used to remove the positive artifact caused by gases absorption after sampling. The collected filter samples were stored in a freezer at -4°C to prevent the volatilisation of particles. Sampling duration was approximately 24 hours starting at 09:30 each day. There were altogether 13, 40, 27, and 35 sets of filters collected in Guangzhou, Shanghai, Beijing, and Lanzhou, respectively.

5.1.3 Tapered Element Oscillating Microbalance

Real-time $PM_{2.5}$ mass concentrations were obtained from Tapered Element Oscillating Microbalance (TEOM, Thermo Electron Corporation, TEOM1400a). The photo of TEOM is shown in Figure 5.4. It incorporates an inertial balance that directly measures the mass collected on an exchangeable filter cartridge by monitoring the corresponding frequency changes of a tapered element. As more mass collects on the exchangeable filter, the tube’s natural frequency of oscillation decreases. The sample flow passes through the filter, where particulate matter collects, and then continues through the hollow tapered element on its way to an active volumetric flow control system and vacuum pump. Because of the hygroscopic particles, the mass collected on the filter can be very sensitive to changes in the ambient water vapor concentration. To eliminate the effect of water, associated with hygroscopic salts, the TEOM filter is kept at 50^{o}C (Thermo Electron Corporation, 2005). More detailed of the principle and the operation of TEOM is available elsewhere in Patashnick and Rupprecht, 1991.

Figure 5.4. The photo of Tapered Element Oscillating Microbalance.

Quality control and assurance of Tapered Element Oscillating Microbalance

In this study, the flow rate of TEOM was kept at 3L/min and the calibration was performed with a Gillibrator bubble flow meter. The TEOM mass response was calibrated using a series of filters with measured masses.

5.1.4 Aerosol optical properties measurement

5.1.4.1 Aerosol light scattering coefficient

An integrating nephelometer manufactured by Optec Inc. (model: NGN-2), featured with an open-air design without any heater was used in this study. The measurement principle was based on the scattering of light caused by particle scattering as it passed through a measurement chamber. The instrument was equipped with a light source with Lamertian diffuser to diffuse the light from 5° to 175°. Two photodiode light detectors (D1 and D2) were used to measure the scattering intensity of particles associated with the 550nm wavelength of light.

During the measurement, light beams were emitted from the light source passing through the heat absorbing glass filter. The light was then radiated by the diffuser with angle from 5° to 175° to the normal of diffuser's surface. The initial and scattered light intensities are detected by photodiode detectors D1 and D2. Finally, the NGN-2 electronic output was converted to the light scattering coefficient based on the result of a span and zero calibration.

5.1.4.2 Aerosol light absorption coefficient

Aerosol light absorption coefficient was measured by the PSAP (Particle Soot / Absorption Photometer) based on the integrating plate technique which was manufactured by Radiance Research Company of US.

The air stream was drawn from inlet without particles size-cut device by a vacuum pump, and then passed through the black conductive tubing with ½" OD. After passing through the conductive tubing, the air was drawn into the detection chamber, by a vacuum pump, where photodiode detectors were equipped to measure the light transmittance between signal and reference filters. Inside a chamber, a LED lamp with 565nm wavelength was installed to generate a light source which closed to the most sensitive wavelength (550nm) of the human eyesight. The particle samples were deposited only on the signal filter. The changes of light transmittance in signal filter can be calculated by the difference of light transmittance between the signal filter and reference filter. The air flow and the filter transmittance were recorded which was later used in the calculation of B_{ap}.

5.1.5 Gas analyzers

In addition to the measurement of particulate matters, gaseous measurements were also conducted. Measurement instruments were housed in a laboratory. Ambient air samples were drawn through a PFA Teflon tube. The sample inlet was located at the rooftop (Guangzhou, Shanghai) or nearby (Beijing and Lanzhou) the laboratory. The other end of the sampling tube was connected to a perfluoroalkoxy (PFA) made manifold with a bypass pump drawing air. The intakes of the analyzers for O_3, CO, SO_2, and NO were connected to the manifold, while the NO_y channel used a separate ¼" (outside diameter) Teflon line which was connected to an enclosure placed outside at the same level of the sampling tube inlet. The photo showing the set up of the sample inlet and the gas analyzers were shown in Figures 5.5 and 5.6, respectively. Brief descriptions of the gas analyzers are given below.

Figure 5.5. The photo showing the set up of the sample inlet in Lanzhou.

Figure 5.6. The set up of the gas analyzers inside the laboratory in Lanzhou.

Ozone was measured using a commercial UV photometric analyzer (Thermo Environmental Instrument (TEI) Inc., model 49C). The limit of detection is 2ppbv and the precision is ±2ppbv. The instrument was checked automatically every day using scrubbed ambient air (TEI, model 111) and with a span standard generated in a multi-gas calibrator (TEI, model 146).

SO_2 was measured by pulsed UV fluorescence (TEI, Model 43S), with a detection limit of 0.06ppbv and 2s precision of 3% for ambient levels of 10ppbv (2-min average). The uncertainty was estimated to be about 9%.

CO was measured with a gas filter correlation, nondispersive infrared analyzer (Advanced Pollution Instrumentation, Inc., Model 300) with a heated catalytic scrubber to convert CO to carbon dioxide (CO_2) for baseline determination. Zeroing was conducted every 2 hour, each lasting for 12 min. The 2-min data at the end of each zeroing were taken as the baseline. The detection limit was 30ppbv for a 2-min average. The 2s precision was about 1% for a level of 500ppbv (2-min average) and the overall uncertainty was estimated to be 10%.

NO and NO_y were detected with a modified commercial MoO/chemiluminescence analyzer (TEI, Model 42S). The modification was made to relocate the internal catalytic converter to a separate enclosure which was placed outside the laboratory near the sample inlet, in order to reduce the loss of NO_y in the sample line prior to the catalytic converter. The enclosure also housed a temperature controller (for the MoO catalyst) and solenoid valves for zero and span tests. NO_y was converted to NO on the surface of MoO maintained at 350 degree Celsius, with NO subsequently measured by the chemiluminescent detector. The instrument automatically switched among zero, NO, and NO_y modes. A bypass pump was installed at the NO_y line to maintain a flow of 1.5L/min through the converter when the instrument was in NO mode. The analyzer had a detection limit of 0.05ppbv. The 2s precision of this instrument was 4% (for NO = 10ppbv) and the uncertainty was about 10%.

The data of the trace gases were collected by a data logger (Environmental Systems Corporation, 8816) [Wang et al., 2001; Wang et al., 2003].

Quality control and assurance of gas analyzers

The analyzers were calibrated by injecting scrubbed ambient air (TEI, Model 111) and a span gas mixture. A NIST-traceable standard (Scott-Marrin, Inc., California) containing 153.8ppmv CO, 15.19ppmv SO_2, and 15.14ppmv NO was diluted using a dynamic calibrator (Environics, Inc., Model 6100). The NO_y conversion efficiency on MoO was checked using a 5.41ppm N-propylnitrate (NPN) standard (Scott-Marrin, Inc., California), which was chosen as the surrogate for NO_y. The zero and span were carried out every day in the early morning. A data logger (Environmental Systems Corporation, Model 8816) was used to control the zero/span calibration and to collect 1-s data, which were averaged to 1-min values.

5.1.6 Meteorological measurements

In addition to the above chemical measurements, several meteorological parameters were also measured at the site. Wind direction and wind speed were recorded by the wind monitor (R.M. Young Company, 05305VM). Ambient relative humidity and temperature were measured by relative humidity / temperature probe (R.M. Young Company, 41372VC/CF). The meteorological parameter sensors output were also collected by a data logger (Environmental Systems Corporation, 8816) [Wang et al., 2001; Wang et al., 2003].

5.2 Filter analysis

Teflon filters were used for the analysis of ion compositions from the filters. The filters were extracted with 10mL of ultra-pure water in an ultrasonic bath for 30 minutes. The water extracts were filtered through a 0.2µm pore size 13-mm filter (MFS, 13JP020AN) and then stored in a bottle. 100µL extracts were injected into the ion chromatographies for analysis. The flow diagram showing the procedures of the filter analysis was shown in Figure 5.7.

Figure 5.7. The flow diagram showing the procedures of the filter analysis.

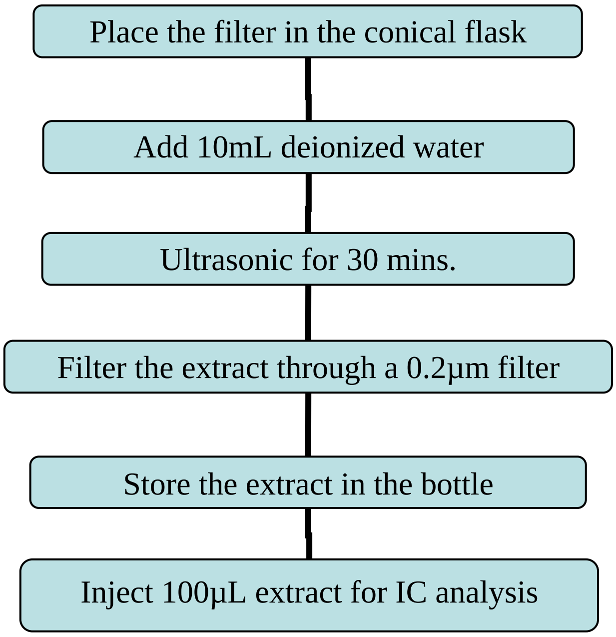

Quality control and assurance of filter analysis

Multi-point calibrations were performed for both ICs before the sample analysis by using commercially available calibration standard solutions (Dionex

Corporation, Six Cation-II standard for cation and seven anion standard for anion). Good calibrations (R^2 >0.993) were obtained for all ions.

Recoveries of the ions were performed before the sample analysis. The aim of the recovery was to determine whether the analytes were loss during the extraction process. The procedures of the recovery were identical to the sample analysis procedures except known concentrations of standards were used instead of the field samples. The recovery could finally be calculated based on the measured concentration against the initial concentration of the respective ion. The average recovery efficiencies were over 80% for all ions.

The ion balance expressed by the ratio of cation sum to anion sum ($\mu eq/m^3$) is calculated and the mean ratios of cation sum to anion sum were 0.72 for Shanghai, 0.82 for Beijing, 0.97 for Lanzhou and 0.92 for Guangzhou. The imbalance of the molar ratios of cation sum to anion sum in Shanghai and Beijing indicated the acidity of the aerosols in these two locations. More detailed will be discussed in the later section.

5.3 Summary of the sampling species in each monitoring station

In this study, there were altogether five field measurements. The sampling species measured in each field study had some difference. Table 5.2 summarized the instruments that have used in each sampling location.

Table 5.2. Summary of the instruments that have used in each monitoring station.

	Guangzhou	Hong Kong	Shanghai	Beijing	Lanzhou
AIM		√	√	√	
Thermo Andersen Chemical Speciation Monitor	√		√	√	√
TEOM			√	√	√
Gas analyzers	√		√	√	√
Meteorological measurements	√		√	√	√

Section III: Results and Discussions

Chapter 6: Intercomparison of the AIM with different sampling methods

As mentioned earlier, the AIM is a newly developed instrument. Up to this moment, there is still no literature or report discussing on the accuracy and/or reliability of this instrument. Thus, data quality and accuracy is the most critical issue to deal with before using the AIM instrument. In order to know the performance of this instrument, I have conducted two different kinds of comparison to verify the AIM instrument. They are (1) comparing with another semi-continuous sulfate (model: R&P8400S) and nitrate (model: R&P8400N) instruments, and (2) comparing with traditional filter analysis method. In this chapter, I will present these two comparison results.

6.1 Comparison with different semi-continuous instruments (R&P8400S and R&P8400N)

The first comparison was done in Tsuen Wan, Hong Kong. One of the reasons for choosing this site was due to the availability of other semi-continuous instruments – Ambient Particulate Sulfate Monitor (APSM, R&P8400S), and Ambient Particulate Nitrate Monitor (APNM, R&P8400N) for measuring the concentrations of particulate sulfate and nitrate, respectively in $PM_{2.5}$, which was operated by the Hong Kong Environmental Protection Department (HKEPD).

Ambient Particulate Sulfate and Nitrate Monitors employ different operating principles from the AIM. For the comparison purpose, it is good to have two entirely different instruments operating with different principles. It is because the same problem should not be present for the two instruments working with different principles. I will firstly summarize the operating principles of these two instruments. After that, I will present and discuss the comparison results in this study.

6.1.1 Operating principles of the Ambient Particulate Sulfate and Nitrate Monitor

The Ambient Particulate Sulfate and Nitrate Monitors are developed by the Aerosol Dynamics, Inc. Each sampling cycle is 10 minutes with an 8 minute sample collection period followed by a 2 minute analysis phase. Ambient air firstly enters the sample flow line in which a $PM_{2.5}$ sharp cut cyclone is installed to remove the large particles from the sample stream. The air then passes through an activated charcoal denuder to remove acidic gases that could interfere with the measurements of the ambient particulate sulfate and nitrate concentrations. The monitor collects the fine particulate matter through means of critical impaction. To achieve high collection efficiencies for very small secondary aerosols, a humidifier moistens the sample stream and causes the hygroscopic sulfate and nitrate particles to grow. The remaining part of the sample stream forms a jet as it passes through a critical orifice. During the sample collection phase, particles collect on an impactor / flashing strip. The instrument automatically changes its internal flow pattern during the sample analysis phase. The sample stream that passes through the $PM_{2.5}$ sharp cut cyclone continues to flow, but is bypassed around the integrated collection and vaporization cell while the sample processing takes place.

For the sulfate analysis, the monitor purges the analysis cell with zero air, and then sends a high current through the impactor / flashing strip that lasts approximately 0.05 second and heats the collected particulate matters to over 600°C. The vaporization decomposition process converts the particulate sulfate contained in the collected samples to SO_2. The SO_2 pulse monitor, a specially-tuned SO_2 pulsed fluorescence analyzer, quantifies the amount of SO_2 generated by this process. The monitor measures total particulate sulfur. The instrument automatically computes the final result as the ambient particulate sulfate concentrations in micrograms per cubic meter. The flow diagram showing the components of the Ambient Particulate Sulfate Monitor is shown in Figure 6.1.

Figure 6.1. The flow diagram of the Ambient Particulate Sulfate Monitor.

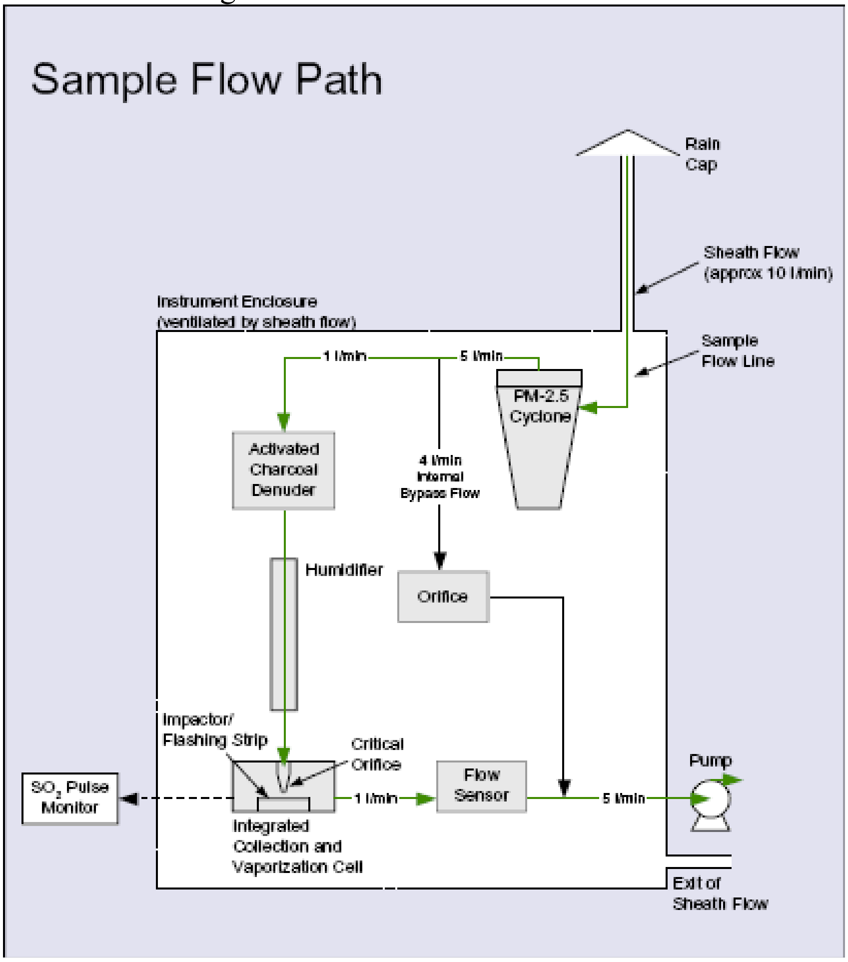

For the measurement of nitrate, the monitor purges the analysis cell with nitrogen, and then sends a high current through the impactor / flashing strip that lasts approximately 0.05 second and heats the collected particulate matters to about 350°C. The vaporization decomposition process converts the particulate nitrate contained in the collected samples to NO_x. The NO_x pulse monitor, a specially-tuned chemiluminescent NO_x analyzer, quantifies the amount of NO_x generated by this process. The instrument automatically computes the final result as the ambient particulate nitrate concentrations in micrograms per cubic meter. Figure 6.2 showed the flow diagram of the Ambient Particulate Nitrate Monitor.

Figure 6.2. The flow diagram of the Ambient Particulate Nitrate Monitor.

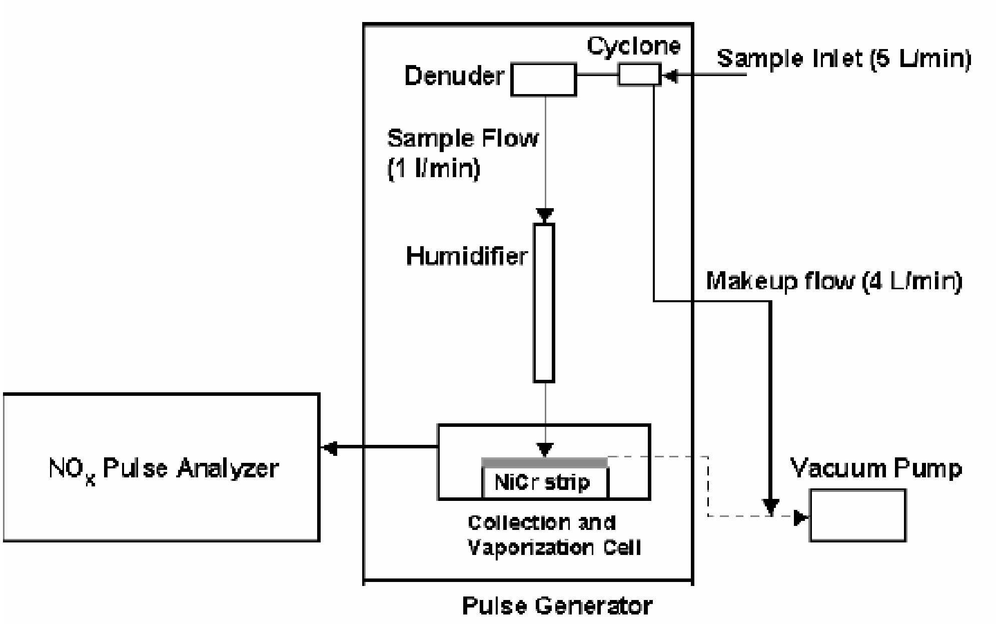

From the above two diagrams, we could see that APSM and APNM actually worked on very similar principles despite of different vaporization processes and different detectors.

6.1.2 Comparison results of sulfate

The overall time series of sulfate as measured by both instruments (the AIM and the APSM) are shown in Figure 6.3. Red line represented the measurement result of sulfate from the AIM, while blue line represented the result from the APSM. According to Figure 6.3, the overall temporal variations of the AIM sulfate were similar to the APSM. However, the AIM showed generally smaller sulfate concentrations (about 28% for the whole study) than the APSM. During the whole measurement period, the average concentrations of sulfate measured by the APSM and the AIM were 18.5 ± 9.1μg/m^3 and 13.4 ± 8.2μg/m^3, respectively. However, at the days with high sulfate pollution plumes such as 28 Jan, 7, and 10 Feb, the measurement results were reversed with the AIM showing higher concentrations of sulfate than the APSM. Figure 6.4 showed the ratio of sulfate as calculated by dividing the concentrations obtained from the APSM with the AIM. The average value was around 1.4 which suggested that the APSM showed higher concentrations of sulfate. Moreover, the ratio was quite constant during the whole measurement period except at the days with high sulfate concentrations. During the high sulfate events, the ratio dropped to about 0.5.

Figure 6.3. Intercomparison result of sulfate between the AIM and the APSM.

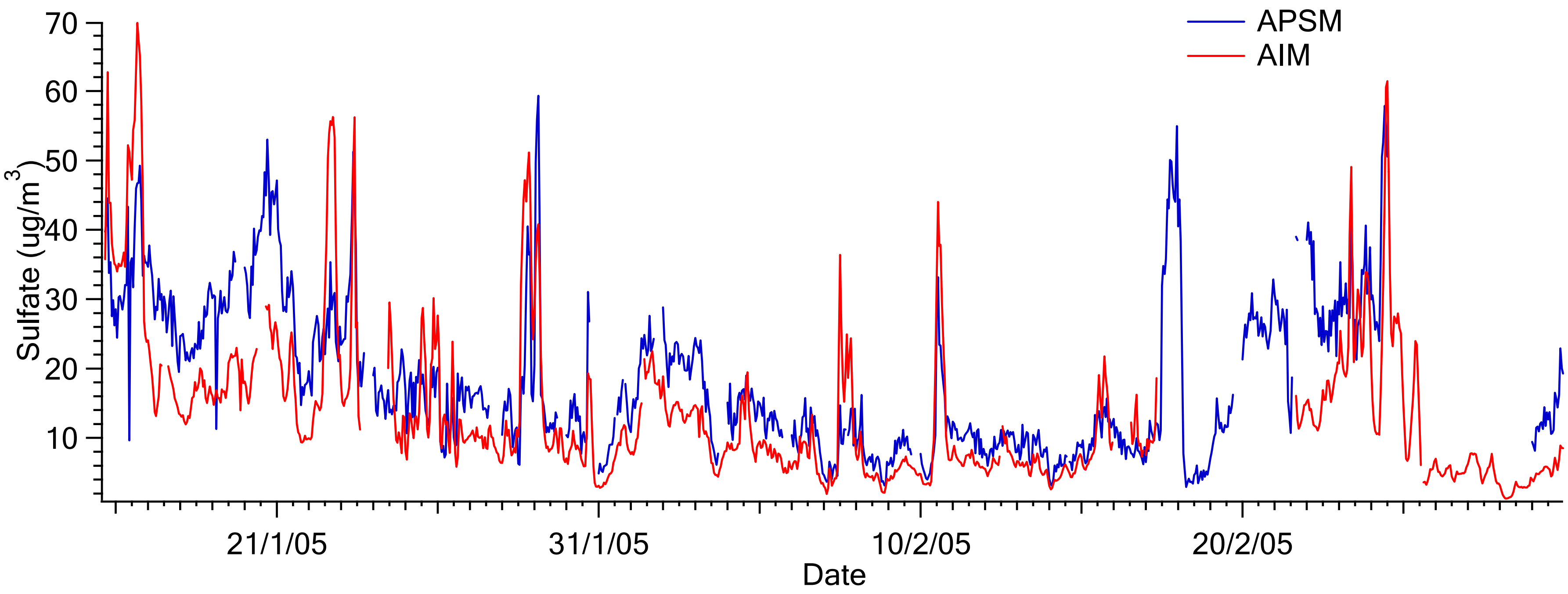

Figure 6.4. The ratio of sulfate as calculated by dividing the concentrations obtained from the APSM with the AIM.

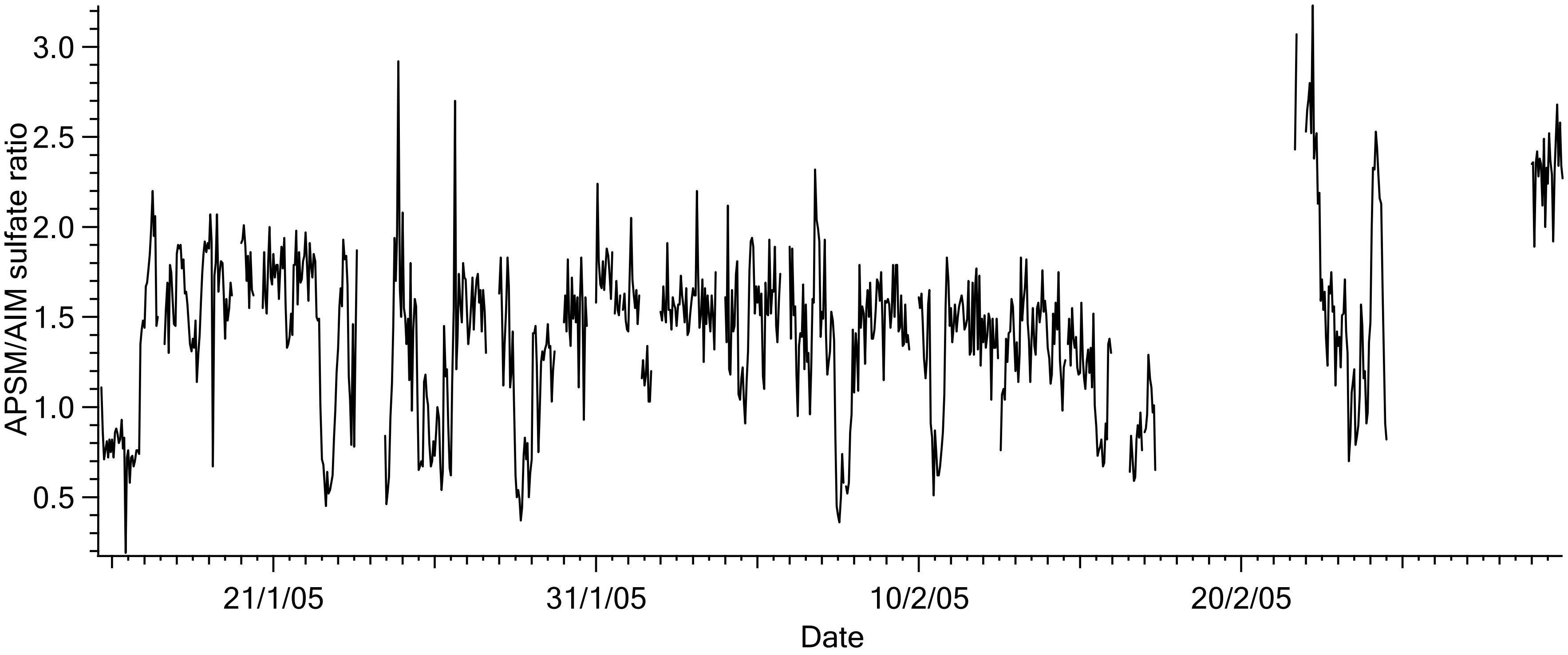

According to the report of the twelve-month particulate matter study in Hong Kong, the concentrations of sulfate in Tsuen Wan were around 10 and 13μg/m^3, respectively in January and February 2001. These values were more resemble to the AIM results (13.4μg/m^3) in comparison with the APSM (18.5μg/m^3) during the measurement period. However, this data was only obtained from 2001, I could not make a definite conclusion on the correctness of these two instruments. Therefore, other analysis has also been performed.

As sulfate is a secondary pollutant which is formed from SO_2, comparison between SO_2 and sulfate is made and shown in Figure 6.5. The top of Figure 6.5 showed the time series of SO_2 and the AIM sulfate, while the bottom of it showed the time series of SO_2 and the APSM sulfate. Results showed that when the concentrations of SO_2 were high such as 22, 23 Jan, and 7, 10 Feb, the AIM instrument showed consistent higher sulfate concentrations. However, the APSM didn't follow the trend of SO_2. This meant that the presence of the SO_2 plume did not contribute to the high concentrations of sulfate in the APSM.

Figure 6.5. Time series of SO_2 and the AIM sulfate (Top). Time series of SO_2 and the APSM sulfate (Bottom).

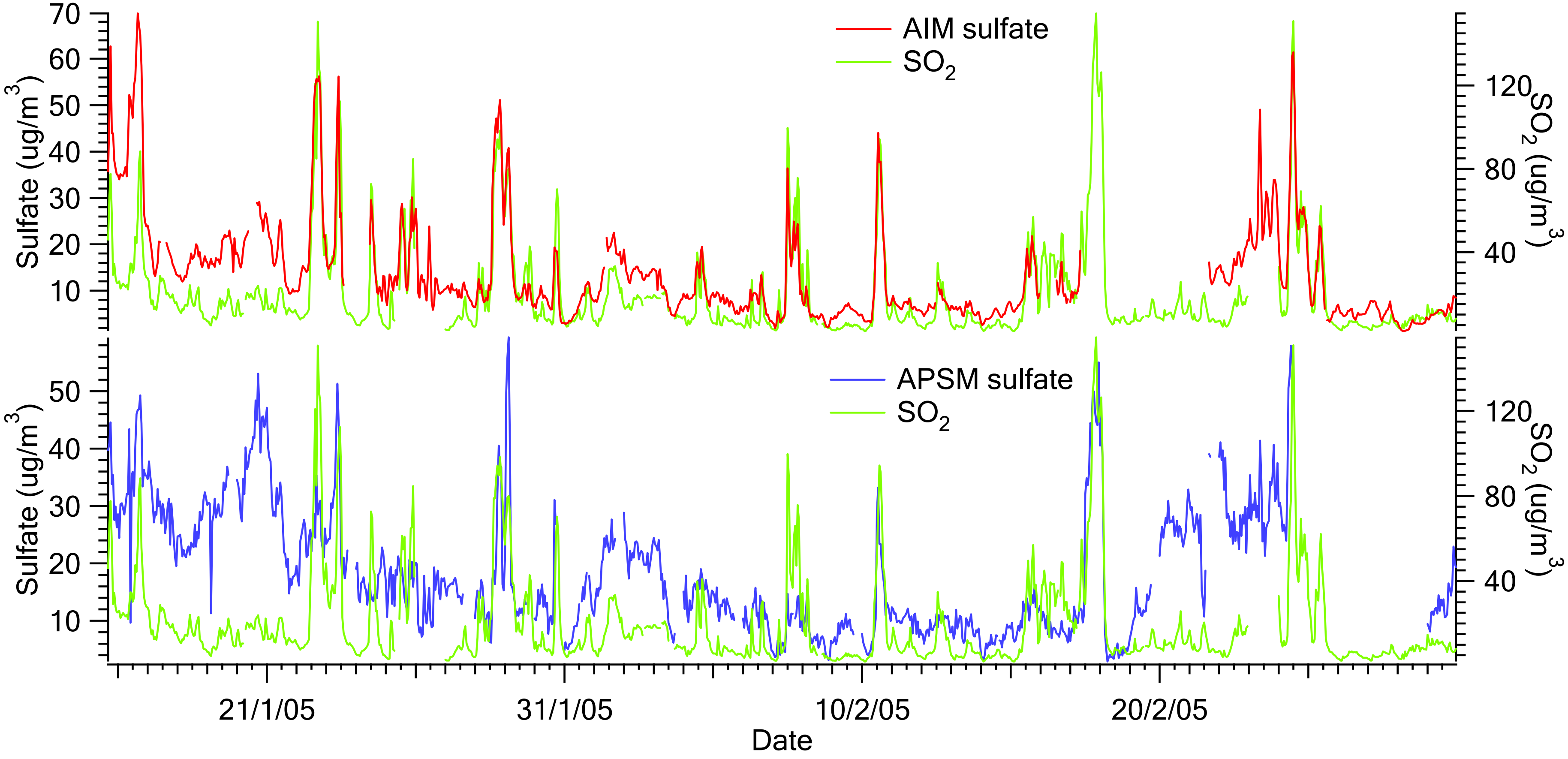

Figure 6.6 showed the molar ratio of sulfate to total sulfur (SO_2 + SO_4^{2-}). The average sulfate to total sulfur ratio for the APSM and the AIM were 0.44 and 0.36, respectively. According to the report of the study of visibility reduction and its causes in Hong Kong, the molar ratio of sulfate to total sulfur was around 0.14 as measured in Tsuen Wan in 2001. Thus, the two instruments were difficult to justify based on the results of molar ratio.

Figure 6.6. The molar ratio of sulfate to total sulfur from the AIM and the APSM.

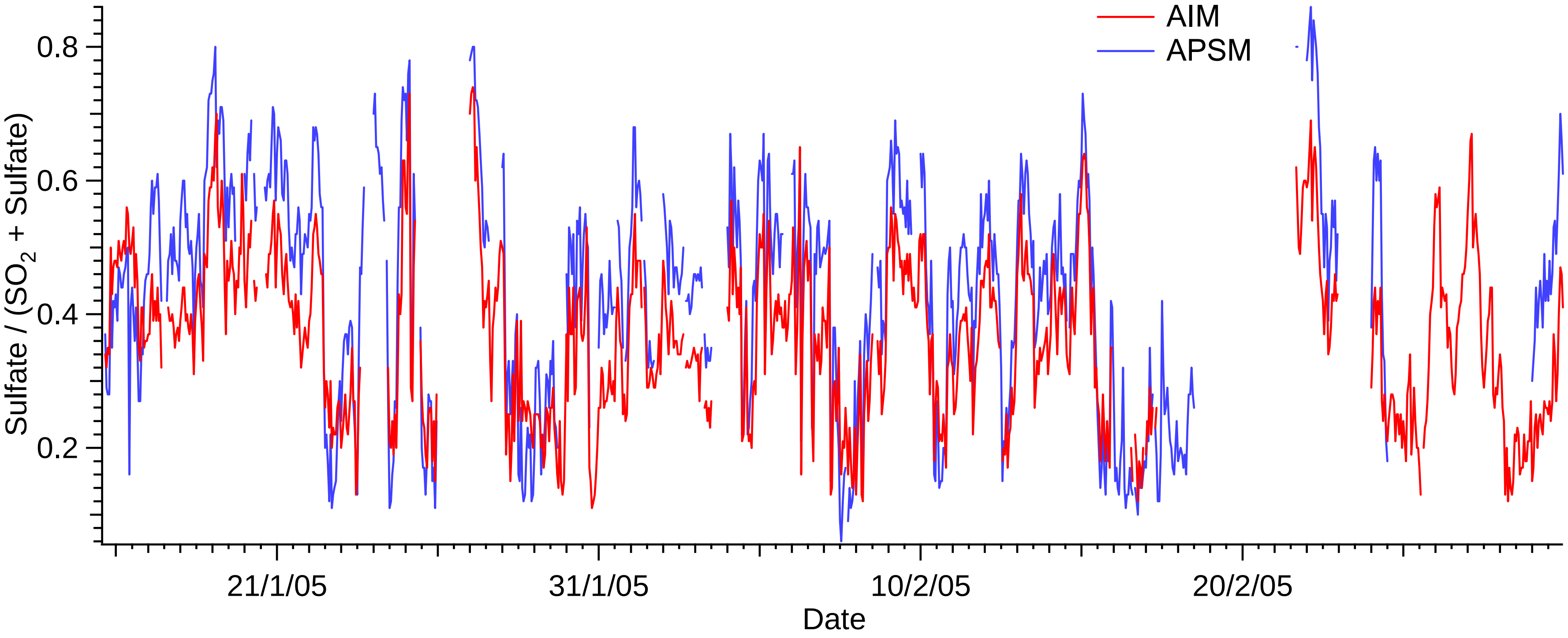

The scatter plot of sulfate between the two instruments was shown in Figure 6.7. The overall correlation of sulfate between the two instruments was 0.46 with the slope and intercept of 0.67 and 9.54, respectively. The scatter plot also suggested that the correlation of sulfate between the two instruments was divided into two groups. One group corresponded to the higher sulfate by the AIM (red circle), while others corresponded to the higher sulfate by the APSM (blue circle).

Figure 6.7. Scatter plot of sulfate between the AIM and the APSM.

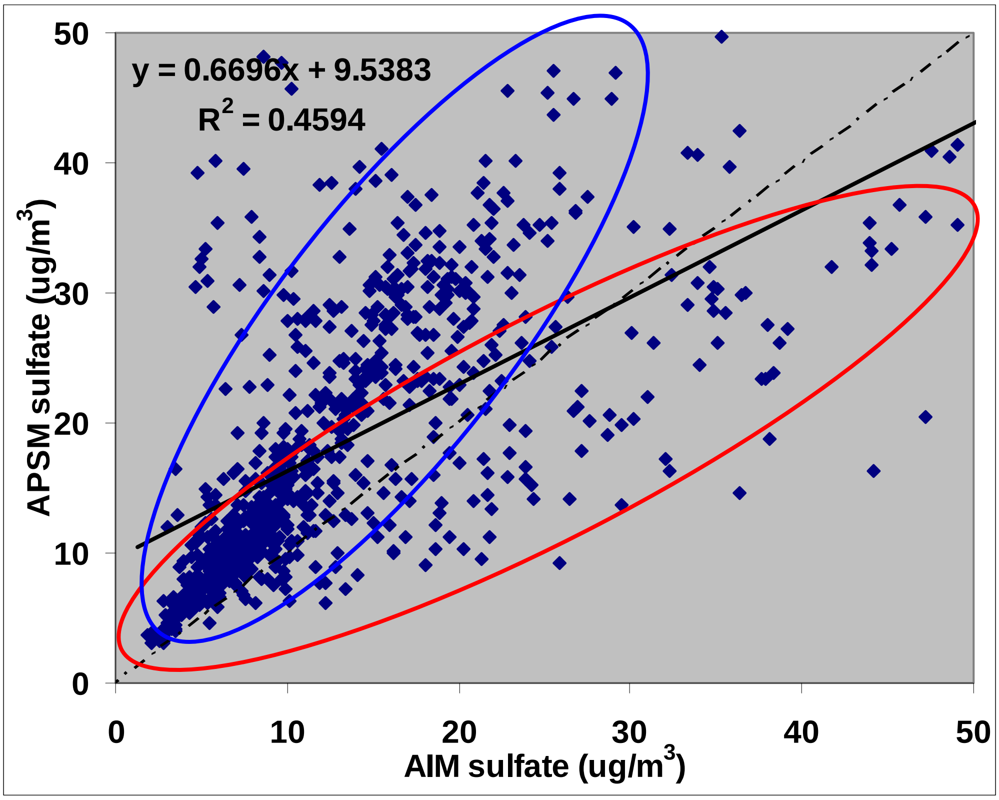

6.1.3 Comparison results of nitrate

The time series of nitrate measured by the AIM and the APNM was shown in Figure 6.8. Results showed that the two instruments gave out an overall similar pattern. However, the two instruments still had an overall of about 15% difference in which the APNM showed lower values. The overall average concentrations of nitrate measured by the APNM and the AIM were 3.0 ±

1.7μg/m^3 and 3.4 ± 2.0μg/m^3, respectively. According to the report of the twelve-month particulate matter study in Hong Kong, the concentrations of nitrate in Tsuen Wan were around 2 and 5μg/m^3, respectively in January and February 2001. Figure 6.9 showed the ratio of nitrate as calculated by dividing the concentrations of the AIM from the concentrations of the APNM. The average ratio was around 0.9 which suggested that the APNM showed lower concentrations of nitrate. It was therefore difficult to make the judgment on the correctness of the two instruments.

Figure 6.8. Intercomparison result of nitrate between the AIM and the APNM.

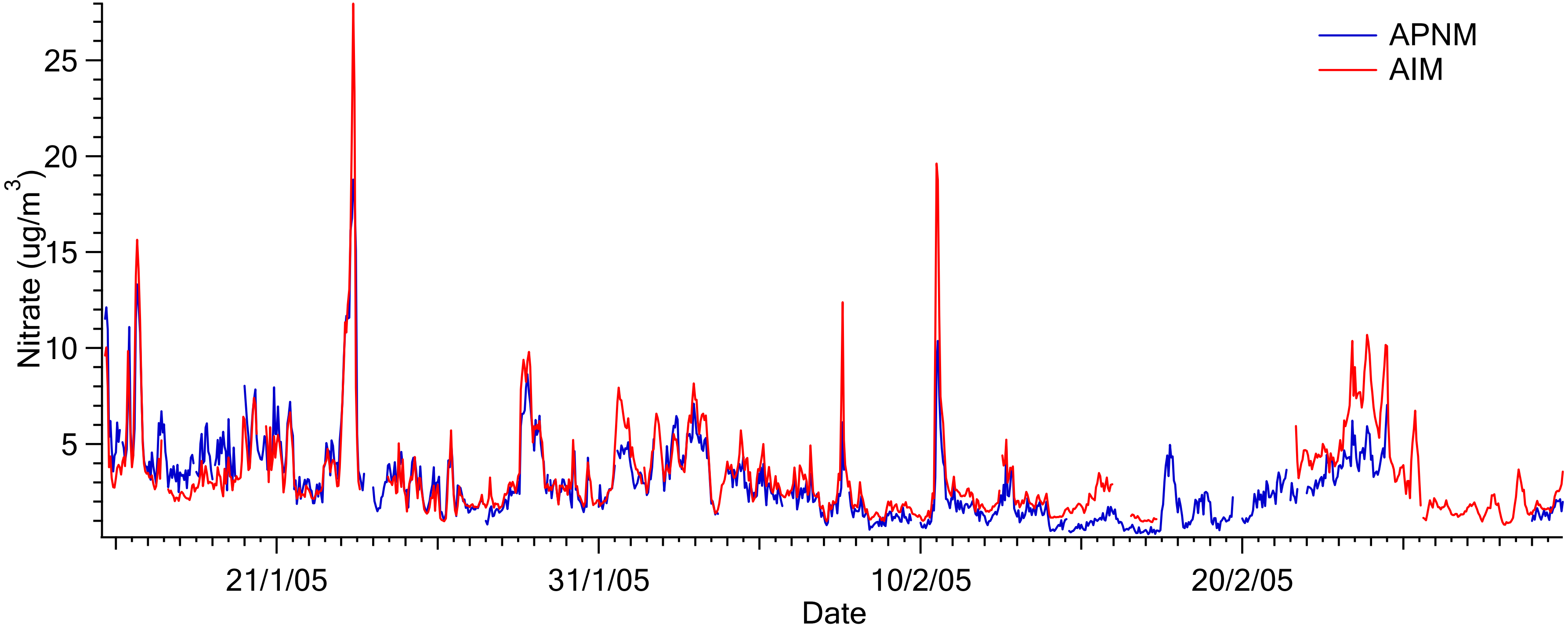

Figure 6.9. The ratio of nitrate as calculated by dividing the concentrations of the AIM from the concentrations of the APNM.

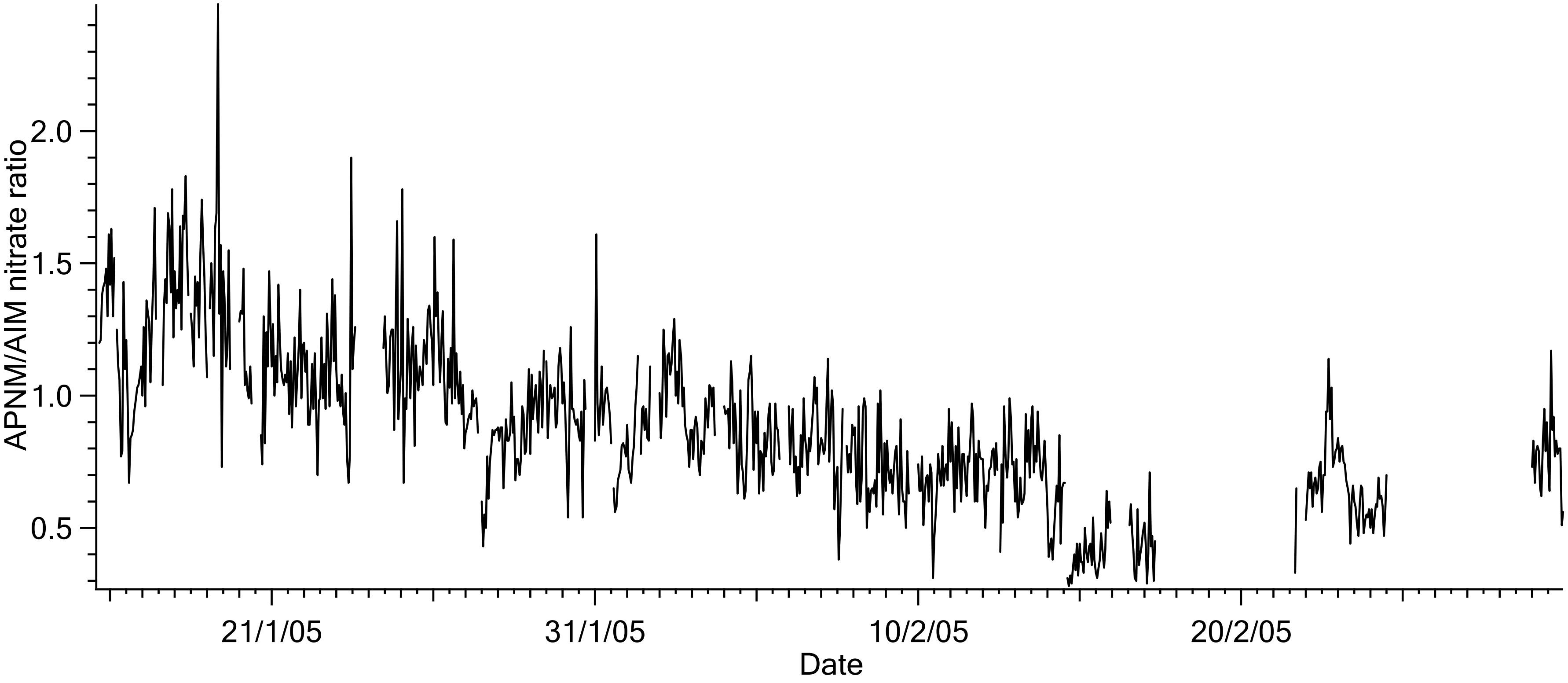

The scatter plot of nitrate between the AIM and the APNM was shown in Figure 6.10. The correlation of nitrate between the two instruments was moderate (R^2 = 0.76), but it was much better than the comparison results of sulfate. Comparing with the scatter plot of sulfate, the data points of nitrate were much less scattered. However, the result in Figure 6.10 still showed the derivations of the two instruments with the slope and intercept of 0.74 and 0.49, respectively. This suggested that there was difference between the AIM and the APNM.

Figure 6.10. Scatter plot of nitrate between the AIM and the APNM.

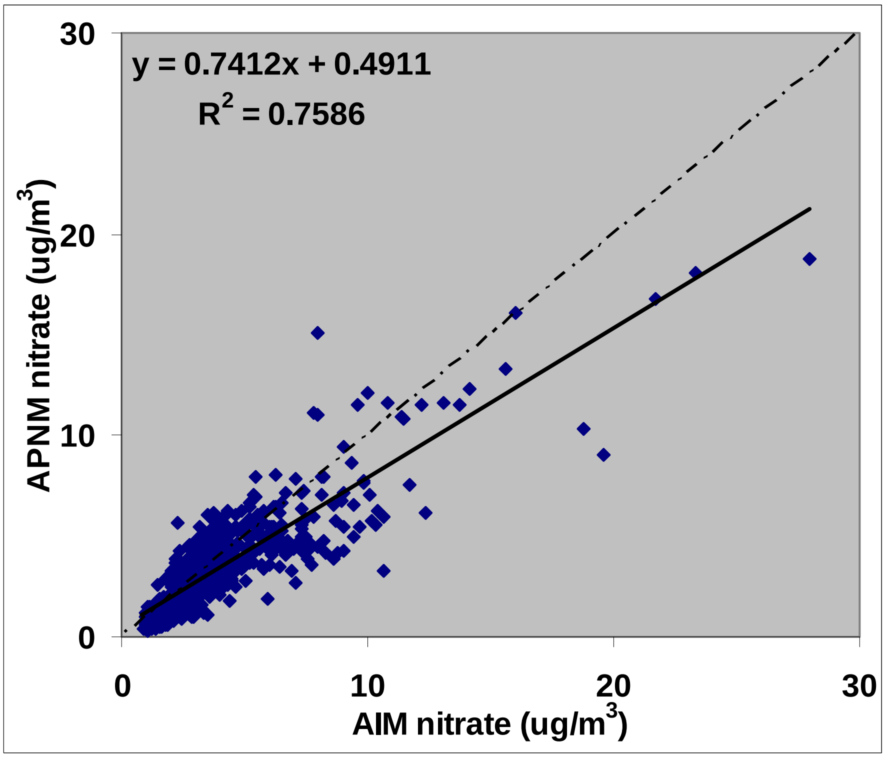

6.2 Comparison with filter measurements

Although several comparisons have been performed to figure out the correctness of the data for the AIM, there is still no definite conclusion that can be drawn based on the results from Tsuen Wan. Therefore, the second comparison of the AIM with the filter-based measurements has been performed in Shanghai and Beijing in order to confirm the accuracy of the AIM data.

Up to this moment, the filter-based measurements are the most reliable and accurate technique for the determination of water soluble ion species.

6.2.1 Overall comparison of sulfate and nitrate in Shanghai and Beijing

The overall comparison results of the AIM sulfate and the filter sulfate in Shanghai and Beijing are shown in Figures 6.11 and 6.12, respectively. The correlation between the two methods in Shanghai was good, with $R^2 = 0.67$ and a RMA slope of 1.28 and an intercept of 2.71, indicating that the AIM gave larger sulfate values than the filter samples. As shown in the following section, the higher sulfate readings in the AIM could be attributed to the positive interference from the high concentrations of SO_2 observed at this site. In contrast to Shanghai, data from Beijing showed an excellent overall correlation ($R^2 = 0.97$) of sulfate between the two methods (Figure 6.12), but overall RMA slope was only 0.58 with a positive intercept of 2.75. The AIM gave lower sulfate values than the filter-based method and the difference between the two data sets increased at higher sulfate levels.

Figure 6.11. Overall comparison results of sulfate in Shanghai.

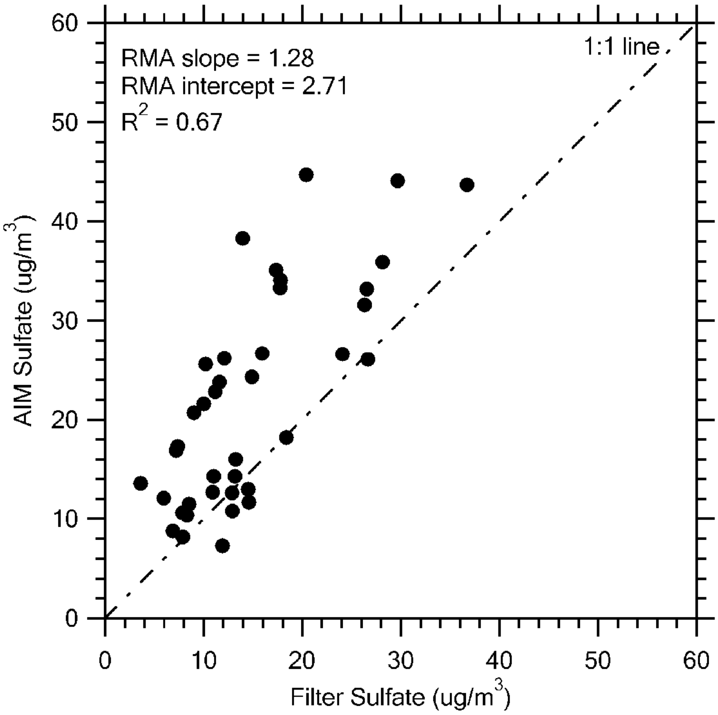

Figure 6.12. Overall comparison results of sulfate in Beijing.

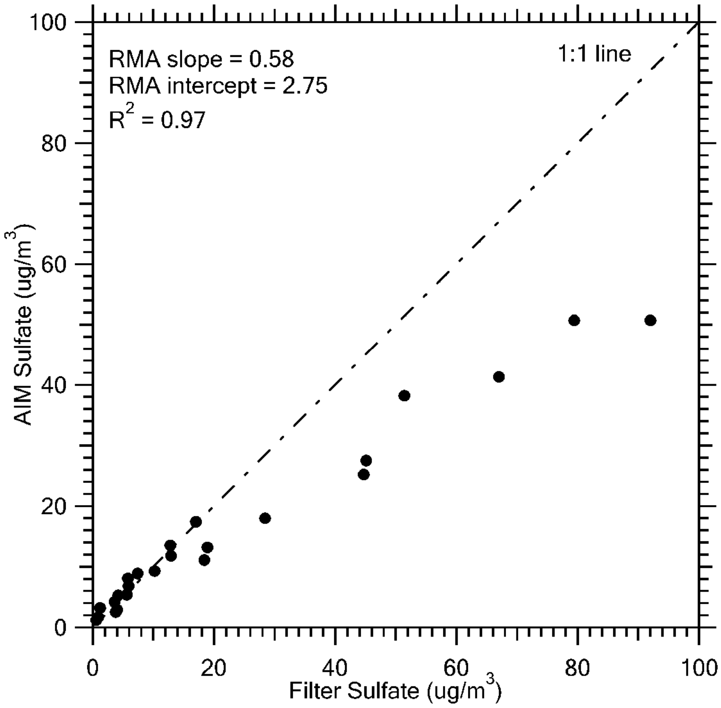

The nitrate results in Shanghai and Beijing are shown in Figures 6.13 and 6.14, respectively. The AIM nitrate was highly correlated with filter nitrate in both Shanghai (R^2 = 0.96) and Beijing (R^2 = 0.88), but the AIM gave lower nitrate concentrations. The AIM showed 83% of filter nitrate in Shanghai but only 45% in Beijing, with intercepts of 0.00 for Shanghai and 1.54 for Beijing. Similar to sulfate, deviations between the two methods for nitrate in Beijing became large at high nitrate loadings.

Figure 6.13. Overall comparison results of nitrate in Shanghai.

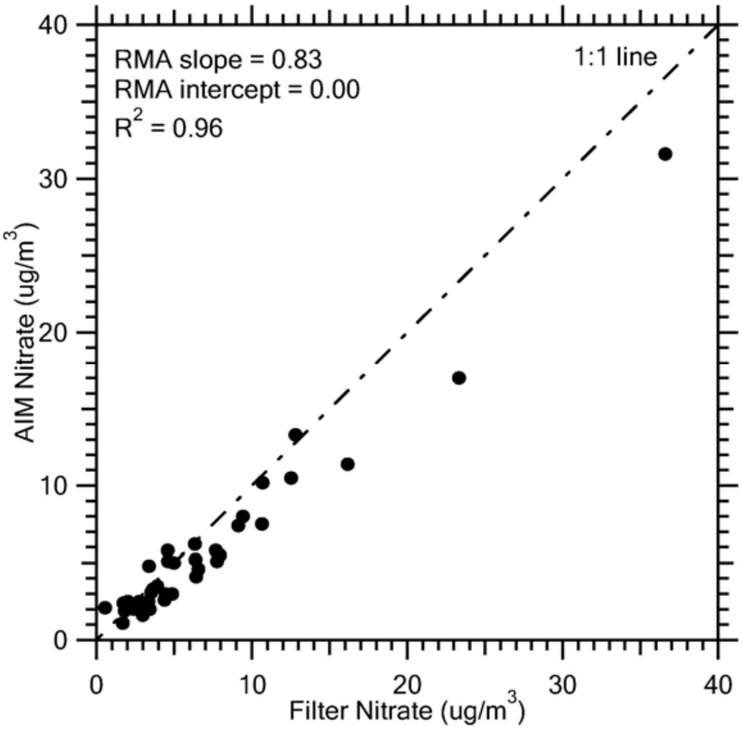

Figure 6.14. Overall comparison results of nitrate in Beijing.

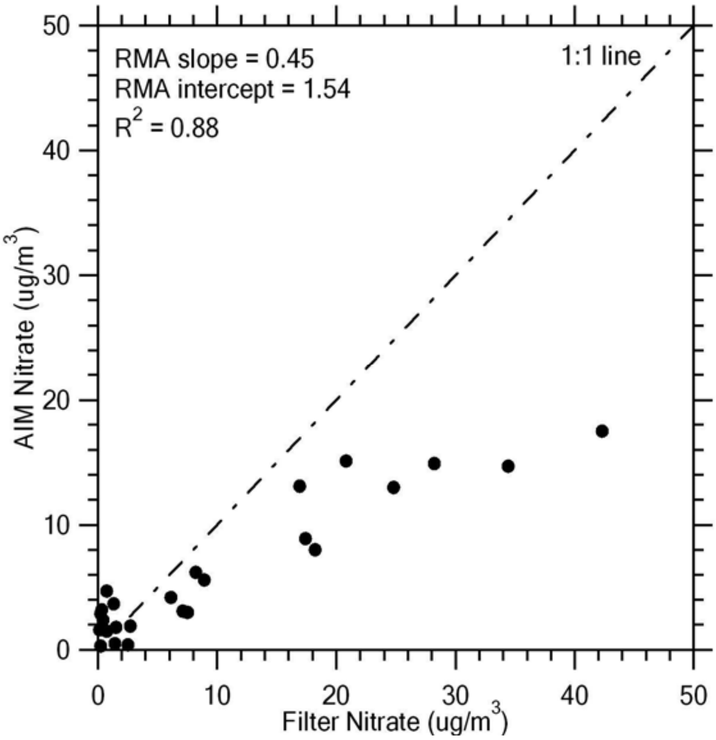

6.2.2 Performance of the AIM at different ion loadings

6.2.2.1 Low concentrations of sulfate and nitrate

While the overall result in Beijing indicated lower sulfate concentrations from the AIM as compared to the filter measurements, we note that for sulfate concentrations of less than 20μg/m^3, the two methods showed an excellent agreement with a slope of 0.97 and an intercept of 0.60 (R^2 = 0.94, N = 16, Figure 6.15). For Shanghai, after removing the positive interference of SO_2 to the AIM by omitting the samples collected on days with peak SO_2 concentrations larger than 30ppbv (see section below), the correlation between the two measurements at low sulfate levels was also greatly improved, yielding a slope of 0.95 and an intercept of 1.41 (R^2 = 0.89, N = 13, Figure 6.16).

Figure 6.15. The concentrations of sulfate with less than 20μg/m^3 in Beijing.

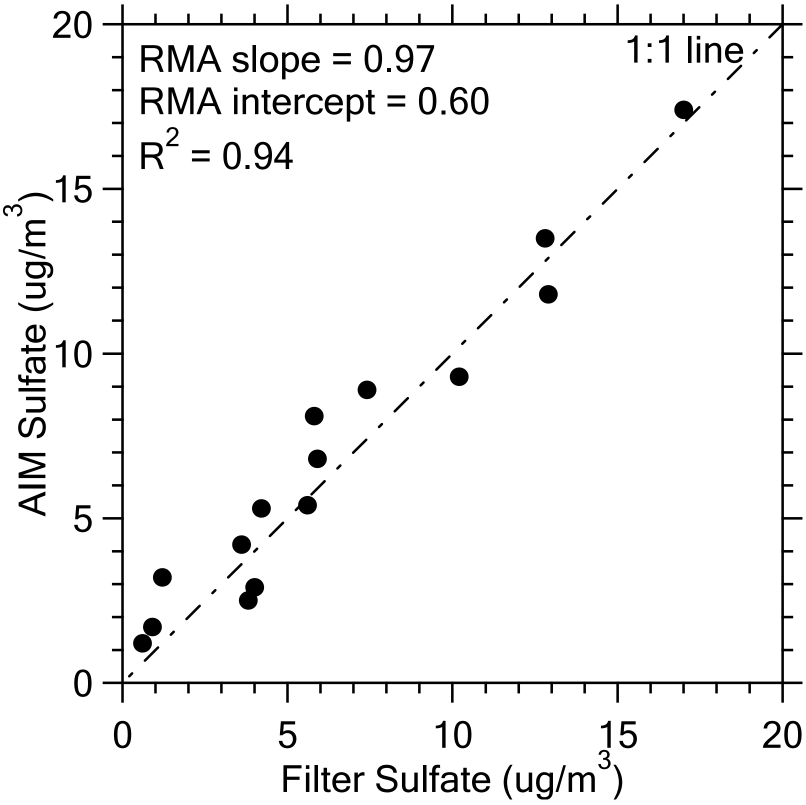

Figure 6.16. The concentrations of sulfate with less than 20μg/m^3 and peak SO_2 concentration less than 30ppbv in Shanghai.

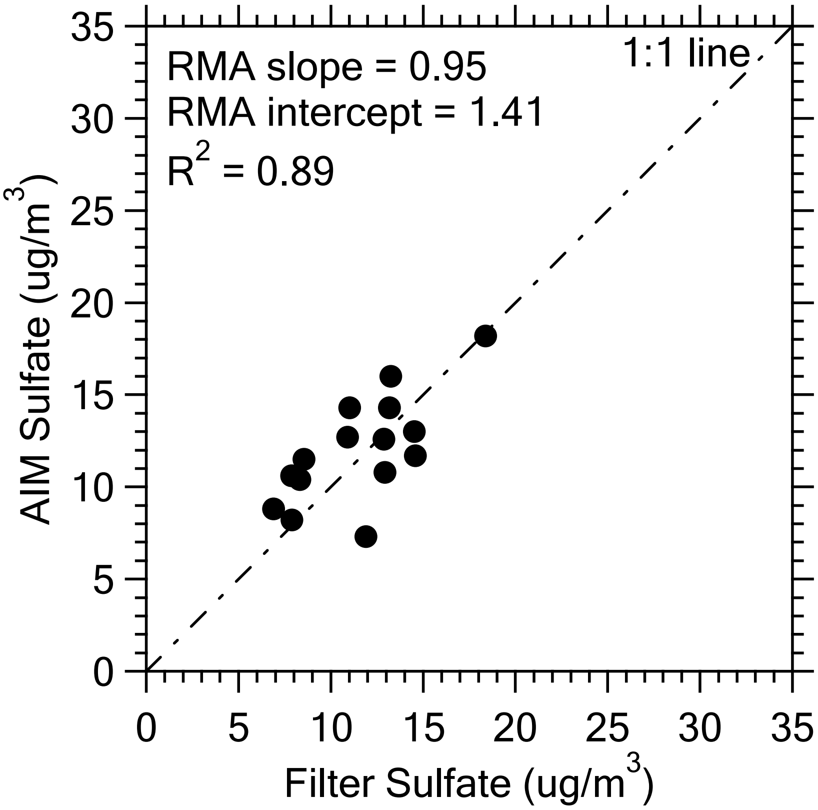

Table 6.1 summarized the results of previous comparison studies in United States and that from the present study for 'low' (i.e. <20μg/m^3) sulfate condition. It should be noted that all the previous comparisons were conducted in a comparatively clean environment, with the concentrations of generally less than 25μg/m^3. Even though most of these studies were conducted in urban areas such as Atlanta, New York City, and Pittsburgh, the aerosol concentrations were much smaller than those observed from our study obtained at suburban / rural areas near Shanghai and Beijing. This reflects more serious particulate pollution in eastern China. Table 6.1 indicated that the correlations between different types of semi-continuous instruments with the filter-based measurements were good (R^2 = 0.83 – 0.95), and a majority of them gave lower sulfate values than the filter-based method.

Table 6.1. Summary of intercomparison results of different semi-continuous instruments with filter-based method for sulfate.

Location	Instrument	Period	Range ($\mu g/m^3$)	R^2	Slope	Intercept	Reference
New York, US	Particle into liquid sampler	Jun 01 – Aug 01	0 – 25	0.91	0.71	0.13	Drewnick et al. (2003)
New York, US	R&P 8400S	Jun 01 – Aug 01	0 – 25	0.95	0.73	0.34	Drewnick et al. (2003)
New York, US	HSHP continuous sulfate monitor	Jun 01 – Aug 01	0 – 25	0.92	0.68	0.63	Drewnick et al. (2003)
Pittsburg, US	R&P 8400S	Jul 01 – Aug 02	0 – 25	0.83	0.71	0.42	Wittig et al. (2004)
Seattle, US	R&P8400S	May 02 – Jan 03	0.5 – 5	0.89	1.22	0.28	Homolya et al. (2005)
Chicago, US	R&P8400S	May 02 – Jan 03	0.5 – 21	0.84	0.47	0.99	Homolya et al. (2005)
Indianapolis, US	R&P8400S	Jul 02 – Jan 03	0.5 – 21	0.83	0.59	0.99	Homolya et al. (2005)
Deer Park, US	R&P8400S	Sept 02 – Dec 02	1 – 6	0.87	0.74	1.65	Homolya et al. (2005)
Shanghai, China[a]	URG9000B	May 05 – Jun 05	0 – 20	0.89	0.95	1.41	This study
Beijing, China	URG9000B	Jun 05 – Aug 05	0 – 20	0.94	0.97	0.60	This study

[a] Only include data with the average daily top five SO_2 concentrations less than 30ppbv.

Similar to sulfate, the AIM nitrate had good correlation (0.86 in Shanghai and 0.90 in Beijing), with the filter data for nitrate levels lower than 15µg/m^3 (Figures 6.17 and 6.18). It should be pointed out that collection of nitrate on filters suffers from both positive and negative artifacts. Positive artifact was due to the reaction of nitric acid with particles to form nitrate or the absorption of HNO_3 on filter which is then measured as nitrate by IC, while the negative artifact arose from the evaporation of volatile nitrate during sampling (e.g. Chow, 1995). Evaporative loss of nitrate on filters was prominent on some days in Beijing when temperatures were high. Figure 6.19 showed a scatter plot of the AIM nitrate versus filter nitrate in Beijing, colour-coded according to average daily temperatures. There was significant nitrate loss on filters at temperatures greater than 28ºC. We discarded these data points in the following comparison. At nitrate level <15µg/m^3, the AIM showed 89% of the filter nitrate in Shanghai (N = 35) and 69% in Beijing (N = 9). These results are consistent with other comparison studies as shown in Table 6.2. Most of the semi-continuous techniques gave comparable correlation coefficients with R^2 ranging from 0.82 to 0.98, and the slopes from 0.46 to 1.23.

Figure 6.17. The concentrations of nitrate with less than 15μg/m^3 in Shanghai.

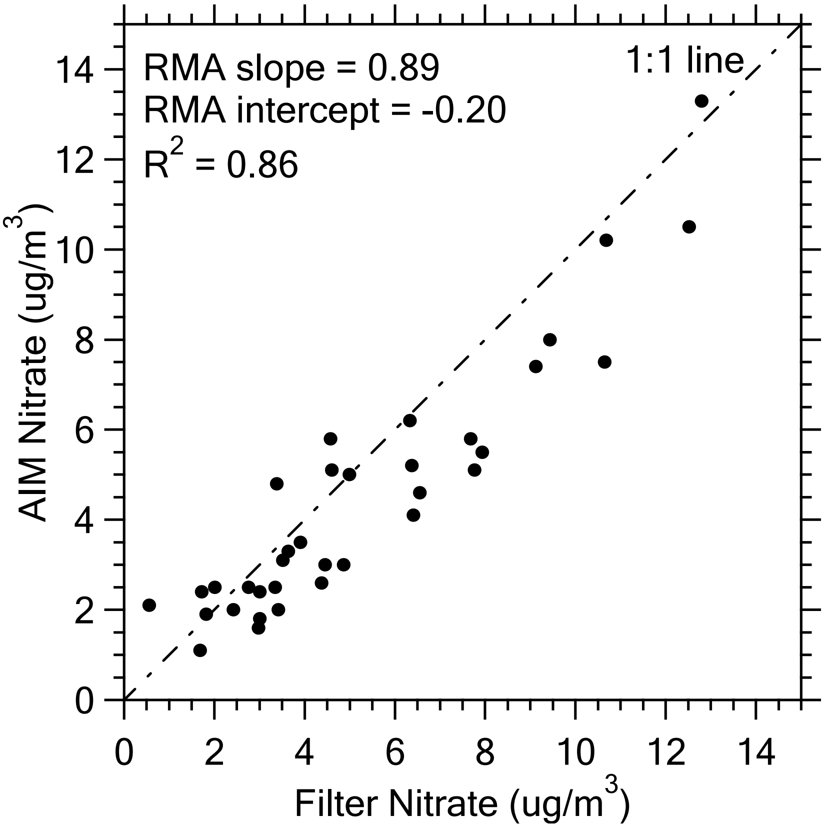

Figure 6.18. The concentrations of nitrate with less than 15μg/m^3 in Beijing.

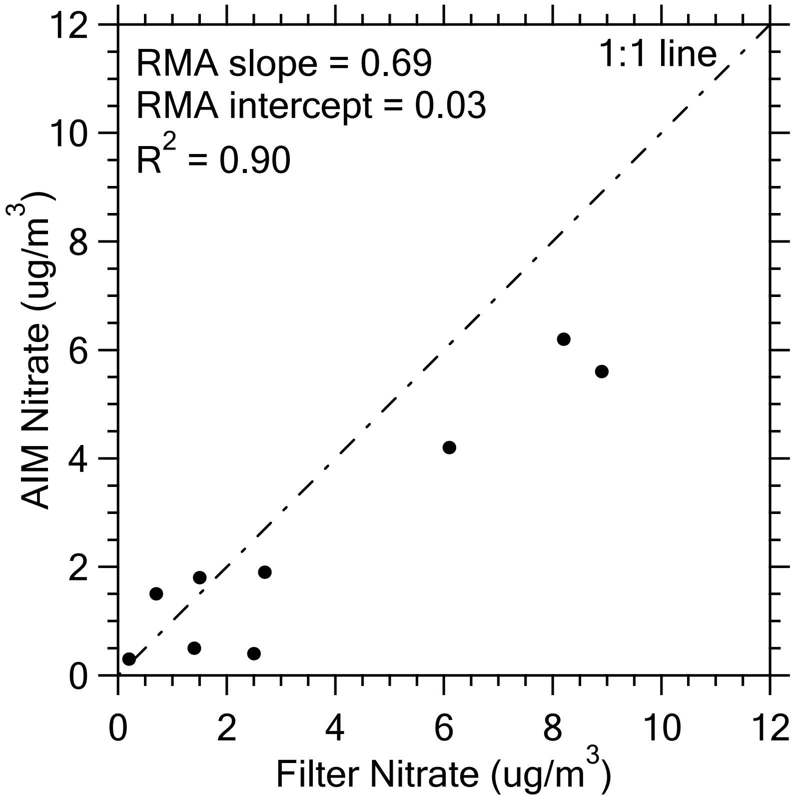

Figure 6.19. Comparison results of nitrate between the AIM and the filter in Beijing with different colors corresponding to different average daily temperatures.

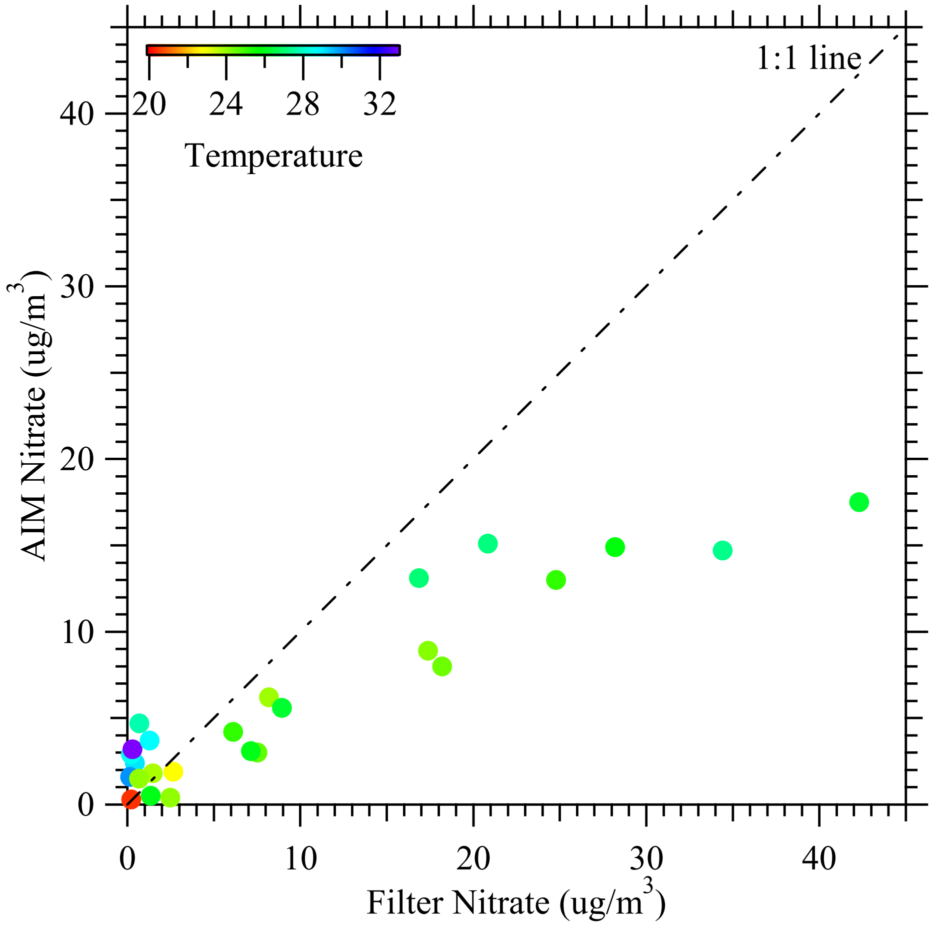

Table 6.2. Summary of intercomparison results of different semi-continuous instruments with filter-based method for nitrate.

Location	Instrument	Period	Range ($\mu g/m^3$)	R^2	Slope	Intercept	Reference
Atlanta, US	Steam jet aerosol collector	Jan 00	0 – 8	0.98	1.04	0.20	Slanina et al. (2001)
Pittsburg, US	R&P 8400N	Jul 01 – Aug 02	0 – 8	0.84	0.83	0.20	Wittig et al. (2004)
Seattle, US	R&P8400N	May 02 – Jan 03	0.2 – 5	0.89	0.78	0.20	Homolya et al. (2005)
Chicago, US	R&P8400N	May 02 – Jan 03	0.2 – 14	0.82	0.46	0.51	Homolya et al. (2005)
Indianapolis, US	R&P8400N	Jul 02 – Jan 03	0.2 – 12	0.85	0.56	0.25	Homolya et al. (2005)
Deer Park, US	R&P8400N	Sept 02 – Dec 02	0.2 – 2	0.21	1.23	0.53	Homolya et al. (2005)
Phoenix, US	R&P8400N	Sept 02 – Feb 03	0.2 – 15	0.86	0.59	0.99	Homolya et al. (2005)
Shanghai, China	URG9000B	May 05 – Jun 05	0 – 15	0.86	0.89	-0.20	This study
Beijing, China	URG9000B	Jun 05 – Aug 05	0 – 15	0.90	0.69	0.03	This study

6.2.2.2 High concentrations of sulfate and nitrate

At high concentrations of sulfate and nitrate, the AIM showed large deviations from the filter data, which was particularly evident in Beijing (Figures 6.12 and 6.14). This may be due to insufficient water vapour in the AIM's steam generator to dissolve all the water-soluble ions under high ionic loadings. In Shanghai, the AIM suffered from the mixed effects of high ion loadings that would give a lower signal, and of high SO_2 (and NO_x) concentrations which may yield positive bias due to denuder breakthroughs. Thus, the effect of high ion loadings in Shanghai was not as obvious as in Beijing. Laboratory studies will be needed to confirm the effect of ambient aerosol loadings on the particle capture efficiency in the AIM in future.

6.2.3 The influence of SO_2

6.2.3.1 Comparison with filter measurements

As mentioned previously, some samples collected near Shanghai showed larger sulfate values from the AIM than those from the filters. Due to the close proximity of the site to several large coal-fired power plants, the SO_2 concentrations were very high. Plumes containing hourly SO_2 greater than 50ppbv were observed on a number of occasions, with the maximum value reaching 156ppbv. Inspection of a time series of sulfate and SO_2 has shown that the data with larger AIM values than filter data were associated with these SO_2 plumes. Figure 6.20 showed the AIM versus filter measurements in Shanghai, colour-coded according to the average concentrations of the five highest hourly SO_2 data during the 24-hour filter sampling. It can be seen that when the mean top five SO_2 concentrations were larger than 30ppbv, the AIM gave larger sulfate values than the filter samples. In contrast, when the mean top five SO_2 levels were smaller than 30ppbv, the two methods gave similar sulfate concentrations.

Figure 6.20. Comparison results of sulfate between the AIM and the filter in Shanghai with different colours corresponding to different daily top five SO_2 concentrations.

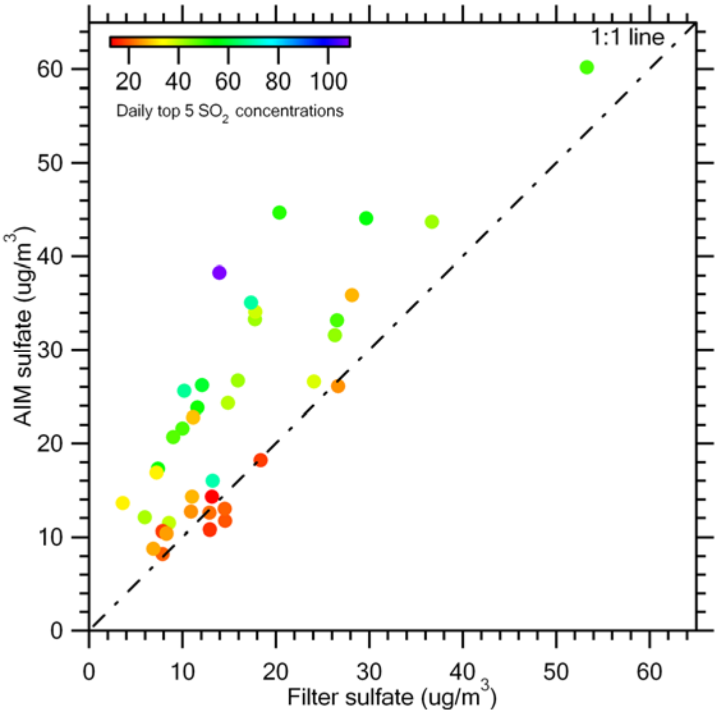

Although a denuder was installed in the AIM to remove interfering gases such as SO_2, it appeared that the SO_2 levels in the site near Shanghai were so high that the gas could not be completely removed and thus penetrated the denuder. SO_2 would then dissolve in water and undergo oxidation to become sulfate during the one-hour sampling stage resulting in larger sulfate values in the AIM. Laboratory tests after the field studies have confirmed the breakthrough of SO_2: when 80ppbv of SO_2 standard was introduced to the sample inlet, about 2% of SO_2 was converted to sulfate.

In Beijing, the average concentrations of SO_2 were 6ppbv with standard deviations of 7ppbv. There were only four days that had the hourly SO_2 greater than 30ppbv. Therefore, interference from SO_2 in Beijing was minimal.

Furthermore, the same problem was also occurred in Tsuen Wan, Hong Kong. As shown previously, when the concentrations of SO_2 were high, the AIM showed much higher sulfate values than the APSN (Figure 6.5). This was in conjunction with the measurement results in Shanghai. Therefore, the results in Tsuen Wan could further confirm the interference of SO_2 to the AIM.

6.2.3.2 Laboratory test confirming the interference of SO_2 to the AIM

In previous section, field measurement data has been used to illustrate the effect of high concentrations of SO_2 to the positive sulfate artifact in the AIM. Apart from the field measurement data, lab experiments have been performed to further verify the SO_2 effect.

The first experiment is done by using 20mL Milli-Q water. The water is then purged with 40ppbv and 80ppbv SO_2 for 1 hour. After that, the water is injected into the anion IC at different time period. The experiment has been done for 48 hours. Figure 6.21 showed the results of the sulfate production at 40ppbv and 80ppbv SO_2 at different time period.

Figure 6.21. The results of the sulfate production at 40ppbv and 80ppbv SO_2 at different time period.

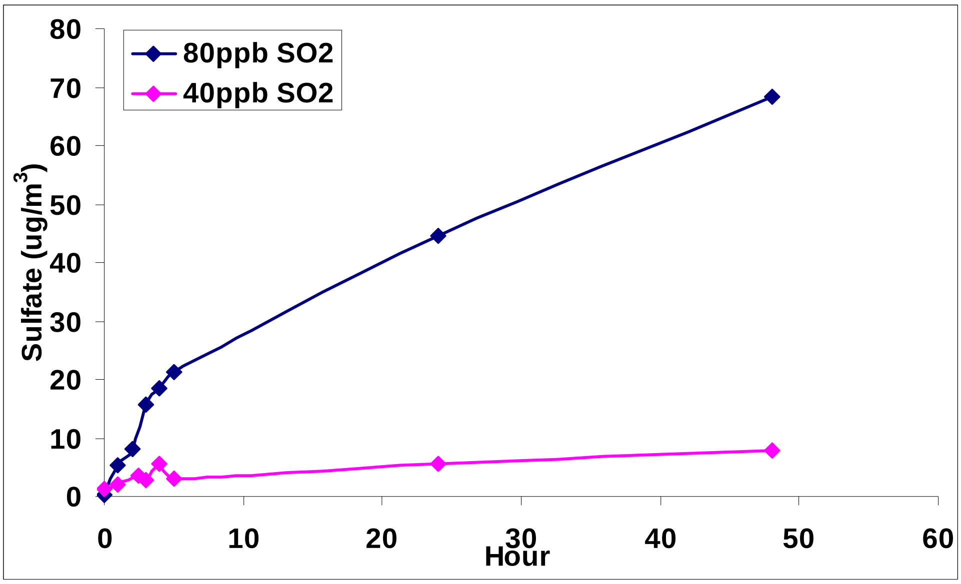

From the above results, we could see that using different levels of SO_2 purging the water, different amount of sulfate was formed at the same time interval. For instance, injecting the samples after 1 hour, 5μg/m^3 and 2μg/m^3 of sulfate were formed for purging with 80ppbv and 40ppbv SO_2, respectively. After 48 hours, sulfate could even reach to around 70μg/m^3 and 8μg/m^3 for purging with 80ppbv and 40ppbv SO_2, respectively. It should be noted that the AIM would not retain the samples for such a long period of time. This experiment is conducted for 48 hours because I wanted to explore the production of sulfate after substantial time period.

In addition to the sulfate peak present in the chromatogram, there were one additional peak present which showed high abundant (according to the peak area) in the beginning (immediately after purging). After that, the peak area decreased continuously during the experiment. I suggested that this peak was most possibly the bisulfate (HSO_3^-) peak, which was the intermediate product for forming sulfate from SO_2 in the aqueous phase reaction. Due to the lack of the HSO_3^- standard, this point could not be further identified.

The second experiment is done by purging the sample inlet of the AIM continuously with 80ppbv SO_2. This experiment is resembled to the actual sampling of the AIM, except continuously injecting high concentrations of SO_2. The experiment has been done for 6 hours. Figure 6.22 showed the results of the sulfate production at different time periods.

Figure 6.22. The results of the sulfate production at different time periods.

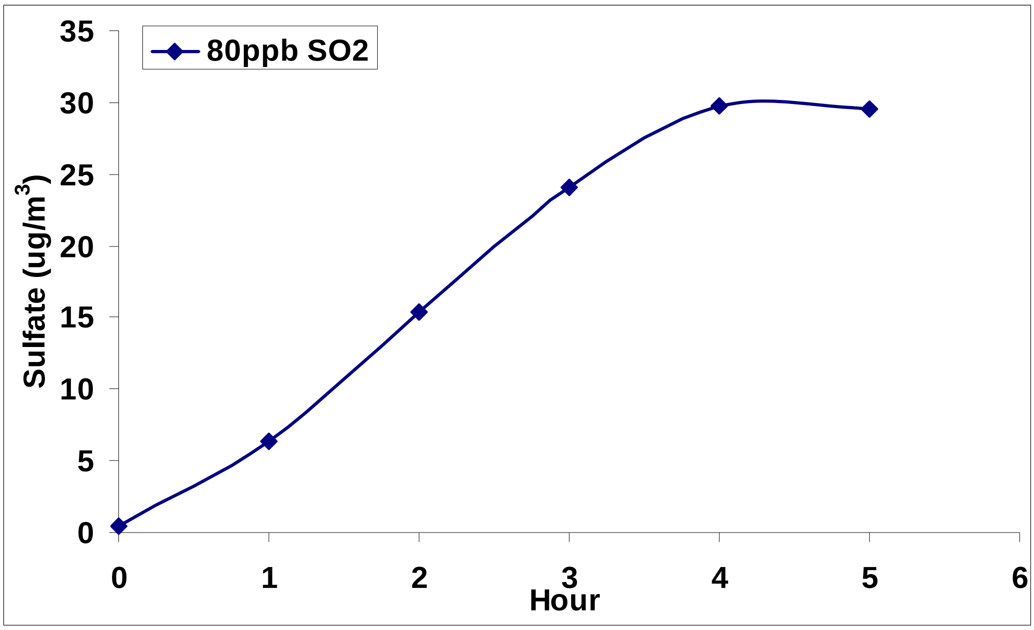

With the continuous purging of the high concentrations of SO_2, sulfate was formed in the AIM (Figure 6.22). At 0 hour (immediate after purging for 1 hour of SO_2), the sulfate concentration was low (about 0.5µg/m^3). However, when purging 80ppbv SO_2 continuously, the sulfate concentrations increased steadily to about 30µg/m^3. This result suggested that time is required for the production of sulfate in the AIM. This experiment was similar to the measurements conducted in Hong Kong and Shanghai. Because the SO_2 plume in the atmosphere usually kept at high levels for several hours so that sulfate could be formed in the AIM just like the above experiment. Conversely, this experiment could also confirm the results in Hong Kong and Shanghai. When the concentrations of SO_2 were high, the removal efficiency of SO_2 for the denuder in the AIM was not good enough so that penetration of SO_2 through the denuder is occurred. If the ambient levels of SO_2 remained high for several hours, the effect of the sulfate production was much more prominent.

6.2.4 Comparison of other ions in Shanghai and Beijing

6.2.4.1 Other ions in Shanghai

The comparison of ions other than sulfate and nitrate has also been performed. Figures 6.23 and 6.24 showed the comparison results of the AIM ammonium and calcium with the filter measurements in Shanghai. Other ions such as fluoride, phosphate, bromide, magnesium, lithium, nitrite are not detected due to the low ambient concentrations of these ions. Moreover, some ions such as chloride, sodium are interfered by the unknown board large peak that was present in the chromatogram, thus the comparison of these ions were not possible. The correlations of the AIM calcium and ammonium with the filter measurements were not good with $R^2 < 0.4$. The poor correlation of calcium was mainly due to the low ambient concentrations of this ion. The low concentrations of calcium made the comparison complicated because small derivation between the two measurements will largely affect the result of the correlation. In contrast, the moderate correlation of ammonium was due to the presence of some scattered points. The slope and intercept between the AIM and the filter measurement were 0.52 and 2.47, respectively for ammonium, and 0.55 and 0.42, respectively for calcium. This meant that the comparison results of the AIM with the filter measurements had some difference.

Figure 6.23. The comparison of the AIM ammonium with the filter ammonium in Shanghai.

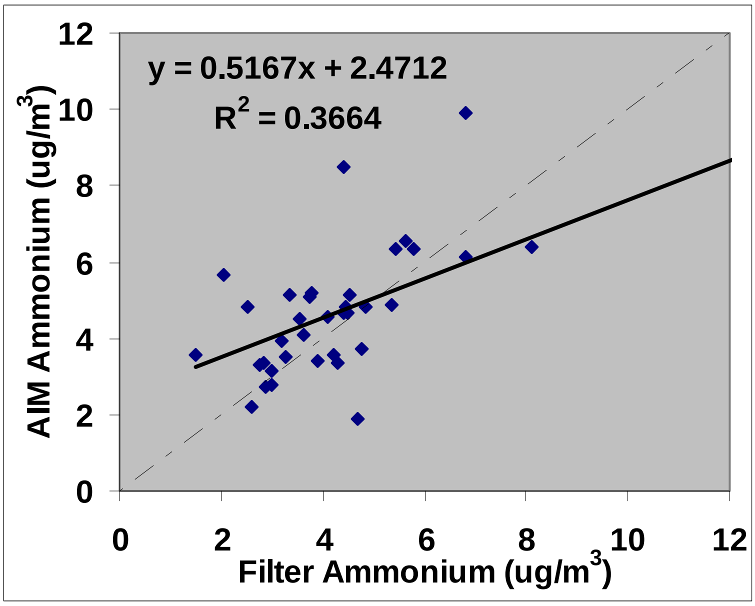

Figure 6.24. The comparison of the AIM calcium with the filter calcium in Shanghai.

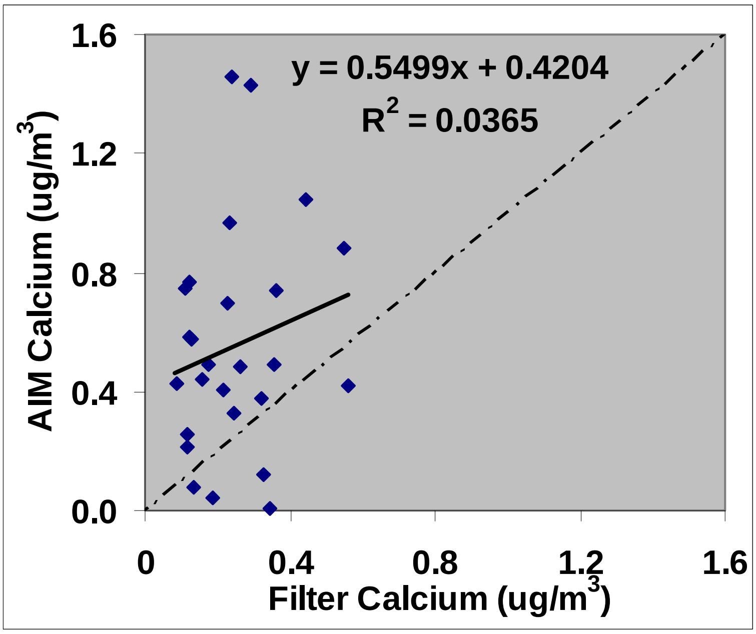

6.2.4.2 Other ions in Beijing

The comparison of other ions in Beijing has also been made. Figures 6.25 – 6.29 showed the comparison results of the AIM calcium, potassium, ammonium, magnesium, and sodium with the filter measurements in Beijing.

Other ions such as fluoride, phosphate are not detected due to the low ambient concentrations of these ions. Among the comparisons of these five ions, the correlations of potassium and ammonium were good with $R^2 > 0.84$, the correlation of magnesium was moderate ($R^2 = 0.59$), and the correlations of calcium and sodium were poor with $R^2 < 0.1$. The poor correlations of calcium and sodium were mainly due to the low ambient concentrations of these respective ions. As mentioned before, these low concentrations of ions made the comparisons complicated. The slopes of the comparisons of these ions ranged from 0.76 to 1.24, while the intercepts are approached to 0.

Figure 6.25. Comparison result of the AIM calcium and the filter calcium in Beijing.

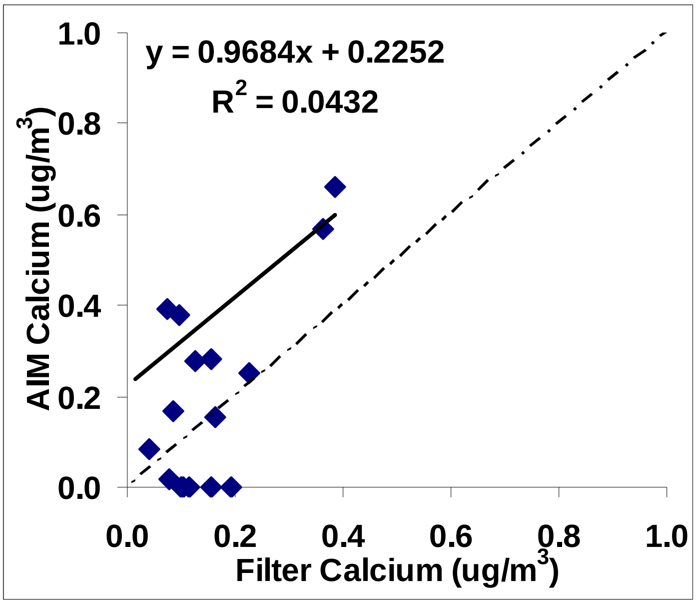

Figure 6.26. Comparison result of the AIM potassium and the filter potassium in Beijing.

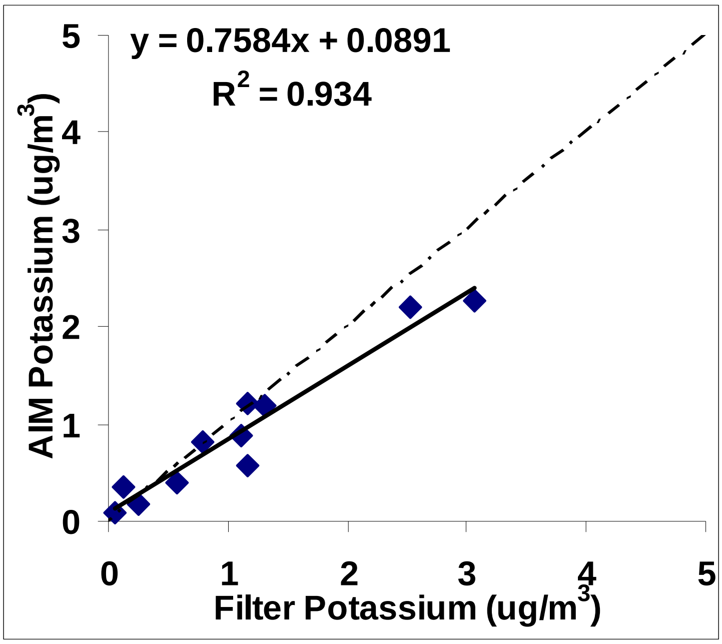

Figure 6.27. Comparison result of the AIM ammonium and the filter ammonium in Beijing.

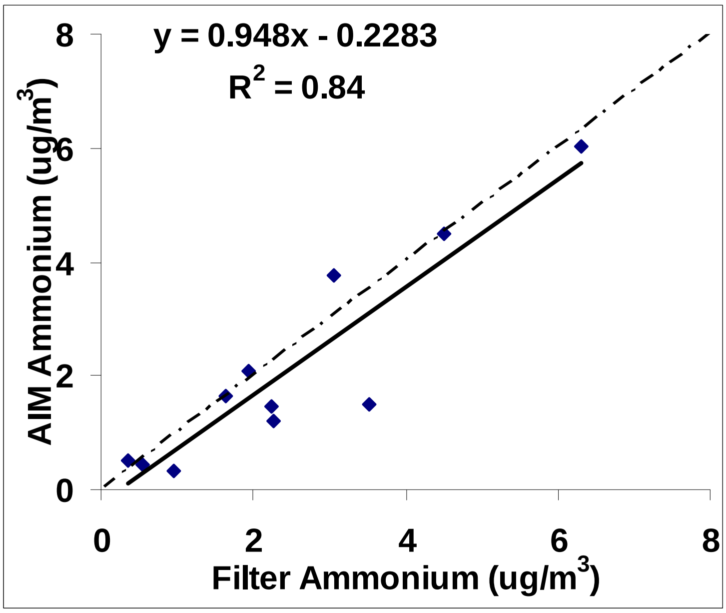

Figure 6.28. Comparison result of the AIM magnesium and the filter magnesium in Beijing.

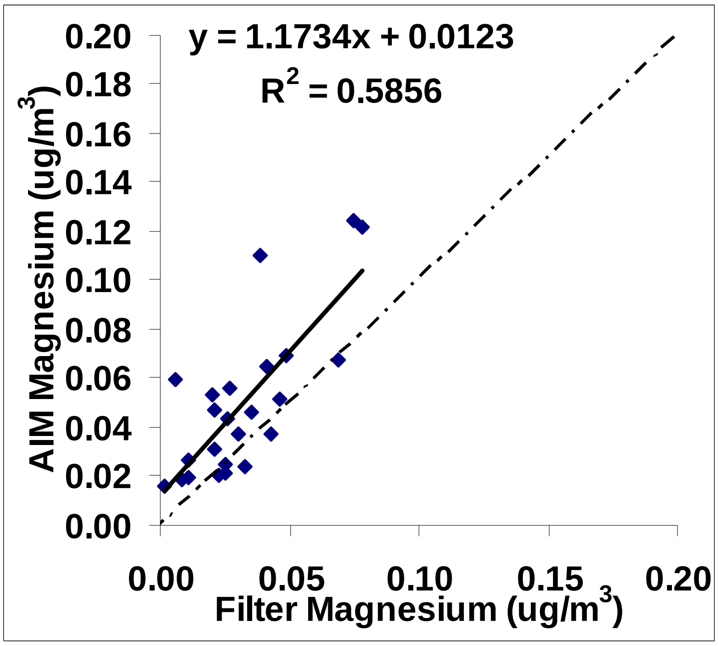

Figure 6.29. Comparison result of the AIM sodium and the filter sodium in Beijing.

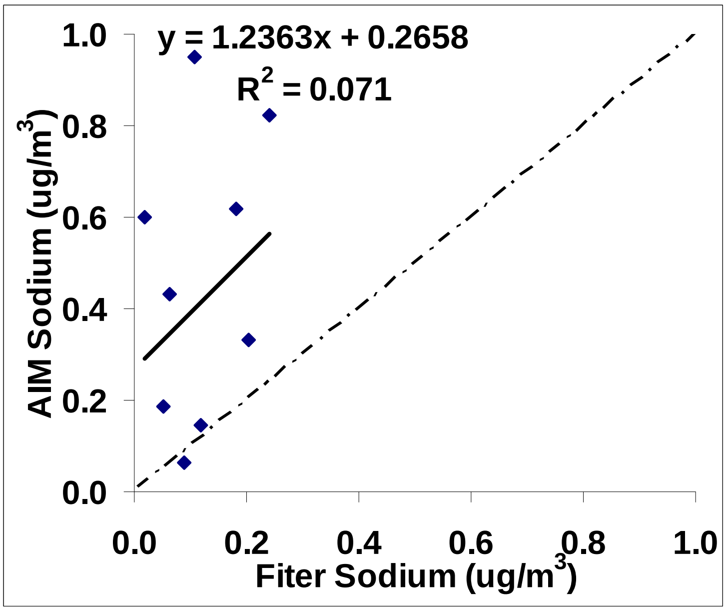

6.3 Suggestions for the improvement of the AIM

Several modifications of the AIM are suggested here to improve its performance under conditions of:

(a) High particulate concentrations

(1) Decrease the flow rate of the AIM: To reduce the amount of water-soluble ions entering the instrument.

(2) Increase the rate of water supply to the steam generator: To enhance capacity for dissolving water-soluble ions.

(b) High SO_2 concentrations

(1) Use a larger denuder.

(2) Put another denuder upstream in series.

(3) Use H_2O_2 or an alkaline solution as opposed to pure water in the denuder.

All the above suggestions in (b) are to increase the efficiency of the liquid diffusion denuder in removing interfering gases such as SO_2.

6.4 Data correction of the AIM

6.4.1 Hong Kong

As there was no filter measurement data in Hong Kong, data correction could only be made to sulfate during high SO_2 concentrations. Here, the assumption has been made. The AIM will be affected by SO_2 at the same level as that in Shanghai. Thus, the sulfate data in Hong Kong is removed at SO_2 concentrations greater than 30ppbv. For the nitrate data in Hong Kong, no correction has been made.

6.4.2 Shanghai

For the sulfate data in Shanghai, the data with the SO_2 concentrations greater than 30ppbv are not used. After this deletion, the AIM sulfate were well correlated ($R^2 = 0.89$) with filter sulfate with the RMA slope and intercept of

0.95 and 1.41, respectively. Figure 6.30 showed the comparison result of the AIM sulfate and the filter sulfate in Shanghai after correction.

Figure 6.30. Comparison result of the AIM sulfate and the filter sulfate in Shanghai after correction.

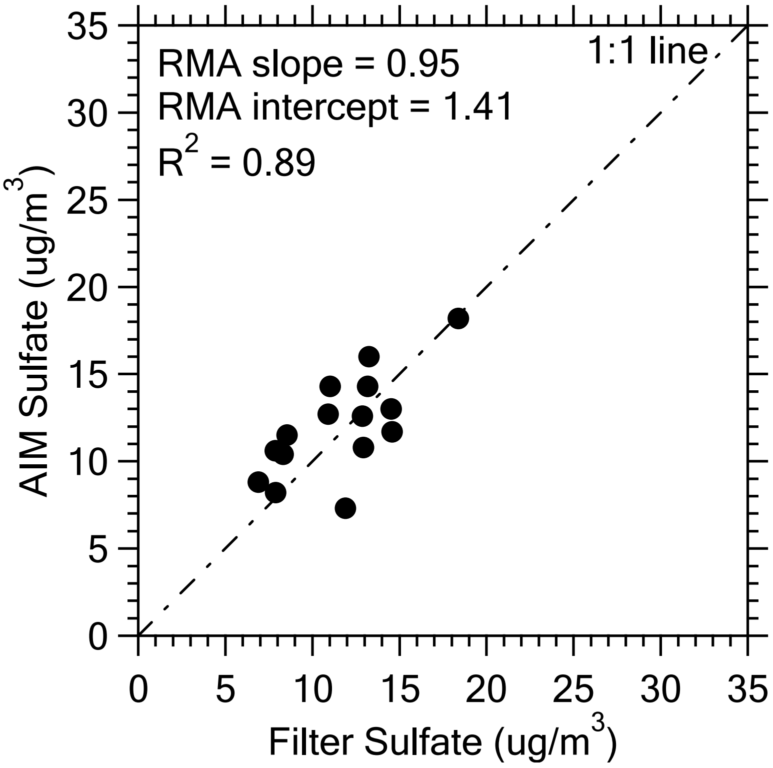

As the comparison result between the AIM nitrate and the filter nitrate was good (R^2 = 0.96, AIM nitrate = 0.83 x filter nitrate + 0.00) in Shanghai, the nitrate data in Shanghai is not corrected.

6.4.3 Beijing

From the previous discussion, we could see that the semi-continuous sulfate and nitrate data in Beijing had its problem during high sulfate and nitrate levels. In order to use the data more accurately, the AIM sulfate and nitrate data at high ion loadings in Beijing have been corrected based on the regression results assuming that the filter-based measurements were accurate at high aerosol loadings. Figure 6.31 showed the scatter plot between the AIM sulfate and the filter sulfate before and after correction, while Figure 6.32 showed the nitrate result before and after correction. The adjusted AIM sulfate and nitrate yielded an overall good correlation ($R^2 > 0.90$) with the regression equations of AIM = 1.01 x filter – 0.5 for sulfate, and AIM = 0.91 x filter + 0.1 for nitrate.

Figure 6.31. The scatter plot between the AIM sulfate and the filter sulfate before and after correction.

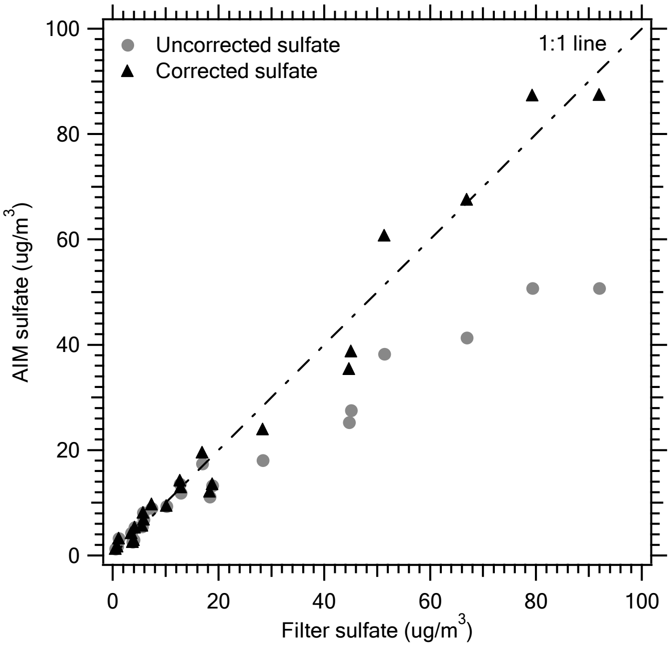

Figure 6.32. The scatter plot between the AIM nitrate and the filter nitrate before and after correction.

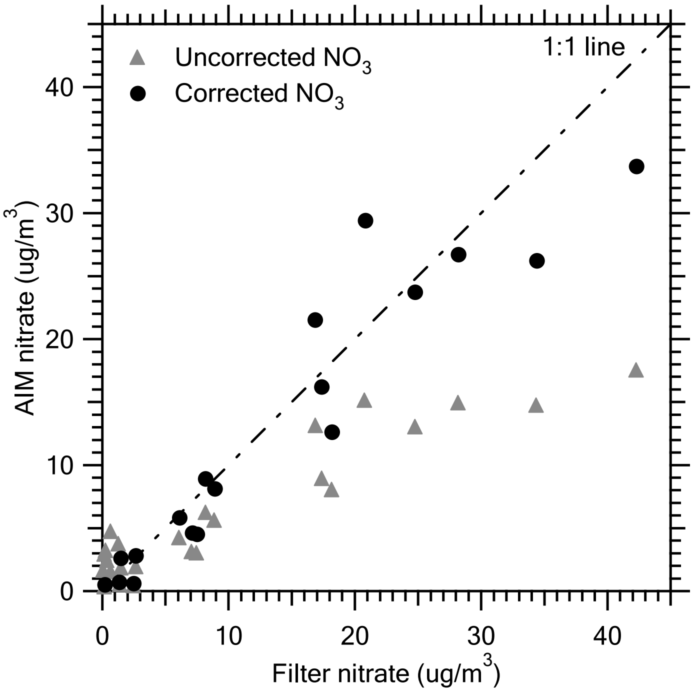

6.5 Data correction of the TEOM

Figures 6.33 and 6.34 showed the comparisons between the $PM_{2.5}$ mass concentrations obtained from the filter measurements and the TEOM instrument in Shanghai and Beijing, respectively. In both Shanghai and Beijing studies, the two methods are found to give similar results. The correlations between the two instruments were excellent in Shanghai and Beijing with r^2 of 0.98 and 0.98, respectively. However, the $PM_{2.5}$ mass obtained from the filter measurements was larger than that from the TEOM instrument with the slopes of 1.19 and 1.35, respectively in Shanghai and Beijing. This difference was due to the loss of the volatile particles such as nitrate when passing through the 50^oC chamber in the TEOM instrument. Moreover, the difference of the slope between the two studies indicated the difference of the existence of the volatile species in these two sites. Based on the above results, the correction factors (1.19 for Shanghai and 1.35 for Beijing) have been applied to the results obtained from the TEOM instrument.

Figure 6.33. Correlation of the $PM_{2.5}$ mass concentrations in Shanghai obtained from the filter measurements and the TEOM instrument.

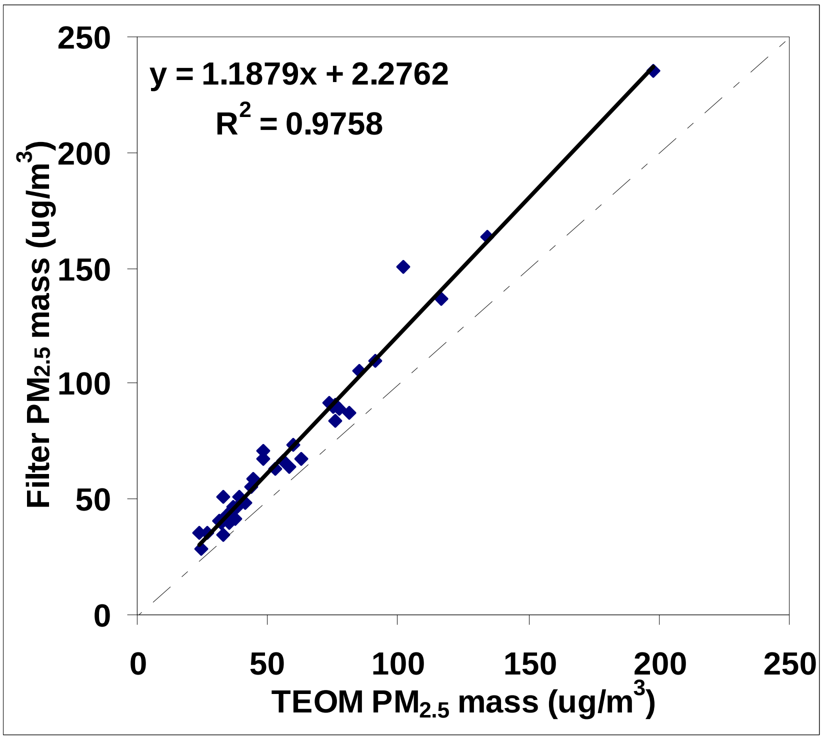

Figure 6.34. Correlation of the $PM_{2.5}$ mass concentrations in Beijing obtained from the filter measurements and the TEOM instrument.

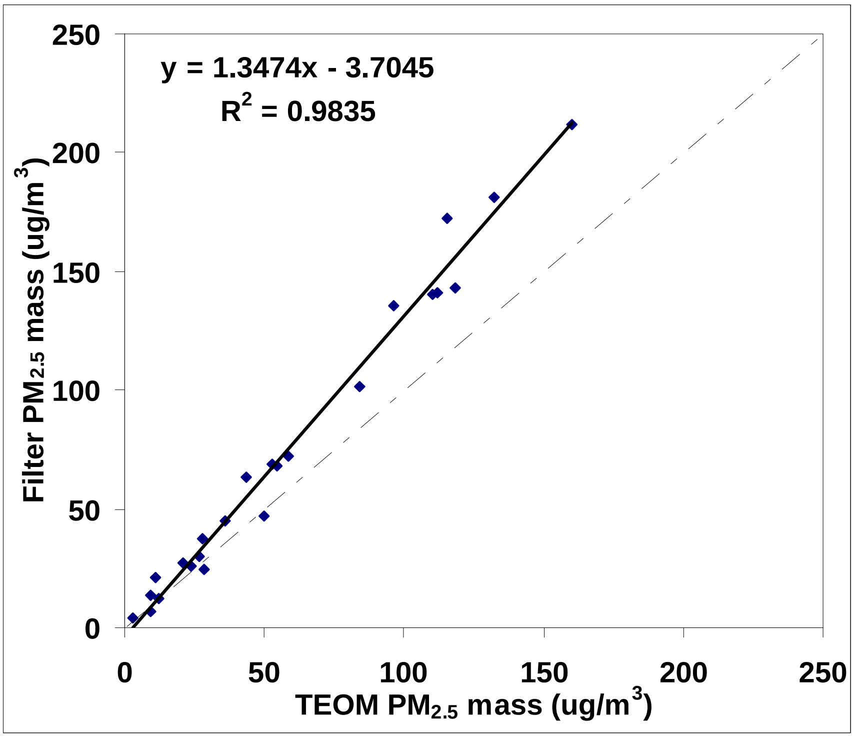

Figure 6.35 also showed the comparison between the $PM_{2.5}$ mass concentrations obtained from the filter measurements and the TEOM instrument as conducted in Lanzhou. The correlation between the two methods was still good (R^2 = 0.71), but it was worse than the Beijing and Shanghai studies. This was possibly due to the unique environment in Lanzhou combined with the fundamental measuring errors of the TEOM instrument. As the air masses in Lanzhou changed abruptly from high concentrations to low concentrations or vice versa, the measurement of the TEOM instrument could not respond in such a short time period. Thus, the correlation result in Lanzhou was worse than the previous studies. The TEOM data of Lanzhou has not been corrected as the slope and the intercept of the comparison was 1.00 and 18.80, respectively.

Figure 6.35. Correlation of the $PM_{2.5}$ mass concentrations in Lanzhou obtained from the filter measurements and the TEOM instrument.

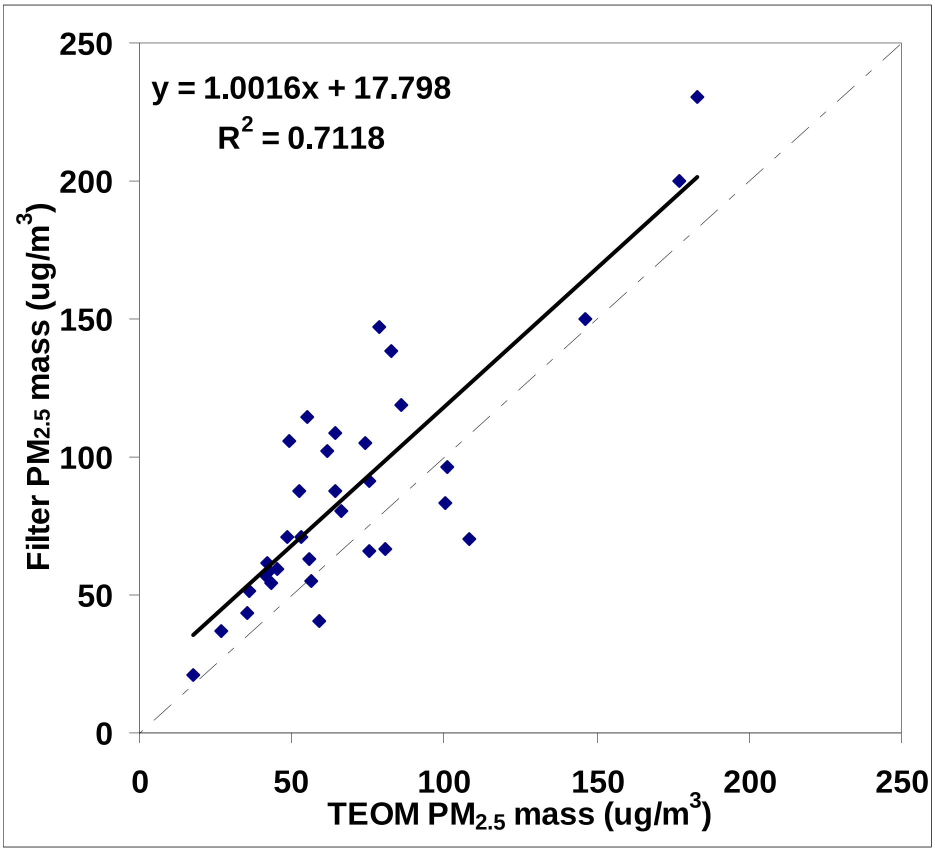

Chapter 7: Measurement results in Beijing, Shanghai, and Hong Kong

7.1 Beijing

7.1.1 Temporal variations and overall results

The time series of hourly concentrations of sulfate, nitrate, and $PM_{2.5}$ mass together with several trace gases (O_3, SO_2, and NO_y), and meteorological parameters (wind, relative and specific humidity, and solar radiation) are shown in Figure 7.1. Two kinds of wind data, surface observed wind and 950hPa National Centre for Environmental Prediction (NCEP) re-analysis wind (at 500m a.s.l.), are used to represent local and regional flow, respectively. Figure 7.1 indicated large day-to-day variations in the concentrations of fine particles and trace gases during the measurement period, which was strongly associated with the changes in meteorological conditions.

Figure 7.1. Time series of hourly concentrations of trace gases (SO_2, NO_y, and O_3), aerosols (sulfate, nitrate, and $PM_{2.5}$ mass), and meteorological parameters [solar radiation, surface wind at the site, NCEP 950hPa re-analysis wind, relative humidity (RH), and specific humidity (SH)].

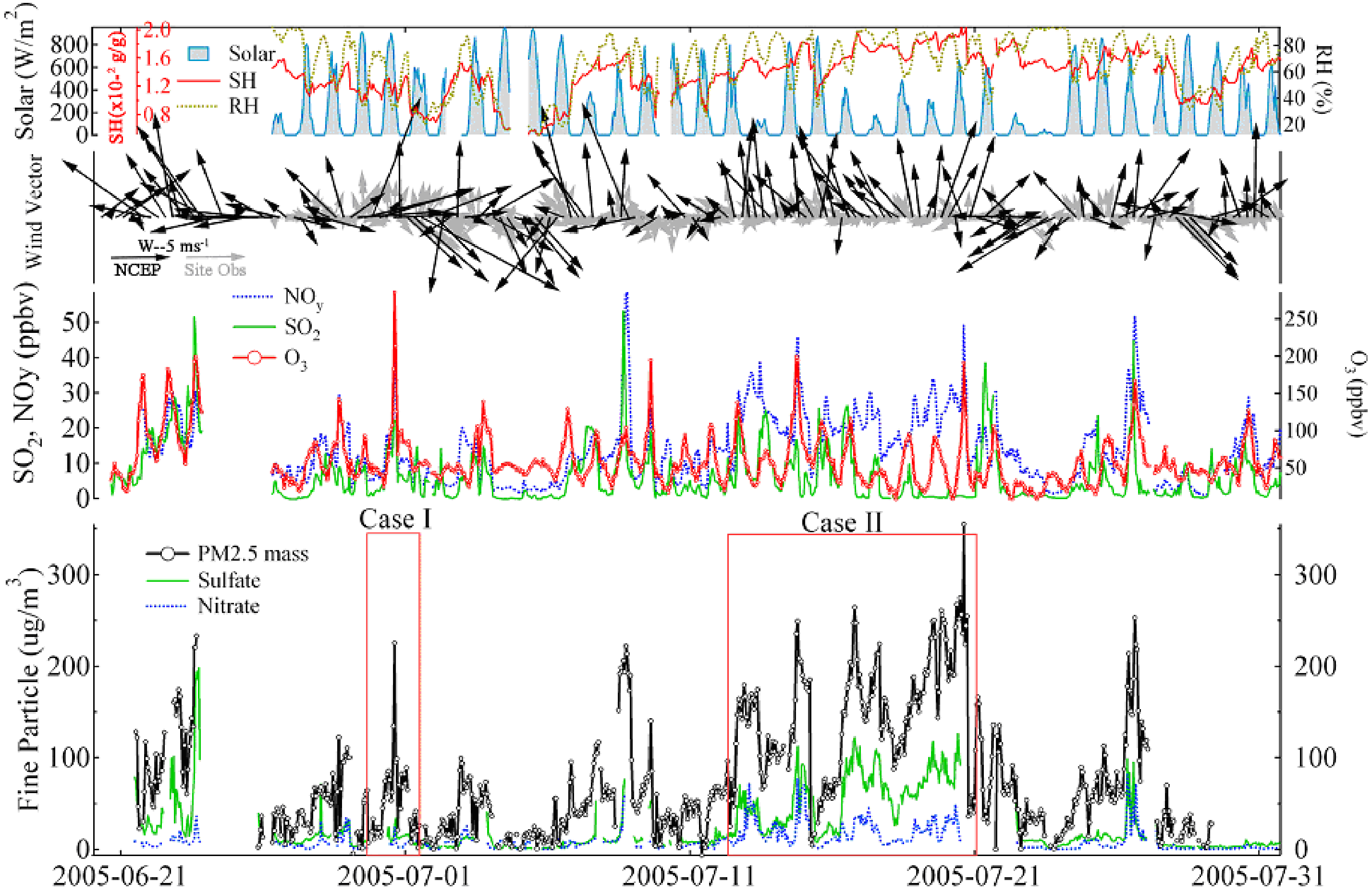

The synoptic weather condition in the study period is characterised by the frequent influence of summer monsoons, which brought humid air from the Pacific, bringing cloudy weather, even storms, to Beijing [Wang et al., 2006]. The southerly monsoons often carried regional air pollutants from the North China Plains (NCPs) mixed with Beijing's urban plumes to the site. A continuous southerly monsoon over several days gave rise to very high concentrations of both primary and secondary pollutants. For example, on 12 – 20 July, when the 950hPa wind continuously blew from the south (see Figure 8.1), the concentrations of $PM_{2.5}$ mass were above 100μg/m^3 for most of the time. Sulfate levels also reached over 50μg/m^3 along with other trace gases, and the daily 1-hour ozone was often above 100ppbv. Several shorter episodes (lasting 1 – 3 days) on 21 – 23 June, 30 June, 6 – 7 July, and 25 – 26 July, were also associated with the southerly winds. In comparison, continental air masses originated from Siberia occasionally impacted the site, with strong north-westerly or north-easterly winds bringing in air with low concentrations of aerosols and trace gases (1 – 2 July, 4 – 6 July, 22 – 24 July, and 30 – 31 July). In these few days, very low concentrations of aerosols (<10μg/m^3 for sulfate, nitrate, and <25μg/m^3 for $PM_{2.5}$ mass) as well as trace gases (CO, SO_2, NO_y) are obtained. The data on these days can be considered as the background for Beijing and the NCPs during the summer.

The mean hourly concentrations (± standard derivation) of sulfate, nitrate, and $PM_{2.5}$ mass from this study were 24.3 (±30.6)μg/m^3, 9.7 (±12.5)μg/m^3, and 79.3 (±65.4)μg/m^3, respectively. These values were much higher than those reported in rural or even urban areas of the United States. For example, Rattigan et al. (2006) reported the average sulfate and nitrate concentrations of 5.1μg/m^3

and 1.3μg/m^3, respectively, in an urban site of New York city. Hu et al. (2002) reported the average sulfate and nitrate concentrations of 21.4μg/m^3 and 14.7μg/m^3, respectively on the campus of Peking University (about 40km from the present site) in June – July 2000, and Wang et al. (2005) found the mean values of $PM_{2.5}$ mass, sulfate, and nitrate of 93.3, 18.4, and 11.2μg/m^3, respectively in the summer season from 2001 – 2003 in Beijing. The similar values of our measurement to the urban / suburban results suggested that fine aerosol pollution in Beijing has not been improving in the past few years, and that it existed beyond the urban centre. In our study, the maximum hourly $PM_{2.5}$ mass, sulfate, and nitrate were 355.1μg/m^3, 198.3μg/m^3, and 81.5μg/m^3, respectively. These extremely high particulate loadings would seriously impair visibility and may also affect the regional climate. On average, sulfate and nitrate contributed to 31% and 12%, respectively of total $PM_{2.5}$ mass.

To explore the relative importance of mobile source versus stationary source, the mass ratio of nitrate / sulfate could be used [Arimoto et al., 1996; Xiao and Liu, 2004]. High nitrate / sulfate mass ratio represents the predominance of mobile source over stationary source of pollutants [Wang et al., 2005]. During this six-week intensive measurement, the average nitrate / sulfate ratio was 0.64 (standard derivation: 1.17). This value was comparable to the measurement conducted in Beijing in 2001 – 2003 with the average value of 0.71 [Wang et al., 2005], and in 1999 – 2000 with the average value of 0.58 [Yao et al., 2002]. This result suggested that mobile sources such as vehicle emissions would be dominant pollution sources in Beijing. However, on some days such as 21 – 23 June, and 14 – 18 July during the pollution plume events, the nitrate /

sulfate ratio showed much lower values (< 0.2), which implied the significant contribution of the stationary sources (e.g. steel factories) to the sampling site.

7.1.2 Diurnal profiles of sulfate, nitrate, and $PM_{2.5}$ mass

The average diurnal variations of sulfate, nitrate, and $PM_{2.5}$ mass over the entire study period are shown in Figure 7.2. The continuous line with vertical bars represented the mean and the standard errors of respective particulates. The dotted line represented the corresponding median value. According to the figure, $PM_{2.5}$ mass showed a distinctive diurnal profile. This pattern was similar to other trace gases (e.g. NO_y and SO_2, Figure not shown) conducted at the same time as reported by Wang et al., 2006. The $PM_{2.5}$ mass concentrations increased steadily from the early morning and reached the maximum in the afternoon at around three and it showed the minimum at the night time. The afternoon maximum of the $PM_{2.5}$ mass is related to the transport of pollution from Beijing and other regional pollution by the mountain-valley breezes to the sampling site in the afternoon [Wang et al., 2006] and could be supported by the overall south-easterly winds at that time, while the $PM_{2.5}$ mass minimum is associated with the influence of the background air mass from the north-westerly wind direction.

Figure 7.2. Average diurnal variations of sulfate, nitrate, $PM_{2.5}$ mass, and vector wind at the site. The vertical bars represented the standard errors, and the dotted line represented the median value.

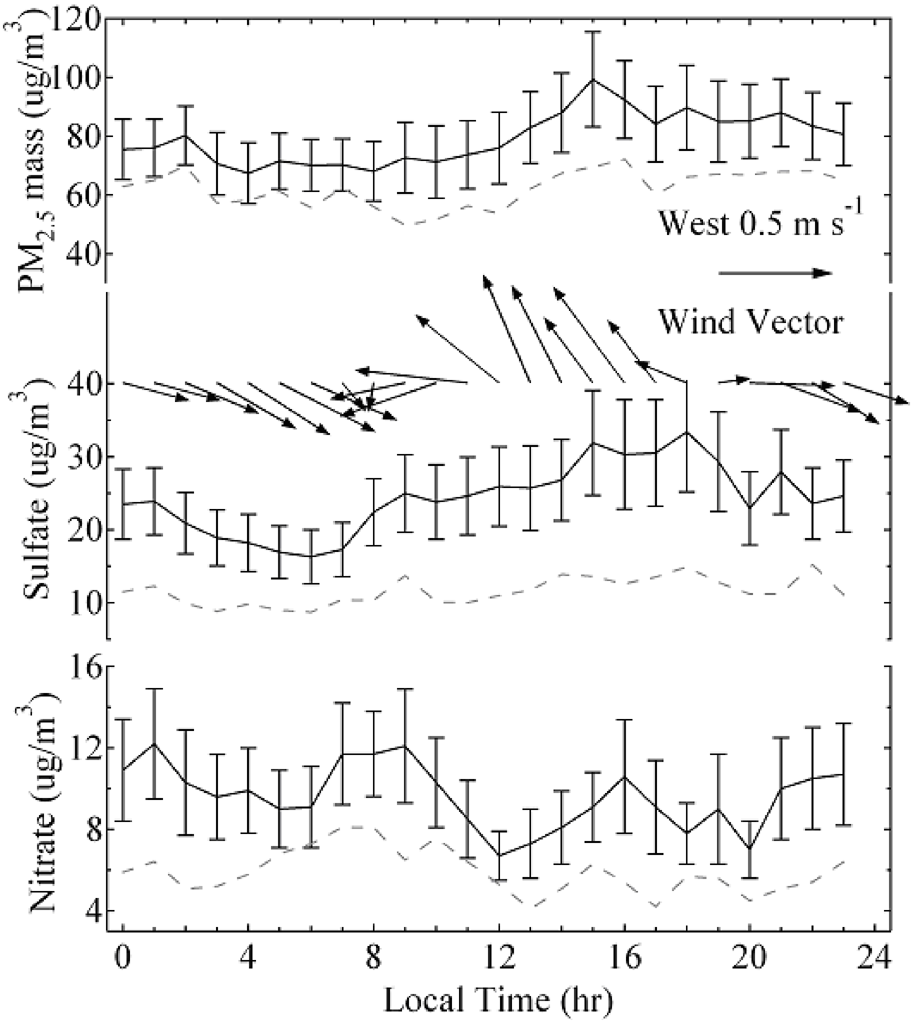

In contrast, sulfate showed no distinctive diurnal pattern. The difference between the daily maximum and minimum was only about 10µg/m^3 with the presence of large standard errors. Although the diurnal profile appeared to have maxima in the afternoon, they are actually caused by several high concentration pollution plumes reaching the site such as 23 June, 16 – 19 July. This could be more clearly indicated by the diurnal profile from the plot of median sulfate (dotted line), which showed the difference of less than 5µg/m^3 for the whole day. Edgerton et al. (2006) also reported the lack of the diurnal profile of sulfate at the urban and rural areas in US. This lack of diurnal pattern indicated a regional sulfate pollution problem in the Beijing area.

The diurnal profile of nitrate was different from trace gases with the maximum occurring in the morning. It appeared that it had the second maximum occurring in the afternoon. This second maximum was similar to sulfate and is caused by the high concentration pollution events. As shown from the median values, the afternoon maximum is removed after neglecting the plumes. At night, the nitrate concentrations kept rather constant. This pattern could be due to the equilibrium reaction between the nitric acid and ammonia as shown from the following equation:

$$HNO_3 + NH_3 \leftrightarrow NH_4NO_3$$ [Stelson and Seinfeld, 1982]

The above equation is sensitive to the change in temperature. When the temperature increases during daytime, the reaction would favour gas-phase nitric acid leading to a reduced aerosol nitrate. At night, the opposite is true. Thus, the observed diurnal pattern of nitrate would be consistent with the temperature pattern for the measurement period in which the temperature was high in the afternoon.

7.1.3 Other ions in Beijing

Figure 8.3 showed the overall time series of the ions other than sulfate and nitrate in Beijing. The overall average concentrations (± standard derivation) of ammonium, potassium, sodium, magnesium, and calcium were 3.2 (± 2.7)$\mu g/m^3$, 1.5 (± 1.9)$\mu g/m^3$, 0.5 (± 1.2)$\mu g/m^3$, 0.1 (± 0.1)$\mu g/m^3$, and 0.3 (± 0.5)$\mu g/m^3$, respectively. Ions such as lithium, fluoride are not detected in the whole study. Except sulfate and nitrate, ammonium was the most abundant ion.

According to Figure 7.3, the concentrations of ammonium, sodium, and potassium were high on 8 July, which was consistent with the high $PM_{2.5}$ mass, sulfate, and nitrate concentrations. Moreover, the concentrations of potassium ion were high on some days such as 23 June, 3, 7, and 8 July, which suggested the influence of the biomass burning in the study region. For the ions such as magnesium, calcium, the ion concentrations kept at relatively low levels for all days.

Figure 7.3. The overall time series of the ions other than sulfate and nitrate in Beijing.

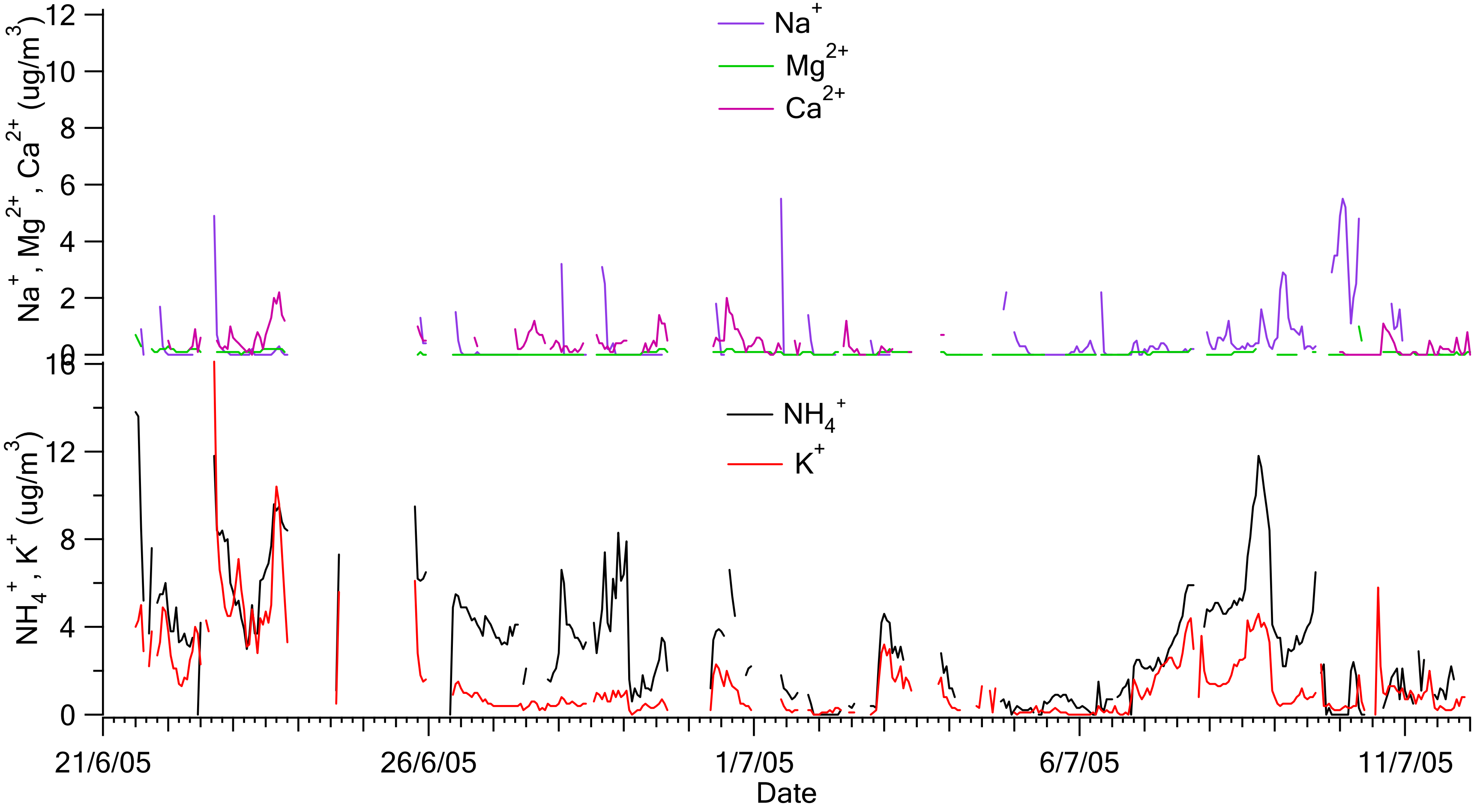

The diurnal profiles of ammonium and potassium are shown in Figures 7.4 and 7.5, respectively. Both potassium and ammonium showed the maximum in the afternoon. This afternoon maximum is related to the transport of pollution from the urban centre of Beijing and other regional pollution by the mountain-valley breezes to the sampling site in the afternoon [Wang et al., 2006] and can be supported by the overall south-easterly winds at that time.

Figure 7.4. The diurnal profile of ammonium in Beijing.

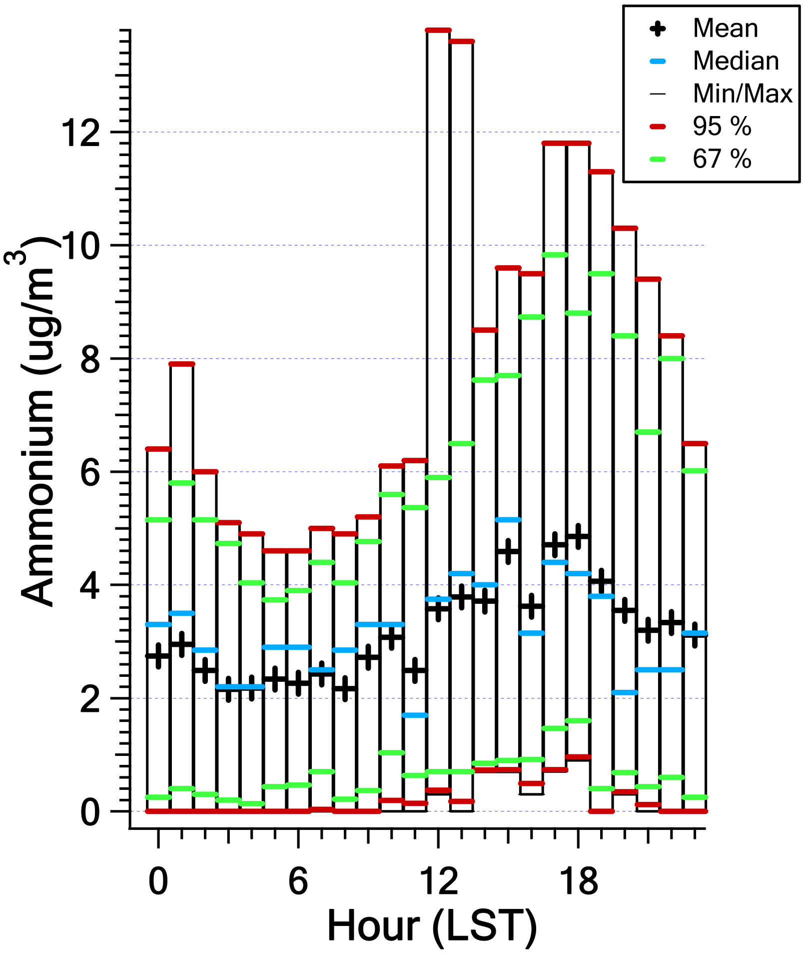

Figure 7.5. The diurnal profile of potassium in Beijing.

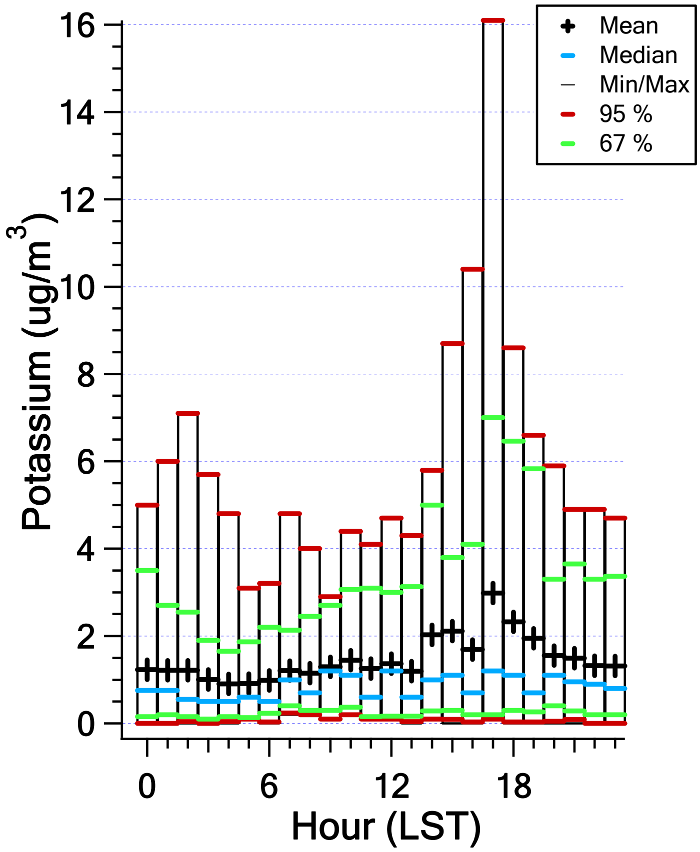

7.2 Shanghai

7.2.1 Temporal variations and overall results

Table 7.1 gave the statistics of sulfate, nitrate, SO_2, $PM_{2.5}$ mass, temperature, and relative humidity. The additional chemical data and the meteorological parameters could provide useful insights into the characteristics of the study site. The study site in Shanghai is surrounded by pollution sources in the Yangtze River Delta. The SO_2 concentrations were high (mean = 21.5ppbv), revealing the large impact of fresh emissions from coal-fired power plants in Shanghai. Moreover, the study site also suffered from severe fine aerosol pollution events. The average concentrations of sulfate, nitrate, and $PM_{2.5}$ mass were 17.9 (± 11.2)μg/m^3, 5.8 (± 7.4)μg/m^3, and 59.7 (± 47.4)μg/m^3, respectively. Yao et al. (2002) also reported similar result in Shanghai in which the concentrations of sulfate and nitrate were 15.9μg/m^3 and 6.8μg/m^3, respectively in the downtown of Shanghai. This again suggested that fine aerosols were not only the locally pollution problem, but also affected regionally. The maximum 1 hour sulfate and nitrate concentrations were 74μg/m^3 and 69μg/m^3, respectively with the maximum hourly $PM_{2.5}$ mass reaching to about 400μg/m^3. These extremely high particulate loadings would seriously impair visibility and may also affect the regional climate. On average, sulfate and nitrate contributed to 30% and 10%, respectively of total $PM_{2.5}$ mass.

Table 7.1. Statistics of sulfate, nitrate, SO_2, $PM_{2.5}$ mass, temperature, and relative humidity.

	Sulfate ($\mu g/m^3$)	Nitrate ($\mu g/m^3$)	SO_2 (ppbv)	$PM_{2.5}$ mass ($\mu g/m^3$)	Temperature (℃)	Relative humidity (%)
Average	17.9	5.8	21.5	59.7	22	65
St. Der.[a]	11.2	7.4	15.4	47.4	4	17
Median	15.7	3.5	17.7	46.8	22	66
Min.	1.1	0.2	1.9	1.8	13	21
Max.	74.4	69.1	155.7	396.4	33	95

[a] St. Der. stands for standard derivation.

The time series of hourly concentrations of sulfate, nitrate, and $PM_{2.5}$ mass together with several trace gases (CO, O_3, SO_2, NO, and NO_y) and meteorological parameters (temperature and relative humidity) are shown in Figure 7.6. Figure 7.6 indicated large day-to-day variations in the concentrations of fine particles and trace gases during the measurement period. For example, from 1 – 3 June, there was presence of consecutive ozone episodes (maximum ozone >120ppbv), in which the primary trace gases also reached to very high levels (CO >1000ppbv, SO_2 >40ppbv, NO_y >60ppbv), whereas the levels of $PM_{2.5}$ mass, sulfate, and nitrate were also very high. The high concentrations of gases and aerosols in these few days were possibly due to the transport of the urban plumes to the sampling location. Figure 7.7 showed the enlarged time series from 1 – 3 June and the respective trajectories at different time periods. We could see that when the concentrations of primary gases and aerosols were high, the trajectory results (the first left three) showed that the air masses are transported through the urban centre of Shanghai and then arrived at the sampling site. In contrast, in the afternoon of 3 June, the concentrations of all gases and aerosols were low. According to the trajectory result (the right one), the air masses did not pass through the urban centre of Shanghai and are mainly come from the ocean, thus the levels of all the species decreased. From this example, we could see that the high concentrations of the species were mostly due to the transport of the air masses through the urban centre of Shanghai.

Figure 7.6. Time series of hourly concentrations of trace gases (CO, SO_2, NO, NO_y, and O_3), aerosols (sulfate, nitrate, and $PM_{2.5}$ mass), and meteorological parameters [temperature (Temp) and relative humidity (RH)].

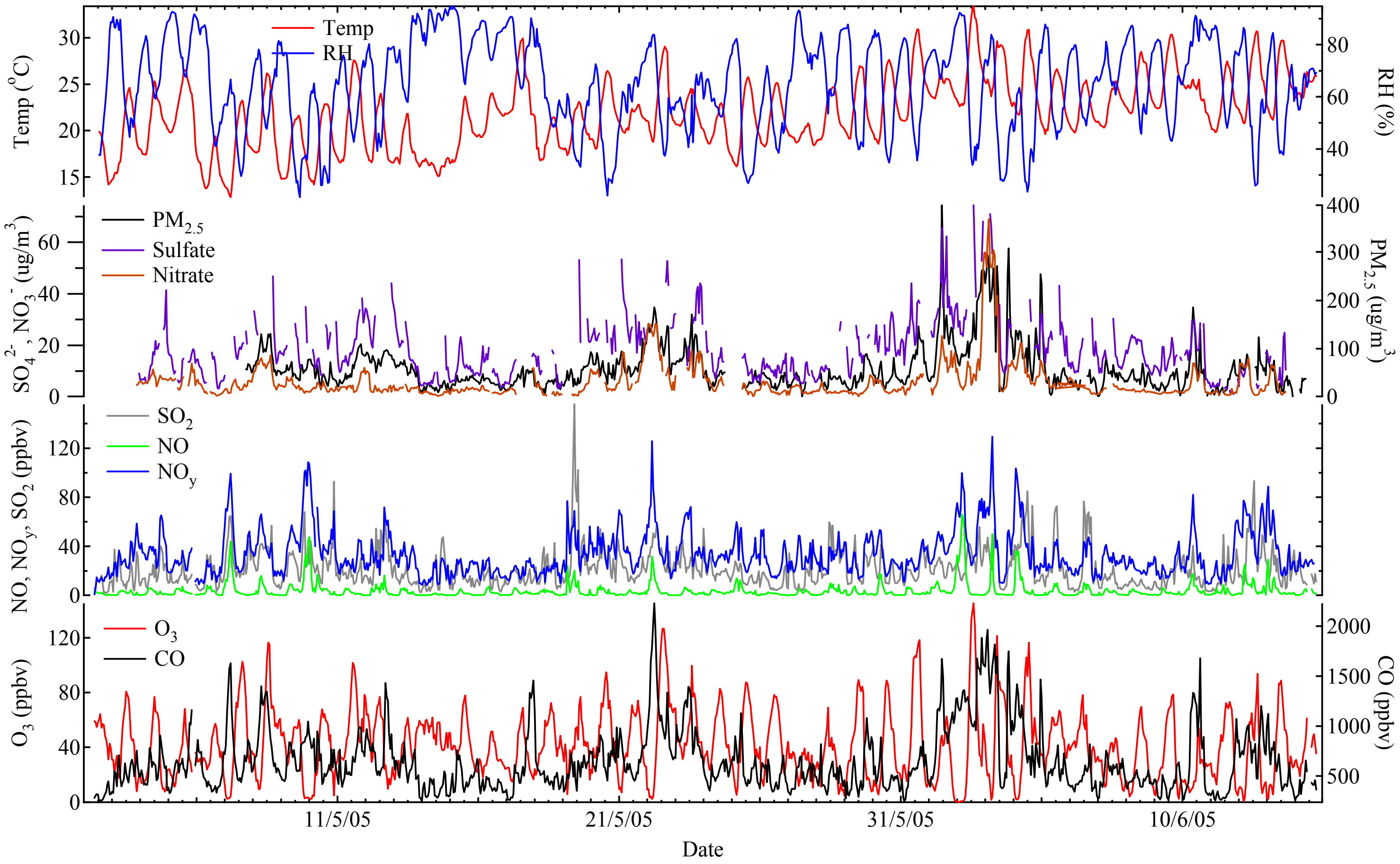

Figure 7.7. Time series of trace gases from 1 – 3 June and the respective trajectories at different time periods.

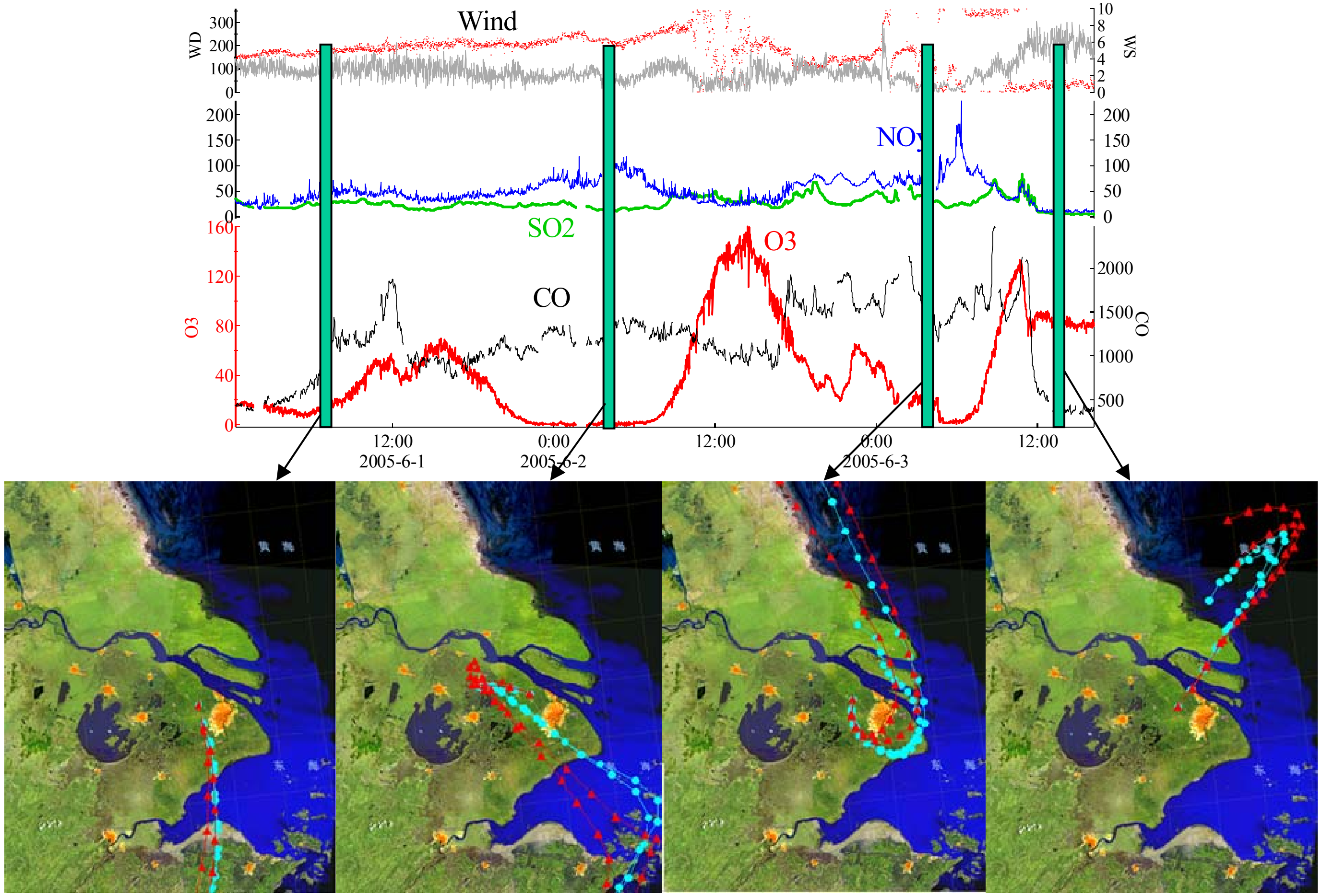

Apart from the days which showed high concentrations of aerosol loadings, some days had low abundance of aerosols such as 26 – 30 May. In these few days, the $PM_{2.5}$ mass was usually lower than 50μg/m^3, while sulfate and nitrate were lower than 10μg/m^3.

The mass ratio of nitrate / sulfate is presented here in order to explore the relative importance of mobile source versus stationary source [Arimoto et al., 1996; Xiao and Liu, 2004]. During this six-week intensive measurement, the average nitrate / sulfate ratio was 0.29 (standard derivation: 0.21). This result suggested that stationary sources such as emissions from power plants would be dominant pollution sources in Shanghai. However, in the nighttime of 11 June, the nitrate / sulfate ratio is raised to above 1, which implied the significant contribution of the mobile sources (e.g. vehicles) arriving to the sampling site.

7.2.2 Diurnal profiles of sulfate, nitrate, and $PM_{2.5}$ mass

The diurnal profiles of sulfate, nitrate, and $PM_{2.5}$ mass are shown in Figures 7.8 – 7.10. The sulfate concentrations were relatively stable over the course of a day. This result was similar to those reported by Wittig et al. (2004) in which they found that in spring, fall and winter, the sulfate concentrations were relatively stable during a day. Similarly, the nitrate concentrations also kept rather constant during the whole day (about 5 – 7μg/m^3). However, the nitrate concentrations showed little decrease (about 1 – 2 μg/m^3) in the afternoon. This could possibly due to the elevated temperature in which NH_4NO_3 undergone thermal decomposition, shifting nitrate into nitric acid. Thus, NO_3 concentrations declined in the afternoon. The same observation is also reported in Rattigan et al.

(2006) and Wittig et al. (2004), which conducted the measurements in New York and Pittsburgh, US, respectively.

Apart from sulfate and nitrate, $PM_{2.5}$ mass showed no distinctive diurnal profile. The daily $PM_{2.5}$ mass ranged from 65μg/m^3 to 80μg/m^3, which suggested that the fine particulate pollution was a regional pollution problem. The pollution problem was extremely serious all the times (greatly violate the US air quality standard) and would theatre the people living there.

Figure 7.8. The diurnal profile of sulfate in Shanghai.

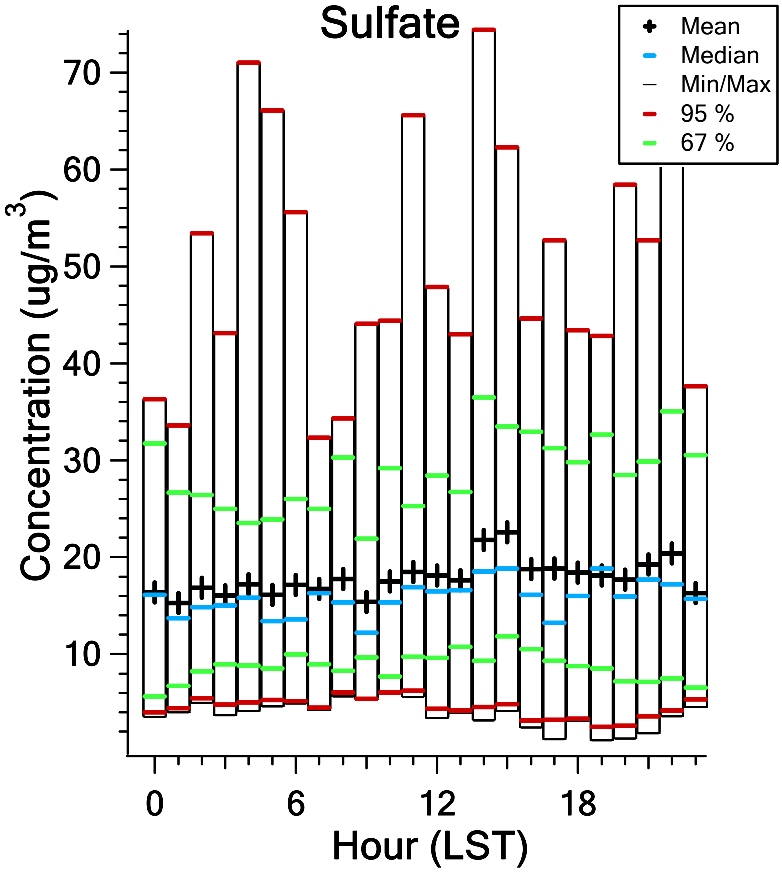

Figure 7.9. The diurnal profile of nitrate in Shanghai.

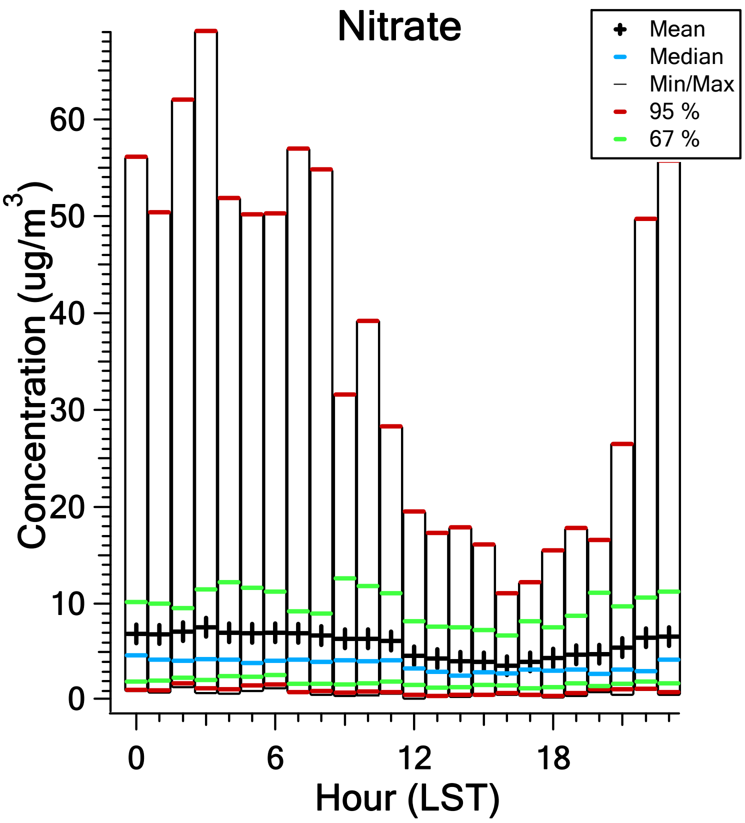

Figure 7.10. The diurnal profile of $PM_{2.5}$ mass in Shanghai.

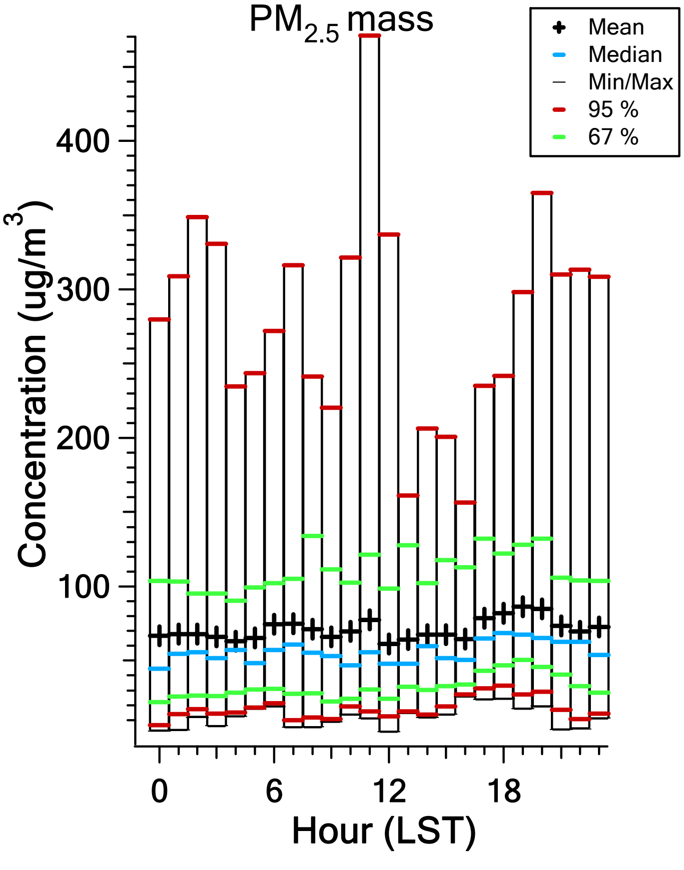

7.2.3 Other ions in Shanghai

Figure 7.11 showed the overall time series of the ions other than sulfate and nitrate in Shanghai. There were some missing data for both ions in the figure and is caused by either the instrument error or the unknown board peak present in the chromatogram. The overall average concentrations (± standard derivation) of ammonium, and calcium were 4.7 (± 2.5)μg/m^3, and 0.8 (± 0.6)μg/m^3, respectively. Other than sulfate and nitrate, ammonium was the most abundant ion. The ambient concentrations of ammonium varied from days-to-days. For instance, the ammonium concentrations were low (about 2 – 4μg/m^3) from May 9 to May 11. In contrast, it rose to over 10μg/m^3 in June 3. On that day, all the gaseous as well as particulate pollutants also reached to very high levels (refer to Figure 7.6).

Figure 7.11. The overall time series of calcium and ammonium in Shanghai.

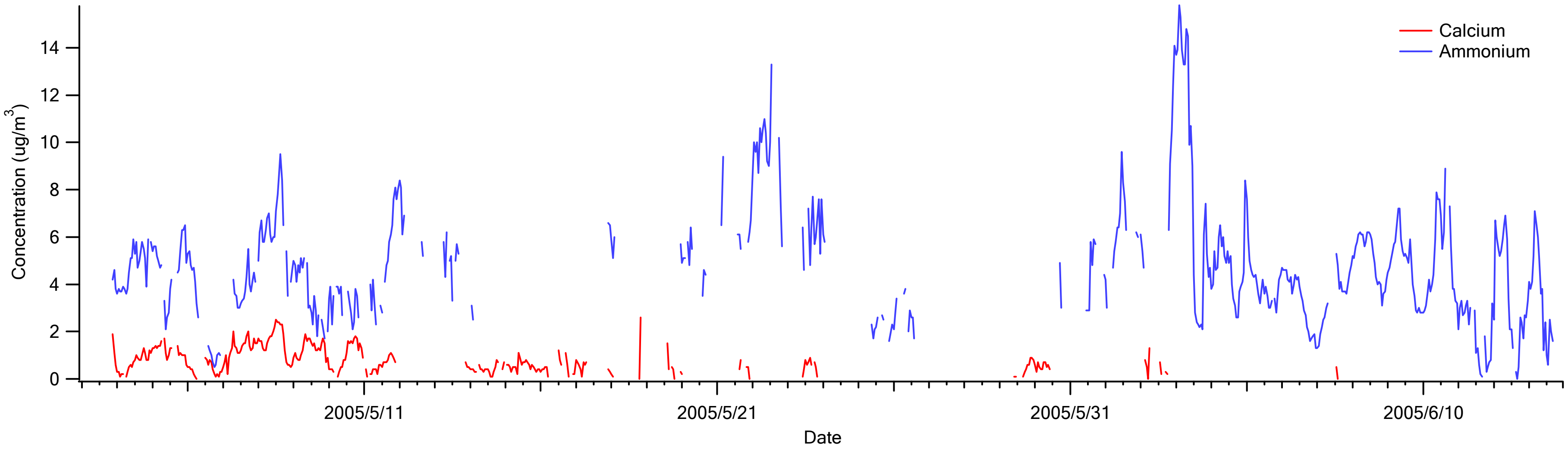

The diurnal profiles of calcium and ammonium are shown in Figures 7.12 and 7.13, respectively. The diurnal profile of calcium showed the minimum in the early morning and maximum in the afternoon. In contrast, the diurnal profile of ammonium was in reverse with the maximum occurring in the morning and minimum in the afternoon. The diurnal pattern of ammonium was similar to the diurnal profile of nitrate (Refer to Figure 7.9) and NO_y (Figure 7.14). The morning NO_y pulse most likely contributed to the ammonium peak. During elevated temperatures NH_4NO_3, however, undergone thermal decomposition, shifting ammonium into ammonia as shown in the following equation:

$$NH_4^+ \leftrightarrow NH_3 + H^+$$

Figure 7.12. The diurnal profile of calcium in Shanghai.

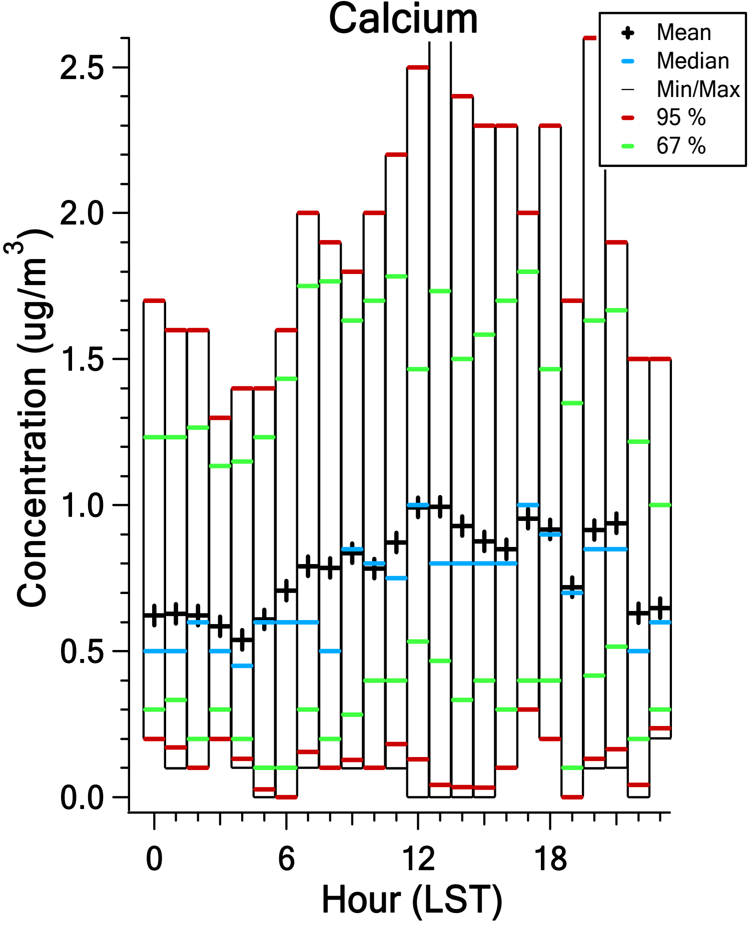

Figure 7.13. The diurnal profile of ammonium in Shanghai.

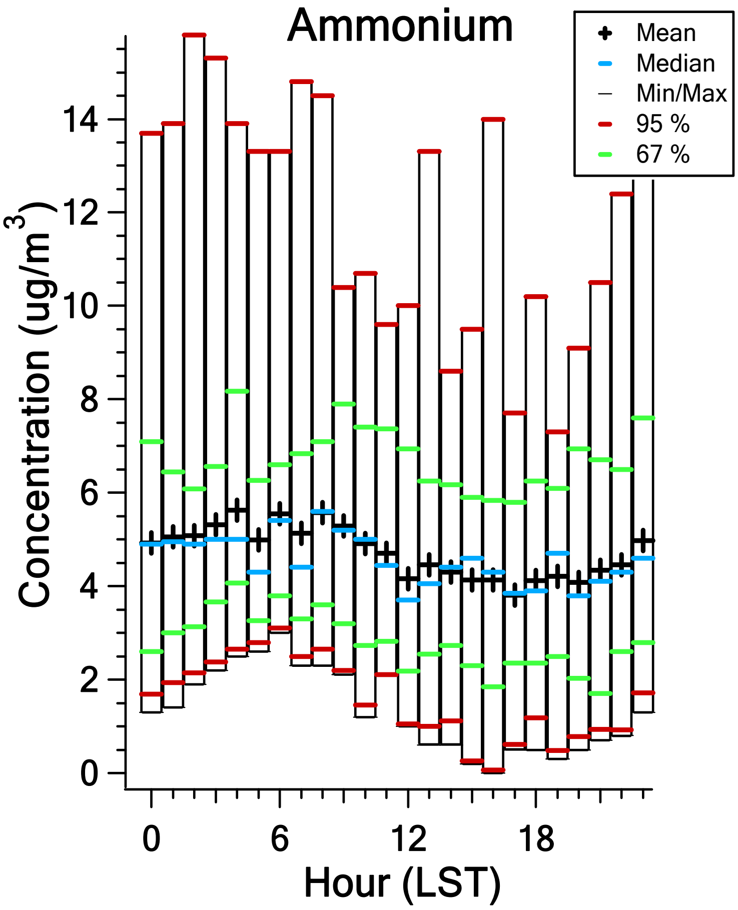

Figure 7.14. The diurnal profile of NO$_y$ in Shanghai.

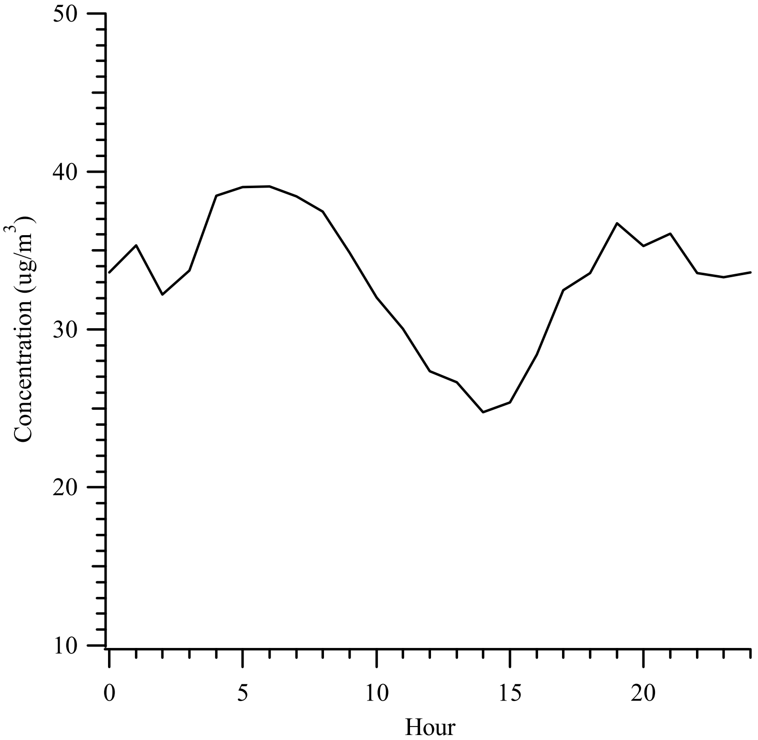

7.3 Hong Kong – Tsuen Wan

7.3.1 Temporal variations and overall results

The time series of hourly concentrations of sulfate and nitrate together with trace gases (SO_2 and NO_2) are shown in Figure 7.15. Please note that the data of the trace gases are obtained from the HKEPD. The mean hourly concentrations (± standard derivation) of sulfate and nitrate were 10.6 (±7.2)$\mu g/m^3$, and 3.4 (±2.6)$\mu g/m^3$, respectively. These values were much lower than our measurements conducted in Beijing (Sulfate: 24.3$\mu g/m^3$ and Nitrate: 9.7$\mu g/m^3$) and Shanghai (Sulfate: 17.9$\mu g/m^3$ and Nitrate: 5.8$\mu g/m^3$), where the measurement took place in the rural and suburban areas of China, respectively. This result reflected the more serious air pollution problems existing in China in comparison with the situation in Hong Kong. Hagler et al. (2006) also reported the average sulfate and nitrate concentrations of 9.3$\mu g/m^3$ and 1.0$\mu g/m^3$, respectively, in urban area of Hong Kong during 2002 - 2003. Our reported values showed little higher concentrations of sulfate and nitrate than the previous year. In this study, the maximum hourly sulfate and nitrate were 52.2$\mu g/m^3$ and 28.0$\mu g/m^3$, respectively. However, the particulate pollution problem in Hong Kong is still not good in comparison with other countries. For instance, the sulfate and nitrate concentrations in Milan (Italy) were 4.0$\mu g/m^3$ and 4.6$\mu g/m^3$, respectively [Lonati et al., 2005], while in Chongju (Korea), the sulfate and nitrate concentrations were 8.2$\mu g/m^3$ and 3.6$\mu g/m^3$, respectively [Lee and Kang, 2001]. At the same period of time, the average concentrations of SO_2 and NO_2 were 19.7 (±23.1)ppbv and 65.4 (±26.2)ppbv, respectively.

Figure 7.15. Time series of hourly concentrations of trace gases (SO_2 and NO_2) and aerosols (sulfate and nitrate) in Tsuen Wan.

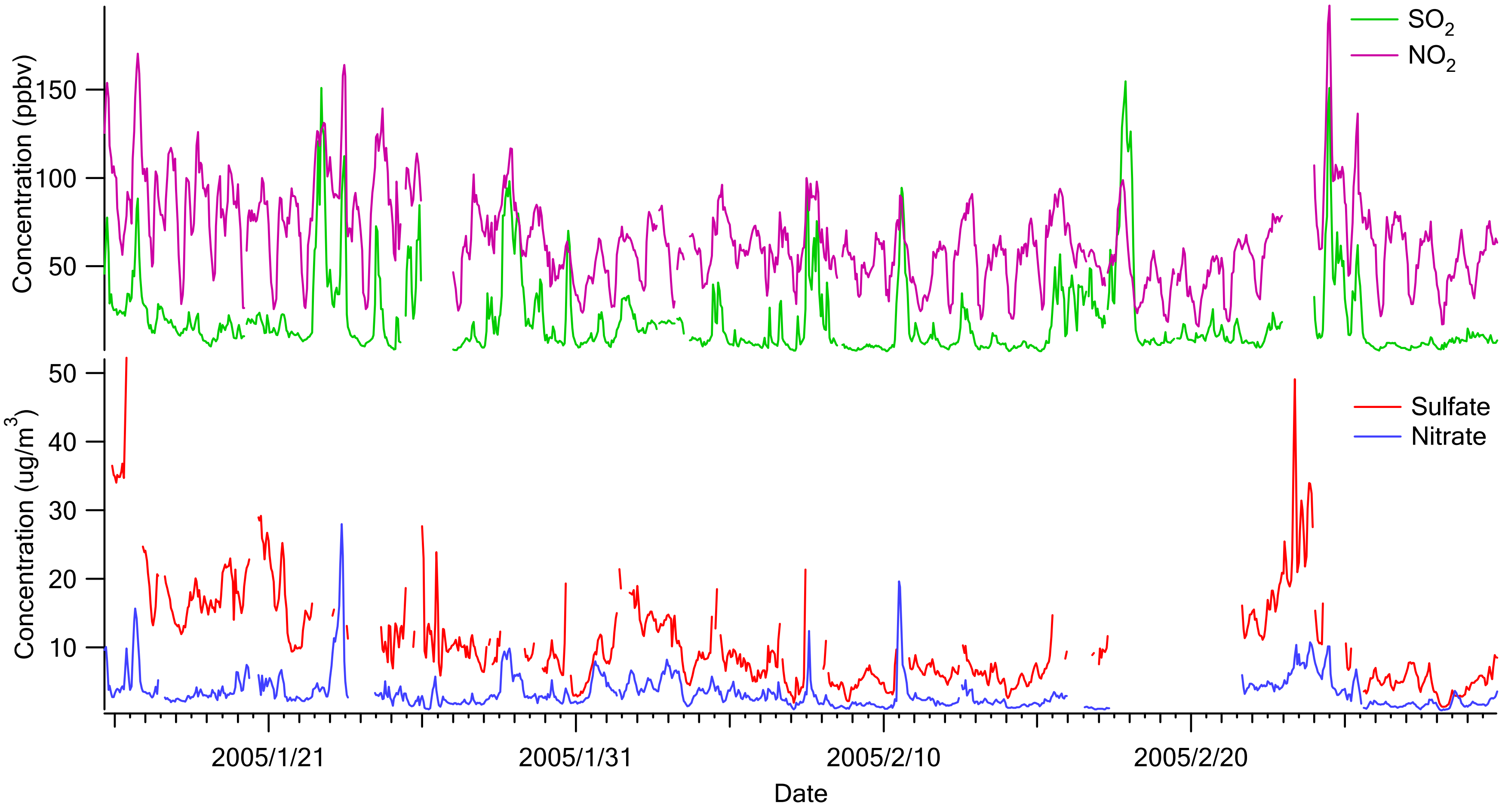

In contrast to the measurement result in Beijing, which showed large day-to-day variations in the concentrations of fine particles and trace gases during the measurement period, the measurement result in Hong Kong showed comparatively less fluctuations, especially for the nitrate concentrations. Only several pollution plumes are detected during the whole measurement period such as 23 Jan, 10 Feb, in which the nitrate concentrations reached to 20μg/m^3. In contrast, more pollution plumes of sulfate are found. The most prominent one was from 23 and 24 February, in which the sulfate concentrations kept at high levels (over 25μg/m^3) for almost the whole day. Besides, the high concentrations of sulfate and nitrate are usually associated with westerly wind, in which the major power plants in Hong Kong are located there.

One case study (23 Jan) is presented below to discuss the pollution plume present on that day. Figure 7.16 showed the time series of hourly concentrations of trace gases (CO, SO_2, and NO_x), aerosols (RSP, sulfate, and nitrate), and meteorological parameters (wind speed and wind direction) at 23 January morning in Tsuen Wan. On that day, the sulfate and nitrate reached to the maximum of about 60μg/m^3 and 30μg/m^3, respectively, while all the other gases showed very high concentrations. In addition, two peaks of sulfate and nitrate are found at around 9:00am and 11:00am, which may be attributed by different sources. Table 7.2 showed the comparison of the ratio of the trace gases between $\Delta CO/\Delta NO_x$ and $\Delta SO_2/\Delta NO_x$. At 9:00am, $\Delta CO/\Delta NO_x$ was 3.40 and $\Delta SO_2/\Delta NO_x$ was 0.11. These ratios were similar to the inventories in Hong Kong as reported by Streets et al. (2003). Thus, the first sulfate and nitrate peak was most possibly due to the transport during the morning rush hour. Similarly, at 11:00am, $\Delta SO_2/\Delta NO_x$ was 0.47. This value would be more resemble to the power plant emissions. These power plant emissions could be due to Lung Kwu Tan power station and Castle Peak power station, which are located on the west side of Hong Kong as the wind direction at that time also supported these pollution sources.

Figure 7.16. Time series of hourly concentrations of trace gases (CO, SO_2 and NO_x), aerosols (RSP, sulfate, and nitrate), and meteorological parameters (wind speed and wind direction) at 23 January morning in Tsuen Wan.

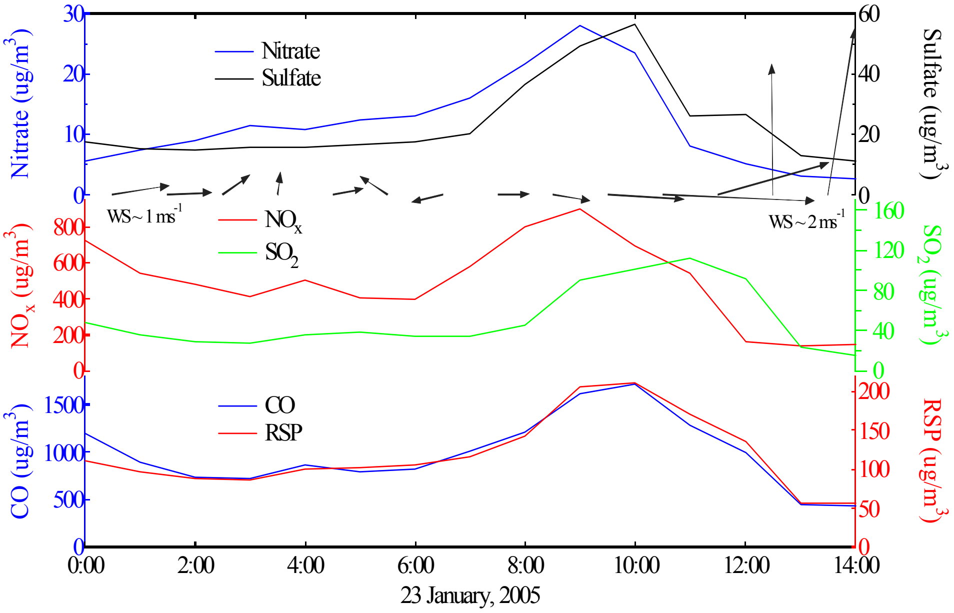

Table 7.2. Comparison of the ratio of the trace gases between $\Delta CO/\Delta NO_x$ and $\Delta SO_2/\Delta NO_x$

	23 Jan 2005		Hong Kong (Streets et al., 2003)	
	09:00	11:00	Transport	Power plants
$\Delta CO/\Delta NO_x$	3.40	5.88	4	-
$\Delta SO_2/\Delta NO_x$	0.11	0.47	0.01	0.57

During this six-week measurement, the average nitrate / sulfate ratio was 0.32 (standard derivation: 0.14). This result suggested that stationary source such as power plant emissions would be comparatively more dominant pollution sources in Hong Kong. However, on 31 January and 28 February afternoon, the nitrate / sulfate values were over 0.8 implying the significant contribution of the mobile sources (e.g. vehicles) at some of the times.

The correlation between sulfate and sulfur dioxide is shown in Figure 7.17. The correlation between sulfate and SO_2 was moderate with $r^2 = 0.40$. The existence of certain relationship between these two parameters indicated the importance of SO_2 on the formation of sulfate.

Figure 7.17. Correlation between sulfate and sulfur dioxide in Tsuen Wan.

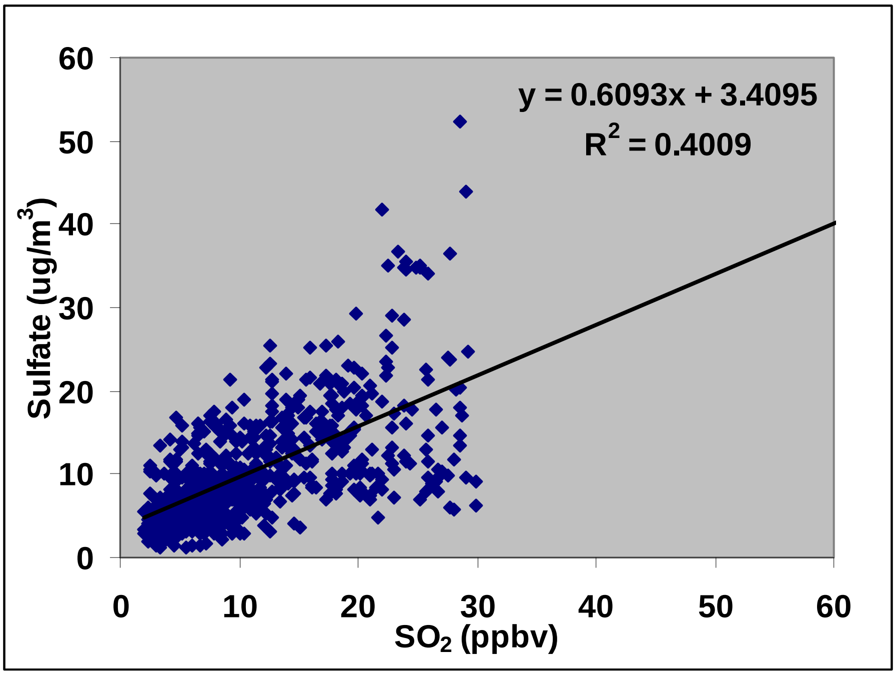

7.3.2 Diurnal profiles of sulfate and nitrate

The average diurnal variations of sulfate and nitrate in the measurement period are shown in Figures 7.18 and 7.19, respectively. The bar represented the average concentrations of the respective species, while the vertical line represented the standard derivation of the respective species. Similar to the result in Beijing, sulfate showed no distinctive diurnal pattern. The mean difference was only several micrograms per cubic meter for the whole day. The lack of diurnal pattern indicated a regional sulfate pollution problem in Hong Kong.

Figure 7.18. The diurnal profile of sulfate in Tsuen Wan.

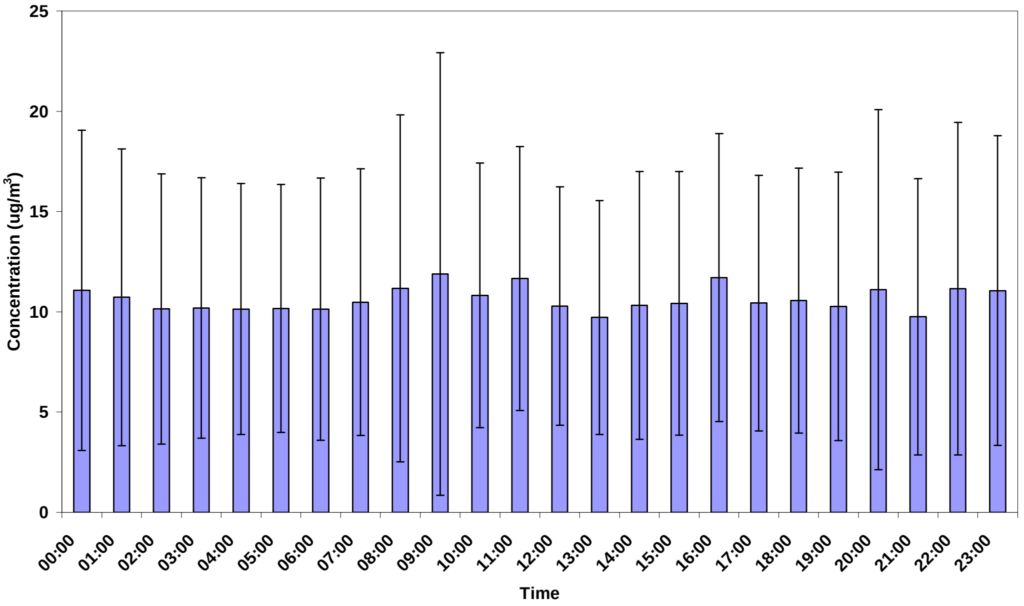

Figure 7.19. The diurnal profile of nitrate in Tsuen Wan.

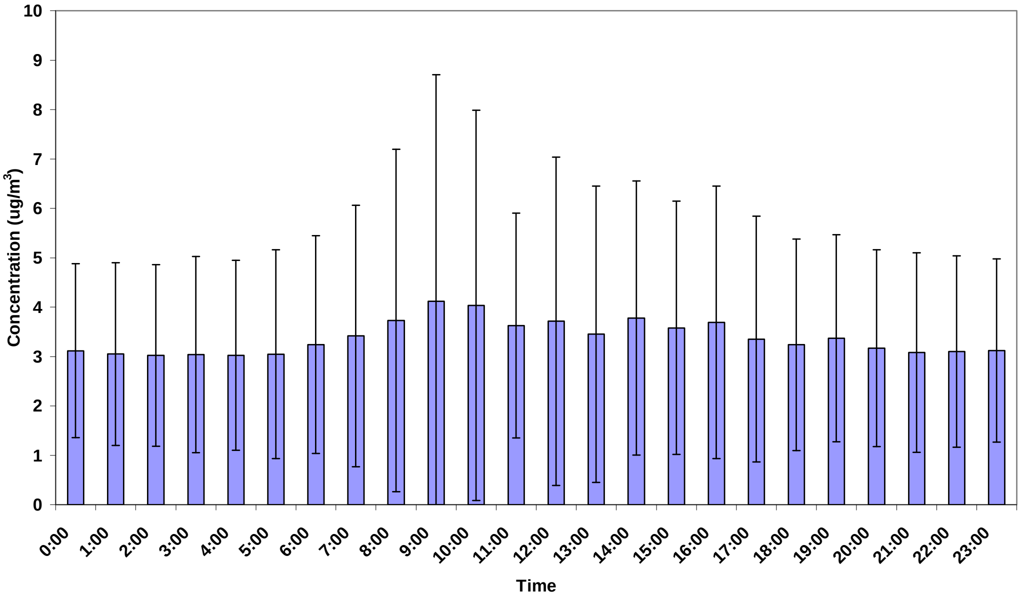

The diurnal profile of nitrate showed two maximum. The first maximum occurred in the morning at 9:00am and the other one was in the afternoon at 2:00pm to 4:00pm. This pattern was different from those measured from Beijing and Shanghai, which showed the minimum in the afternoon. This could be due to the difference between the two environments. The measuring site in Hong Kong is an urban area, while in Beijing and Shanghai are rural and suburban areas, respectively. The measuring environment in Hong Kong is more affected by the near-by densely vehicles, thus the two maximum nitrate peak could be corresponded to the emissions from vehicles during rush hours.

Chapter 8: Results and Analysis of $PM_{2.5}$ mass and water soluble ion species from filter measurements

In this chapter, the filter measurement results and analysis of $PM_{2.5}$ mass and water soluble ion species from Guangdong, Shanghai, Beijing, and Lanzhou will be presented. Although semi-continuous measurements of water soluble ion species have its own advantages, problems have been arisen due to variety of reasons as discussed in the previous chapter. Thus, the results from filter analysis are still the most accurate and reliable method for determining water soluble ion species at present. Thus, filter analysis results are also included in this study.

8.1 Shanghai

8.1.1 Concentrations of $PM_{2.5}$ mass and ions

From the gravimetric analysis, the concentrations of $PM_{2.5}$ mass in Shanghai were in the range of 28.8 – 235.4µg/m^3, with a mean and standard derivation of 71.9 and 41.7µg/m^3, respectively, which was similar to the value of 77.5µg/m^3 as conducted in Beijing in 1989 (Chen et al., 1994). Compared with the USEPA standard in which the daily average of the standard value of 65µg/m^3 for $PM_{2.5}$ (USEPA, 1997), about 44% of the daily $PM_{2.5}$ mass concentrations exceed USEPA standard, showing that fine particle pollution problem is serious in Shanghai. The concentrations of $PM_{2.5}$ mass in each day are plotted in Figure 9.1. From the figure, we could see that there were six days (21, 22 May and 1 – 4 June) which had the daily $PM_{2.5}$ mass concentrations higher than 100µg/m^3. These particularly high $PM_{2.5}$ mass concentrations would pose serious health effects to the human beings.

Figure 8.1. The concentrations of $PM_{2.5}$ mass at Shanghai in each day.

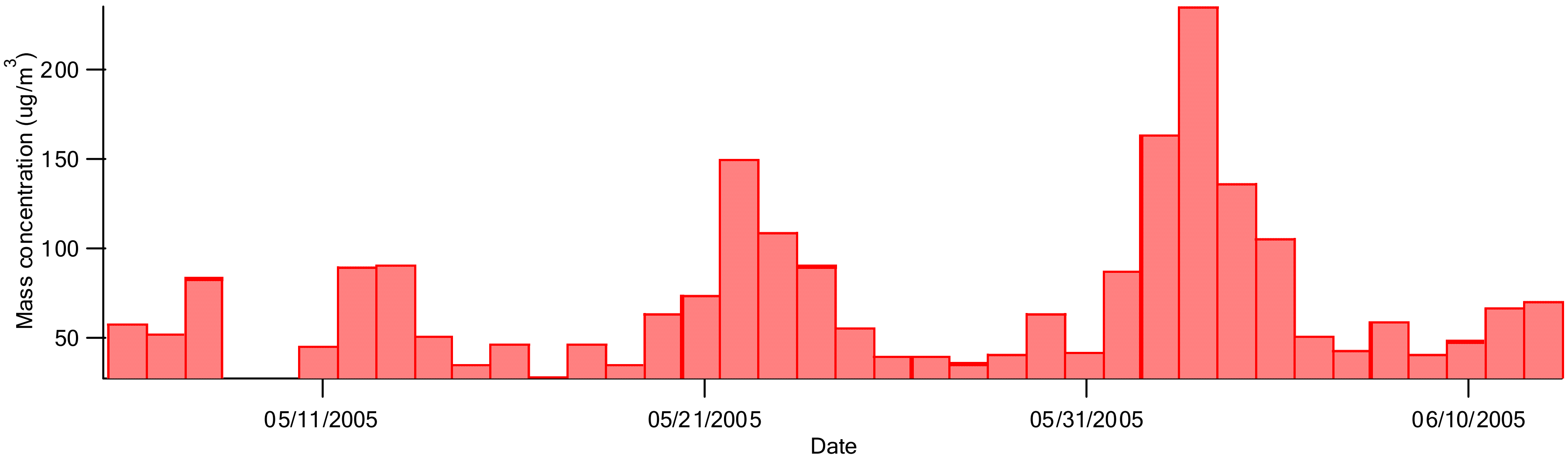

Moreover, strong day-to-day variations of $PM_{2.5}$ mass concentrations are observed in Shanghai. As illustrated in Figure 8.1, $PM_{2.5}$ mass concentrations could be reached as high as 235µg/m^3. However, under the clean condition, the mass concentrations were below 30µg/m^3. These strong temporal variations could be due to different air masses and/or different meteorological conditions arriving the sampling site during the measurement period. Please refer to Chapter 7 for more detailed analysis.

The average, standard derivation, minimum, maximum, and median of water soluble ion species for both cations and anions in Shanghai are shown in Table 8.1. The total water soluble ion species contributed to about 45% of the $PM_{2.5}$ mass concentrations. Among all the water soluble ions, SO_4^{2-}, NO_3^-, and NH_4^+ were the top three most abundant species. The average SO_4^{2-} concentration was 15.8µg/m^3 and accounted for 49% of the total mass of inorganic ions. Sulfate alone has already exceeded the US NAAQS annual $PM_{2.5}$ standard of 15µg/m^3. The second most abundant species was NO_3^- with the average concentration of 7.1µg/m^3, which accounted for 22% of the total mass of inorganic ions. For ammonium, the average concentration was 4.3µg/m^3 in Shanghai. These measured values were similar to those reported by Yao et al., 2002 in Shanghai. Yao et al. (2002) reported the annual average SO_4^{2-}, NO_3^-, and NH_4^+ concentrations were 15.9µg/m^3, 6.8µg/m^3, and 6.6µg/m^3, respectively at Hainan Road in Shanghai. The sum of the remaining ions accounted for about 16% of the total mass of inorganic ions in Shanghai. The distribution of the ion composition in Shanghai is shown in Figure 8.2. According to the figure, we could see that SO_4^{2-}, NO_3^-, and NH_4^+ were the three most dominant ion species.

K^+ and Cl^- were the fourth and fifth and accounted for 7% and 6%, respectively of the total ion mass. Other ions accounted for less than 1% of the total ion mass.

Table 8.1. The average, standard derivation, minimum, maximum, and median of the water soluble ion species for both cations and anions in Shanghai.

	Cations						Anions						
	Li^+	Na^+	NH_4^+	K^+	Mg^{2+}	Ca^{2+}	F^-	Cl^-	NO_2^-	Br^-	NO_3^-	PO_4^{3-}	SO_4^{2-}
Average	N.A.	0.4	4.3	2.3	0.1	0.2	N.A.	1.9	0.2	N.A.	7.1	N.A.	15.8
[a]St. der.	N.A.	0.2	2.0	3.1	0.0	0.1	N.A.	2.3	0.2	N.A.	6.7	N.A.	9.6
Minimum	N.A.	0.1	1.5	0.3	0.0	0.1	N.A.	0.1	0.0	N.A.	0.6	N.A.	3.6
Maximum	N.A.	1.1	12.9	14.4	0.2	0.6	N.A.	9.1	0.7	N.A.	36.6	N.A.	53.3
Median	N.A.	0.3	4.1	1.2	0.1	0.2	N.A.	1.0	0.1	N.A.	4.7	N.A.	13.1

[a]St. der. represents standard derivation.

Figure 8.2. The distribution of the ion composition in Shanghai.

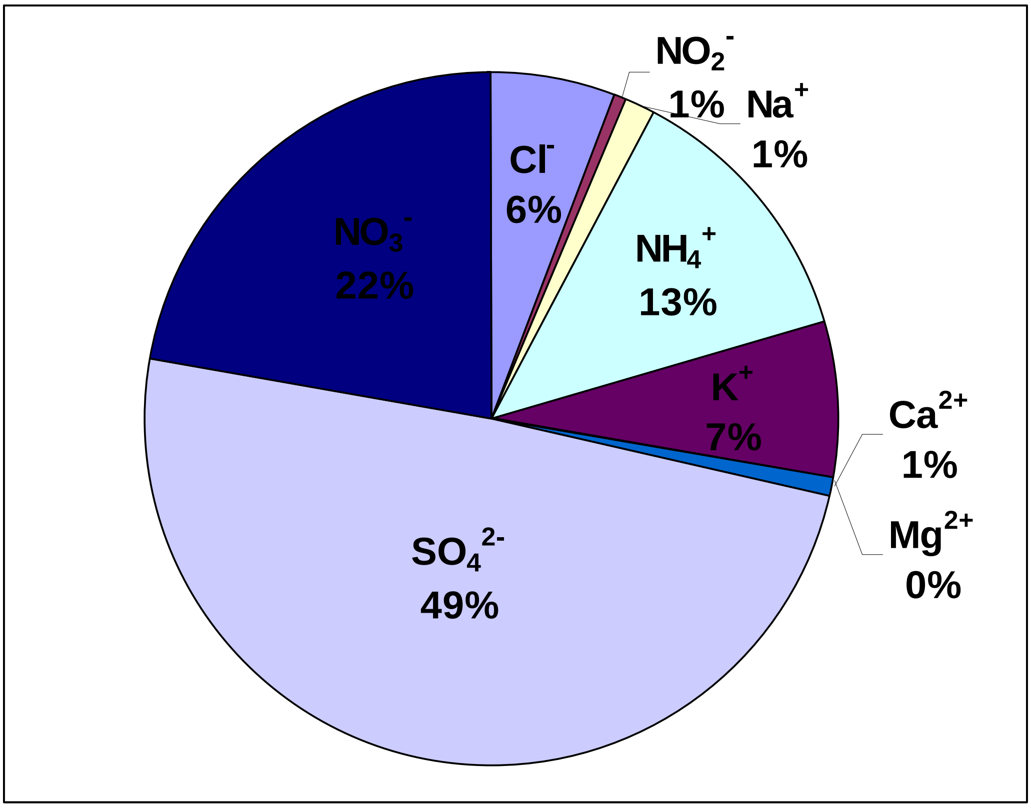

Figure 8.3 showed the daily ion composition in Shanghai. Red line represented $PM_{2.5}$ mass concentration. Generally speaking, the ion distribution in each day was similar and was proportional to the $PM_{2.5}$ mass. However, K^+ ion (yellow in color) only showed remarkable levels on some days, especially during the day of the highest $PM_{2.5}$ mass concentrations. This suggested that the contribution of biomass burning was one of the causes for the high levels of $PM_{2.5}$ mass.

Figure 8.3. The daily ion composition in Shanghai.

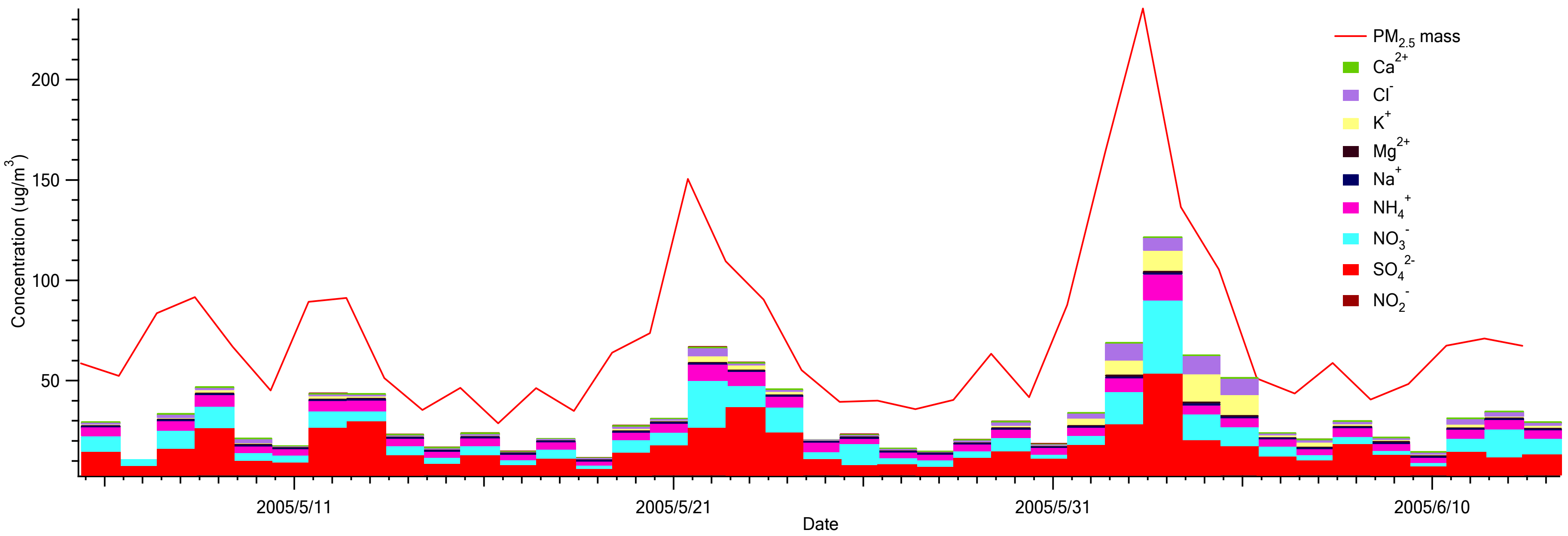

8.1.2 The source of SO_4^{2-} and NO_3^- in $PM_{2.5}$

As shown previously, the mass ratio of $[NO_3^-]/[SO_4^{2-}]$ has been used as an indicator of the relative importance of mobile versus stationary sources [Arimoto et al., 1996; Xiao and Liu, 2004; Yao et al., 2002]. Arimoto et al. (1996) ascribed high $[NO_3^-]/[SO_4^{2-}]$ mass ratio to the predominance of mobile source over stationary source of pollutants. In China, gasoline and diesel fuel contain 0.12% and 0.2% sulfur (by weight), respectively [Kato, 1996]. The estimated ratios of NO_x to SO_x from the emission of gasoline and diesel fuel burning are 13:1 and 8:1, respectively. The sulfur content in coal is 1% and the estimated ratio of NO_x to SO_x is 1:2 from coal burning [Wang et al., 2005; Yao et al., 2002]. Thus, it is reasonable to use SO_4^{2-} as an indicator of stationary emission and NO_3^- of mobile emission. Figure 8.4 showed the daily $[NO_3^-]/[SO_4^{2-}]$ ratio for the whole measurement period. From the figure, we could see that the mass ratio was below 0.5 for most of the days. This indicated that the influence of the stationary source was predominant at the sampling site, while the ratio could reach over 1 for some of the days such as 25 May, 11 June, which indicated the influence of the mobile source. In this study, the average mass ratio of $[NO_3^-]/[SO_4^{2-}]$ during the measurement period was 0.44. This value was similar to those reported by Yao et al., 2002. The relatively low $[NO_3^-]/[SO_4^{2-}]$ ratio suggested that the more influence of the stationary source over the mobile source of pollutants in our study site. This was because there were several small to medium scale power plants located around the sampling site.

Figure 8.4. The daily $[NO_3^-]/[SO_4^{2-}]$ ratio in Shanghai for the whole measurement period.

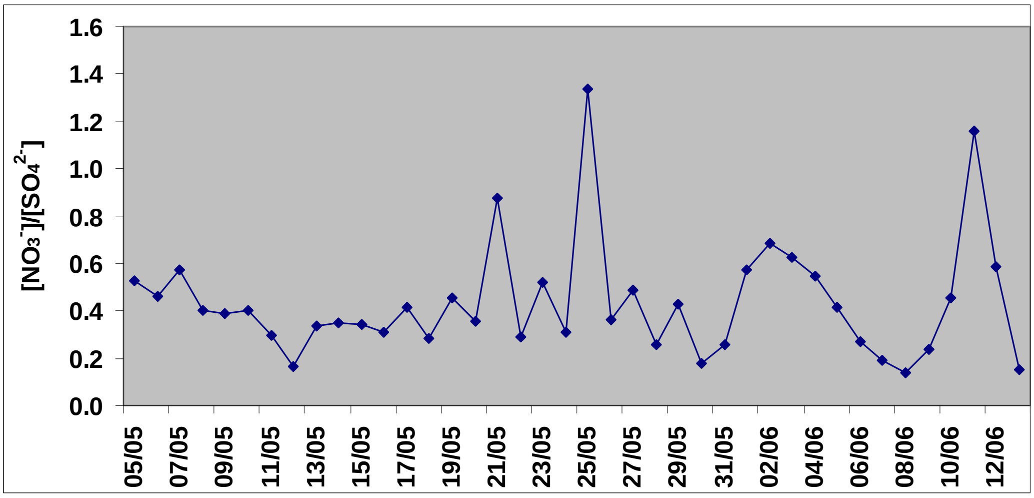

8.1.3 The speciation of the major ions

The chemical forms of the major ions in aerosols in Shanghai are identified by bivariate correlations. Table 8.2 showed the summary of the correlation coefficients among these major ions. It could be seen that NH_4^+ is closely correlated with SO_4^{2-} and NO_3^-, while Cl^- is correlated well with Na^+ and K^+. These suggested that $(NH_4)_2SO_4$, NH_4NO_3, NaCl, and KCl are found to be the major chemical species in the aerosol particles based on their correlation coefficients.

Table 8.2. The summary of the correlation coefficients among the major ions in Shanghai.

R^2	SO_4^{2-}	NO_3^-	Cl^-	NO_2^-
Na^+	0.39	0.39	**0.70**	0.02
Mg^{2+}	0.14	0.13	0.02	0.00
K^+	0.31	0.38	**0.84**	0.01
Ca^{2+}	0.45	0.43	0.20	0.01
NH_4^+	**0.85**	**0.78**	0.17	0.02

8.1.4 The oxidation of sulfur and nitrogen

Sulfur oxidation ratio (SOR) is defined as $SO_4^{2-}/(SO_4^{2-}+SO_2)$, and nitrogen oxidation ratio (NOR) is defined as $NO_3^-/(NO_3^-+NO_y)$. These could be the indicators of the secondary transformation processes. SOR expressed the degree of oxidation of sulfur in terms of the ratio of sulfur in sulfate to total sulfur. Similarly, NOR expressed the degree of oxidation of nitrogen in terms of the ratio of nitrogen in nitrate to total nitrogen. Higher SOR and NOR suggested that the oxidation of gaseous species have occurred and more secondary aerosols could exist in the atmosphere [Wang et al., 2005]. The SOR and NOR of $PM_{2.5}$ aerosols in Shanghai are shown in Figure 8.5. From the figure, we could see that SOR and NOR ranged from 0.05 – 0.30, and 0.01 – 0.19, respectively. The average SOR and NOR for the whole measurement period were 0.16 and 0.07, respectively. Ohta and Okita (1990) suggested that when the ratio value was greater than 0.10, photochemical oxidation of SO_2 would occur in the atmosphere. The SOR of Shanghai $PM_{2.5}$ aerosols were greater than 0.10 in the study period. This result suggested that secondary formation of SO_4^{2-} from SO_2 is occurred. In contrast, the low NOR in Shanghai $PM_{2.5}$ aerosols suggested that the secondary formation of NO_3^- from NO_y is weakly occurred in Shanghai compared to that of SO_4^{2-}.

Figure 8.5. The SOR and NOR of $PM_{2.5}$ aerosols in Shanghai.

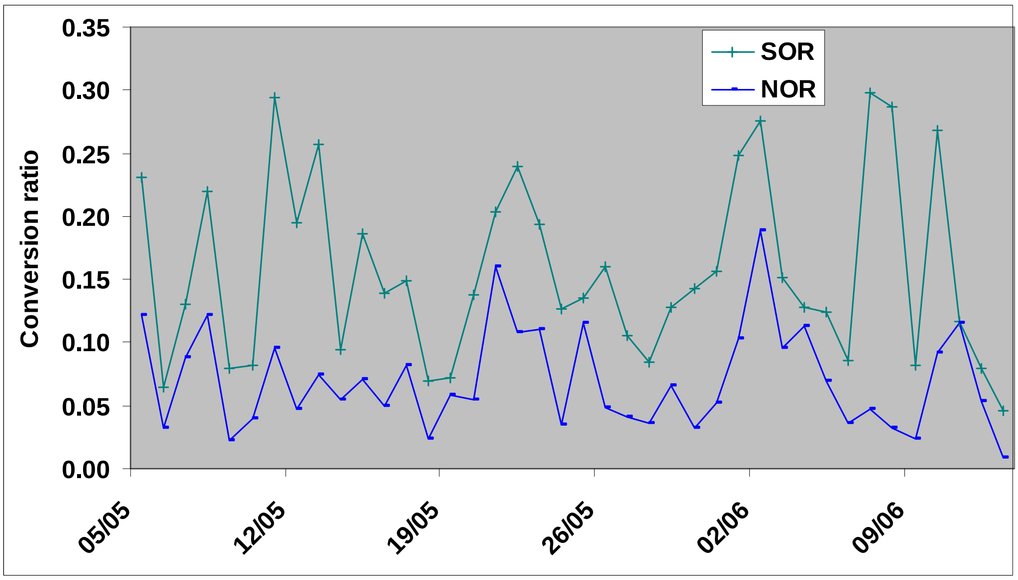

To identify the factors controlling the formation of secondary ions (SO_4^{2-} and NO_3^-), the correlation coefficients between SOR, NOR, and other parameters are calculated and the results are shown in Table 8.3. SOR and NOR showed very weak correlations with O_3, temperature, relative humidity, and solar radiation. These suggested that the formation of secondary aerosols were very complex and many reactions might occur at the same time and lead to the formation of secondary aerosols. Therefore, no good correlations with individual species are found.

Table 8.3. Correlation coefficients between SOR, NOR, and other parameters (ozone, temperature, relative humidity, and solar radiation) in Shanghai.

	O_3	Temperature	RH	Solar radiation
SOR	0.04	0.04	0.13	0.13
NOR	0.18	0.04	0.01	0.00

8.2 Beijing

8.2.1 Concentrations of $PM_{2.5}$ mass and ions

In this study, the mean concentrations of $PM_{2.5}$ mass in Beijing were in the range of 12.2 – 211.9μg/m^3, with a mean and standard derivation of 76.6μg/m^3 and 59.6μg/m^3, respectively. Wang et al. (2005) found a mean value of $PM_{2.5}$ mass of 93.3μg/m^3 in the summer season of Beijing in 2001 – 2003. The similar value of our measurement to the urban/suburban results suggested that fine aerosol pollution problem in Beijing had not been improved in the past few years and that it existed beyond the urban center. In addition, about 48% of the daily $PM_{2.5}$ mass concentrations were higher than the USEPA standard, showing that fine particle pollution was serious in Beijing. The concentrations of $PM_{2.5}$ mass in each day were plotted in Figure 8.6. There were altogether 24 $PM_{2.5}$ samples collected during the whole measurement period.

Figure 8.6. The concentrations of $PM_{2.5}$ mass in each day in Beijing.

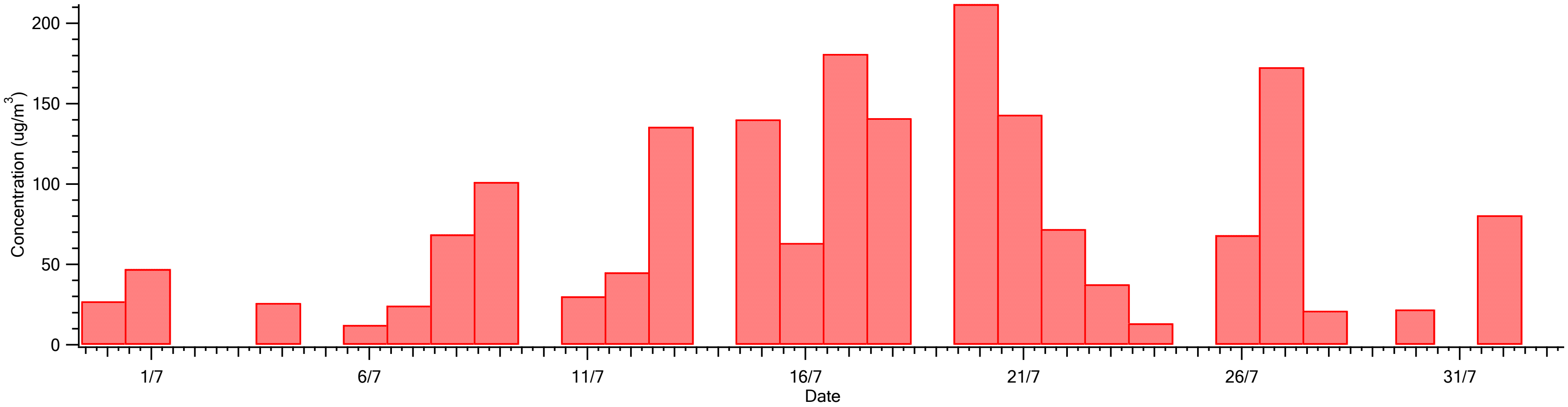

Again, strong day-to-day variations of $PM_{2.5}$ mass concentrations were observed in Beijing. As illustrated in Figure 8.6, there were several days which had the daily $PM_{2.5}$ mass concentration greater than 100µg/m^3 and the highest $PM_{2.5}$ mass concentration could be reached as high as 212µg/m^3. However, under the clean condition, the $PM_{2.5}$ mass concentrations could be as low as only several micrograms per cubic meter. This could also be seen from the large standard derivation (60µg/m^3) of $PM_{2.5}$ mass. These strong temporal variations of $PM_{2.5}$ mass could be reflecting a sharp contrast between regional background air from the north and urban plumes from the south attacking the sampling site.

The average, standard derivation, minimum, maximum and median of the water soluble ionic species of both cations and anions in Beijing were shown in Table 8.4. The total water soluble ion species contributed to about 53% of $PM_{2.5}$ mass concentrations. Among all the water soluble ions, SO_4^{2-}, NO_3^- and NH_4^+ were the top three most abundant species. The average SO_4^{2-} concentration was 23µg/m^3, which accounted for 55% of the total mass of inorganic ions. The average NO_3^- concentration was 9.9µg/m^3, which accounted for 24% of the total mass of inorganic ions. The average NH_4^+ concentration was 5.7µg/m^3 in Beijing, which contributed to about 14% of the total mass of inorganic ions. The measured values were similar to those measured by Hu et al., 2002. He reported the average sulfate and nitrate concentrations of 21.4µg/m^3 and 14.7ug/m^3, respectively on the campus of Peking University in June – July 2000. Moreover, the maximum sulfate and nitrate reached to 92.0µg/m^3 and 42.3µg/m^3, respectively. These extremely high particulate loadings would seriously affect the environment. As sulfate and nitrate were the precursors of the formation of acid rain, the high concentrations of sulfate and nitrate would lead to the problem of acid rain. The sum of other ions only accounted for 6% of the total mass of inorganic ions in Beijing. The distribution of the ion composition was shown in Figure 8.7. According to the figure, we could see that SO_4^{2-}, NO_3^- and NH_4^+ were the dominant ion species, followed by K^+ (3%), NO_2^- (2%) and Cl^- (1%).

Table 8.4. The average, standard derivation, minimum, maximum and median of the water soluble ionic species of both cations and anions in Beijing.

	Cations						Anions						
	Li^+	Na^+	NH_4^+	K^+	Mg^{2+}	Ca^{2+}	F^-	Cl^-	NO_2^-	Br^-	NO_3^-	PO_4^{3-}	SO_4^{2-}
Average	N.A.	0.1	5.7	1.3	0.0	0.1	N.A.	0.4	0.7	N.A.	9.9	N.A.	22.6
[a]St. der.	N.A.	0.1	5.1	1.1	0.0	0.1	N.A.	0.6	0.8	N.A.	11.9	N.A.	26.0
Minimum	N.A.	0.0	0.4	0.0	0.0	0.0	N.A.	0.0	0.0	N.A.	0.2	N.A.	0.6
Maximum	N.A.	0.3	19.4	4.0	0.1	0.4	N.A.	1.9	2.7	N.A.	42.3	N.A.	92.0
Median	N.A.	0.1	3.6	1.1	0.0	0.1	N.A.	0.1	0.4	N.A.	5.7	N.A.	12.8

[a]St. der. represents standard derivation.

Figure 8.7. The distribution of the ion composition in Beijing.

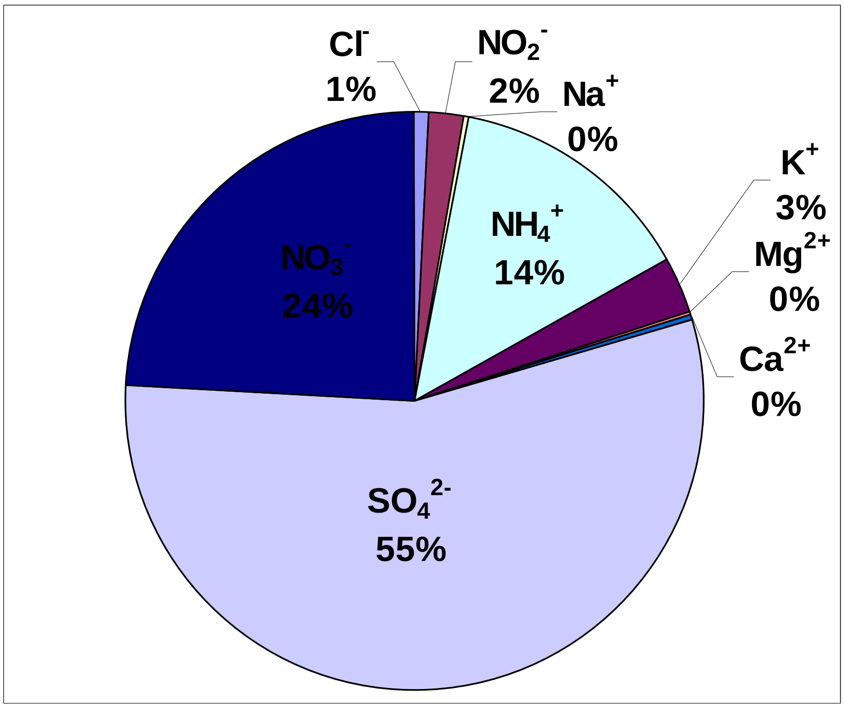

8.2.2 The source of SO_4^{2-} and NO_3^- in $PM_{2.5}$

The mass ratio of $[NO_3^-]/[SO_4^{2-}]$ during the whole measurement period was shown in Figure 8.8. The average $[NO_3^-]/[SO_4^{2-}]$ during the measurement period was 0.40. From the figure, we could see that the mass ratio was below 0.5 for most of the days which indicated the influence of the stationary source was predominant. However, the ratio was larger than 1 on 10 July. This suggested that the sampling location was occasionally affected more by the mobile source. The measured value was similar to those reported by Yao et al., 2002. The relatively low $[NO_3^-]/[SO_4^{2-}]$ ratio suggested that the more influence of the stationary source over the mobile source of pollutants in our study site.

Figure 8.8. The mass ratio of $[NO_3^-]/[SO_4^{2-}]$ in Beijing.

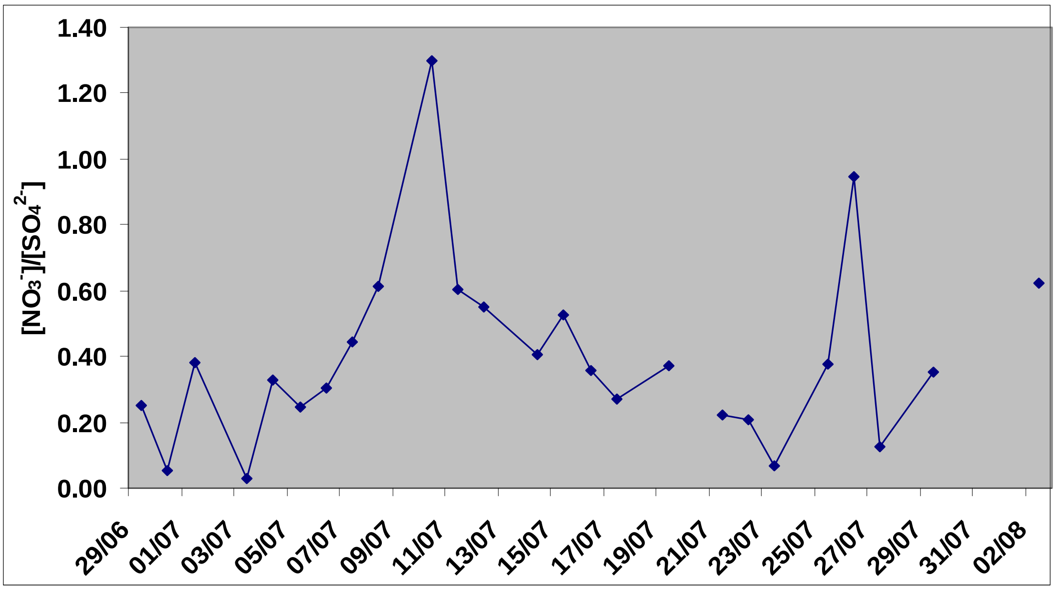

8.2.3 The speciation of major ions

The chemical forms of those major ions in aerosols in Beijing were identified by bivariate correlations. Table 8.5 showed the summary of the correlation coefficients among these major ions. It could be seen that NH_4^+ was closely correlated with SO_4^{2-}, NO_3^- and Cl^- while Na^+ was correlated well with Cl^-, NO_3^- and K^+ was correlated well with SO_4^{2-}. These suggested that $(NH_4)_2SO_4$, NH_4NO_3, NH_4Cl, NaCl, $NaNO_3$ and K_2SO_4 were found to be the major chemical species in the aerosol particles based on their correlation coefficients.

Table 8.5. The summary of the correlation coefficients among the major ions in Beijing.

R^2	SO_4^{2-}	NO_3^-	Cl^-	NO_2^-
Na^+	0.57	**0.67**	**0.64**	0.45
Mg^{2+}	0.02	0.06	0.02	0.02
K^+	**0.62**	0.55	0.58	0.42
Ca^{2+}	0.00	0.01	0.00	0.00
NH_4^+	**0.75**	**0.76**	**0.83**	0.59

8.2.4 The oxidation of sulfur and nitrogen

The SOR and NOR obtained for $PM_{2.5}$ aerosols in Beijing was shown in Figure 8.9. From the figure, we could see that the SOR and NOR ranged from 0.05 – 0.98 and 0.01 – 0.36, respectively. The average SOR and NOR during the whole measurement period was 0.45 and 0.16, respectively. The SOR and NOR of Beijing $PM_{2.5}$ aerosols were both higher than 0.10 in the study period. These results suggested that secondary formation of SO_4^{2-} from SO_2 as well as NO_3^- from NO_y components were occurred in the rural area of Beijing. Furthermore, the conversion of SO_2 was almost complete (Over 80%) for certain days.

To identify the factors controlling the formation of secondary ions (SO_4^{2-} and NO_3^-), the correlation coefficients between SOR, NOR and other parameters were calculated and the results were shown in Table 8.6. SOR showed moderate correlation with relative humidity. As discussed previously, SO_4^{2-} formation has three main major formation mechanisms. The moderately good correlation of SOR with relative humidity would suggest that the formation of sulfate would be more favor towards the aqueous phase reaction of SO_2.

Figure 8.9. The SOR and NOR obtained for $PM_{2.5}$ aerosols in Beijing.

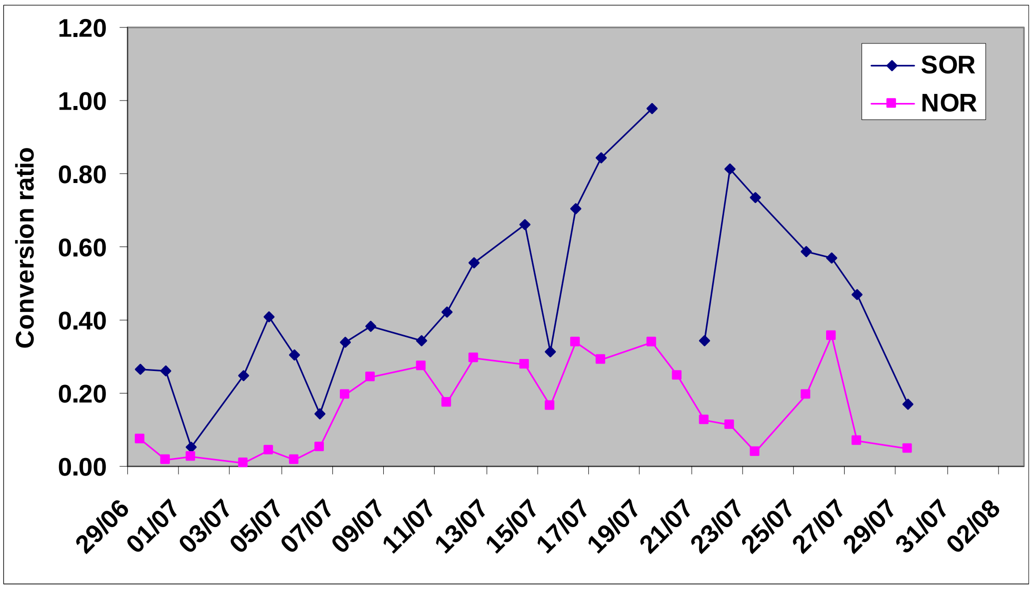

Table 8.6. The correlation coefficients between SOR, NOR and other parameters (Ozone, temperature, relative humidity and solar radiation) in Beijing.

	Ozone	Temperature	Relative humidity	Solar radiation
SOR	0.07	0.15	0.50	0.22
NOR	0.03	0.06	0.36	0.18

8.3 Lanzhou

8.3.1 Concentrations of $PM_{2.5}$ mass and ions

Particulate pollution in the Lanzhou Valley of Gansu Province is a well-known public health problem (Ta et al., 2004). However, the aerosol study in this region is very limited. In this section, I will report the aerosol measurements conducted in Lanzhou. The concentrations of $PM_{2.5}$ mass in each day were plotted in Figure 8.10. Please note that there were 11 filters which had shorter collection time so that the width of the bar shown in Figure 8.10 was much narrower than others. We have selected the days that had high ozone to conduct shorter time aerosol sampling in order to get the diurnal profile of the aerosol samples. During the high ozone period, the collection time for the filter was 2 hours instead of 24 hours. Except during the ozone episode period, $PM_{2.5}$ mass concentrations were usually below 80μg/m^3. However, for the time with the ozone episode, $PM_{2.5}$ mass could reach over 150μg/m^3. In the whole study period, the mean concentrations of $PM_{2.5}$ mass in Lanzhou were in the range of 27.1 – 183.1μg/m^3, with a mean and standard derivation of 73.1 and 38.5μg/m^3, respectively.

Figure 8.10. The concentrations of $PM_{2.5}$ mass in each day in Lanzhou.

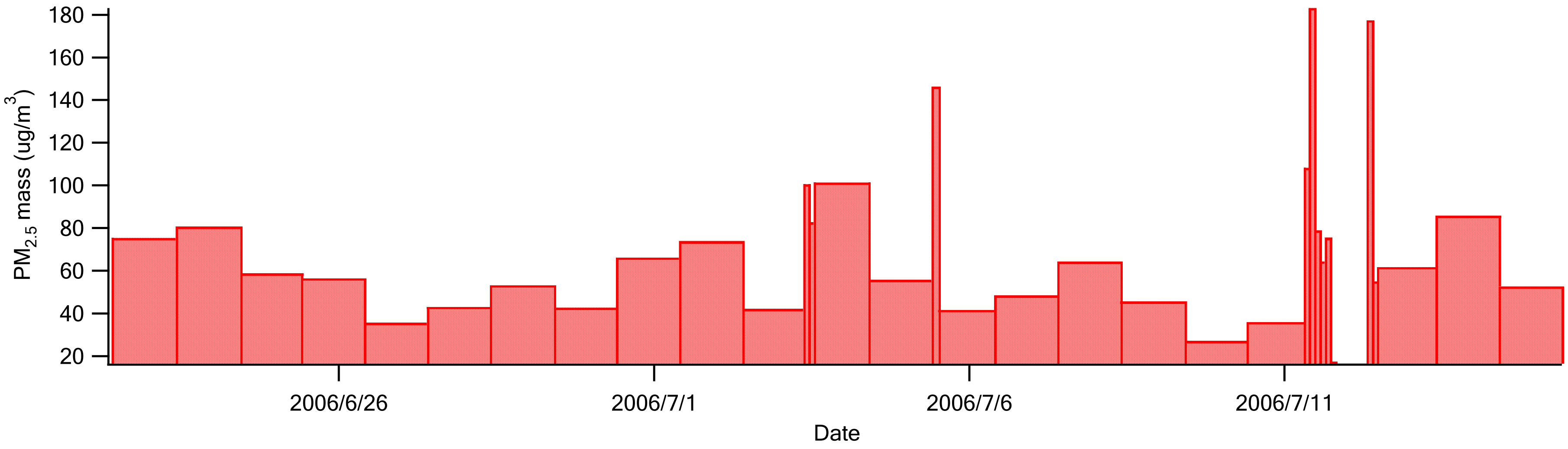

The case in Lanzhou was different from the previous as the particle concentrations could change quickly within a few hours. This could see more clearly from the TEOM as well as the gaseous pollutant measurements. Figure 9.11 showed one of the cases in Lanzhou. In this figure, several gaseous pollutants such as CO, O_3, NO_y were shown. We could see that in the morning of June 25, all the primary pollutants increased to very high levels (CO >1000ppbv, SO_2, NO_y >40ppbv) together with O_3 (>100ppbv). However, after around 12 o'clock, all the pollutant levels sharply decreased to very low values. This kind of change could be associated with the change in wind direction (From south-westerly to northerly wind). Thus, the mass concentrations obtained from filter measurements at 24-hour interval would miss out this abrupt change of pollution levels. Comparing with Qian et al., 2001, our measured results of $PM_{2.5}$ mass were lower than the urban (115ug/m^3) and suburban (98ug/m^3) measurements in Lanzhou during 1995 – 1996. In addition, about 38% of the daily $PM_{2.5}$ mass concentrations were higher than the USEPA standard, showing that fine particle pollution problem is also serious in Lanzhou.

Figure 8.11. The time series plot of gaseous pollutants (CO, O_3, NO, NO_y, SO_2, PAN) and meteorological parameters (solar radiation, wind speed and wind direction) on 24 to 26 June in Lanzhou.

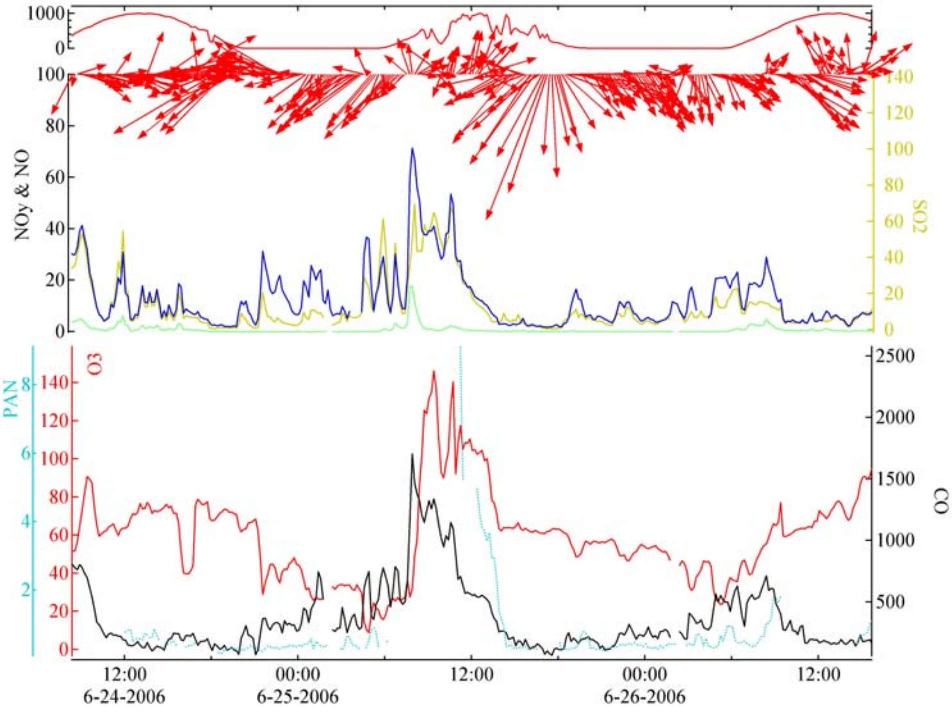

Figure 8.12 showed one of the representative diurnal profile of $PM_{2.5}$ mass obtained from filters (11 July). The $PM_{2.5}$ mass concentration was high in the morning and increased to about 180µg/m^3 at around 9am. Afterwards, the $PM_{2.5}$ mass decreased rapidly to around 80ug/m^3 at around noon time and remained steady until late afternoon which dropped to only 15ug/m^3. This pattern was similar to the CO pattern in the same day which reached to about 1000ppbv in the morning and continuous to decrease until late afternoon.

Figure 8.12. The diurnal profile of $PM_{2.5}$ mass obtained from filters (11 July) in Lanzhou.

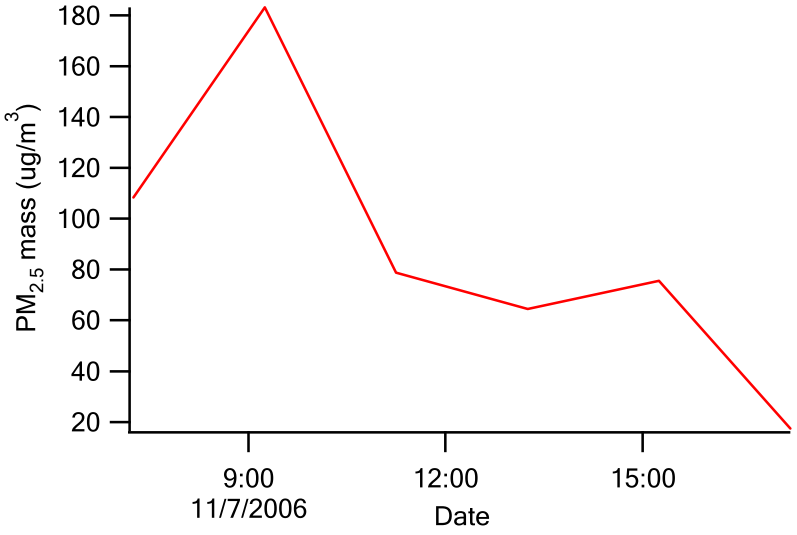

The average, standard derivation, minimum, maximum and median of the water soluble ionic species of both cations and anions in Lanzhou were shown in Table 8.7. The total water soluble ion species contributed to about 43% of the $PM_{2.5}$ mass concentration. Among all the water soluble ions, SO_4^{2-}, Cl^- and NH_4^+ were the top three most abundant species. The average SO_4^{2-} concentration was 11µg/m^3, which accounted for 35% of the total mass of inorganic ions. The average Cl^- concentration was 5.9µg/m^3, which accounted for 19% of the total mass of the inorganic ions. Thirdly, the average NH_4^+ concentration was 5.1µg/m^3, which contributed to about 16% of the total mass of inorganic ions. Moreover, the maximum sulfate and nitrate were 33.1 and 17.2µg/m^3, respectively. The sum of the remaining ions accounted for 30% of the total mass of inorganic ions. The distribution of the ion composition was shown in Figure 8.13. According to the figure, we could see that SO_4^{2-}, Cl^- and NH_4^+ were the dominant ion species, followed by NO_3^- (12%), NO_2^- (7%) and Ca^+ (4%).

Table 8.7. The average, standard derivation, minimum, maximum and median of the water soluble ionic species of both cations and anions in Lanzhou.

	Cations						Anions						
	Li^+	Na^+	NH_4^+	K^+	Mg^{2+}	Ca^{2+}	F^-	Cl^-	NO_2^-	Br^-	NO_3^-	PO_4^{3-}	SO_4^{2-}
Average	N.A.	0.5	5.1	0.8	0.4	1.3	0.5	5.9	2.3	N.A.	3.7	N.A.	10.8
[a]St. der.	N.A.	0.5	4.8	0.4	0.7	1.6	0.3	5.3	2.8	N.A.	3.3	N.A.	6.8
Minimum	N.A.	0.0	0.7	0.2	0.0	0.0	0.2	0.2	0.2	N.A.	0.7	N.A.	3.4
Maximum	N.A.	2.3	23.4	2.2	1.5	6.9	1.0	20.1	11.4	N.A.	17.2	N.A.	33.1
Median	N.A.	0.4	3.7	0.8	0.4	1.6	0.4	4.0	1.2	N.A.	2.6	N.A.	10.0

[a] St. der. represents standard derivation.

Figure 8.13. The distribution of the ion composition in Lanzhou.

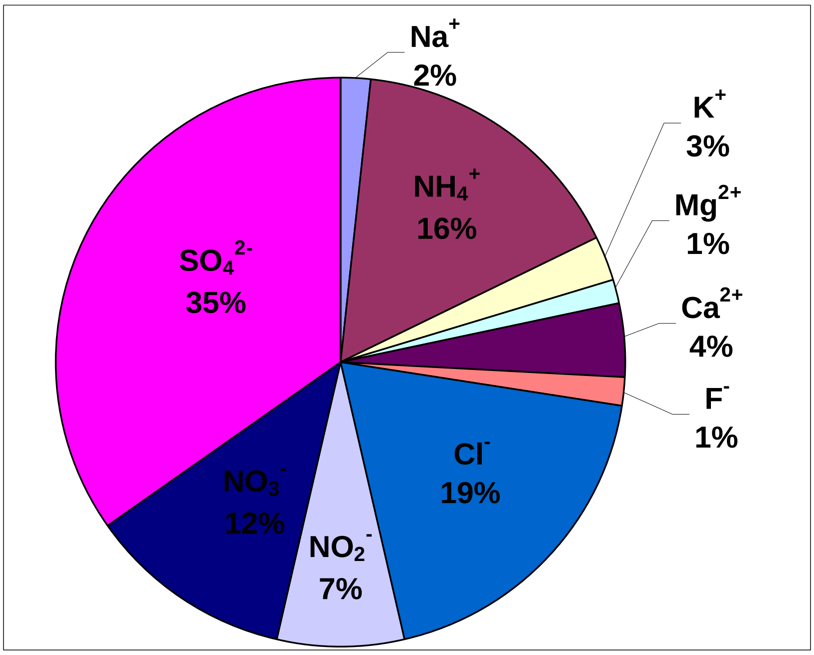

8.3.2 The source of SO_4^{2-} and NO_3^- in $PM_{2.5}$

The mass ratio of $[NO_3^-]/[SO_4^{2-}]$ during the whole measurement period was shown in Figure 8.14. The average $[NO_3^-]/[SO_4^{2-}]$ ratio during the measurement period was 0.38. According to the figure, the mass ratio was below 0.4 for most of the days which indicated the predominant of the influence of the stationary source. The relatively low $[NO_3^-]/[SO_4^{2-}]$ ratio suggested that the more influence of the stationary source over the mobile source of pollutants in our study site as there were many power plants located at the west side of the sampling site. Sometimes the plume from the power plant was clearly seen at the sampling site (Figure 8.15).

Figure 8.14. The mass ratio of $[NO_3^-]/[SO_4^{2-}]$ during the whole measurement period in Lanzhou.

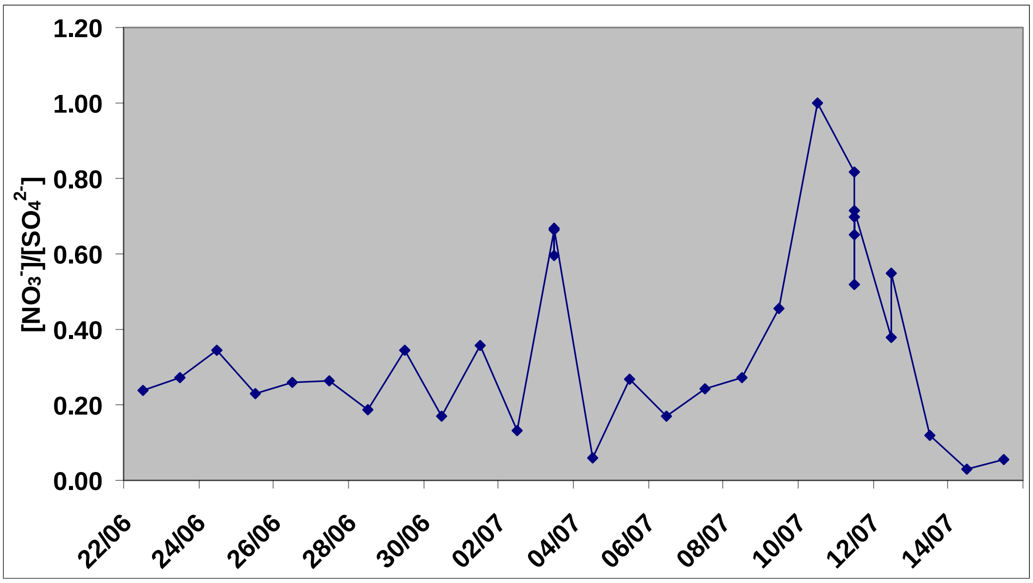

Figure 8.15. The plume from the power plant as seen from the sampling site.

8.3.3 The speciation of the major ions

The chemical forms of the major ions in aerosols in Lanzhou were identified by bivariate correlations. Table 8.8 showed the summary of the correlation coefficients among these major ions. It could be seen that NH_4^+ was moderately correlated with SO_4^{2-} while NO_2^- was correlated with Ca^{2+}. These suggested that $(NH_4)_2SO_4$ and $Ca(NO_2)_2$ were found to be the major chemical species in the aerosol particles based on their correlation coefficients.

Table 8.8. The summary of the correlation coefficients among the major ions in Lanzhou.

R^2	SO_4^{2-}	NO_3^-	Cl^-	NO_2^-
Na^+	0.01	0.14	0.03	0.32
Mg^{2+}	0.01	0.12	0.08	0.18
K^+	0.01	0.01	0.07	0.04
Ca^{2+}	0.02	0.01	0.01	**0.48**
NH_4^+	**0.41**	0.35	0.14	0.05

8.3.4 The oxidation of sulfur and nitrogen

The SOR and NOR for $PM_{2.5}$ aerosols in Lanzhou was shown in Figure 8.16. The SOR and NOR ranged from 0.05 – 0.47 and 0.02 – 0.37, respectively. The average SOR and NOR during the whole measurement period was 0.18 and 0.09, respectively. SOR of $PM_{2.5}$ aerosols in Lanzhou was higher than 0.10 in the study period. This result suggested that secondary formation of SO_4^{2-} from SO_2 was occurred.

Figure 8.16. The SOR and NOR for $PM_{2.5}$ aerosols in Lanzhou.

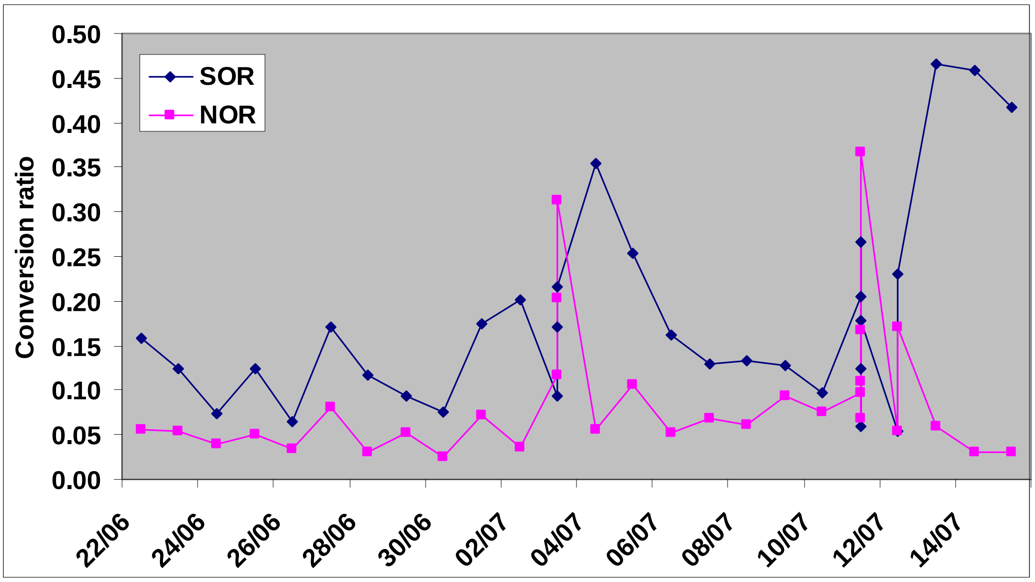

The factors controlling the formation of secondary ions (SO_4^{2-} and NO_3^-) were identified by the correlation coefficients between SOR, NOR and other parameters. The results were shown in Table 8.9. SOR and NOR don't show any good correlation with the meteorological parameters and ozone. This suggested that the SO_4^{2-} and NO_3^- formation was very complex and might involve varies simultaneous formation pathways. As discussed earlier, the air mass changed abruptly in this sampling site, this would be another reason for the poor correlation.

Table 8.9. The correlation coefficients between SOR, NOR and other parameters (Ozone, temperature, relative humidity and solar radiation) in Lanzhou.

	Ozone	Temperature	Relative humidity	Solar radiation
SOR	0.08	0.01	0.19	0.04
NOR	0.00	0.00	0.01	0.00

8.4 Guangzhou

Guangzhou is one of the fastest developing cities in China. This rapid development has raised the living condition of the citizens; however, this fast-paced growth in population and energy use has degraded the local air quality. In this section, I will describe the fine particulate pollution problem in Guangzhou. The study site was located at Wan Qing Sha, which has already described before.

8.4.1 Concentrations of $PM_{2.5}$ mass and ions

The daily variation of $PM_{2.5}$ mass concentrations was shown in Figure 8.17. There were altogether 13 filter samples collected in the six weeks intensive study. The average $PM_{2.5}$ mass during the whole measurement period was 54.7μg/m^3 with standard derivation of 27.7μg/m^3. Hagler et al. (2006) reported the mean $PM_{2.5}$ mass was 70.6 ± 30.2μg/m^3 conducted in the urban area of Guangzhou during 2002 – 2003. The reported value was comparable with our measured results. However, we should note that the measurement of Hagler et al. (2006) was conducted in the urban area of Guangzhou while our measurements were done in the suburban area. Thus, fine particulate pollution was not only locally pollution problem, but also affected the whole Guangzhou region. According to Figure 8.17, the daily variation of $PM_{2.5}$ mass was moderate. It ranged from 16.5µg/m^3 to 93.2µg/m^3. Among the 13 sampling days, there were 5 days (38%) exceeding the USEPA standard of 65µg/m^3. This reflected the seriousness of the fine particle pollution problem in the Guangzhou region.

Figure 8.17. The day-to-day variation of $PM_{2.5}$ mass concentrations in Guangzhou.

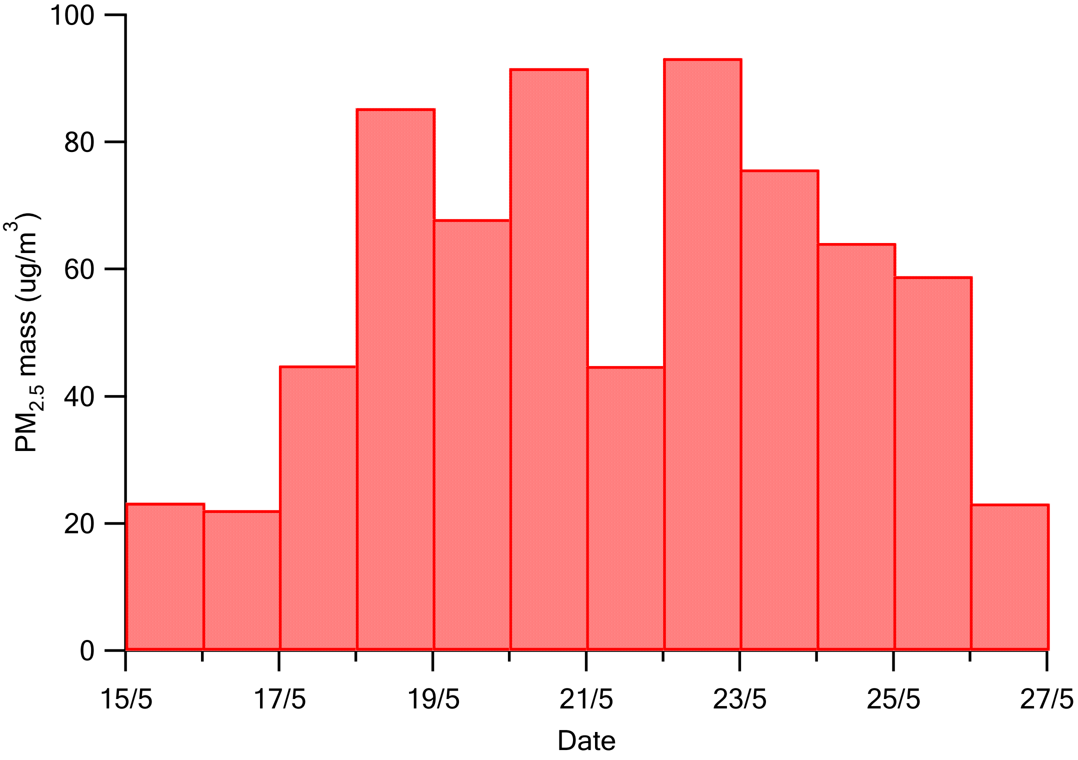

The overall average concentration, together with standard derivation, minimum, maximum and median of the water soluble ion species of both cations and anions in Guangzhou were shown in Table 8.10. Among all the measured water soluble ions, SO_4^{2-}, NO_3^- and NH_4^+ were the dominating species. The average (± standard derivation) SO_4^{2-} concentration was 13.1 (±6.0)µg/m^3, which accounted for 49% of the total water soluble ion species as shown in Figure 8.18. Figure 8.18 showed the relative contribution of individual ion species to the total water soluble ions. The second most abundant ion species was NO_3^-, which accounted for 20% of the total water soluble ions. The mean NO_3^- concentration was 5.2 (±3.8)μg/m^3. Following NO_3^-, NH_4^+ was the third dominating ion species. The mean NH_4^+ concentration was 5.2 (±2.2)μg/m^3, which contributed to 20% of the total water soluble ions. The above three ions have already accounted for 89% of the total water soluble ion species. For the remaining ions, only trace amount of them were detected. For instance, the average Na^+ and K^+ concentrations were 0.4 (±0.1)μg/m^3 and 1.0 (±0.5)μg/m^3, respectively. Furthermore, several ions such as Li^+, Mg^{2+}, F^-, Br^-, PO_4^{3-} were not detected during the whole measurement period. As a whole, the total water soluble ion species contributed to about 48% of the $PM_{2.5}$ mass concentrations. This large percentage of total water soluble ion species to the $PM_{2.5}$ mass concentrations reflected the importance of the ion species in the atmosphere.

Table 8.10. The average, standard derivation, minimum, maximum and median of the individual water soluble ion species (Both cations and anions) in Guangzhou.

	Cations						Anions						
	Li^+	Na^+	NH_4^+	K^+	Mg^{2+}	Ca^{2+}	F^-	Cl^-	NO_2^-	Br^-	NO_3^-	PO_4^{3-}	SO_4^{2-}
Average	N.A.	0.4	5.2	1.0	N.A.	0.3	N.A.	0.8	0.6	N.A.	5.2	N.A.	13.1
[a]St. der.	N.A.	0.1	2.2	0.5	N.A.	0.2	N.A.	0.6	0.2	N.A.	3.8	N.A.	6.0
Minimum	N.A.	0.2	1.7	0.1	N.A.	0.0	N.A.	0.2	0.3	N.A.	1.0	N.A.	3.5
Maximum	N.A.	0.5	8.3	1.7	N.A.	0.6	N.A.	2.2	1.0	N.A.	12.2	N.A.	23.3
Median	N.A.	0.4	6.3	0.9	N.A.	0.3	N.A.	0.7	0.5	N.A.	4.4	N.A.	12.9

[a] St. der. represents standard derivation.

Figure 8.18. The relative contribution of individual ion species to the total water soluble ions in Guangzhou.

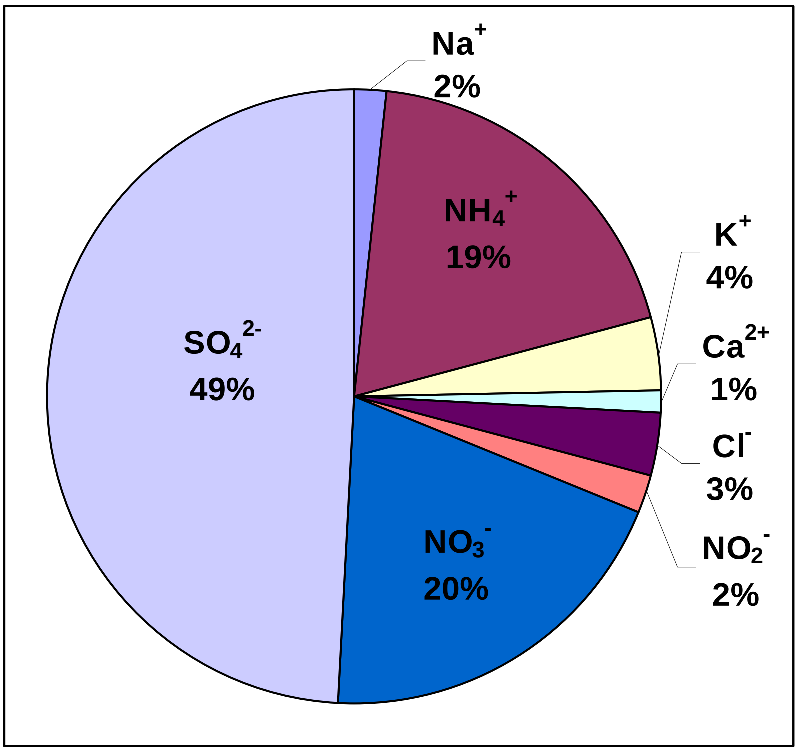

Figure 8.19 showed the daily variation of individual ion species in Guangzhou. As shown in the figure, the daily distribution of ion species was similar and the concentrations of the ions were generally proportional to the $PM_{2.5}$ mass. Moreover, the K^+ ion was present in all the samples and was the indication of the presence of biomass burning. This was different from the Beijing study in which the K^+ ion only present during the $PM_{2.5}$ episode day.

Figure 8.19. The day-to-day variation of individual water soluble ion species in Guangzhou.

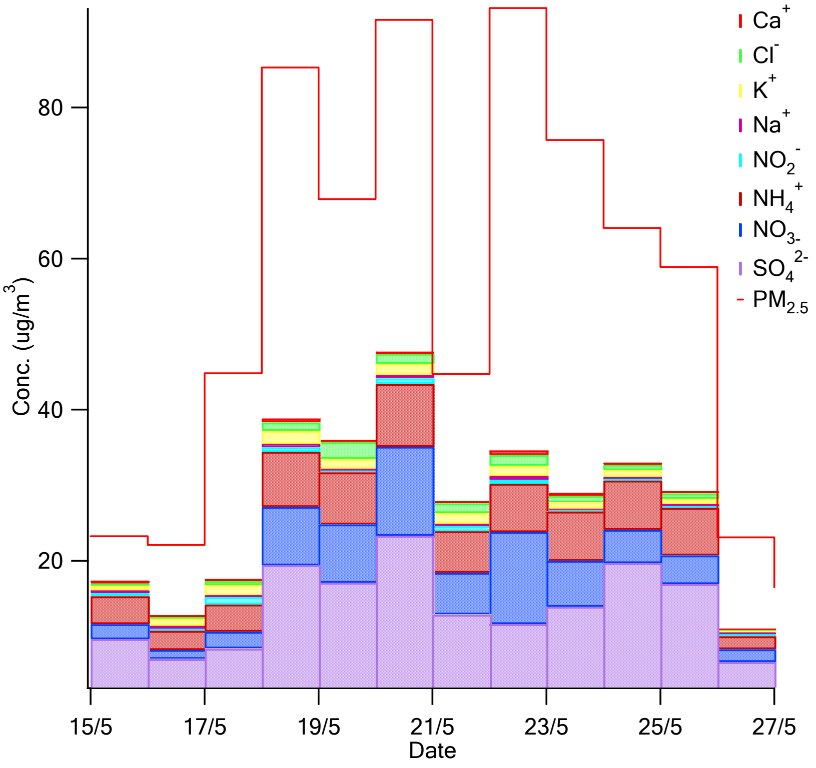

8.4.2 The source of SO_4^{2-} and NO_3^- in $PM_{2.5}$

The daily variation of the mass ratio of $[NO_3^-]/[SO_4^{2-}]$ for the whole measurement period was shown in Figure 8.20. In this study, the average $[NO_3^-]/[SO_4^{2-}]$ ratio was 0.38. The low $[NO_3^-]/[SO_4^{2-}]$ ratio suggested that stationary source emissions were more important than the mobile source emissions in the study area. From Figure 8.20, the mass ratio was below 0.4 for most of the days which indicated the influence of the stationary source was predominant. However, there was a day (22 May) in reach the ratio was larger than 1. This suggested that the sampling location was also affected by the mobile source.

Figure 8.20. The daily variation of the mass ratio of $[NO_3^-]/[SO_4^{2-}]$ in Guangzhou.

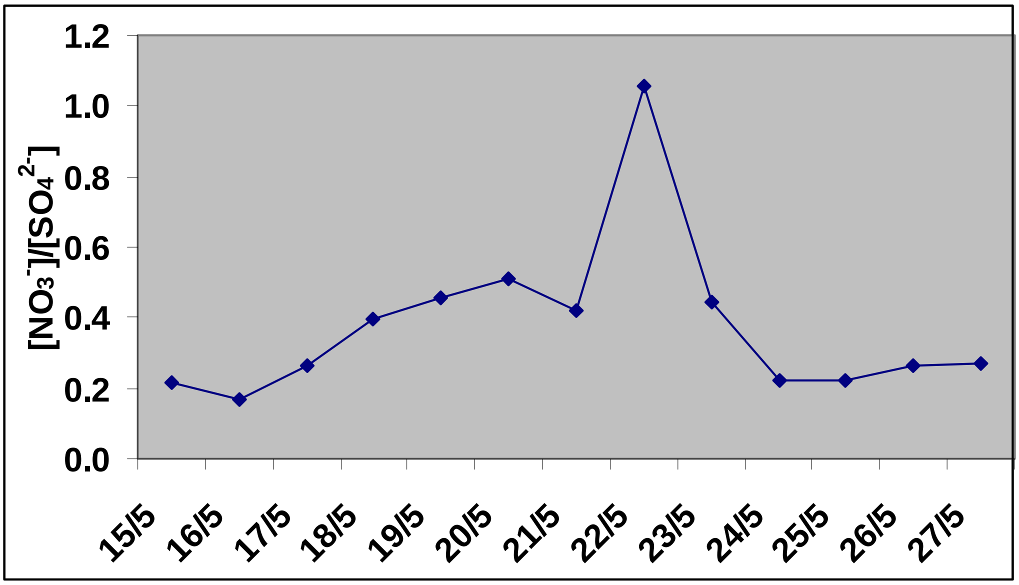

8.4.3 The speciation of major ions

The chemical forms of the major ions in aerosols in Guangzhou were identified by bivariate correlations here. Table 8.11 showed the summary of the correlation coefficients among these major ions. It could be seen that NH_4^+ was well correlated with SO_4^{2-}, NO_3^- and Cl^- while Na^+ was also well correlated with SO_4^{2-}. These suggested that $(NH_4)_2SO_4$, NH_4NO_3, NH_4Cl and Na_2SO_4 were found to be the major chemical species in the aerosol particles based on their correlation coefficients.

Table 8.11. The summary of the correlation coefficients among the major ions in Guangzhou.

R^2	SO_4^{2-}	NO_3^-	Cl^-	NO_2^-
Na^+	**0.66**	0.41	0.31	0.14
K^+	0.37	0.45	0.48	0.17
Ca^{2+}	0.20	0.42	0.22	0.01
NH_4^+	**0.87**	**0.69**	**0.60**	0.02

8.5 Comparison between different megacities

In the previous section of this chapter, I have reported the concentrations, variations and compositions of $PM_{2.5}$ mass and water soluble ion species.

Moreover, the sources, speciation and oxidation of major ions in each sampling location were also discussed. In the section, I would try to compare the findings from different megacities. As the four measurement sites were located at roughly the east (Shanghai), south (Guangzhou), west (Lanzhou) and north (Beijing) of China, the comparison between these four locations could give us some ideas about the difference of particulate loadings and/or conversion routes between different geographical locations. We should note that the comparisons in this study would have some derivations due to the difference of the sampling time at different locations, but at least all the measurements were conducted at the summer time.

8.5.1 Comparison of $PM_{2.5}$ mass

Figure 8.21 showed the comparison of the average $PM_{2.5}$ mass concentrations during the whole measurement period collected at the four sampling sites with the vertical line corresponding to the standard derivation of the measurement. The $PM_{2.5}$ mass showed similar concentrations at different cities. Shanghai, Beijing and Lanzhou showed the levels of around 70µg/m^3 whereas Guangzhou showed a little lower (Around 60µg/m^3). The standard derivation of $PM_{2.5}$ mass at the four locations was also roughly the same with Beijing showing a little larger derivation. The average levels of $PM_{2.5}$ mass in Shanghai, Beijing and Lanzhou have already violated the USEPA standard. The above results suggested that fine particulate pollution problem was not only limited to one or two cities, but affecting the whole country of China. We should also bear in mind that all the measurements conducted in this study were in the suburban and/or rural areas of China, the fine particulate pollution problem in the urban area of China would expect to be more serious. This severe pollution problem would cause harmful effects to the human beings and the environment. As shown in the introduction part, the greater the particulate pollution problem, the number of mortality and morbidity is increased correspondingly.

Figure 8.21. Comparison of $PM_{2.5}$ mass at four sampling locations.

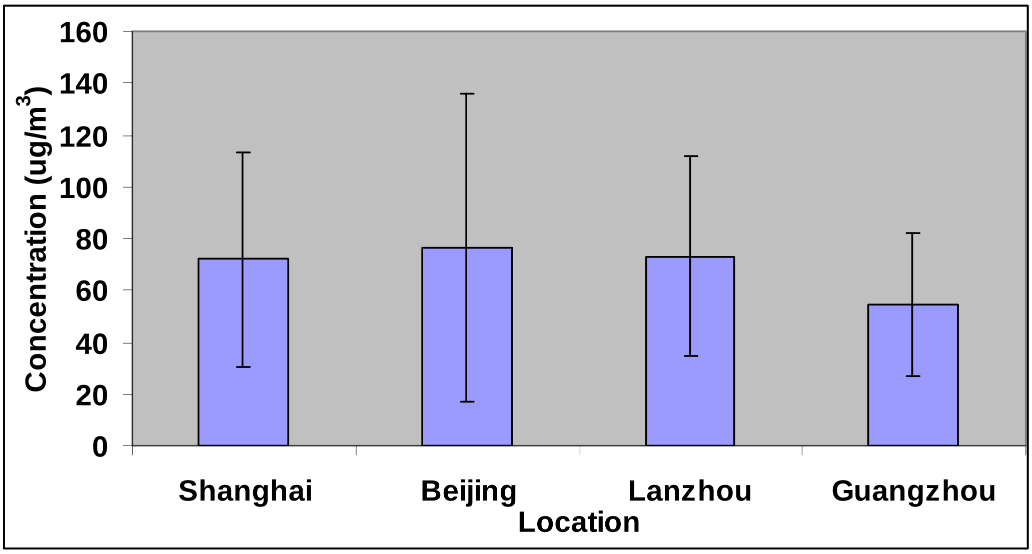

Table 8.12 tabulated the $PM_{2.5}$ mass concentrations in this study as well as other studies in the world. In this table, all the studies were conducted in the rural and/or suburban areas during summer time. Referring to Table 8.12, the concentrations of $PM_{2.5}$ mass were below 25µg/m^3 for the studies conducted in rural and/or suburban areas (Including Japan, Korea, United States, United Kingdom, Austria). However, the levels of $PM_{2.5}$ mass in China (This study) were two to seven folds higher than others. Thus, this comparison could serve as an example to illustrate the seriousness of the fine particulate pollution problem in China and China could also be one of the most polluted countries in the world.

Table 8.12. Comparison of $PM_{2.5}$ mass concentrations with other studies in the world.

City, Country	Sampling period	Land type	$PM_{2.5}$ mass ($\mu g/m^3$)	Reference
Birmingham, United Kingdom	Jun – Aug (98 – 00)	Rural	~10	Dingenen et al., 2004
Vienna, Austria	Jun – Aug 99	Rural	~13	Hauck et al., 2004
Tokyo, Japan	Jul 02	Suburban	18.0	Sasaki and Sakamoto, 2006
Tennessee, United States	Jul – Aug 02	Rural	21.1	Tanner et al., 2005
Gosan, Korea	Aug 03	Rural	10.9	Kim et al., 2007
Guangzhou, China	May 04	Suburban	54.7	This study
Shanghai, China	May – Jun 05	Suburban	71.9	This study
Beijing, China	Jun – Aug 05	Rural	76.6	This study
Lanzhou, China	Jun – Jul 06	Suburban	73.1	This study

8.5.2 Comparison of water soluble ions

8.5.2.1 Comparison of the concentrations of total water soluble ions

Figure 8.22 showed the comparison of the concentrations of total water soluble ions at four sampling locations. The vertical bar represents the standard derivation of total water soluble ions. We could see that the levels of total water soluble ions were similar at four different sampling locations in which Beijing showing a little higher concentration (38.7µg/m^3) than others (26.4µg/m^3 – 32.0µg/m^3). Combined with the data showed previously in which the $PM_{2.5}$ mass at four sites were similar, we should be able to deduce that the contribution of water soluble ions to $PM_{2.5}$ mass was the highest in Beijing (About 53%). One of the reasons was that the sampling location in Beijing was located at the mountain top and was the most rural in comparison with the other three sites. For the remaining three locations, we could only classify them as suburban areas. As the ions such as sulfate and nitrate were primarily secondary in nature, sampling at more rural area could provide more time for the formation of secondary species and thus higher levels of ions in $PM_{2.5}$. As a consequent, the higher concentrations of ions, especially sulfate (Larger contribution to the chemical light extinction), would have great effect on visibility and the environment. As observed from each sampling site, the visibility problem was the most serious in the Beijing area. The clean day and the poor visibility day in Beijing sampling site were shown in Figure 8.23. Figure 8.23a showed the photo taken on 23 July. On that day, the $PM_{2.5}$ mass and sulfate concentration were only 13.3µg/m^3 and 3.6µg/m^3, respectively. In contrast, Figure 8.23b showed the photo taken on 17 July from the same view as that of Figure 8.23a. The $PM_{2.5}$ mass and sulfate concentration were 141.0μg/m^3 and 67.0μg/m^3, respectively on that day. Therefore, the visibility problem was clearly seen from these two photos.

Figure 8.22. Comparison of the concentrations of total water soluble ions at four sampling locations.

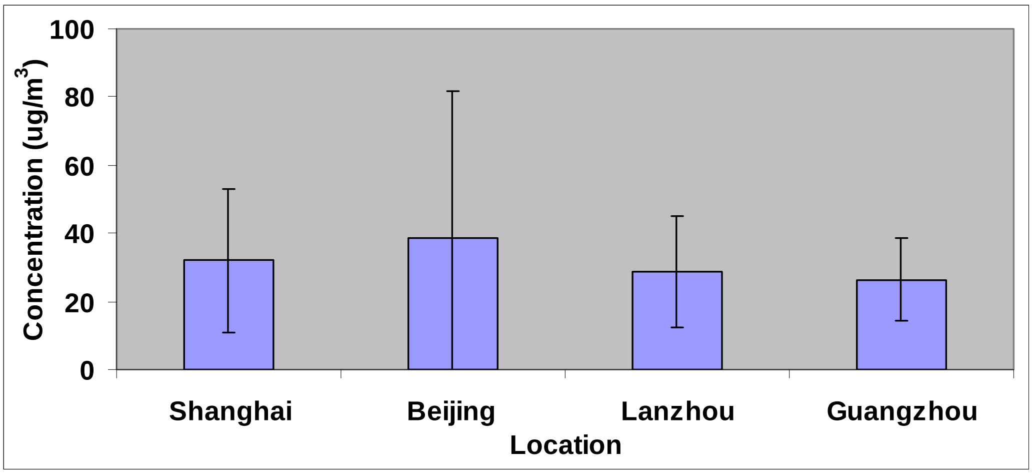

Figure 8.23. Photo taken on (a) 23 July (b) 17 July.

(a)

(b)

Besides, the standard derivation of ions in Beijing was the largest in comparison with the others as shown in Figure 8.24. This was due to the contrasting air mass from the south (urban centre) and the north (background air mass) reaching the sampling site at different periods of time. This has been discussed before and will not be further elaborate here. Apart from Beijing, Lanzhou should have similar situation (as discussed in section 8.3.1), but couldn’t reflect in this figure. This was because the change of air masses in Lanzhou occurred within a few hours and on the same day so that the effect was mask. However, for the Beijing situation, the air mass changed for days or even weeks. This could also serve as one of the good examples of using continuous instruments rather than the filter collection method.

8.5.2.2 Comparison of the ion compositions

The ion distribution at the four sampling sites was basically similar. Sulfate was the most dominant ion species in all sampling locations and accounted for 35% – 57% of the total water soluble ions. Except Lanzhou, nitrate and ammonium were the second and third most dominant ion species. Lanzhou showed a little different ion composition in which chloride and ammonium were the second and third dominant ion species. The difference in this ion composition suggested that the source of chloride in Lanzhou was different from others. From the correlation plot of sodium and chloride ions in each sampling site, we could see that the correlation of sodium and chloride was moderate in Shanghai (0.70), Beijing (0.64) and Guangzhou (0.31), while no correlation was found in Lanzhou (0.03). This also provided an additional support of different source of chloride in Lanzhou from the others. The good correlation of chloride with sodium suggested that chloride was mainly from the marine source. In contrast, the marine influence on the levels of chloride might be minor in Lanzhou and the chloride ion might be associated with the burning activities in the surrounding area. For the rest of the ions, it contributed to less than 10% for each individual ion.

8.5.2.3 Comparison of the sources of sulfate and nitrate in $PM_{2.5}$

The source of sulfate and nitrate was identified in previous section based on the $[NO_3^-]/[SO_4^{2-}]$ ratio. The results obtained from the four sampling sites were similar (0.44 in Shanghai, 0.40 in Beijing, 0.38 in Lanzhou and 0.38 in Guangzhou) which indicated the more influence of the stationary sources over the mobile sources in the whole region of China. Streets and Waldhoff (2000) has reported the emissions of SO_2 and NO_x in 1995 in various cities of China. The emissions of SO_2 in Shanghai, Beijing and Guangzhou were 544kt, 304kt and 250kt, respectively, while the emissions of NO_x in Shanghai, Beijing and Guangzhou were 352kt, 243kt and 138kt, respectively. Thus, the corresponding

$[NO_x]/[SO_2]$ ratio were 0.65, 0.80, 0.55 in Shanghai, Beijing and Guangzhou, respectively. The ratios obtained in 1995 were comparatively larger than our studies. This indicated that China was more affected by the emissions of mobile sources at that time. More recent work from Streets et al. (2003) also reported the emissions of SO_2 and NO_x in China in 2000 and were 20,385Gg and 11,347Gg, respectively, which corresponded to the $[NO_x]/[SO_2]$ ratio of 0.56. This reflected the more important of the stationary sources in 2000 when comparing with 1995. This result could be expected as China has grown rapidly during the past ten years. Many industries have been built and in turn the energy consumption was also rapidly increased. Streets et al. (2003) reported the fuel consumption in China by stationary sources such as industries, power plants were 31955PJ, whereas the fuel consumption by mobile sources were only 4246PJ in 2000. Our studies in 2004 – 2006 could suggest that pollution from stationary sources was becoming more important in the whole region of China.

8.5.2.4 Comparison of the speciation of the major ions

The chemical forms of the major ions in aerosols at the four sampling sites were identified. Results suggested that ammonium sulfate $[(NH_4)_2SO_4]$ was the most common form of ions exist in $PM_{2.5}$ mass. All the sampling sites have shown good correlations among these two ions. The second most common ion form was ammonium nitrate (NH_4NO_3). Except Lanzhou, all of them showed good correlations. The remaining ion forms were varied among different locations. For example, sodium chloride (NaCl) and potassium chloride (KCl) showed good correlations in Shanghai and Beijing. This suggested the influence of the marine sources and biomass burning at these two locations. In contrast, sodium sulfate (Na_2SO_4) showed good correlations in Beijing and Guangzhou only. We could see that different locations had different sources of ions so as to contribute different major form of ions.

8.5.2.5 Comparison of the oxidation of sulfur and nitrogen

The sulfur oxidation ratio and nitrogen oxidation ratio has been reported previously. Shanghai and Lanzhou showed similar overall SOR and NOR values (Shanghai – SOR: 0.16, NOR: 0.07, Lanzhou – SOR: 0.18, NOR: 0.09). This was because the two sampling sites were located at the suburban areas and the time for the formation of ions was roughly similar. In Beijing, larger SOR and NOR values (SOR: 0.45, NOR: 0.16) were obtained. This indicated the more processing air masses reaching the station than other sites as the sampling site in Beijing was located at the rural area and more time was given for the ion to form during the transport from the sources to the monitoring station.

Finally, SOR and NOR was correlate with the possible controlling factors governing the sulfate and nitrate formation. Most of the correlation was not good except the correlation between the SOR and the relative humidity in Beijing. The results suggested that multiple reaction pathways for the formation of ions occurred simultaneously. In addition, filter-based sampling was also not good enough method to determine the reaction pathways due to the long sampling time.

Chapter 9: Formation mechanisms of sulfate, nitrate and the contribution of aerosols to the visibility impairment in Beijing

The formation mechanisms of sulfate and nitrate are worth studying because these two ions are the major components of water-soluble ion species in the atmosphere. It also contributes to a significant fraction in $PM_{2.5}$. In this chapter, I will explore and discuss the formation routes of sulfate and nitrate based on the results obtained from both the AIM and the filter analysis. In addition, visibility is largely affected by the presence of aerosols in the atmosphere. Thus, I will also discuss the significant of aerosols which lead to the visibility reduction in Beijing

9.1 Formation of sulfate

9.1.1 Formation of sulfate in Beijing under different meteorological conditions

As discussed previously in section 7.1.1, the concentrations of fine aerosols at the Beijing study site are strongly influenced by the change in the weather conditions. In the following discussion, I will examine two cases in details to show the relation of the formation of sulfate to the meteorological condition and long-range / meso-scale transport.

Case I: June 30. Figure 9.1 showed the time series of 30 June of aerosols ($PM_{2.5}$ mass, sulfate, nitrate), trace gases (CO, SO_2, NO, NO_y, O_3), and meteorological parameters (solar, total ultraviolet, relative humidity, temperature, wind direction, wind speed). This was the “super” ozone episode with the maximum O_3 hourly mixing ratio of 286ppbv, which was the highest reported value in open literature for China [Wang et al., 2006]. We could see that the local weather condition on that day is characterised by strong solar radiation and low relative humidity. Most of the primary trace gases, O_3, and $PM_{2.5}$ mass concentrations reached very high levels in the afternoon (NO_y ~49ppbv, SO_2 ~22ppbv, and $PM_{2.5}$ mass ~225μg/m^3). However, fine sulfate and nitrate only accounted for 14% and 10%, respectively, of total $PM_{2.5}$ mass, suggesting significant contribution of organic aerosols to the $PM_{2.5}$ mass [Black carbon only contributed to a small fraction (4%) of the $PM_{2.5}$ mass].

Figure 9.1. Time series of 30 June of aerosols ($PM_{2.5}$ mass, sulfate, nitrate), trace gases (CO, SO_2, NO, NO_y, O_3), and meteorological parameters (solar, total ultraviolet, relative humidity, temperature, wind direction, wind speed).

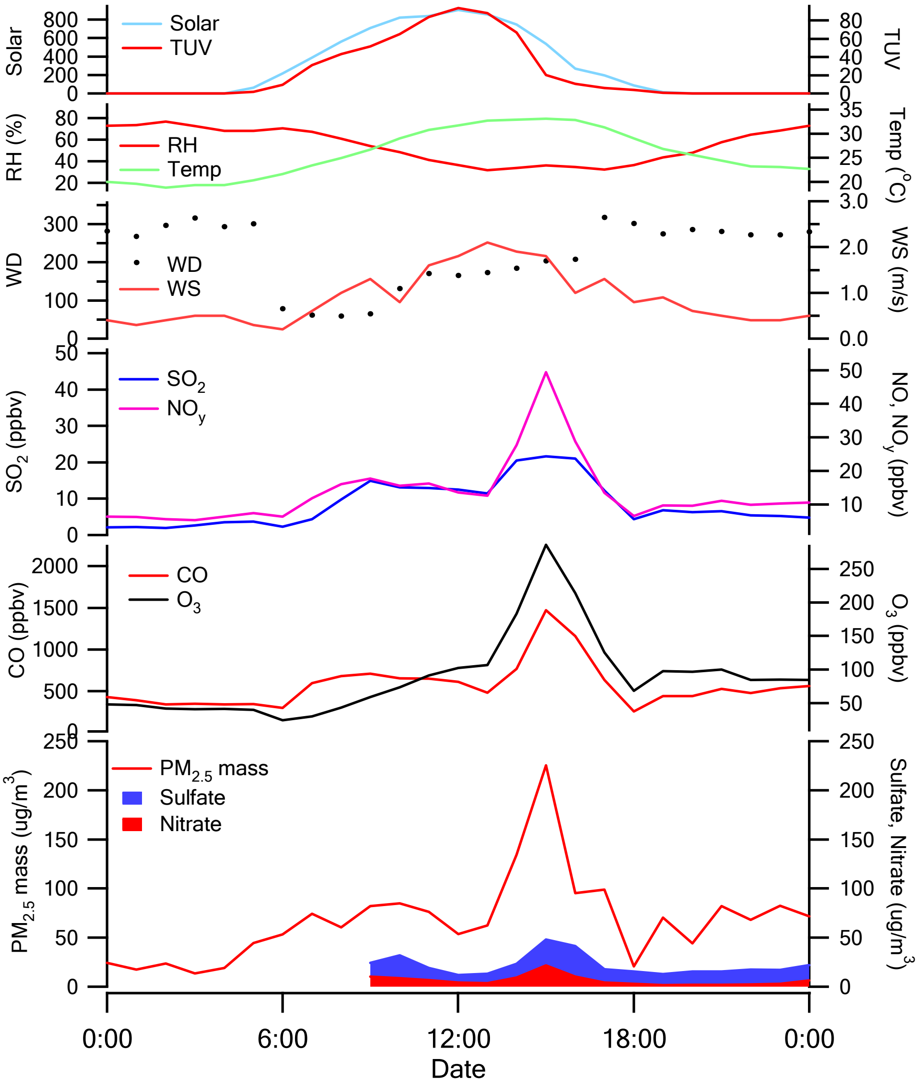

To learn about the synoptic condition related to this episode, the mean potential height and wind stream at 950hPa on 29 June – 1 July are shown in Figure 9.2a. A low-pressure system was situated in north-eastern China with a strong Pacific High at low latitude; Beijing is located in the convergence zone between the air from the southwest and that from the remote areas to the west. Three-day backward back trajectories ending at 100m AGL over the site before, during and after arrival of the plumes are plotted on a mean MODIS Aerosol Optical Depth (AOD) map during these three days (Figure 10.2b) (The MODIS data are obtained from http://disc1.sci.gsfc.nasa.gov/daac-bin/G3/gui.cgi?instance_id=MODIS_DAILY_L3). The back trajectories are calculated using the HYSPLIT model (HYbrid Single-Particle Lagrangian Integrated Trajectory, NOAA Air Resources Laboratory) driven by MM5 nesting simulations [Ding et al., 2004; Wang et al., 2006], and the left bottom of Figure 9.2b showed the magnified picture of hourly trajectories on a topographic map. It showed that the very high concentrations of fine aerosols (and ozone) in the afternoon of June 30 were due to the transport of urban emissions from Beijing. The AOD map of this day suggested that there was no regional aerosol pollution around Beijing.

In addition, this low formation of sulfate could be attributed to the low ambient water content. The average ambient water content on that day was 0.012g/g which did not favor the conversion of SO_2. Details will be discussed in the following section. Although it was a sunny day with high SO_2 concentrations, the conversion of SO_2 was still low.

Figure 9.2. (a) Mean 950hPa geopotential height and wind stream during 29 June – 1 July, and (b) 3-day back-trajectories ending at 100m AGL over the site for the episode hour and pre-/post-episode hours on averaged MODIS Terra Aerosol Optical Depth map during these three days. The bottom left of Figure 10.2b showed the magnified picture of hourly trajectories on the topographic map. The red dot on both figures represented the sampling site.

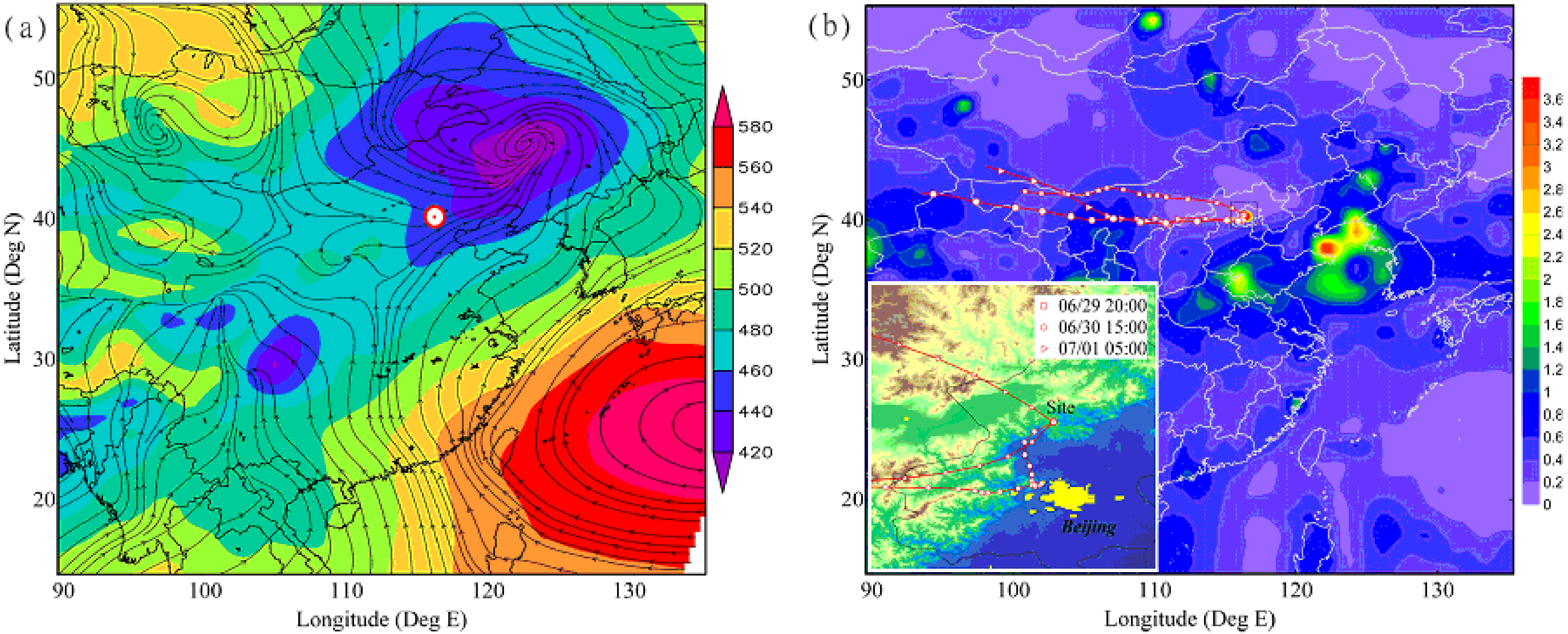

Case II: 12 – 20 July. Figure 9.3 showed the time series of 12 – 20 July of aerosols ($PM_{2.5}$ mass, sulfate, nitrate), trace gases (CO, SO_2, NO, NO_y, O_3), and meteorological parameters (solar, total ultraviolet, relative humidity, temperature, wind direction, wind speed). This multi-day episode could be clearly seen from the time series in the figure. The weather during this period was mostly cloudy and the humidity was high (average: 75%). The maximum hourly O_3 concentrations were mostly above 100ppbv indicating moderate photochemical pollution. The concentrations of the primary gases were moderately high whereas the levels of the $PM_{2.5}$ mass were very high, with the maximum hourly levels in each day ranging from 188μg/m^3 to 355μg/m^3. Sulfate and nitrate contributed to about 40% and 13% of total $PM_{2.5}$ mass, respectively. SO_2 is completely depleted on the last day of the episode (being converted to sulfate) while the NO_y levels remained high, indicating NO_y is not subjected to a significant degree of removal.

Figure 9.3. Time series of 12 – 20 July of aerosols (PM$_{2.5}$ mass, sulfate, nitrate), trace gases (CO, SO$_2$, NO, NO$_y$, O$_3$), and meteorological parameters (solar, total ultraviolet, relative humidity, temperature, wind direction, wind speed).

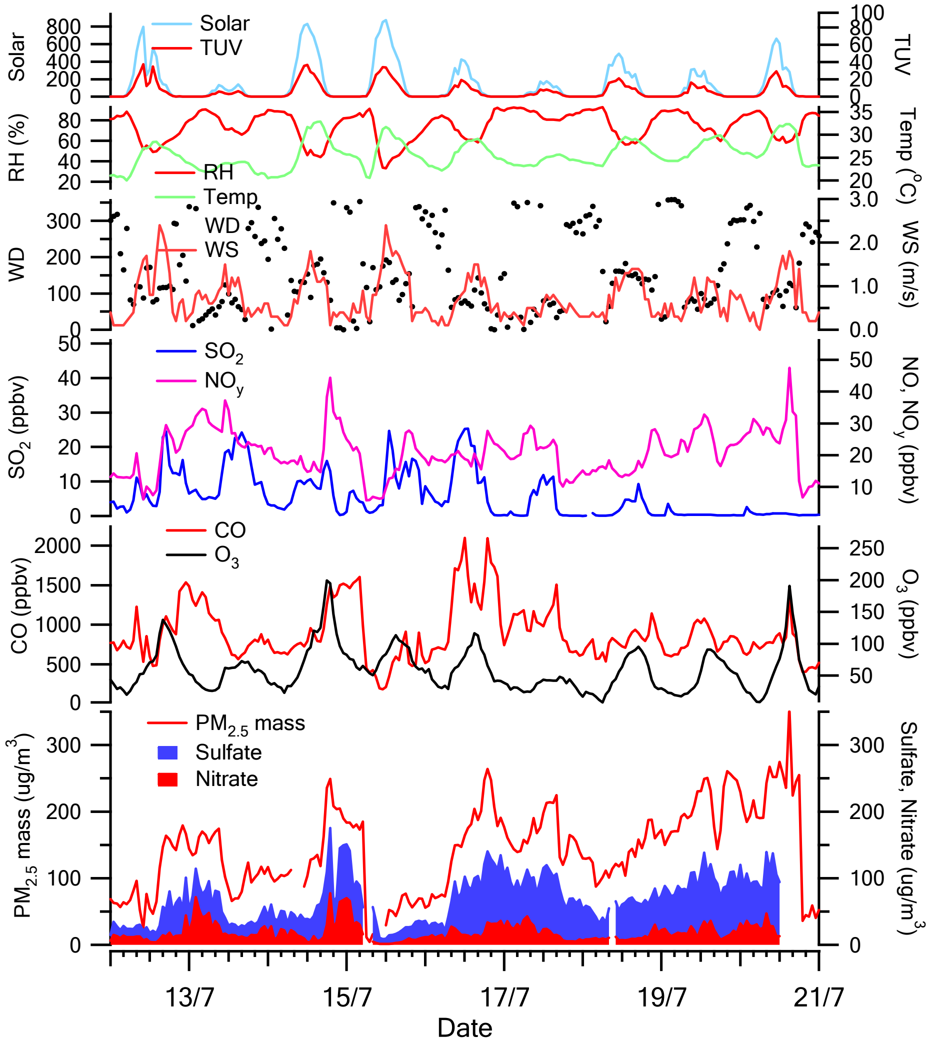

The mean 950hPa potential height and wind stream during 12 – 20 July is shown in Figure 9.4a, and 3-day back-trajectories ending at 100, 300, and 500m (see marker size) at the hour of aerosol peaks are shown in Figure 9.4b. Typhoon HAITANG landed in southeast China. Associated with this cyclone, the Pacific High is situated in a more northern location than in Case I, giving continuous south-easterly and southerly winds in the Eastern China and the NCPs. The AOD data revealed very severe aerosol pollution in the NCPs (with an AOD value of up to 3.8). Back trajectories showed that air masses arriving at the site during this episode came from the southeast, south and southwest, suggesting that the very high concentrations of sulfate aerosol were due to the impact of regional sources in the NCPs under humid conditions. In addition, the results also suggested that cloudy weather and high water content would favor the conversion of SO_2 by aqueous phase reaction.

Figure 9.4. Same as Figure 10.2 but for the period of 12 – 20 July. Note: Back-trajectories for this period are calculated for three altitudes: 100m, 300m, and 500m above ground level.

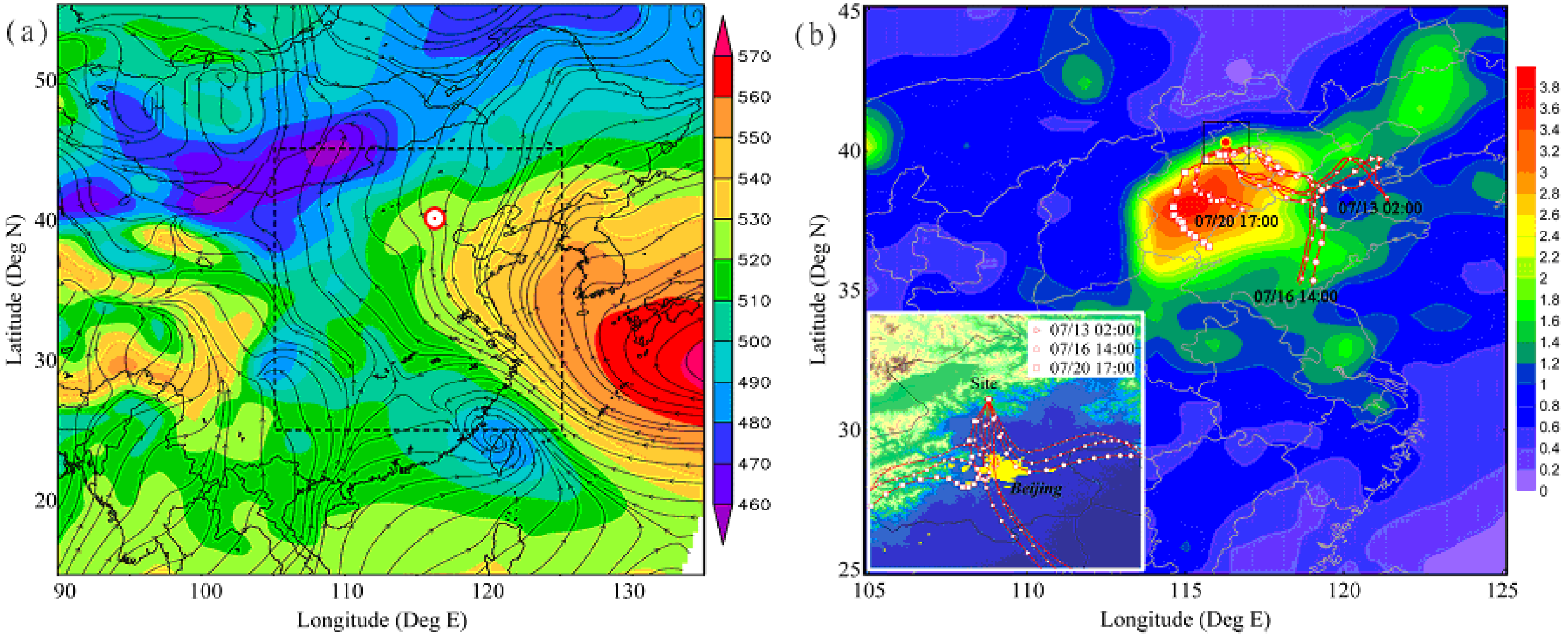

9.1.2 Formation of sulfate in downwind area of Beijing

Figure 9.5a showed the scatter plot of sulfate and total sulfur ([SO_2] + [Sulfate], unit: ppbv) colour-coded with specific humidity (SH) for all data. The sulfur conversion ratio [sulfate / total sulfur] increased with humidity: SO_2 is almost completely converted to sulfate when SH reached 2×10^{-2}g/g. The average sulfur conversion ratio was 77% for SH $\geq$ 0.016g/g. In contrast, the average sulfur conversion ratio was 40% for SH $\leq$ 0.014g/g. The increased conversion of SO_2 to sulfate under humid conditions is consistent with the current understanding of sulfur chemistry indicating the importance of aqueous phase reactions in the formation of sulfate from SO_2 [Seinfeld and Pandis, 1998].

Figure 9.5a. Scatter plot of Sulfate and Total sulfur (SO_2 + sulfate) colour-coded according to specific humidity for all data.

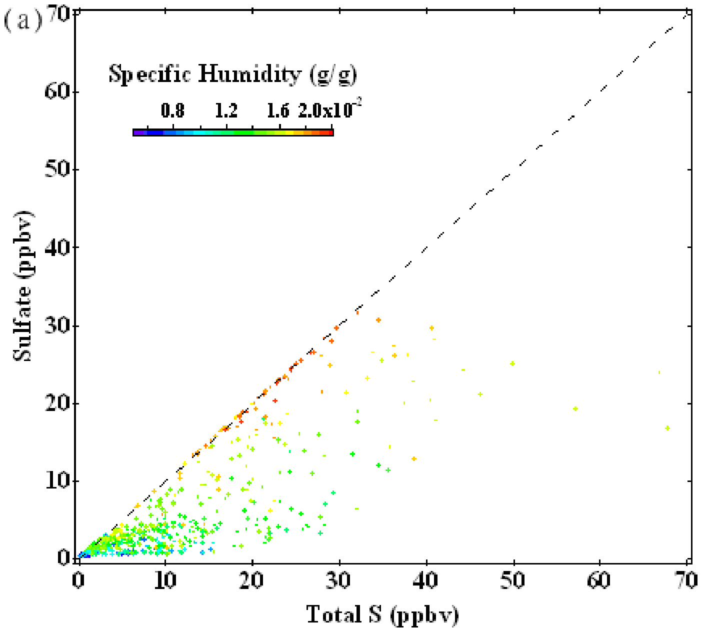

The detail of this reaction is shown in the followings:

SO_2 firstly dissolves in water to form sulfurous acid.

$$SO_2 + H_2O \rightarrow H_2SO_3$$

After that, the major aqueous sulfate formation includes the reactions of dissolved SO_2 with H_2O_2, O_3 or O_2 (catalyzed by Mn^{2+} or Fe^{3+}).

$$SO_2 + \frac{1}{2} O_2 + Mn^{2+} \text{ or } Fe^{3+} \rightarrow H_2SO_4$$

$$SO_2 + H_2O_2 \rightarrow H_2SO_4 + H_2O$$

$$SO_2 + O_3 \rightarrow H_2SO_4 + O_2$$

[Khoder, 2002; Saxena and Seigneur, 1987]

As shown from the above, ambient water content played an important role for the conversion of SO_2 to sulfate in the study region. Therefore, we believed that aqueous phase reaction was a dominant reaction pathway for the oxidation of SO_2 in Beijing. Apart from that, the abundant O_3 and possibly other oxidants in northern Beijing may have accelerated the formation of sulfate, and the presence of large amounts of particulate matter around Beijing could also provide larger surface areas for the aqueous phase and heterogeneous reactions to occur [Sharma et al., 2003; Foltescu et al., 1996].

To examine the extent of SO_2 conversion in different episodes, Figure 9.5b showed the scatter plot of Case I and II plus five additional cases during which a well defined plume (with O_3 >180ppbv) from Beijing impacted the study site. It was supported by the well-defined shape and narrow width of the plumes for the trace gases (not shown here). This suggested that the plumes have not experienced significant degree of dispersion and mixing since emission. Thus, the plumes should come from a large source not far away from the site. As Beijing is the closest metropolitan area in the upwind direction with strong emissions, plumes from the city could reach the site in a few hours without much dispersion, giving rise to the high concentrations of ozone and other primary gases. In addition, the calculated 3-day back trajectories with HYSPLIT4 model (Hybrid Single-Particle Lagrangian Integrated Trajectory model version 4.7) also supported the above. Therefore, the plumes from these episode cases could be classified as the urban plumes coming from Beijing. More details about these cases could refer to Wang et al., 2006.

Figure 9.5b. Scatter plot of Case I (denoted by crosses) and II (denoted by dots) plus urban plumes (denoted by open circles).

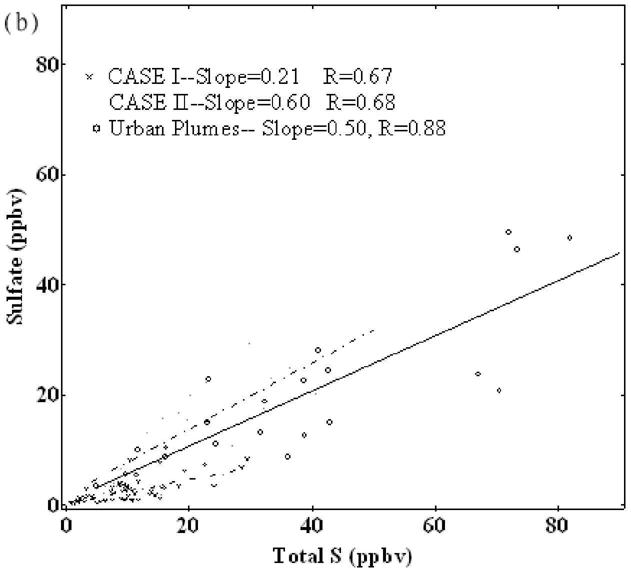

In these episode cases, the sulfate concentrations together with the $PM_{2.5}$ mass were high. The concentrations of sulfate ranged from $18\mu g/m^3$ to $131\mu g/m^3$ during the pollution events while the $PM_{2.5}$ mass ranged from $81\mu g/m^3$ to $262\mu g/m^3$. These high particulate concentrations clearly indicated that the great impact of the urban plumes to the regional air quality. As seen in Figure 9.5b, Case I and II had a very different slope, 0.21 vs. 0.6, and Case II contained most of the points with high humidity. The remaining five episodes gave a good overall linear correlation (r =

0.88) and a slope of 0.50. Given an average transport time of about 6 hours from the Beijing urban area (based on the trajectories result), the conversion rate of SO_2 was approximately 8% per hour in these plumes and about 4% per hour for 30 June when the air was drier. The conversion rates in most of the cases in our study appeared to be on the high end of the observed values reported in previous studies [Edgerton et al., 2006; Warneck, 2000]. Given the high hygroscopicity of sulfate aerosols, the large loading of sulfate observed at this site indicates severe impairment of summertime visibility by secondary air pollution. The high concentrations of sulfate may also lead to the formation of acid rain and may also affect the weather pattern of the study region.

9.1.3 Formation of sulfate in Shanghai

Figure 9.6 showed the scatter plot of sulfate and total sulfur ($[SO_2]$ + [Sulfate], unit: ppbv) colour-coded with relative humidity for all data. The sulfur conversion ratio [sulfate / total sulfur] did not show any relation with humidity. The result was in contrast to the findings in Beijing in which the SO_2 is almost completely converted to sulfate at high humidity. The average sulfur conversion ratio was 23% during the whole measurement period. The above result suggested that sulfate formation mechanisms in Shanghai were much more complex than in Beijing. In Shanghai, several formation mechanisms may be occurred simultaneously so that single factor contributing to the reaction could not be easily identified.

Figure 9.6. Scatter plot of Sulfate and Total sulfur (SO_2 + sulfate) colour-coded according to the relative humidity for all data.

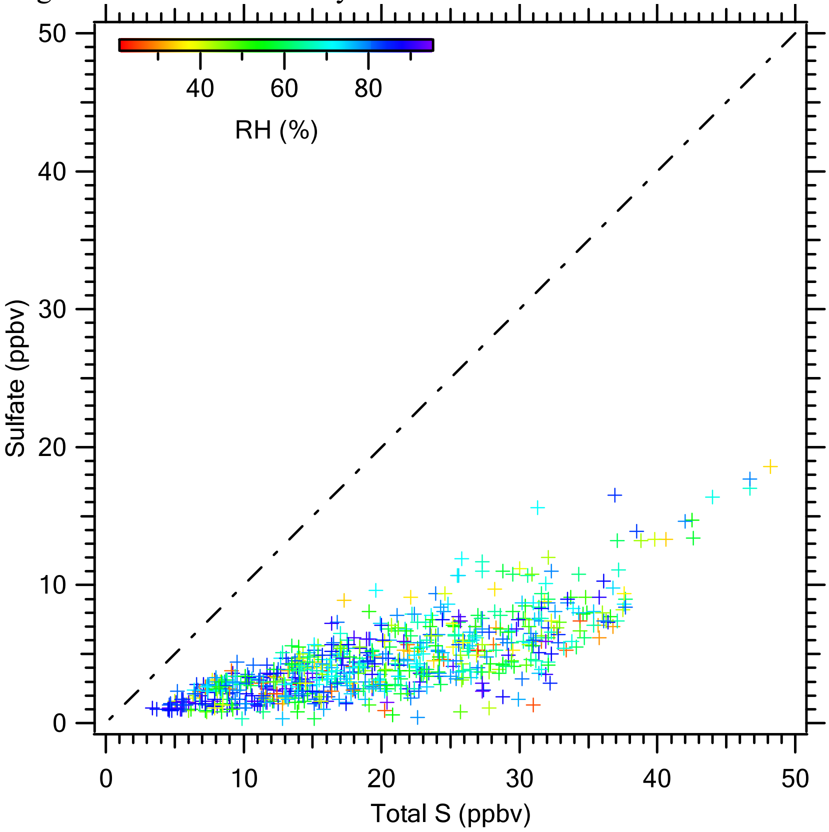

9.2 Formation of nitrate

After discussing the formation of sulfate in previous section, I will continue to examine the formation of nitrate at the four study sites. The formation of nitrate can mainly divide into two types: ammonium-rich samples and ammonium-poor samples.

Figure 9.7 showed the molar ratio of [nitrate]/[sulfate] versus molar ratio of [ammonium]/[sulfate] for the samples in the four study sites as well as those from the literature. These ratios indicated the reaction between ammonia and nitric acid and other formation processes of nitrate under different sulfate concentrations. From the figure, we could see that the relative abundance of nitrate increased when the molar ratio of ammonium to sulfate increased for the ammonium rich samples ($[NH_4^+]/[SO_4^{2-}] > 1.5$). This indicated that more nitrate is added in the sulfate-nitrate-ammonium system by the increase in ammonium concentrations.

Figure 9.7. Molar ratio of nitrate to sulfate versus molar ratio of ammonium to sulfate.

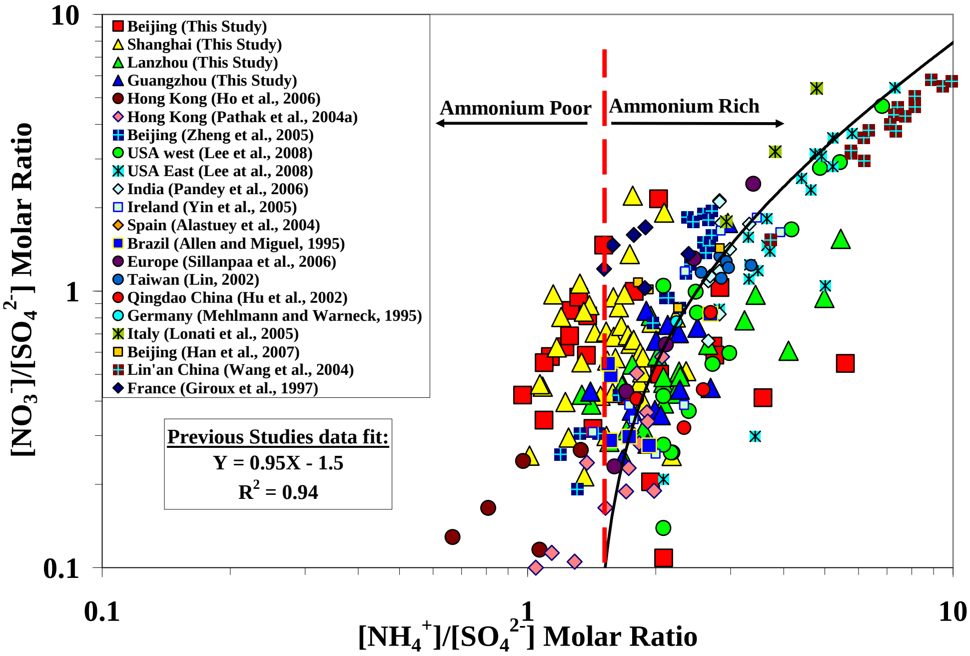

Recall from Chapter 1, nitrate could be formed from two major reaction pathways: gas-phase homogeneous reaction ($HNO_3 + NH_3 \leftrightarrow NH_4NO_3$) as well as heterogeneous reaction ($NO_3 + N_2O_5 \rightarrow$ aerosol NO_3^-). As shown in Figure 9.8, the excess ammonium was similar to the nitrate concentrations. Excess ammonium was equal to $[NH_4^+]/[SO_4^{2-}] - 1.5$ times $[SO_4^{2-}]$. This figure showed that the responsible reaction pathway for the increase in the nitrate concentration with almost similar increase in the excess ammonium was due to the gas-phase homogeneous reaction between ambient ammonia and nitric acid in the ammonium rich samples. We could see that most of the previous studies followed this trend (solid line in Figure 9.7) indicating the nitrate formation was through this reaction pathway. The scattering of the data in Figure 9.8 could be due to the influence of other atmospheric processes such as sodium nitrate formation.

Figure 9.8. Nitrate concentration as a function of “excess ammonium”.

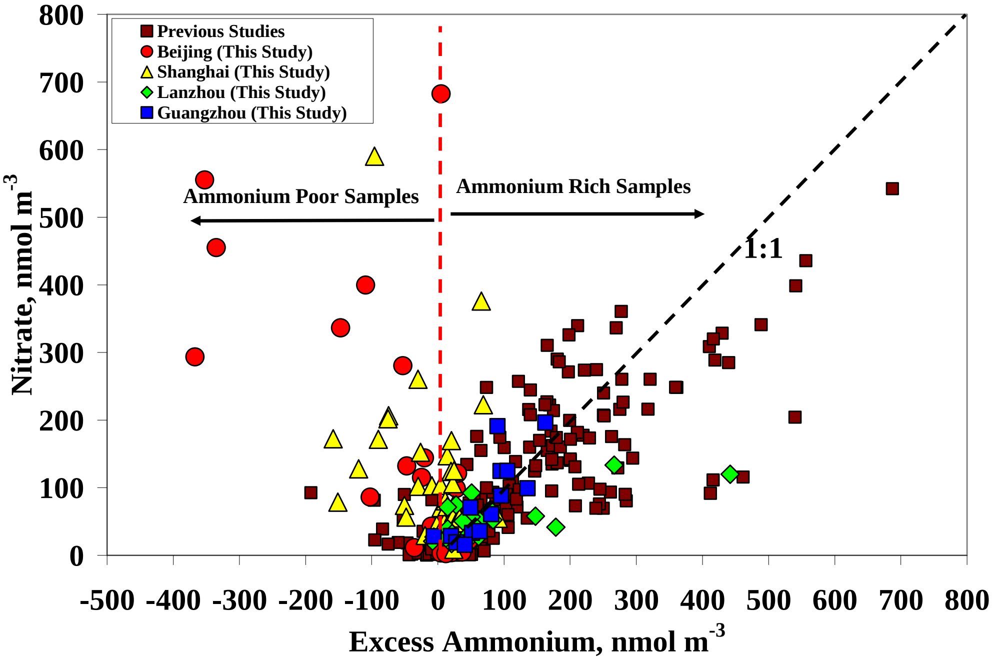

In our Lanzhou and Guangzhou studies, most of the samples were ammonium rich (indicated by green and blue colour, respectively in Figure 9.8) and the nitrate formation in these two sampling sites are most possibly formed from the gas-phase homogeneous reaction between ammonia and nitric acid similar to the previous reported results.

As shown in Figure 9.7, few samples from Hong Kong and Europe in the previous studies showed low nitrate to sulfate molar ratio and scattered at $[NH_4^+]/[SO_4^{2-}]$ below 1.5. This suggested the formation of nitrate was not important when the ammonia was not rich enough. However, for the Beijing and Shanghai samples, the formation mechanisms of nitrate were different from the previous reported literature as well as Lanzhou and Guangzhou samples. We could see clearly from Figure 9.7 that the molar ratio of ammonium to sulfate was below 1.5 for most of the samples in Shanghai and Beijing, but it was different from those previously reported results (i.e. the nitrate concentrations were low at low ammonium to sulfate molar ratio). Figure 9.8 further showed that the molar ratio of nitrate to sulfate increased with decreasing excess ammonium indicating nitrate is associated with acidity. This result suggested that the high nitrate concentrations in Beijing and Shanghai could not be explained by the homogeneous gas-phase reaction between ammonia and nitric acid.

Instead, the high concentrations of nitrate in Shanghai and Beijing were more related to the heterogeneous hydrolysis of N_2O_5. The high concentrations of $PM_{2.5}$ mass and large fractions of water soluble ion species in $PM_{2.5}$ in Beijing and Shanghai suggested that the aerosols there were largely hydroscopic with large surface areas as well as highly acidic as discussed in Chapter 8. According to previous studies, high hygroscopicity, surface area, and acidity of the pre-exisiting particles promote heterogeneous hydrolysis of N_2O_5 [Anttila et al., 2006; Hallquist et al., 2003; Hu and Abbat, 1997; Martinez et al., 2000; McLaren et al., 2004]. Thus, these conditions would favour the hydrolysis of N_2O_5 leading to the formation of nitrate on pre-existing aerosols. A strong positive correlation between sulfate and nitrate (Figure 9.9) was found and high concentrations of sulfate and nitrate were found at high RH. These could be explained as nitrate was produced on the preexisting sulfate aerosols, which could provide sufficient surface areas, aerosol water content and aerosol acidity for the N_2O_5 hydrolysis.

Figure 9.9. Nitrate versus sulfate concentrations colour-coded with ambient RH.

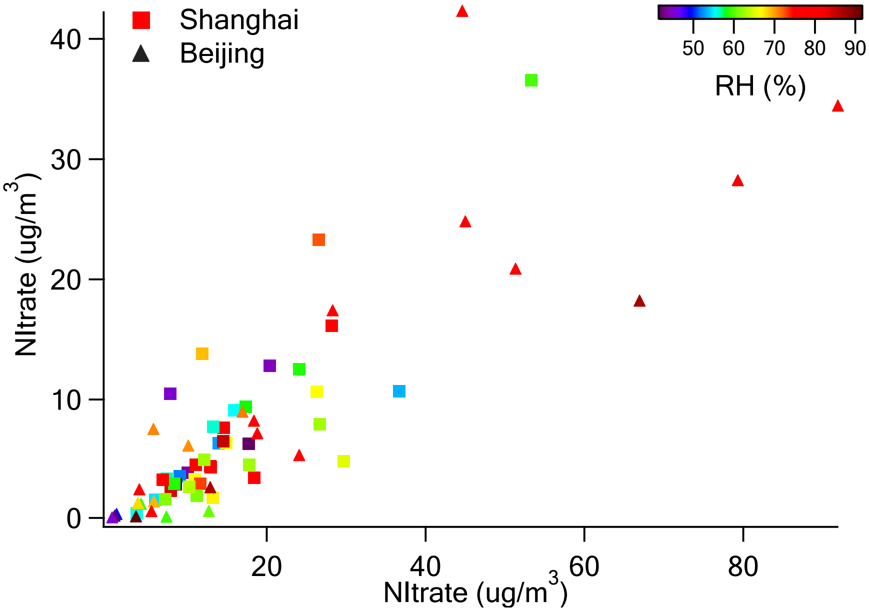

Another indication for the role of hydrolysis in producing the nitrate can be seen from the scatter plot between nitrate and total reactive nitrogen as shown in Figure 9.10. Figure 9.10 showed that the high concentrations of nitrate are mostly associated with high aerosol water content and are less dependent on NO_y, which indicated the importance of heterogeneous hydrolysis in the production of nitrate in these samples.

Figure 9.10. Nitrate concentrations as a function of total reactive nitrogen (NO_y).

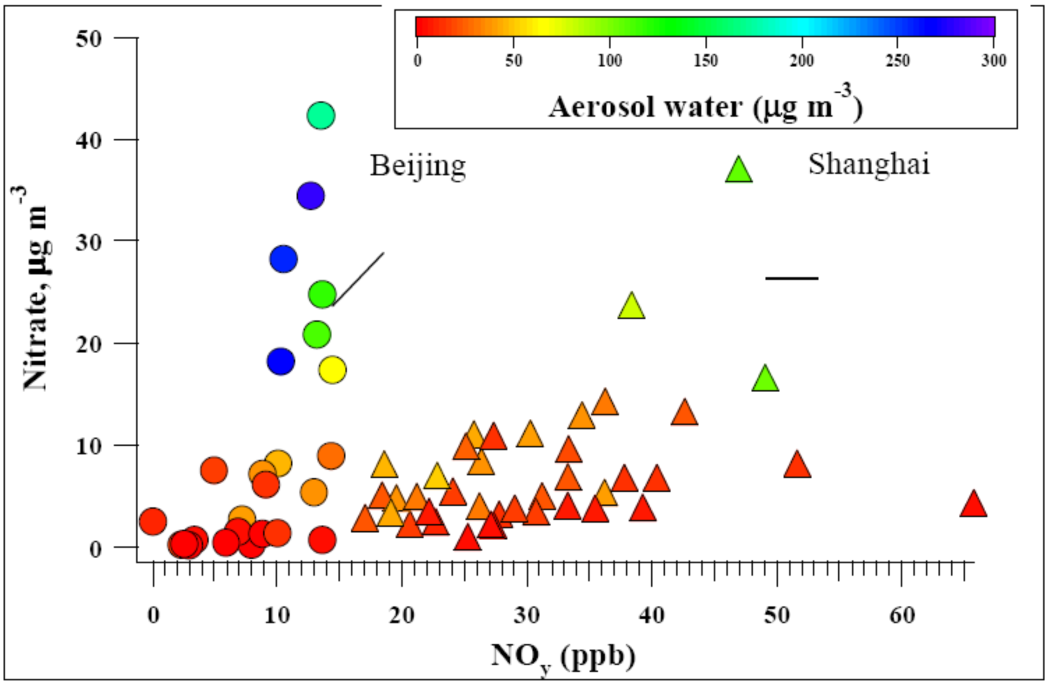

In this chapter, I have clearly demonstrated the different formation routes of sulfate and nitrate at different locations. Their formation pathways are largely depended on the environmental conditions as well as the existing precursor gases and aerosols in that area. In order to reduce the sulfate and nitrate concentrations in a place, we should learn their responsible precursor gases and aerosols first. Thus, this study is of great importance for helping to find out the relevant substances responsible for the sulfate and nitrate formation.

9.3 Impact of water soluble ions to the visibility reduction in Beijing

9.3.1 The seriousness of visibility problem in Beijing

As discussed in previous chapter, the particulate pollution problems in different part of China were very serious. More simplicity, these could also be evidenced by serious visibility degradation in China. In this section, I will discuss the visibility pollution problem in Beijing.

Visibility can be defined as the greatest distance at which an observer can just see a black object viewed against the horizon sky [Malm, 1999]. According to the Koschmeider equation, visibility can be estimated from the atmospheric extinction coefficient:

$$\text{Visibility} = \text{Constant} / b_{ext}$$

where the constant has been found to vary from place to place, depending on how visual ranges are observed as well as on atmospheric characteristics and b_{ext} refers to light extinction coefficient. In addition, the B_{ext} can be expressed as the summation of radiation scattering and absorption by particles:

$$B_{ext} = B_{sp} + B_{ap} + B_{sg} + B_{ag}$$

Where B_{sp} and B_{ap} refer to scattering and absorption of light by particles, respectively, and B_{sg} and B_{ag} refer to scattering and absorption by gases, respectively [Chen et al., 2003].

Here, I will briefly discuss the aerosol light scattering (B_{sp}) and absorption coefficients (B_{ap}), which was an important component of B_{ext}. Figure 9.11 showed the time series of scattering of light by particles (B_{sp}), absorption of light by particles (B_{ap}), wind speed and wind direction at the Beijing study site. As shown in the figure, the variations in B_{sp} and B_{ap} within the study period were significant. For example, the B_{sp} and B_{ap} value ranged from 1.4 to 2207.9Mm^{-1}, and 0.7 to 71.5Mm^{-1}, respectively in Beijing. The average B_{sp} and B_{ap} at Beijing were 306.4 ± 350.9Mm^{-1} and 15.5 ± 11.6Mm^{-1}, respectively observed at the study site.

Figure 9.11. Time series of B_{sp}, B_{ap}, and meteorological parameters (Wind speed and wind direction) at Beijing study site.

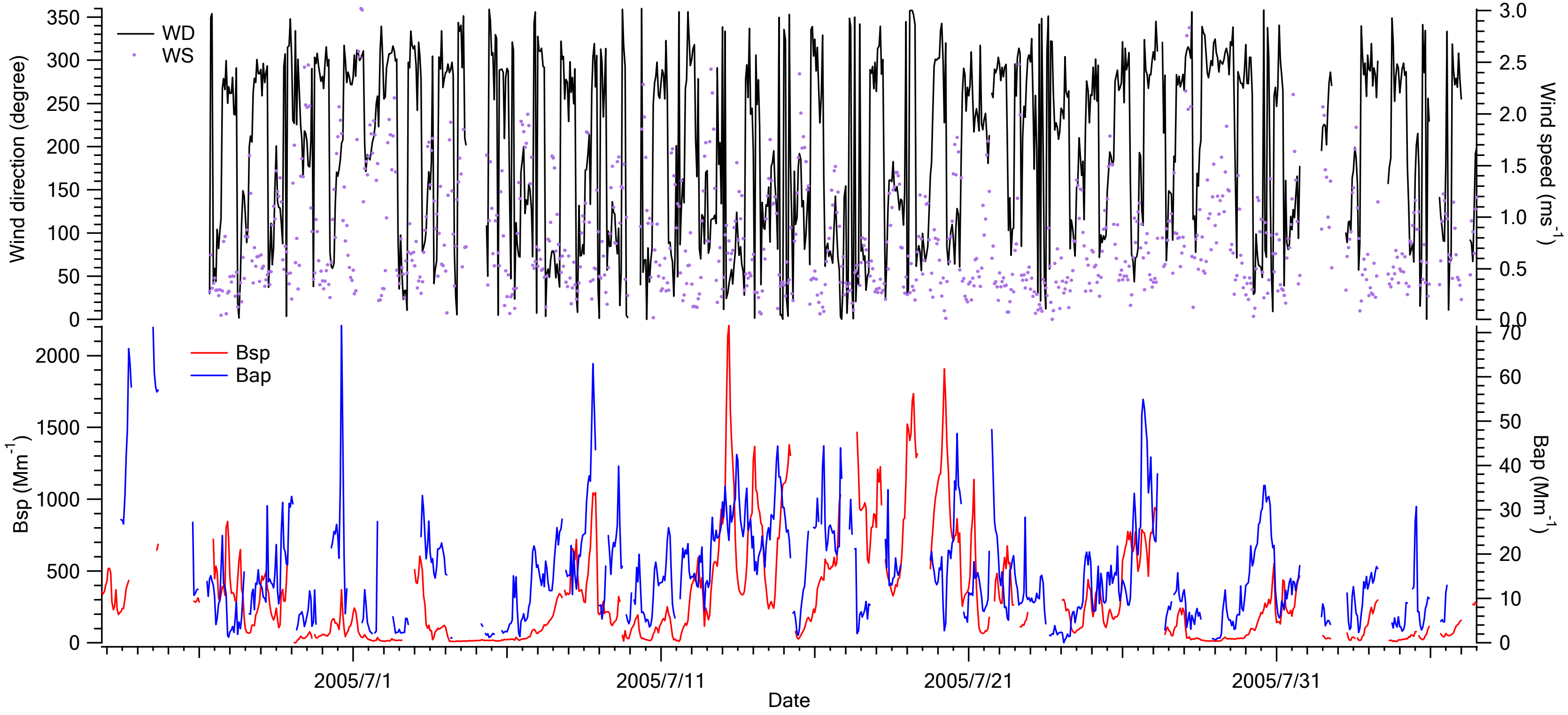

Comparing with the studies in United States, the B_{sp} and B_{ap} values in Beijing were much higher. These two values were even higher than those measured in the urban area of United States. Anderson et al. [2000] made the measurement of visibility in the urban area of Bondville, US. He found that the B_{sp} and B_{ap} values were 52 ± 57 and 5 ± 4Mm^{-1}, respectively. The B_{sp} and B_{ap} values in Beijing were about 6 and 3 times higher than the US study. Thus, the visibility problem in Beijing was much more serious in comparison with the US.

Apart from US, there was also some visibility studies conducted in China. Our studies in Beijing were similar to those measured in the rural area of Linan [Xu et al., 2002] and sub-urban area of Wan Qing Sha [Cheung, 2006]. The B_{sp} and B_{ap} values in Linan studies were 353 ± 202 and 23 ± 14Mm^{-1}, respectively, while the B_{sp} and B_{ap} values in Wan Qing Sha studies were 334 ± 268 and 24 ± 24Mm^{-1}, respectively. The previous study together with our present study suggested that the visibility problem was serious in different parts of China. Table 9.1 tabulated the aerosol light scattering and absorption values obtained in China (together with the present study) and US.

Table 9.1. Aerosol light scattering and absorption obtained in China and United States.

Site	Period	B_{sp} (Mm^{-1})	B_{ap} (Mm^{-1})	Source
China				
Hok Tsui (Rural)	Nov 98 – Feb 99	56 ± 31	20 ± 10	Man and Shih, 2001
Beijing (Urban)	Jun 99	480 ± 370	83 ± 40	Bergin et al., 2001
Linan (Rural)	Nov 99	353 ± 202	23 ± 14	Xu et al., 2002
Yulin (Rural)	Mar 01 – Apr 01	158 ± 193	6 ± 11	Xu et al., 2004
Tai O (Rural)	Oct 02 – Dec 02	224 ± 255	22 ± 16	Cheung, 2006
Taishan (Rural)	Oct 03 – Nov 03	184 ± 269	6 ± 6	Cheung, 2006
Qingyuan (Rural)	Feb 04 – Apr 04	435 ± 380	9 ± 10	Cheung, 2006
Wan Qing Sha (Sub-urban)	Apr 04 – Jun 04	334 ± 268	24 ± 24	Cheung, 2006
Beijing (Rural)	Jun 05 – Aug 05	306 ± 351	16 ± 12	This study
US				
Atlanta (Urban)	Jul 99 – Sept 99	121 ± 48	16 ± 12	Carrico et al., 2003
Bondville (Urban)	Aug 99 – Sept 99	52 ± 57	5 ± 4	Anderson et al., 2000

The aerosol optical property can be altered by the ambient RH. In order to minimize the influence of RH on the aerosol optical data, two sets of diurnal variations of B_{sp} and B_{ap} were calculated. The first set included all data, while the other set included only the data with RH less than or equal to 80%.

Figure 9.12a illustrated the diurnal profiles of B_{sp} and B_{ap}. The red and blank lines represented B_{sp} and B_{ap} for all the collected data, respectively, while the blue and green dotted lines represented B_{sp} and B_{ap} for the data with RH smaller than or equal to 80%, respectively. From the figure, we could see that B_{sp} was found to be the highest in the early morning. This could be due to the high RH in the early morning (illustrated in Figure 9.12b). As shown in the same figure, when the high RH data was removed (RH >80%), the value of B_{sp} was low. Thus, the visibility impairment in the early morning was possibly due to the hygroscopic species such as $(NH_4)_2SO_4$ and NH_4NO_3 in the atmosphere.

The peak values of B_{sp} and B_{ap} (RH ≤80%) were appeared in the afternoon, which was attributed by the secondary pollution formed during the transport of air pollutants from the urban area of Beijing to the sampling site. The formation of secondary pollutants increased the $PM_{2.5}$ concentrations in the atmosphere and consequently increased in the light scattering properties, resulting in a high B_{sp} and B_{ap} in the afternoon. The concurrent enhancement of primary as well as secondary pollutants (as shown in section 7.2) together with the high B_{sp} and B_{ap} were found in the afternoon. This should be due to the influence of the aged pollution plumes from distinct sources, which was then transported to the sampling site and subsequently affected the visibility.

Figure 9.12. Diurnal variations of (a) B_{sp} and B_{ap}, and (b) Temperature and relative humidity in Beijing.

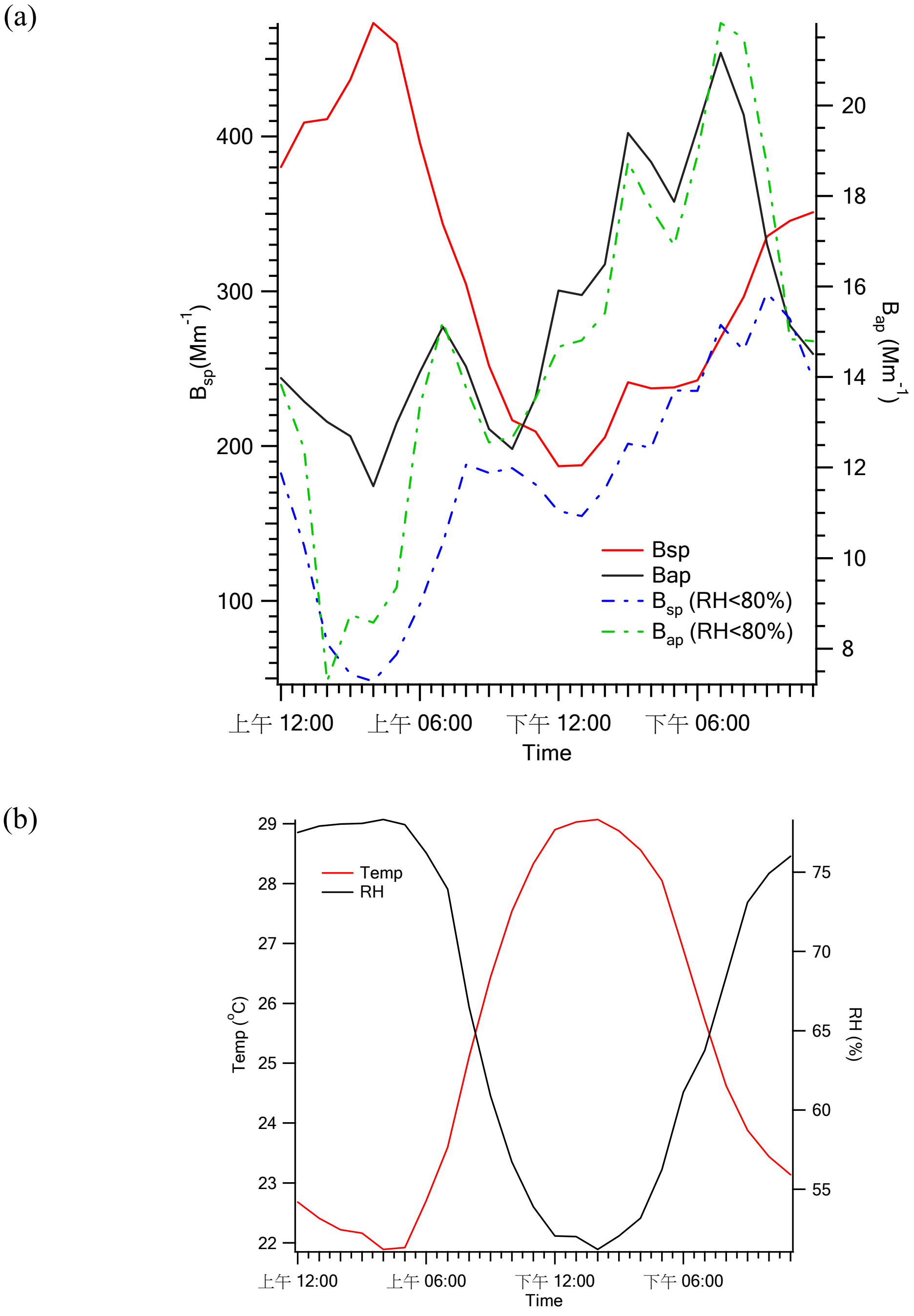

After discussing the aerosol optical properties, B_{ext} was then discussed here. The value of 2.6 was applied for the visibility equation showing at the beginning of this section. This value was adopted from the previous visibility studies in Tai O, Hong Kong conducted by Wang, 2003. He has shown that the value 2.6 was appropriate in the Hong Kong situation. Thus, I assumed that this value was also applicable in the Beijing area. Figure 9.13 showed the results of the daily visibility in Beijing. During the whole measurement period, about 60% of the days (excluding the days with mean RH >80%) had the visibility of less than 8km. As ambient RH could greatly influence the aerosol optical property and in turn the visibility, thus the data with RH >80% was neglected in order to minimize the influence of RH on the calculated visibility. On some selected days such as 16, 18 and 19 July, the visibility was even reduced to about 2km. Figures 9.14a and 9.14b showed the photos taken on different days with contrasting visibility. The two photos were taken at the same location. On July 16, the mountains surrounding the sampling site are totally masked by the poor visibility and showing great contrast with the good visibility day on July 29. This percentage of visibility impairment was extremely high in comparison with the studies conducted in Hong Kong and Shenzhen. Comparing with the same month in 2001, there were only 4% and 2% of the days with visibility <8km in Hong Kong and Shenzhen, respectively. Based on the same study, the worst visibility impairment was occurred in September in both Hong Kong and Shenzhen with 17% and 25% of the days with visibility <8km, respectively [Wang, 2003]. This comparison could clearly demonstrate the seriousness of the visibility problem in Beijing.

Figure 9.13. The results of the daily visibility in Beijing.

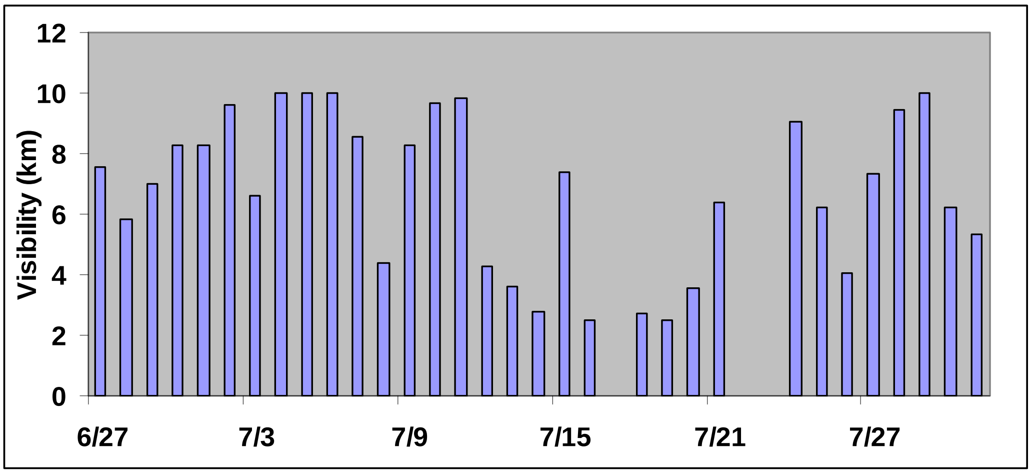

Figure 9.14. (a) Photo taken on 16 July with the visibility of only 2.5km on that day. (b) Photo taken on 29 July with the visibility of over 10km on that day.

(a)

(b)

9.3.2 The contribution of water soluble ions to the visibility impairment in Beijing

After showing the visibility situation in Beijing, I will now discuss the causes of the visibility problems. The correlation of daily B_{ext} and various aerosols with RH ≤80% was shown in Figure 9.15. According to the figure, it could be seen clearly that visibility reduction was strongly correlated with aerosols – $PM_{2.5}$ mass, sulfate, nitrate and ammonium ions, and to a lesser extent, NO_y ($R^2 = 0.55$, not shown in the figure). The correlation between B_{ext} and NO_y was due to the brown nature of the NO_2 species, which caused the absorption of light. If the concentrations of NO_2 in the atmosphere were high, the sky would appear as reddish brown which was the indication of the NO_2 haze problem. More importantly, the results indicated that fine particulates, especially sulfate, nitrate and ammonium were the major visibility reducing aerosol components in the polluted atmosphere. They have shown good correlations (R^2 ranged from 0.63 to 0.81) with B_{ext}. This was consistent with the findings in Chin (1997) and Wang (2003). Both of them found that fine particulates (sulfate, nitrate and ammonium) were the major visibility reducing aerosol components in the polluted atmosphere in Hong Kong. In the following, I will further discuss the contribution of the particulates to the visibility reduction in Beijing.

Figure 9.15. The correlations of B_{ext} versus (a) $PM_{2.5}$ mass, (b) SO_4^{2-}, (c) NO_3^- and (d) NH_4^+ with RH ≤80%.

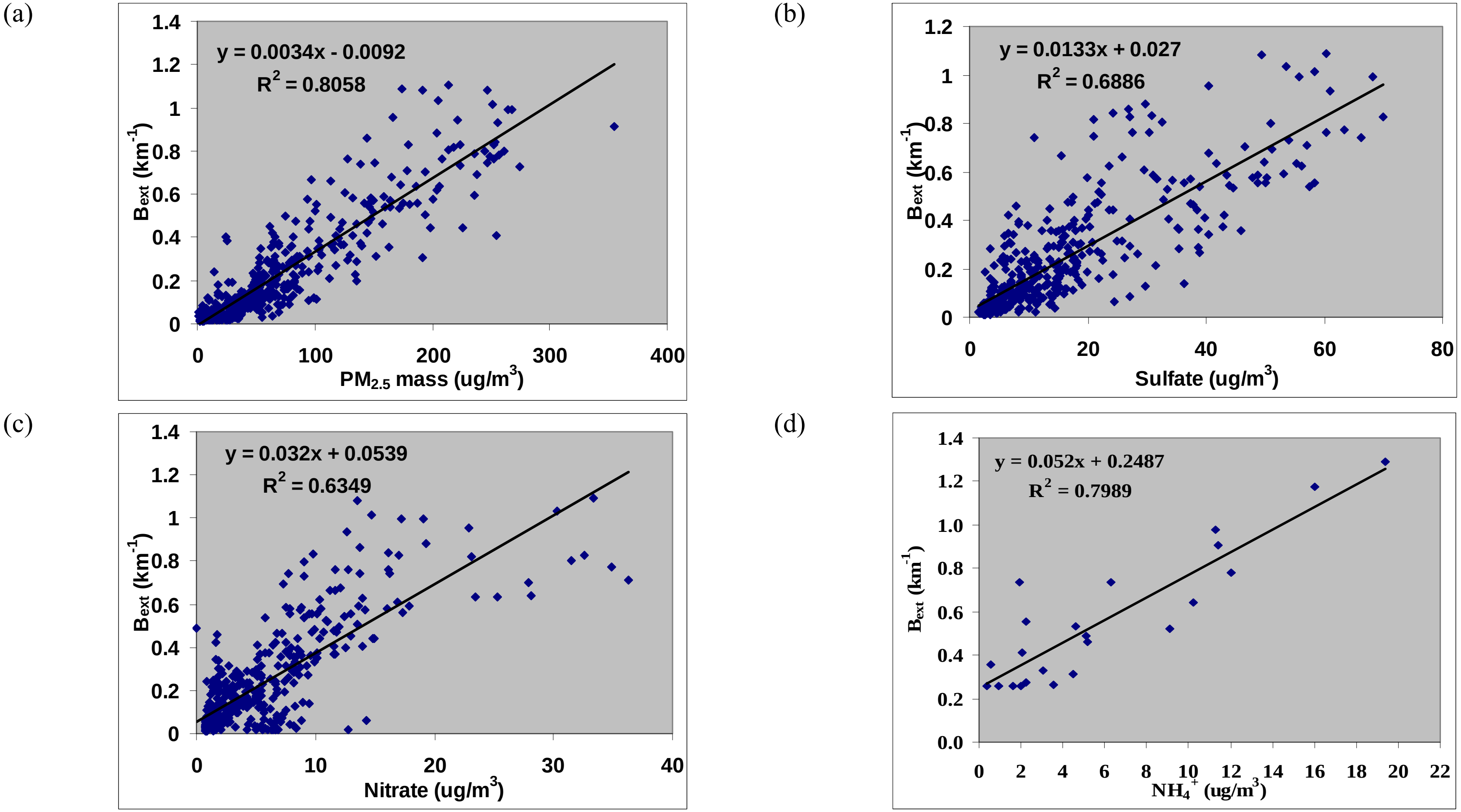

The following equation is used to estimate the extinction coefficient (B_{ext}):

b_{ext} = (3)f(RH)[Sulfate] + (3)f(RH)[Nitrate] + (4)f_{org}(RH)[OMC] + (1)[SOIL] + (0.6)[CM]

where 3m^2/g is the dry specific scattering for sulfates and nitrates, 4m^2/g for organic carbon and 1m^2/g and 0.6m^2/g are the respective scattering efficiencies for soil and coarse mass, [Sulfate] = $(NH_4)_2SO_4$, [Nitrate] = NH_4NO_3, [OMC] = 1.4[OC], [Soil] = 2.2[Al] + 2.19[Si] + 1.63[Ca] + 2.42[Fe] + 1.94[Ti] and [CM] = [RSP] - [FSP] and f(rh) = hygroscopic species growth function. The hygroscopic species growth function was adopted the data from Dr. William Malm and the respective growth curve was shown in Figure 9.16 [Sisler and Malm, 2000 and Wang, 2003].

Figure 9.16. Hygroscopic growth curve from Dr. William Malm.

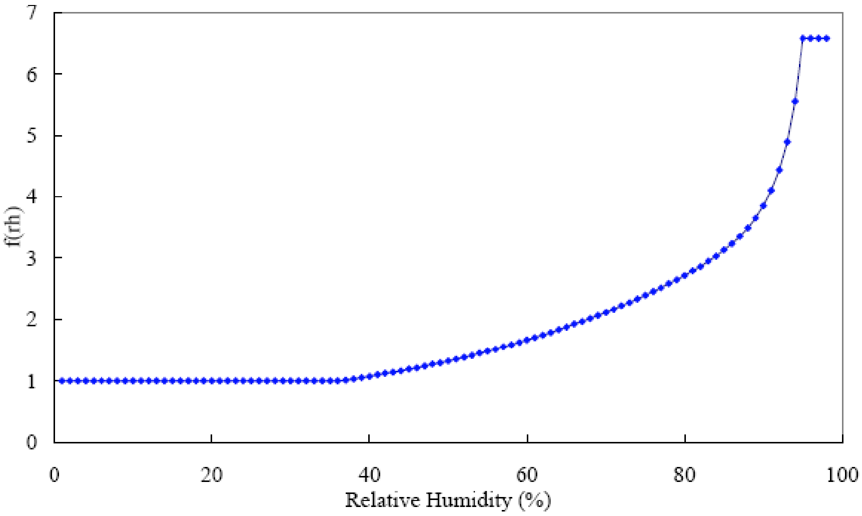

The above formula assumed that sulfate and nitrate ions were fully neutralized by ammonium ions. However, during the discussion of the formation of nitrate, I have shown that the ammonium ions in Beijing could not fully neutralize the nitrate ions. Thus, I assumed that the above formula still hold in the present situation.

Based on the above equation, the contributions of $(NH_4)_2SO_4$ and NH_4NO_3 to the light extinction were computed. Figure 9.17 showed the daily contributions of ammonium sulfate and ammonium nitrate to the light extinction. The overall $(NH_4)_2SO_4$ and NH_4NO_3 were found to contribute 26% and 11%, respectively of the light extinction. These two species alone have already contributed to about one-third of the visibility reduction. The result of the ammonium sulfate to the light extinction was similar to those reported by Wang, 2003 in Tsuen Wan, Hong Kong in which the ammonium sulfate contributed to 33% of the light extinction there. In contrast, the ammonium nitrate showed a larger contribution in Beijing (11%) than the studies conducted by Wang, 2003 in Hong Kong (4% – 5%). However, the contributions of ammonium sulfate and ammonium nitrate to the visibility reduction were much larger in Beijing than in US. Malm (1999) found that the contributions of the ammonium sulfate and ammonium nitrate to the visibility reduction were only 10% and 5%, respectively in the Eastern US, and 5% and 4%, respectively in the western US. The greatest contribution to the visibility reduction in US was come from organics. Thus, this study has shown the importance of the role of ammonium sulfate and ammonium nitrate to the visibility impairment in the Beijing area.

Figure 9.17. The daily contributions of ammonium sulfate and ammonium nitrate to the light extinction.

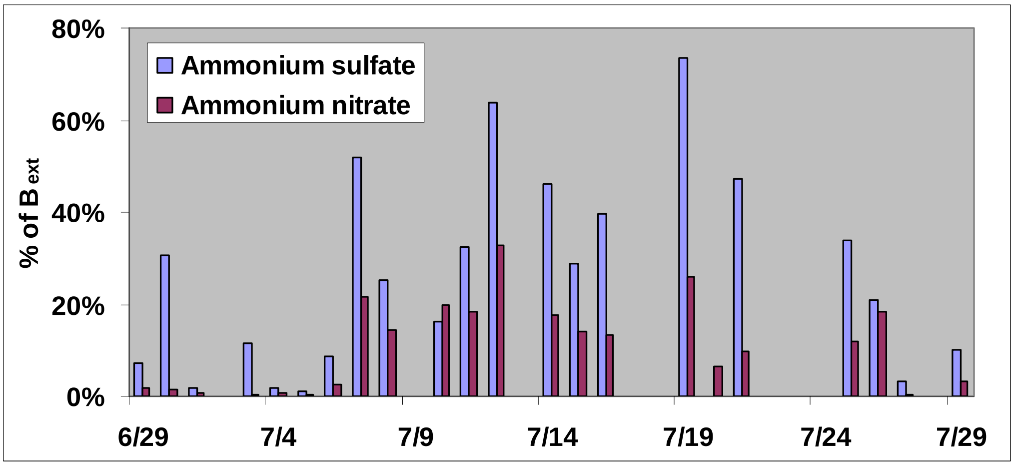

Furthermore, the contributions of ammonium sulfate and ammonium nitrate to the light extinction were greatly increased during the pollution days. The contributions of $(NH_4)_2SO_4$ and NH_4NO_3 could reach to as high as 73% and 33%, respectively to the light extinction during the episode days. These significant contributions of ammonium sulfate and ammonium nitrate to visibility degradation are due to the high concentrations of sulfate, nitrate and its ability to absorb water vapor which enhance light scattering. It was because the relative humidity (RH) in Beijing during the study period was relatively high. The average RH for the whole measurement period was 66 ± 20%. Neglecting the RH data that was greater than 80%, the average RH still had 55 ± 17%. As sulfate and nitrate species were water associated and therefore contributed to relatively larger light extinction in the study area.

In the following section, I will use the semi-continuous data to have further investigation on the contribution of the particulates to the visibility problem in Beijing. In computing the contributions of $(NH_4)_2SO_4$ and NH_4NO_3 to the light extinction, the dry mass scattering efficiencies of 2.2m^2/g and 2.4m^2/g for ammonium sulfate and ammonium nitrate are used, respectively instead of 3m^2/g. Malm et al. (2007) suggested that the dry mass extinction efficiencies were variable. In this study, the original improve formula for calculating the $(NH_4)_2SO_4$ and NH_4NO_3 to the light extinction was not the most appropriate due to the unbalance of sulfate, nitrate and ammonium and leaded to the overestimation of the total contribution. Thus, the dry mass scattering efficiencies as suggested by the revised improve formula [Malm et al., 2007] is applied in this study as the original formula would lead to the overestimation of the total contributions under these conditions.

The light extinction contributed by $(NH_4)_2SO_4$ and NH_4NO_3 is computed again by using the high resolution data. The high resolution data could provide us a more in-depth understanding of the visibility changes in a short period of time. The overall contributions of $(NH_4)_2SO_4$ and NH_4NO_3 to the light extinction in Beijing are shown in Figure 9.18. In comparison with Figure 7.1, more data were rejected in Figure 9.18 due to the high relative humidity in Beijing. As discussed before, the scattering efficiencies of sulfate and nitrate in $PM_{2.5}$ are greatly affected by relative humidity due to the hygroscopic properties of sulfate and nitrate. Thus, the data with relative humidity greater than 80% is rejected.

The overall light extinction contributed by $(NH_4)_2SO_4$ and NH_4NO_3 were 15% ± 14% and 7% ± 8%, respectively as computed from the high resolution data. According to Figure 9.18, we could see that the percentage contributions of $(NH_4)_2SO_4$ and NH_4NO_3 to the light extinction varied greatly within a day. For example, the percentage contributions of $(NH_4)_2SO_4$ and NH_4NO_3 to the light extinction changed from below 20% in the morning to about 40% in the afternoon on July 25. Moreover, in the mid-July, there were continuously high contributions of $(NH_4)_2SO_4$ and NH_4NO_3 to the light extinction. It would be due to the combined effect of high sulfate and nitrate loadings as well as high relative humidity at that period of time. More detailed will be discussed in the case study below.

Figure 9.18. The overall contributions of $(NH_4)_2SO_4$ and NH_4NO_3 to the light extinction in Beijing by using the high resolution data.

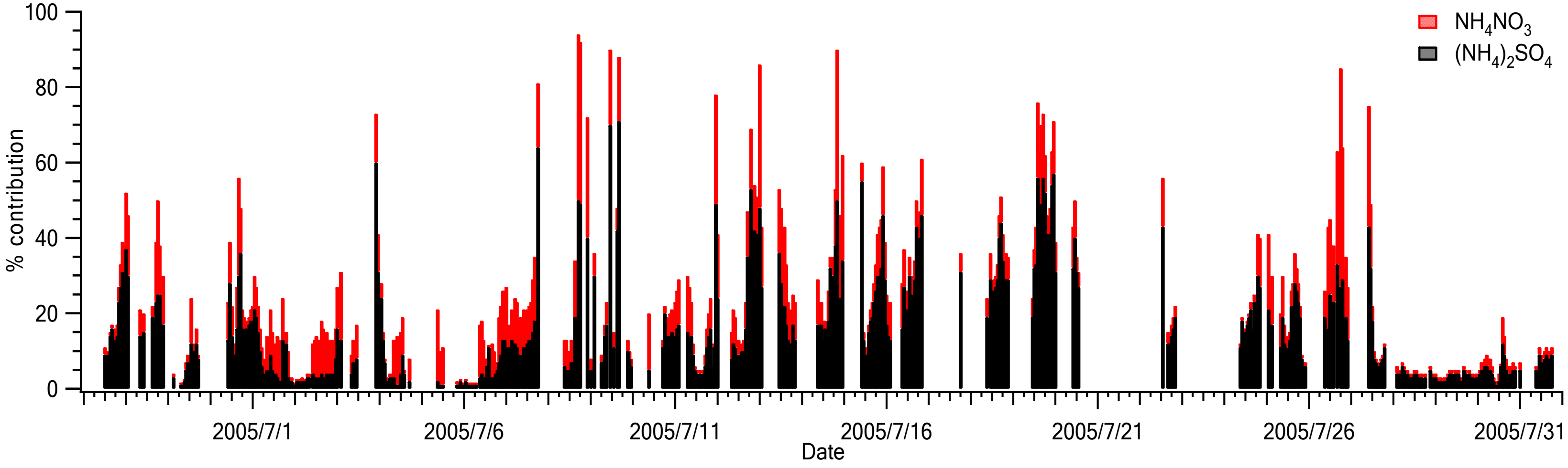

The concentrations of trace gases and particulates are then classified according to different wind direction. Table 9.2 showed the statistics of trace gases, particulates, relative humidity, light extinction and the percentage contributions of $(NH_4)_2SO_4$ and NH_4NO_3 to the light extinction of eight major wind direction. From the table, we could see that primary trace gases and $PM_{2.5}$ particulates varied under different wind direction. Generally, the westerly and northwesterly wind showed the lowest gaseous and particulate concentrations. The concentrations of NO and NO_y were around 0.3 and 11ppb, respectively, while the concentrations of $PM_{2.5}$ mass, sulfate and nitrate were about 60, 10 and 5μg/m^3, respectively under these two wind direction. Moreover, the most evident pollutants were come from CO and SO_2, which showed only around 500 and 3ppb, respectively from the westerly wind direction in comparison with all other direction (about 700ppb for CO and 7ppb for SO_2). This indicated that under westerly and northwesterly wind direction, the air mass was less affected by vehicles or power plants, which is known to be the major pollution sources in Beijing area. These low concentrations of gaseous and particulates were due to the continental air mass originated from Siberia impacting the sampling site. These low concentrations could also be reflected from the B_{ext} value. As shown from Table 9.2, the westerly wind direction showed the lowest B_{ext} value among all the wind direction which was the direct indication of the best visibility. In contrast, the particulate concentrations were high ($PM_{2.5}$ mass: ~100μg/m^3, sulfate: ~23μg/m^3, nitrate: ~10μg/m^3) under easterly wind direction (Northeasterly, easterly and southeasterly). Under these wind direction, the concentrations of primary as well as secondary gases were also high.

Apart from the difference in the concentrations of trace gases and particulates, the contribution of $(NH_4)_2SO_4$ to the light extinction is also varied. Higher contribution of $(NH_4)_2SO_4$ to the light extinction is found under easterly and southeasterly wind direction, which accounted for 18% and 20%, respectively of the light extinction. Conversely, under northerly and northwesterly wind direction, the contribution of $(NH_4)_2SO_4$ to the light extinction is the lowest, which accounted for 10% and 11%, respectively of the light extinction. In contrast to $(NH_4)_2SO_4$, the contribution of NH_4NO_3 to the light extinction showed a little higher under easterly wind direction (9%) in comparison with other direction. These changes of the contributions of $(NH_4)_2SO_4$ and NH_4NO_3 to the light extinction under different wind direction could be due to the changes in the concentrations of sulfate (~25μg/m^3 under easterly and southeasterly wind versus ~10μg/m^3 under northerly and northwesterly wind) and nitrate (~10μg/m^3 under easterly wind versus ~5μg/m^3 for other direction) under different wind direction.

Table 9.2. The statistics of trace gases, particulates, relative humidity, light extinction and the percentage contributions of $(NH_4)_2SO_4$ and NH_4NO_3 to the light extinction of eight major wind directions.

	Easterly wind	Southeasterly wind	Southerly wind	Southwesterly wind	Westerly wind	Northwesterly wind	Northerly wind	Northeasterly wind
RH (%)	60.1	53.9	45.9	46.7	58.5	54.1	51.4	58.4
O_3 (ppb)	60.3	80.7	71.3	52.3	53.0	48.9	49.0	50.6
CO (ppb)	718	679	572	547	519	572	684	737
SO_2 (ppb)	6.8	6.9	7.0	7.5	3.0	3.9	2.9	5.7
NO (ppb)	0.6	0.4	0.5	0.5	0.2	0.3	0.3	0.5
NO_y (ppb)	15.4	15.8	12.4	11.6	10.7	11.6	14.6	15.6
$PM_{2.5}$ mass ($\mu g/m^3$)	97.2	93.0	83.4	60.4	57.1	69.5	95.4	98.3
Sulfate ($\mu g/m^3$)	25.1	23.5	17.7	13.2	9.7	10.2	10.7	19.0
Nitrate ($\mu g/m^3$)	10.9	8.0	5.7	6.2	4.6	4.8	8.7	9.5
B_{ext} (Mm^{-1})	716	502	499	521	452	506	750	705
B $[(NH_4)_2SO_4]$ (%)	18	20	16	15	12	11	10	14
B $[NH_4NO_3]$ (%)	9	7	6	7	6	6	9	9

In the following section, I would present three cases to illustrate the contributions of ammonium sulfate and ammonium nitrate to the light extinction under different synoptic weather. The first case was the case presented in the previous section (section 9.1.1). This case was the “super” ozone episode. This day is characterized by strong solar radiation and low relative humidity, especially in the afternoon. On that day, the wind direction is changed from northwest in the early morning to the south in the afternoon, and then changed back to northwest again at night. Figure 9.19 showed the contributions of $(NH_4)_2SO_4$ and NH_4NO_3 to the light extinction as well as the meteorological parameters on June 30. The visibility on that day was good with the visual range greater than 10km for about half a day. In addition, the $PM_{2.5}$ concentration was comparatively low (about $65\mu g/m^3$) and the concentrations of sulfate and nitrate were also low (about $15\mu g/m^3$ for sulfate and about $6\mu g/m^3$ for nitrate) on that day. From the figure, the contributions of $(NH_4)_2SO_4$ and NH_4NO_3 to the light extinction changed under different wind direction. The contributions of $(NH_4)_2SO_4$ and NH_4NO_3 increased steadily to about 60% of the light extinction when the wind direction changed from northwesterly to southerly. When the wind direction is changed to northwesterly again at night, the contributions decreased to about 20%. Although the concentrations of fine sulfate and nitrate were low on that day, the contributions of $(NH_4)_2SO_4$ and NH_4NO_3 could still reach to about 60% of the light extinction.

Figure 9.19. The contributions of $(NH_4)_2SO_4$ and NH_4NO_3 to the light extinction as well as the meteorological parameters on June 30.

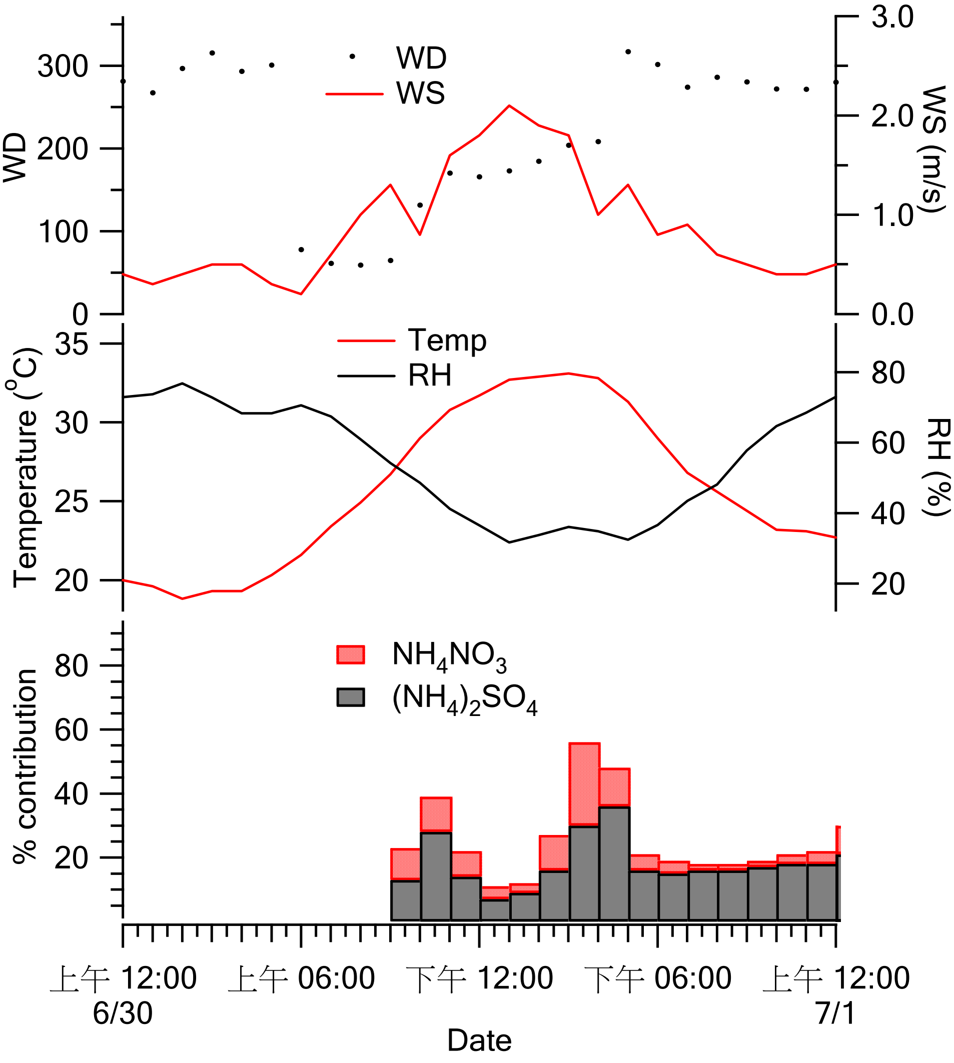

The second case was also the case that discussed before (section 9.1.1). This case was the multi-day episode with high relative humidity (average: 75%) on that period of time. The primary gases as well as the particulates, especially sulfate and nitrate levels are reached to very high levels on that period. Figure 9.20 showed the contributions of $(NH_4)_2SO_4$ and NH_4NO_3 to the light extinction as well as the meteorological parameters on July 12 – 20. Many data points were missing in Figure

9.20. This was because the relative humidity kept at high levels in this period of time and thus the data with RH >80% are neglected. The visibility was very poor (<2km of visual range for most of the time) on these days and it was the worst visibility period among the whole study period in Beijing. The average B_{ext} value was about $1000Mm^{-1}$. In this period of time, the contributions of $(NH_4)_2SO_4$ and NH_4NO_3 to the light extinction were much higher than the first case and are sometimes reached to over 60% of the light extinction. The percentage contributions have shown that the contributions of $(NH_4)_2SO_4$ and NH_4NO_3 are increased from the afternoon to the late night. It was because the concentrations of sulfate and nitrate kept at high levels during this period, the high contributions of $(NH_4)_2SO_4$ and NH_4NO_3 to the light extinction are more related to the increase of relative humidity from the afternoon to the night time. In this case, the variation of the contributions of $(NH_4)_2SO_4$ and NH_4NO_3 are more related to the relative humidity as well as the sulfate and nitrate concentrations and are less related to the wind direction.

Figure 9.20. The contributions of $(NH_4)_2SO_4$ and NH_4NO_3 to the light extinction as well as the meteorological parameters on July 12 – 20.

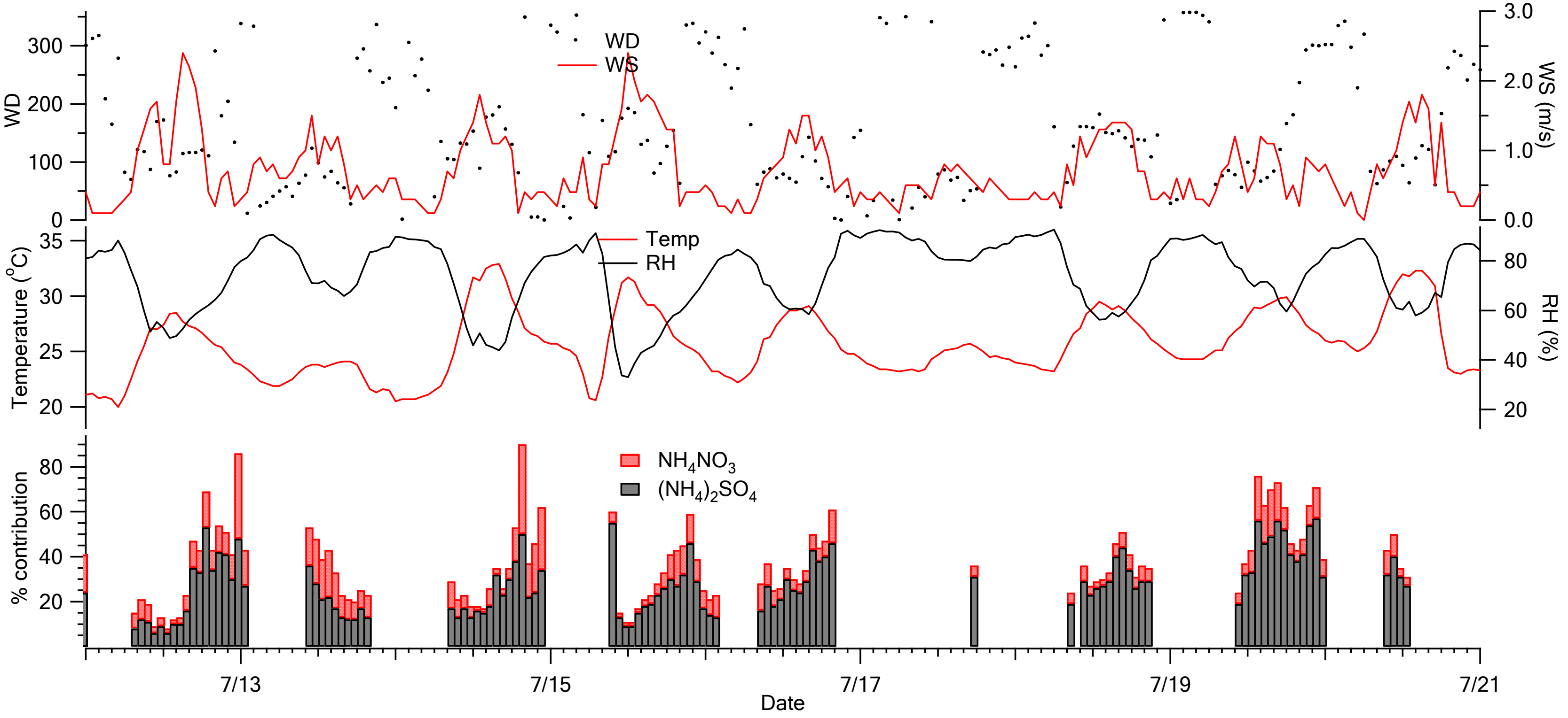

The third case was from July 28 to 29. On these two days, the visibility were good (>10km of the visual range). The concentrations of sulfate and nitrate were at very low levels (<5μg/m^3). The average PM$_{2.5}$ mass were about 20μg/m^3. In this case, we could see that the contributions of $(NH_4)_2SO_4$ and NH_4NO_3 were low (<10%) (Figure 9.21). This low contribution was obviously due to the low levels of sulfate and nitrate in the atmosphere. More importantly, this phenomenon implied that the contribution of other species, possibly organic matter would become significant contributors to the light extinction under the clean weather in Beijing. This case was different from the previous two cases in which $(NH_4)_2SO_4$ and NH_4NO_3 were the major contributors of the light extinction in Beijing.

Figure 9.21. The contributions of $(NH_4)_2SO_4$ and NH_4NO_3 to the light extinction as well as the meteorological parameters on July 28 – 29.

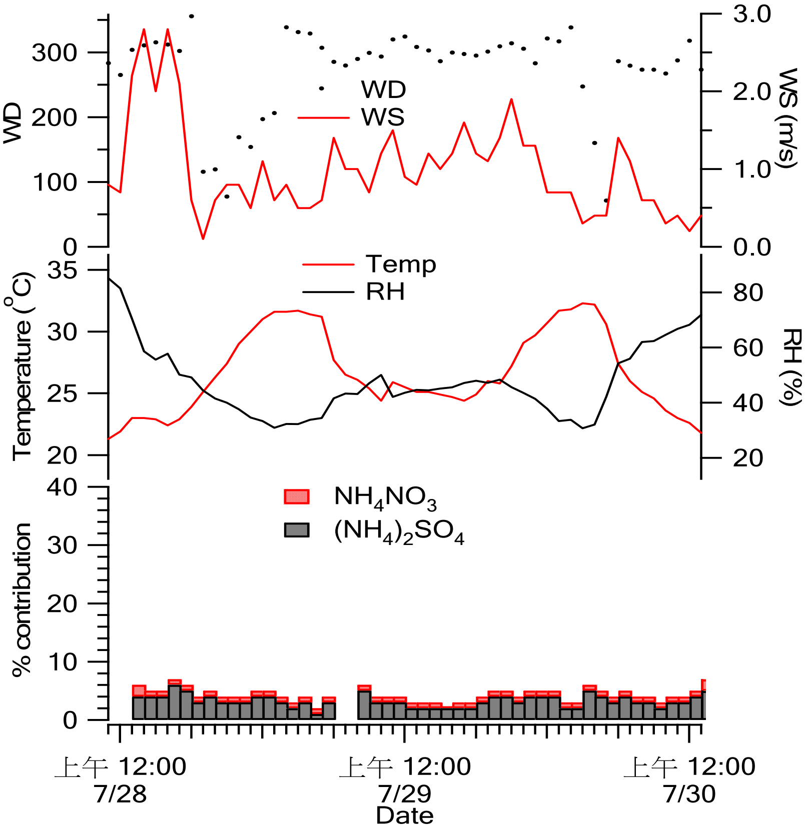

In conclusion, this visibility study has shown that Beijing suffered from serious visibility reduction problem and the main causes were the presence of ammonium sulfate and ammonium nitrate in the atmosphere. It is well known that almost all fine particle sulfates originated from SO_2 oxidation and are associated with ammonium. The major sources of SO_2 in Beijing are combustion of fossil fuels from power generations and industrial operations, while NH_3 are generally emitted from agricultural activities and also from transportation in urban area. Thus, reducing emissions of sulfur dioxide should effectively improve the visibility problem in Beijing area.

Conclusions

In conclusion, the measurement of water soluble ionic species in $PM_{2.5}$ by both semi-continuous instrument (AIM) and traditional filter analysis method were conducted in different parts of China – Hong Kong, Beijing, Shanghai, Lanzhou, and Guangzhou from 2004 – 2006.

The evaluation of data accuracy and quality were firstly performed to verify the performance of the recently developed semi-continuous instrument (AIM). Good correlation results were obtained under low sulfate and nitrate concentrations. However, the AIM instrument showed both positive (e.g. high SO_2 levels) and negative artifacts (e.g. high particle loadings) under different circumstances. Thus, improvement of the AIM instrument was needed.

The measurement results of water soluble ions and $PM_{2.5}$ masses collected in Shanghai, Beijing, Lanzhou, and Guangzhou have shown that the concentrations of the $PM_{2.5}$ mass and water soluble ion species were high. This demonstrated the seriousness of the air pollution problems in the whole China. Generally, sulfate, nitrate and ammonium were the major components of the water soluble ions in these places. Moreover, the temporal variations of the $PM_{2.5}$ mass and water soluble ion species were large within a day and were due to different meteorological and chemical factors.

SO_2 was found to have been converted to sulfate in seven urban pollution plumes examined in Beijing. An examination of SO_2 versus total sulfur under different humidity conditions indicated that the conversion of SO_2 was most efficient under humid conditions in Beijing. The nitrate formation pathways at four study sites were different. Lanzhou and Guangzhou were mainly through gas-phase homogeneous reaction between ammonia and nitric acid, while Beijing and Shanghai were through heterogeneous hydrolysis of N_2O_5.

In addition, the visibility problem in Beijing was very serious, about 60% of the days had the visibility of less than 8km. Results suggested that fine particulates (sulfate, nitrate and ammonium) were the major visibility-reducing aerosol components in the polluted atmosphere in Beijing. Ammonium sulfate and ammonium nitrate played a significant role in the visibility impairment in Beijing.

Suggestions for the future work

After this study, I would like to suggest the following research direction in the future.

From a technical point of view, the improvement of the instrument (AIM) should be done for measuring ions. As discussed before, AIM has problems during high particle loadings as well as high SO_2 concentrations (above 30ppbv), modification of the instrument should be made so that it can be suitable to use in any environment, not only limited to the clean environment.

For the future research direction, I would suggest to conduct the measurements at two or even three locations simultaneously in the same city. At each location, all the necessary parameters for sulfate and nitrate formation such as O_3, H_2O_2, solar radiation should be measured. In this way, we can know clearly the variations of each parameter at each sampling location, the time needed for the air masses to transport from the sources (e.g. urban centre) to the second monitoring stations as well as the changes of the air masses during the transportation. By combining all the information, I believe that more accurate and in-depth formation mechanisms of sulfate and nitrate can be found.

References

1. Air Services Group, 2003. Air Quality in Hong Kong 2003. Environmental Protection Department, The Government of the Hong Kong Special Administrative Region.
2. Alastuey A., Querol X., Rodrıgueza S., Plana F., Lopez-Soler A., Ruiz C., Mantilla E.,2004. Monitoring of atmospheric particulate matter around sources of secondary inorganic aerosol. Atmospheric Environment 38, 4979 – 4992.
3. Allen A.G., Miguel A.H., 1995. Indoor organic and inorganic pollutants: In-situ formation and dry deposition in southeastern Brazil. Atmospheric Environment 29, 3519 – 3526.
4. Andrews E., Saxena P., Musarra S., Hildemann L.M., Koutrakis P., McMurry P.H., Olmez I., White W.H., 2000. Concentration and composition of atmospheric aerosols from the 1995 SEAVS experiment and a review of the closure between chemical and gravimetric measurements. Journal of the Air and Waste Management Association 50, 648 – 664.
5. Anttila T., Kiendler-Scharr A., Tillmann R., Mentel T.F., 2006. On the reactive uptake of gaseous compounds by organic-coated aqueous aerosols: theoretical analysis and application to the heterogeneous hydrolysis of N_2O_5. Journal of Physical Chemistry 110A, 10435 – 10443.
6. Appel B.R., Tokiwa Y., Haik M., Kothny E.L., 1984. Artifact particulate sulfate and nitrate formation on filter media. Atmospheric Environment 18, 2, 409 – 416.

7. Arimoto R., Duce R.A., Savoie D.L., Prospero J.M., Talbot R., Cullen J.D., Tomza U., Lewis N.F., Ray B.J., 1996. Relationships among aerosol constituents from Asia and the North Pacific during Pem-West A. Journal of Geophysical Research 101, 2011 – 2023.

8. Ashbaugh L.L., Eldred R.A., 2004. Loss of Particle Nitrate from Teflon Sampling Filters: Effects on Measured Gravimetric Mass in California and in the IMPROVE Network. Journal of the Air & Waste Management Association 54, 93 – 104.

9. Baldwin A.C., 1982. Heterogeneous reactions of sulfur dioxide with carbonaceous particles. International Journal of Chemical Kinetics 14, 269 – 277.

10. Bari A., Ferraro V., Wilson L.R., Luttinger D., Husain L., 2003. Measurements of gaseous HONO, HNO_3, SO_2, HCl, NH_3, particulate sulfate and $PM_{2.5}$ in New York, NY. Atmospheric Environment 37, 2825 – 2835.

11. Beijing Environmental Protection Bureau (BJEPB). URL: <http://www.bjepb.gov.cn>.

12. Beilke S., Lamb D., Muller J., 1975. On the uncatalized oxidation of atmospheric SO_2 by oxygen in aqueous systems. Atmospheric Environment 9, 1093 – 1090.

13. Chameides W.L., Stelson A.W., 1992. Aqueous-phase chemical processes in deliquescent sea-salt aerosols: a mechanism that couples the atmospheric cycles of S and sea-salt. Journal of Geophysical Research 97, 20565 – 20580.

14. Charlson R.J., Heintzenberg J., 1995. Aerosol Forcing of Climate. Wiley, England, 363 – 382.

15. Chen L.W.A., Chow J.C., Doddrldge B.G., Dlckerson R.R., Ryan W.F., Mueller P.K., 2003. Analysis of a Summertime $PM_{2.5}$ and Haze Episode in the Mid-Atlantic Region. Journal of Air & Waste Management Association 53, 946 – 956.

16. Chen Z.L., Ge S., Zhang J., 1994. Measurement and analysis for atmospheric aerosol particulates in Beijing. Research of Environmental Sciences 7 (3), 1 – 9.

17. Cheng K.H., Swift D.L., 1995. Calculation of total deposition of ultrafine aerosols in human extrathoracic and intrathoracic regions. Aerosol Science and Technology 22, 194 – 201.

18. Cheng Y.H., Tsai C.J., 1997. Evaporation loss of ammonium nitrate particles during filter sampling. Journal of Aerosol Science 28, 1553 – 1567.

19. Cheng Z.L., Lam K.S., Chan L.Y., Wang T., Cheng K.K., 2000. Chemical characteristics of aerosols at coastal station in Hong Kong. I. Seasonal variation of major ions, halogens and mineral dusts between 1995 and 1996. Atmospheric Environment 34, 2771 – 2783.

20. Cheung H.C., Wang T., Baumann K., Guo H., 2005. Influence of regional pollution outflow on the concentrations of fine particulate matter and visibility in the coastal area of southern China. Atmospheric Environment 39, 6463 – 6474.

21. Chow J.C., 1995. Measurement methods to determine compliance with ambient air-quality standards for suspended particles. Journal of the Air & Waste Management Association 45, 5, 320 – 382.

22. Chow J.C., Antony Chen L.W., Watson J.G., Lowenthal D.H., Magliano K.A., Turkiewicz K., Lehrman D.E., 2006. $PM_{2.5}$ chemical composition and spatiotemporal variability during the California Regional $PM_{10}/PM_{2.5}$ Air Quality Study (CRPAQS). Journal of Geophysical Research 111, D10S04, doi:10.1029/2005JD006457.

23. Clegg, S.L., Brimblecombe P., Wexler A.S., 1998. A thermodynamic model of the system H^+–NH_4^+–Na^+– SO_4^{2-}–NO_3^-–Cl^-–H_2O at 298.15K. Journal of Physical Chemistry 102A, 2155–2171.

24. Cohen, B., Xiong, J., Li, W., 1996. The influence of charge on the deposition behavior of aerosol particles with emphasis on singly charged nanometer sized particles. J.M.C. Marijnissen and L. Gardon, Eds, Aerosol Inhalation, Kluwer Academic, Dordrecht, 127.

25. Crutzen, P.J., 1996. The role of particulate matter and ozone photochemistry. M. Kulmala and P.R. Wagner, Eds., Nucleation and Atmospheric Aerosols, Pergamon Press, Oxford, UK.

26. Cyrys J., Dietrich G., Kreyling W., Tuch T., Heinrich J., 2001. $PM_{2.5}$ measurements in ambient aerosol: comparison between Harvard impactor (HI) and the tapered element oscillating microbalance (TEOM) system. The Science of the Total Environment 278, 191 – 197.

27. Dasch J.M., Cadle S.H., Kennedy K.G., Mulawa P.A., 1989. Comparison of annular enuders and filter packs for atmospheric sampling. Atmospheric Environment 23, 2775 – 2782.

28. Dennis R.L., McHenry J.N., Barchet W.R., Binkowski F.S., Byun D.W., 1993. Correcting RADM's sulfate under prediction: discovery and correction of model errors and testing the corrections through comparison against field data. Atmospheric Environment 27A, 975 – 997.

29. Dentener, F.J., Carmichael, G.R., Zhang, Y., Lelieveld, J., Crutzen, P.J., 1996. Role of mineral aerosol as a reactive surface in the global troposphere. Journal of Geophysical Research 101, 22, 22869 – 22889.

30. Ding A., Wang T., Zhao M., Wang T., Li Z.K., 2004. Simulation of sea-land breezes and a discussion of their implications on the transport of air pollution during a multi-day ozone episode in the Pearl River Delta of China. Atmospheric Environment 38, 39, 6737 – 6750.

31. Dingenen R.V., Raes F., Putaud J.P., Baltensperger U., Charron A., Facchini M.C., Decesari S., Fuzzi S., Gehrig R., Hansson H.C., Harrison R.M., Hüglin C., Jones A.M., Laj P., Lorbeer G., Maenhaut W., Palmgren F., Querol X., Rodriguez S., Schneider J., Brink H.T., Tunved P., Tørseth K., Wehner B., Weingartner E., Wiedensohler A., Wåhlin P., 2004. A European aerosol phenomenology – 1: physical characteristics of particulate matter at kerbside, urban, rural and background sites in Europe. Atmospheric Environment 38, 2561 – 2577.

32. Docker, D.W., Pope, C.A., Xu, X.P., Spengler, J.D., Ware, J.H., Fay, M.E., Ferris, B.G., Speizer, F.E., 1993. An association between air pollution and mortality in six U.S. cities. New England Journal of Medicine 329 (24), 1753 – 1759.

33. Drewnick F., Schwab J.J., Hogrefe O., Peters S., Husain L., Diamond D., Weber R., Demerjian K.L., 2003. Intercomparison and evaluation of four

semi-continuous $PM_{2.5}$ sulfate measurements. Atmosphere Environment 37, 3335 – 3350.

34. Drewnick F., Schwab J.J., Jayne J.T., Canagaratna M., Worsnop D.R., Demerjian K.L., 2004. Measurement of Ambient Aerosol Composition During the PMTACS-NY 2001 Using an Aerosol Mass Spectrometer. Part I: Mass Concentrations. Aerosol Science and Technology 38 (S1), 92 – 103.
35. Duan F.K., He K.B., Ma Y.L., Yang F.M., Yu X.C., Cadle S.H., Chan T., Mulawa P.A., 2006. Concentration and chemical characteristics of PM2.5 in Beijing, China: 2001 – 2002. Science of the Total Environment 355, 1 – 3, 264 – 275.
36. Eatough D.J., Lewis L.J., Eatough M., Lewis E.A., 1995. Sampling Artifacts in the Determination of Particulate Sulfate and $SO_{2(g)}$ in the Desert Southwest Using Filter Pack Samplers. Environmental Science & Technology 29, 787 – 791.
37. Edgerton E.S., Hartsell B.E., Saylor R.D., Jansen J.J., Hansen D.A., Hidy G.M., 2006. The Southeastern Aerosol Research and Characterization Study, Part 3: Continuous Measurements of Fine Particulate Matter Mass and Composition. Journal of Air & Waste Management Association 56, 1325 – 1341.
38. Erduran M.S., Tuncel S.G., 2001. Gaseous and particulate air pollutants in the Northeastern Mediterranean Coast. The Science of the Total Environment 281, 205 – 215.
39. Ferin, J., Oberdörster, G., Penney, D.P., Soderholm, S.C., Gelein, R., Piper, H.C., 1990. Increased pulmonary toxicity og ultrafine particles. Journal of Aerosol Science 21, 381 – 384.

40. Fisseha R., Dommen J., Gutzwiller L., Weingartner E., Gysel M., Emmenegger C., Kalberer M., Baltensperger U., 2006. Seasonal and diurnal characteristics of water soluble inorganic compounds in the gas and aerosol phase in the Zurich area. Atmospheric Chemistry and Physics 6, 1895 – 1904.
41. Foltescu V.L., Lindgren E.S., Isakson J., Öblad M., 1996. Gas-to-particle conversion of sulfur and nitrogen compounds as studied at marine stations in northern Europe. Atmospheric Environment 30, 18, 3129 – 3140.
42. Fridlind A.M., Jacobson M.Z., 2000. A study of gas-aerosol equilibrium and aerosol pH in the remote marine boundary layer during the first aerosol characterization experiment (ACE-1). Journal of Geophysical Research 105, 17325 – 17340.
43. Friedlander, S. K., Smoke, Dust, and Haze. Fundamentals of Aerosol Dynamics. Second Edition, Oxford University Press, New York, 2000.
44. Gao S., Ng N.L., Keywood M., Varutbangkul V., Bahreini R., Nenes A., He J., Yoo K.Y., Beauchamp J.L., Hodyss R.P., Flagan R.C., Seinfeld J.H., 2004. Particle phase acidity and oligomer formation in secondary organic aerosol. Environment Science and Technology 38, 6582 – 6589.
45. Giroux J.E., Arnaud C., Jacques J., 1997. Chalk Analysis of levels of nitrates and derivatives of ammonia in an urban atmosphere. Science of Total Environment 196, 247 – 254.
46. Hämeri K., Kulmala M., Aalto P., Leszczynski K., Visuri R., Hämekoski, K., 1996. The investigations of aerosol particle formation in urban background area of Helsinki. Atmospheric Research 41, 281 – 298.

47. Hagler G.S.W., Bergin M.H., Salmon L.G., Yu J.Z., Wan E.C.H., Zheng M., Zeng L.M., Kiang C.S., Zhang Y.H., Lau A.K.H., Schauer J.J., 2006. Source areas and chemical composition of fine particulate matter in the Pearl River Delta region of China. Atmospheric Environment 40, 3802 – 3815.

48. Han L., Zhuang G., Cheng S., Li J., 2007. The mineral aerosol and its impact on urban pollution aerosols over Beijing, China. Atmospheric Environment 41, 7533 – 7546.

49. Hao J., Wang L., Shen M., Li L., Hu J., 2007. Air quality impacts of power plant emissions in Beijing, Environmental Pollution 147, 401 – 408.

50. Harrison D., Park S.S., Ondov J., Buckley T., Kim S.R., Jayanty R.K.M., 2004. Highly time resolved fine particle nitrate measurements at the Baltimore Supersite. Atmospheric Environment 38, 5321 – 5332.

51. Harrison R.M., Sturges W.T., Kitto A.M.N., Li Y., 1990. Kinetics of evaporation of ammonium chloride and ammonium nitrate aerosols. Atmospheric Environment 24A, 1883 – 1888.

52. Hauck H., Berner A., Frischer T., Gomiscek B., Kundi M., Neuberger M., Puxbaum H., Preining O., AUPHEP-Team, 2004. AUPHEP – Austrian Project on Health Effects of Particulates – general overview. Atmospheric Environment 38, 3905 – 3915.

53. Hayami H., 2005. Behavior of secondary inorganic species in gaseous and aerosol phases measured in Fukue Island, Japan, in dust season. Atmospheric Environment 39, 2243 – 2248.

54. He K., Yang F., Ma Y., Zhang Q., Yao X., Chan C.K., Cadle S., Chan T., Mulawa P., 2001. The characteristics of $PM_{2.5}$ in Beijing, China. Atmospheric Environment 35, 4959 – 4970.

55. Heintzenberg J., 1989. Fine particles in global troposphere - a review. Tellus 41B, 149 – 160.

56. Hillamo R., Allegrini I., Sparapani R., Kerminen V.M., 1998. Mass size distributions and precursor gas concentrations of major inorganic ions in Antarctic aerosol. International Journal of Environmental Analytical Chemistry 71, 3 – 4, 353 – 372.

57. Hirsch R.M., Gilroy E.J., 1984. Methods of fitting a straight line to data: Examples in water resources. Water Resources Bulletin 20, 5, 705 – 711.

58. Ho K.F., Lee S.C., Cao J.J., Chow J.C., Watson J.G., Chan C.K., 2005. Seasonal variations and mass closure analysis of particulate matter in Hong Kong. Science of Total Environment 355, 276 – 287.

59. Ho K.F., Lee S.C., Louie P.K.K., Zou S.C., 2002. Seasonal variation of carbonyl compound concentration in urban area of Hong Kong. Atmospheric Environment 36, 1259 – 1265.

60. Hogrefe O., Schwab J.J., Drewnick F., Lala G.G., Peters S., Demerjian K.L., Rhoads K., Felton H.D., Rattigan O.V., Husain L., Dutkiewicz V.A., 2004. Semicontinuous PM2.5 Sulfate and Nitrate Measurements at an Urban and a Rural Location in New York: PMTACS-NY Summer 2001 and 2002 Campaigns. Journal of Air & Waste Management Association 54, 1040 – 1060.

61. Homolya J., Taylor S., Smiley J., Anderson D., Bohlin M., Frost J., Michel E., Pausel S., 2005. A Multi-Site Performance Comparison of Semi-

Continuous Carbon, Nitrate and Sulfate Monitors. URL: http://www.epa.gov/ttnamti1/files/ambient/pm25/workshop/atlanta/cont1.

62. Honrath R.E., Peterson M.C., Dziobak M.P., Dibb J.E., Arsenault M.A., Green S.A., 2000. Release of NOx from sunlight-irradiated midlatitude snow. Geophysical Research Letters 27, 2237 – 2240.

63. Hu J.H., Abbatt J.P.D., 1997. Reaction probabilities for N_2O_5 hydrolysis on sulfuric acid and ammonium sulfate aerosols at room temperature. Journal of Physical Chemistry A 101, 871 – 878.

64. Hu M., He L.Y., Zhang Y.H., Wang M., Kim Y.P., Moon K.C., 2002. Seasonal variation of ionic species in fine particles at Qingdao, China. Atmospheric Environment 36, 5853–5859.

65. Hu M., Zhou F., Shao K., Zhang Y., Tang X., Slanina J., 2002. Diurnal variations of aerosol chemical compositions and related gaseous pollutants in Beijing and Guangzhou. Journal of Environmental Science and Health A37 (4), 479 – 488.

66.

67. Huang X.F., Hu M., He L.Y., Tang X.Y., 2005. Chemical characterization of water-soluble organic acids in $PM_{2.5}$ in Beijing, China. Atmospheric Environment 39, 2819 – 2827.

68. Jayne J.T., Leard D.C., Zhang X., Davidovits P., Smith K.A., Kolb C.E., Worsnop D.R., 2000. Development of an Aerosol Mass Spectrometer for Size and Composition Analysis of Submicron Particles. Aerosol Science and Technology 33, 49 – 70.

69. Jeong C.H., Lee D.W., Kim E., Hopke P.K., 2004. Measurement of real-time $PM_{2.5}$ mass, sulfate, and carbonaceous aerosols at the multiple monitoring sites. Atmospheric Environment 38, 5247 – 5256.

70. Jimenez J.L., Jayne J.T., Shi Q., Kolb C., Worsnop D.R., Yourshaw I., Seinfeld J.H., Flagan R.C., Zhang X., Smith K.A., Morris J.W., Dacidovits P., 2003. Ambient aerosol sampling using the Aerodyne Aerosol Mass Spectrometer. Journal of Geophysical Research 108, D7, 8425, doi:10.1029/2001JD001213.

71. Juozaitis A., Trakumas S., Girgždienė, Girgždys A., Šopauskienė D., Ulevičius V., 1996. Investigations of gas-to-particle conversion in the atmosphere. Atmospheric Research 41, 183 – 201.

72. Kadowaki S., 1986. On the Nature of Atmospheric Oxidation Processes of SO_2 to Sulfate and of NO_2 to Nitrate on the Basis of Diurnal Variations of Sulfate, Nitrate, and Other Pollutants in an Urban Area. Environmental Science and Technology 20, 1249 – 1253.

73. Kane S.M., Caloz F., Leu M.T., 2001. Heterogeneous uptake of gaseous N_2O_5 by $(NH_4)_2SO_4$, NH_4HSO_4, and H_2SO_4 aerosols. Journal of Physical Chemistry A 105, 6465 – 6470.

74. Karamchandani P., Venkatram A., 1992. The role of non-precipitating clouds in producing ambient sulfate during summer: results from simulations with the Acid Deposition and Oxidant Model (ADOM). Atmospheric Environment 26A, 1041 – 1052.

75. Kato N., 1996. Analysis of structure of energy consumption and dynamics of emission of atmospheric species related to the global environmental

change (SO_x, NO_x, and CO_2) in Asia. Atmospheric Environment 30, 757 – 2785.

76. Keeler G.J., Spengler J.D., Castillo R.A., 1991. Acid aerosol measurements at a suburban Connecticut site. Atmospheric Environment 25A, 681 – 690.
77. Khlystov A., Wyers G.P., Slanina J., 1995. The steam-jet aerosol collector. Atmospheric Environment 29, 17, 2229 – 2234.
78. Khoder M.I., 2002. Atmospheric conversion of sulfur dioxide to particulate sulfate and nitrogen dioxide to particulate nitrate and gaseous nitric acid in an urban area. Chemosphere 49, 675 – 684.
79. Kim J.Y., Ghim Y.S., Song C.H., Yoon S.C., Han J.S., 2007. Seasonal characteristics of air masses arriving at Gosan, Korea, using fine particle measurements between November 2001 and August 2003. Journal of Geophysical Research 112, D07202, doi:10.1029/2005JD006946.
80. Kondratyev K.Y., Ivlev L.S., Krapivin V.F., Varotsos C.A., 2006. Atmospheric Aerosol Properties. Formation, Processes and Impacts. Springer, UK.
81. Koutrakis P., Thompson K.M., Wolfson J.M., Spengler J.D., Keeler G.J., Slater J.L., 1992. Determination of aerosol strong acidity losses due to interactions of collected particles: Results from laboratory and field studies. Atmospheric Environment 26A, 987 – 995.
82. Krivácsy Z., Molnár Á., 1998. Size distribution of ions in atmospheric aerosols. Atmospheric Research 46, 279 – 291.
83. Kulmala M., Kerminen V.M., Laaksonen A., 1995. Simulations on the effect of sulfuric acid formation on atmospheric aerosol concentrations. Atmospheric Environment 29, 3, 377 – 382.

84. Lee H.S., Kang B.W., 2001. Chemical characteristics of principal PM2.5 species in Chongju, South Korea. Atmospheric Environment 35, 4, 739 – 746.

85. Lee T., Yu X.Y., Ayres B., Kreidenweis S.M., Malm W.C., Collett J.L.Jr., 2007. Observations of fine and coarse particle nitrate at several rural locations in the United States. Atmospheric Environment, doi:10.1016/j.atmosenv.2007.05.016.

86. Lin J.J., 2002. Characterization of the major chemical species in $PM_{2.5}$ in the Kaohsiung City, Taiwan. Atmospheric Environment 36, 1911 – 1920.

87. Liu S.L.J., Burton R.M., Wilson W.E., Koutrakis P., 1996. Comparison of aerosol acidity in urban and semi-rural environments. Atmospheric Environment 30, 1237 – 1254.

88. Lonati G., GiuglianoM., Butelli P., Romele L., Tardivo R., 2005. Major chemical components of PM2.5 in Milan (Italy). Atmospheric Environment 39, 10, 1925 – 1934.

89. Long R.W., Eatough N.L., Eatough D.J., Meyer M.B., Wilson W.E., 2005. Continuous Determination of Fine Particulate Matter Mass in the Salt Lake City Environmental Monitoring Project: A Comparison of Real-Time and Conventional TEOM Monitor Results. Journal of Air & Waste Management Association 55, 1839 – 1846.

90. Louie P.K.K., Chow J.C., Chen L.W.A., Watson J.G., Leung G., Sin S.W.M., 2005. PM2.5 chemical composition in Hong Kong: urban and regional variations. Science of the Total Environment 338, 267 – 281.

91. Louie P.K.K., Leung G.S.P., Yeung B.T.W., Sin D.W.M., Yu J., Lau A., Bergin M., Zheng M., Chow J., Watson J., 2002. Twelve-month Particulate Matter Study in Hong Kong.

92. Luria M., Sievering H., 1991. Heterogeneous and homogeneous oxidation of SO2 in the remote marine atmosphere. Atmospheric Environment 25A, 8, 1489 – 1496.

93. Ma J., Tang J., Li S.M., Jacobson M.Z., 2003. Size distributions of ionic aerosols measured at Waliguan Observatory: Implication for nitrate gas-to-particle transfer processes in the free troposphere. Journal of Geophysical Research 108, D17, 4541, 10.1029/2002JD003356.

94. Ma Y., Weber R.J., Maxwell-Meier K., Orsini D.A., Lee Y.N., Huebert B.J., Howell S.G., Bertram T., Talbot R.W., Dibb J.E., Scheuer E., 2004. Intercomparisons of airborne measurements of aerosol ionic chemical composition during TRACE-P and ACE-Asia. Journal of Geophysical Research 109, D15S06, doi:10.1029/2003JD003673.

95. Martinez M., Perner D., Hackenthal E.M., Kulzer S., Schutz L., 2000. NO_3 at Helgoland during the NORDEX campaign in October 1996. Journal of Geophysical Research 105, 22685 – 22695.

96. McLaren R., Salmon R.A., John-Liggio J., Hayden K.L, Anlauf K.G., Leaitch W.R., 2004. Nighttime chemistry at a rural site in the Lower Fraser Valley. Atmospheric Environment 38, 5837 – 5848.

97. McMurry P., Shepherd M., Vickery J., 2004. Particulate Matter Science for Policy Makers. A NARSTO Assessment. Cambridge University Press.

98. Mehlmann A., Warneck P., 1995. Atmospheric gaseous HNO_3, particulate nitrate, and aerosol size distributions of major ionic species at a rural site in western Germany. Atmospheric Environment 29, 2359 – 2373.

99. Meng Z., Seinfeld J.H., Saxena P., Kim, Y.P., 1995. Contribution of water to particulate mass in the south coast air basin. Aerosol Science and Technology 22, 111 – 123.

100. Middleton P., Kiang C.S., Mohnen V.A., 1980. Theoretical estimates of the relative importance of various urban sulfate aerosol production mechanisms. Atmospheric Environment 14, 463 – 472.

101. Molina M.J., Molina L.T., 2004. Megacities and atmospheric pollution. Journal of the Air & Waste Management Association 54, 644 – 680.

102. Mouli P.C., Mohan S.V., Reddy S.J., 2003. A study on major ion composition of atmospheric aerosols at Tirupati. Journal of Hazardous Materials B96, 217 – 228.

103. Müller K., 1999. A 3 year study of the aerosol in northwest Saxony (Germany). Atmospheric Environment 33, 1679 – 1685.

104. National Aeronautics and Space Administration (NASA). URL: <http://disc1.sci.gsfc.nasa.gov/daac-bin/G3/gui.cgi?instance_id=MODIS_DAILY_L3>.

105. National Bureau of Statistics of China, 2004. China population statistics yearbook. China Statistics Press, Beijing.

106. National Bureau of Statistics of China, 2005. Statistical yearbook of China 2005. China Statistics Press, China.

107. Nemitz E., Sutton M.A., Wyers G.P., Jongejan P.A.C., 2004. Gas–particle interactions above a Dutch heathland: I surface exchange fluxes of NH_3, SO_2, HNO_3, HCl. Atmospheric Chemistry and Physics 4, 989 – 1005.

108. Oberdörster, G., Gelein, R.M., Ferin, J., Weiss, B., 1995. Association of particulate air pollution and acute mortality: involvement of ultrafine particles. Inhalation toxicology 7, 1, 111 – 124.

109. Ohta S., Okita T., 1990. A chemical characterization of atmospheric aerosol in Sapporo. Atmospheric Environment 24A, 4, 815 – 822.

110. Pandey S.K., Tripathi B.D., Mishra V.K., Prajapati S.K., 2006. Size fractionated speciation of nitrate and sulfate aerosols in a sub-tropical industrial environment. Chemosphere 63, 49 – 57.

111. Pandis S.N., Seinfeld J.H., Pilnis C., 1992. Heterogeneous sulfate production in an urban fog. Atmospheric Environment 26A, 2509 – 2522.

112. Park S.S., Ondov J.M., Harrison D., Nair N.P., 2005. Seasonal and shorter-term variations in particulate atmospheric nitrate in Baltimore. Atmospheric Environment 39, 2011 – 2020.

113. Patashnick H., Rupprecht E.G., 1991. Continuous PM10 measurements using the tapered element oscillating microbalance. Journal of the Air & Waste Management Association 41, 1079 – 1083.

114. Pathak R.K., Chan C.K., 2005. Inter-particle and gas-particle interactions in sampling artifacts of $PM_{2.5}$ in filter-based samplers. Atmospheric Environment 39, 1597 – 1607.

115. Pathak R.K., Liou P.K.K., Chan C.K., 2004b. Characteristics of Aerosol acidity in Hong Kong. Atmospheric Environment 38, 2965 – 2974.

116. Pathak R.K., Yao X., Lau A.K.H., Chan C.K., 2003. Acidity and concentrations of ionic species of $PM_{2.5}$ in Hong Kong. Atmospheric Environment 37, 1113 – 1124.

117. Pathak R.K., Yao X.H., Chan C.K., 2004a. Sampling artifacts of acidity and ionic species in $PM_{2.5}$. Environmental Science and Technology 38, 254 – 259.

118. Qian Z., Zhang J., Wei F., Wilson W.E., Chapman R., 2001. Long-term ambient air pollution levels in four Chinese cities: inter-city and intra-city concentration gradients for epidemiological studies. Journal of Exposure Analysis and Environmental Epidemiology 11, 341 – 351.

119. Rattigan O.V., Hogrefe O., Felton H.D., Schwab J.J., Roychowdhury U.K., Husain L., Dutkiewicz V.A., Demerjian K., 2006. Multi-year urban and rural semi-continuous $PM_{2.5}$ sulfate and nitrate measurements in New York state: Evaluation and comparison with filter based measurements. Atmospheric Environment 40, S192 – S205.

120. Ravishankara A.R., 1997. Heterogeneous and Multiphase Chemistry in the Troposphere. Science 276, 1058 – 1065.

121. Sasaki K., Sakamoto K., 2006. Diurnal characteristics of suspended particulate matter and $PM_{2.5}$ in the urban and suburban atmosphere of the Kanto Plain, Japan. Water, Air, and Soil Pollution 171, 29 – 47.

122. Saxena P., Seigneur C., 1987. On the oxidation of SO_2 to sulfate in atmospheric aerosols. Atmospheric Environment 21, 4, 807 – 812.

123. Seaton, A., McNee, W., Donaldson, K., Godden, D., 1995. Particulate air pollution and acute health effects. Lancet 345, 176 – 178.

124. Seinfeld J.H., Pandis S.N., 1998. Atmospheric Chemistry and Physics: From Air Pollution to Climate Change, John Wiley, New York.

125. Sharma M., Kiran Y.N.V.M., Shandilya K.K., 2003. Investigations into formation of atmospheric sulfate under high PM_{10} concentration. Atmospheric Environment 37, 2005 – 2013.

126. Shwartz J., Zhuang G., Wang Y., Han L., Guo J., Dan M., Zhang W., Wang Z., 2004. The air-borne particulate pollution at Beijing – concentrations, composition, distribution, and sources of Beijing aerosol. Atmospheric Environment 38 (35), 5991 – 6004.

127. Sievering H., Gorman E., Kim Y., Ley T., Seidl W., Boatman J., 1994. Heterogeneous conversion contribution to the sulfate observed over Lake Michigan. Atmospheric Environment 28, 2, 367 – 370.

128. Sievering H., Gorman E., Ley,T., Pszenny A.A.P., Spring-Young M., Boatman J.F., Kim Y., Nagamoto C., Wellman D.L., 1995. Ozone oxidation of sulfur in sea-salt aerosol particles during the Azores marine aerosol and gas exchange experiment. Journal of Geophysical Research 100, 23075 – 23081.

129. Sillanpaa M., Hillamo R., Saarikoski S., Frey A. et al., 2006. Chemical composition and mass closure of particulate matter at six urban sites in Europe. Atmospheric Environment 40, 212 – 223.

130. Simon P.K., Dasgupta P.K., 1993. Wet Effluent Denuder Coupled Liquid/Ion Chromatography Systems: Annular and Parallel Plate Denuders. Analytical Chemistry 65, 1134 – 1139.

131. Sisler J.F., Malm W.C., 2000. Interpretation of Trends of $PM_{2.5}$ and Reconstructed Visibility from the IMPROVE Network. Journal of Air & Waste Management Association 50, 775 – 789.

132. Slanina J., Brink H.M.T., Otjes R.P., Even A., Jongejan P., Khlystov A., Waijers-Ijpelaan A., Hu M., Lu Y., 2001. The continuous analysis and ammonium in aerosols by the steam jet aerosol collector (SJAC): extension and validation of the methodology. Atmospheric Environment 35, 2319 – 2330.

133. Spurny K.R., 2000. Aerosol chemical processes in the environment. 23 – 46 pp., Lewis publishers, U.S.

134. Stelson A.W., Seinfeld J.H., 1982. Relative humidity and temperature dependence of the ammonium nitrate dissociation constant. Atmospheric Environment 16, 984 – 992.

135. Stolzenburg M.R., Hering S.V., 2000. Method for the Automated Measurement of Fine Particle Nitrate in the Atmosphere, Environmental Science & Technology 34, 907 – 914.

136. Streets D.G., Bond T.C., Carmichael G.R., Fernandes S.D., Fu Q., He D., Klimont Z., Nelson S.M., Tsai N.Y., Wang M.Q., Woo J.H., Yarber K.F., 2003. An inventory of gaseous and primary aerosol emissions in Asia in the year 2000. Journal of Geophysical Research 108, D21, 8809, doi:10.1029/2002JD003093.

137. Streets D.G., Fu J.H.S., Jang C.J., Hao J.M., He K.B., Tang X.Y., Zhang Y.H., Wang Z.F., Li Z.P., Zhang Q., Wang L.T., Wang B.Y., Yu C., 2007. Air quality during the 2008 Beijing Olympic Games. Atmospheric Environment 41, 3, 480 – 492.

138. Streets D.G., Waldhoff S.T., 2000. Present and future emissions of air pollutants in China: SO_2, NO_x, and CO. Atmospheric Environment 34, 363 – 374.

139. Surratt J.D., Kroll J.H., Kleindienst T.E., Edney E.O., Claeys M., Sorooshian A., Ng N.L., Offenberg J.H., Lewandowski M., Jaoui M., Flagan R.C., Seinfeld J.H., 2007. Evidence for organosulfates in secondary organic aerosol. Environmental Science and Technology 41, 517 – 527, DOI: 10.1021/es062081q.

140. Ta W., Wang T., Xiao H., Zhu X., Xiao Z., 2004. Gaseous and particulate air pollution in the Lanzhou Valley, China. Science of the Total Environment 320, 163 – 176.

141. Tang I.N., Munkelwitz H.R., 1994. Water activities, densities and refractive indices of aqueous sulfates and sodium nitrate droplets of atmospheric importance. Journal of Geophysical Research 99, 18801 – 18808.

142. Tanner R.L., Bairai S.T., Olszyna K.J., Valente M.L., Valente R.J., 2005. Diurnal patterns in PM2.5 mass and composition at a background, complex terrain site. Atmospheric Environment 39, 3865 – 3875.

143. Thermo Electron Corporation, 2005. TEOM® Series 1400a Ambient Particulate Monitor Operation Manual. Thermo Electron Corporation.

144. Tsai C.J., Perng S.N., 1998. Artifacts of ionic species for Hi-Vol PM_{10} and PM_{10} dichotomous samplers. Atmospheric Environment 32, 1605 – 1613.

145. Tsitouridou R., Voutsa D., Kouimtzis T., 2003. Ionic composition of PM_{10} in the area of Thessaloniki, Greece. Chemosphere 52, 883 – 891.

146. Ueda H., Takemoto T., Kim Y.P., Sha W., 2000. Behaviors of volatile inorganic components in urban aerosols. Atmospheric Environment 34, 353 – 361.

147. URG, 2003. Ambient Ion Monitor URG-9000 Series Operations Manual. URG.

148. US Environmental Protection Agency (USEPA), 1997. National ambient air quality standards for particulate matter, final rule. Federal Register Vol. 62 (138), Part II, EPA, 40 CFR Part 50, 18 July.

149. Van Oss R., Duyzer J., Wyers P., 1998. The influence of gas to particle conversion on measurements of ammonia exchange over forest. Atmospheric Environment 32, 465 – 471.

150. Vedal S., 1997. Critical review—ambient particles and health: lines that divide. Journal of the Air and Waste Management Association 47, 551 – 581.

151. Wang G., Wang H., Yu Y., Gao S., Feng J., Gao S., Wang L., 2003. Chemical characterization of water-soluble components of PM_{10} and $PM_{2.5}$ atmospheric aerosols in five locations of Nanjing, China. Atmospheric Environment 37, 2893 – 2902.

152. Wang T., 2003. Study of Visibility Reduction and its Causes in Hong Kong. The Environmental Protection Department of HKSAR, Air Services Group, Hong Kong, AS 01-286.

153. Wang T., Cheung V.T.F., Lam K.S., Kok G.L., Harris J.M., 2001. The characteristics of ozone and related compounds in the boundary layer of he South China coast: temporal and vertical variations during autumn season. Atmospheric Environment 35, 2735 – 2746.

154. Wang T., Ding A., Gao J., Wu W.S., 2006. Strong ozone production in urban plumes from Beijing, China. Geophysical Research Letters 33, L21806, doi:10.1029/2006GL027689.

155. Wang T., Poon C.N., Kwok Y.H., Li Y.S., 2003. Characterizing the temporal variability and emission patterns of pollution plumes in the Pearl River Delta of China. Atmospheric Environment 37, 3539 – 3550.

156. Wang T., Wong C.H., Chenug T.F., Blake D.R., Arimoto R., Baumann K., Tang J., Ding G.A., Yu X.M., Li Y.S., Streets D.G., Simpson I.J., 2004. Relationships of trace gases and aerosols and the emission characteristics at Lin'an, a rural site in eastern China, during spring 2001. Journal of Geophysical Research, 109, D19S05, doi:10.1029/2003JD004119.

157. Wang T., Wong H.L.A., Tang J., Ding A., Wu W.S., Zhang X.C., 2005. On the origin of surface ozone and reactive nitrogen observed at a remote mountain site in the northeastern Qinghai-Tibetan Plateau, western China. Journal of geophysical research, submitted.

158. Wang Y., Zhuang G., Tang A., Yuan H., Sun Y., Chen S., Zheng A., 2005. The ion chemistry and the source of $PM_{2.5}$ aerosol in Beijing. Atmospheric Environment 39, 3771 – 3784.

159. Wang Y., Zhuang G., Zhang X., Huang K., Xu C., Tang A., Chen J., An Z., 2006. The ion chemistry, seasonal cycle, and sources of $PM_{2.5}$ and TSP aerosol in Shanghai. Atmospheric Environment 40, 2935 – 2952.

160. Wang Y., Zhuang G.S., Sun Y.L., An Z.S., 2006. The variation of characteristics and formation mechanisms of aerosols in dust, haze, and clear days in Beijing. Atmospheric Environment 40, 34, 6579 – 6591.

161. Warneck P., 2000. Chemistry of the Natural Atmosphere. Second edition. Academic Press, New York.

162. Wayne, R.P., 1991. The nitrate radical: Physics, chemistry and the atmosphere. Atmospheric Environment 25A, 1 – 203.

163. Weber R., Orisun D., Duan Y., Baumann K., Kiang C.S., Chameides W., Lee Y. N., Brechtel F., Klotz P., Jongejan P., Brink H.T., Slanina J., Boring C.B., Genfa Z., Dasgupta P., Hering S., Stolzenburg M., Dutcher D.D., Edgerton E., Hartsell B., Solomon P., Tanner R., 2003. Intercomparison of near real time monitors of PM2.5 nitrate and sulfate at the U.S. Environmental Protection Agency Atlanta Supersite. Journal of Geophysical Research 108, D7, 8421, doi:10.1029/2001JD001220.

164. Weber R.J., Orisun D., Daun Y., Lee Y.N., Klotz P.J., Brechtel F., 2001. A Particle-into-Liquid Collector for Rapid Measurement of Aerosol Bulk Chemical Composition. Aerosol Science and Technology 35, 718 – 727.

165. Wei F., Teng E., Wu G., Hu W., Wilson W.E., Chanpman R.S., Pau J.C., Zhang J., 1999. Ambient concentrations and elemental compositions of PM10 and PM2.5 in four Chinese cities. Environmental Science and Technology 33, 4188 – 4193.

166. Winchester J.W., Bi M., 1984. Fine and coarse composition in an urban setting – A case-study in Beijing, China. Atmospheric Environment 18, 7, 1399 – 1409.

167. Wittig A.E., Takahama S., Khlystov A.Y., Pandis S.N., Hering S., Kirby B., Davidson C., 2004. Semi-continuous PM2.5 inorganic composition measurements during the Pittsburgh Air Quality Study. Atmospheric Environment 34, 3201 – 3213.

168. Wu W.S., Wang T., 2007. On the performance of a semi-continuous $PM_{2.5}$ sulfate and nitrate instrument under high loadings of particulate and sulfur dioxide. Atmospheric Environment, doi:10.1016/j.atmosenv.2007.02.025 (in press).

169. Xiao H., Liu C., 2004. Chemical characteristics of water-soluble components in TSP over Guiyang, SW China, 2003. Atmospheric Environment 38, 6297 – 6306.

170. Yang H., Yu J.Z., Ho S.S.H., Xu J., Wu W.S., Wan C.H., Wang X., Wang X., Wang L., 2005. The chemical composition of inorganic and carbonaceous materials in $PM_{2.5}$ in Nanjing, China. Atmospheric Environment 39, 3735 – 3749.

171. Yao X., Chan C.K., Fang M., Cadle S., Chan T., Mulawa P., He K., Ye B., 2002. The water-soluble ionic composition of $PM_{2.5}$ in Shanghai and Beijing, China. Atmospheric Environment 36, 4223 – 4234.

172. Yao X., Ling T.Y., Fang M., Chan C.K., 2006. Comparison of thermodynamic predictions for in situ pH in $PM_{2.5}$. Atmospheric Environment 40, 2835 – 2844.

173. Yao X.H., Chan C.K., Fang M., Cadle S.H., Chan T., Mulawa P.A., He K., Ye B., 2002. The water-soluble ionic composition of $PM_{2.5}$ in Shanghai and Beijing, China. Atmospheric Environment 36, 4223 – 4234.

174. Yao X.H., Fang M., Chan C.K., 2001. Experimental study of the sampling artifact of chloride depletion from collected sea salt aerosols. Environmental Science and Technology 35, 600 – 605.

175. Ye B., Ji X., Yang H., Yao X., Chan C.K., Cadle S.H., Chan T., Mulawa P.A., 2003. Concentration and chemical composition of $PM_{2.5}$ in Shanghai for a 1-year period. Atmospheric Environment 37, 499 – 510.

176. Yin J., Allen A.G., Harrison R.M. et al., 2005. Major component composition of urban PM_{10} and $PM_{2.5}$ in Ireland. Atmospheric Research 78, 149 – 165.

177. Zhang M., Salmon L.G., Schauer J.J., Zeng L., Kiang C.S., Zhang Y., Cass G.R., 2005. Seasonal trends in PM2.5 source contributions in Beijing, China. Atmospheric Environment 39, 3967 – 3976.

178. Zhang X.Q., McMurry P.H., 1992. Evaporative loss of fine particulate nitrates during sampling. Atmospheric Environment 26A, 3305 – 3312.

179. Zhang Y., Seigneur C., Seinfeld J.H., Jacobson M., Clegg S.L., Binkowski F.S., 2000. A comparative review of inorganic aerosol thermodynamic equilibrium modules: similarities, differences, and their likely causes. Atmospheric Environment 34, 117 – 137.

180. Zhuang H., Chan C.K., Fang M., Wexler A.S., 1999. Formation of nitrate and non-sea-salt sulfate on coarse particles. Atmospheric Environment 33, 4223 – 4233.